

# A STUDY OF TRELIS-CODED QAM ON ISI CHANNELS

## A THESIS

*submitted in fulfilment of the  
requirements for the award of the degree*

*of*

DOCTOR OF PHILOSOPHY

*in*

ELECTRONICS AND COMPUTER ENGINEERING



By

**SURESH CHANDRA MOHAN**



DEPARTMENT OF ELECTRONICS AND COMPUTER ENGINEERING  
UNIVERSITY OF ROORKEE  
ROORKEE-247 667 (INDIA)

AUGUST, 1997

## CANDIDATE'S DECLARATION

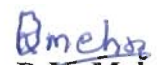
I hereby certify that the work which is being presented in the thesis entitled **A Study of Trellis-Coded QAM on ISI Channels** in fulfilment of the requirement for the award of the degree of *Doctor of Philosophy* and submitted in the Department of Electronics and Computer Engineering of the University, is an authentic record of my own work carried out during a period from April, 1993 to August, 1997 under the supervision of **Dr. D.K. Mehra**.

The matter presented in this thesis has not been submitted by me for the award of any other degree of this or any other University.

  
(SURESH CHANDRA MOHAN)


This is to certify that the above statement made by the candidate is correct to the best of my knowledge.


Date: August 28, 1997

  
Dr. D.K. Mehra  
Professor  
Department of Electronics  
and Computer Engineering  
University of Roorkee  
Roorkee - 247 667, INDIA

The Ph.D. viva-voce examination of Suresh Chandra Mohan, Research Scholar,  
has been held on 14/7/98

  
Signature of Supervisors

  
Signature of H.O.D.  
147

  
Signature of  
External Examiner

## ABSTRACT

In recent years, the ever increasing demand for reliable high-speed information transmission has spurred an active interest in the development of efficient coded communication systems, both in terms of power efficiency and bandwidth (spectral) efficiency. The traditional coding schemes trade bandwidth efficiency for increased power efficiency/coding gain and therefore are considered to be suitable only for power limited channels, where bandwidth is abundant. The rapid growth in digital radio communication and high-speed digital networks, demands a large spectral efficiency to meet the enhanced information rate requirements. Ungerboeck's combined coding and modulation scheme, namely Trellis-coded modulation (TCM), has provided an impetus to achieve high spectral efficiency on bandlimited channels, while providing adequate power efficiency/coding gain. Over the past decade, the TCM has evolved as a robust and efficient coding scheme for information transmission without sacrificing data rate, bandwidth, and signal power. The fact that it promised to fill most of the 9 dB gap between the rates achievable and Shannon's channel capacity limit, prompted an active research as well as wide-spread practical applications of the TCM.

Ungerboeck's TCM scheme is an integrated design approach that regards coding and modulation as a single entity. Essentially, the TCM scheme employs non-binary redundant modulation in conjunction with a finite-state convolutional encoder that governs the selection of channel signals. The key to this unified design approach is a special mapping technique called mapping by set-partitioning, which ensures that the minimum Euclidean distance (ED) between the coded signal sequences is maximized. At the receiver, the noise corrupted signal sequence is decoded by soft-decision maximum-likelihood Viterbi decoder, which is an optimum receiver. Depending upon the code employed, a TCM scheme can improve the robustness of

digital transmission on additive white Gaussian noise (AWGN) channel by 3 to 6 dB relative to an uncoded modulation system, without compromising the bandwidth efficiency or power efficiency.

The present work is concerned with the study of Trellis-coded QAM system on AWGN channels as well as on time-dispersive intersymbol interference (ISI) channels. In an effort to overcome the problem of computational complexity of the optimal receiver structure for bandlimited channels, various reduced complexity sub-optimum receiver structures have been considered and their performance evaluated.

We consider first, the performance of Trellis-coded QAM systems on AWGN channels, which depends on the decoding algorithm and the distance properties of the code employed. An exact analysis of the error probability is difficult, and one normally resorts to either simulation or the evaluation of performance bounds. Simulation is a time consuming process and therefore cannot provide realistic estimates of error performance at high signal-to-noise ratio (SNR). On the other hand, the performance bounds are the most effective tools in the evaluation of performance at moderate to high SNR. The algorithms used to compute the performance need to be fast and efficient. Most of the algorithms proposed in the literature are based on the transfer function approach, which when combined with union bound yields a tight upper bound to the error probability.

In the present work, we have proposed a unidirectional trellis search algorithm based on the shortest-route principle, that computes the distance spectrum of the code using a trellis structure whose state complexity is same as that of the encoder. The algorithm is fast and efficient. The derivation of tight upper bound to error probability requires computation of the complete distance spectrum of the code to evaluate all the terms of the union bounds. In practice, the first few spectral lines of the code are computed to yield a moderately tight upper bound to error probability. Following this approach, the performance of trellis codes on AWGN channel have been evaluated through bounds, using the

proposed distance spectrum computing algorithm, and the results so derived are compared with simulation results. The performance evaluation so derived is found to be nearly tight, in the sense that the simulation result lies well within the computed lower and upper bounds. The proposed method, for the computation of distance spectrum and hence the evaluation of the code performance, is found to be quite effective for Ungerboeck's TCM codes. We observe that, over AWGN channel the TCM schemes achieve a coding gain of nearly 3-5 dB relative to the uncoded reference system.

The large spectral efficiency and high coding gain achieved by TCM on AWGN channels, has stimulated researchers to investigate its performance and consider its application to high-speed data transmission over bandlimited time-dispersive channels. The primary impediments over such a channel are the ISI and AWGN. While TCM can effectively enhance noise immunity without a reduction in data rate, a powerful equalization technique such as maximum-likelihood sequence estimation (MLSE) is desired to mitigate the effects of ISI. Therefore for bandlimited channels, a TCM scheme in combination with an optimum MLSE promises to achieve data rates close to channel capacity. The cascade of TCM encoder and ISI channel can be represented by a combined finite-state machine and hence a combined ISI-Code trellis, whose states is the product of encoder states and ISI states. Consequently, the receiver performs a maximum-likelihood estimation of data sequence using the Viterbi algorithm (VA) that searches for a minimum cost path in the combined ISI-Code trellis and the resulting structure is optimum. A study has been performed to evaluate the error rate performance of the combined ISI-Code receiver structures, used for the decoding of various Trellis-coded QAM signals in the presence of ISI and AWGN, through simulation. Making use of the error structure of the basic trellis-code employed and the ISI channel characteristics, the performance of the optimum combined MLSE receiver structures have also been evaluated through bounds, and are found to be in concurrence with the simulation results. From the simulation results, we find that the performance of the optimum

combined MLSE receiver structures, over certain ISI channels, is very close to that under an ISI-free environment. Although there is a degradation of the order of 1–2 dB relative to the ISI-free performance, the combined ISI-code trellis structure achieves gain of about 2–3 dB over the uncoded MLSE reference system.

Since the computational complexity of the optimum combined MLSE receiver structure grows exponentially with channel memory length the practical implementation becomes prohibitive, even for moderate ISI. This has motivated researchers to find the sub-optimum TCM receiver structures with reduced complexity, that maintains most of the performance advantages of the MLSE. The complexity can be reduced drastically by employing pre-filtering techniques prior to MLSE, as is being used for uncoded modulation schemes. We have proposed, a sub-optimum KFE-MLSE receiver structure comprising of Kalman filter equalizer (KFE) followed by maximum-likelihood Viterbi decoder for the decoding of trellis-coded QAM signals in the presence of ISI and AWGN.

The proposed KFE-MLSE structure is a sub-optimum receiver structure and the performance degradation for the above can be evaluated by assuming that the Viterbi algorithm still operates with a white Gaussian noise, whose variance is the overall variance of the correlated noise and the residual ISI at the equalizer output. The effect of prefiltering on the free distance of the code can be computed by finding the combined channel-KFE impulse response through ‘innovations’ representation of the processes involved, and the spectral factorization techniques. We have evaluated the performance of the KFE-MLSE receiver structure, by finding the performance degradation relative to its performance under an ISI-free environment. The performance bounds so derived are compared with the simulation results of several trellis-coded QAM schemes employing KFE-MLSE structure on different ISI channels. Also, the performance of the KFE-MLSE receiver structure is compared with that of the optimum combined ISI-code trellis structure for limited ISI memory length. The proposed suboptimal KFE-MLSE structure achieves significant gain of about 2–2.5 dB over the uncoded KFE

reference system, although it suffers a performance loss of about 1.0–2.0 dB relative to the optimum combined MLSE structure.

An alternative to the prefiltering technique is the use of reduced-state algorithms, which aim at reducing the states of the optimum combined ISI-code trellis by incorporating a built-in decision-feedback mechanism within the Viterbi decoder. The Reduced State Sequence Estimation (RSSE) and the Parallel Decision Feedback Decoding (PDFD) are two such sequence estimation algorithms, which provide a good performance/complexity trade-off, the latter being a special case of RSSE. In RSSE, the complexity reduction is achieved by using the channel truncation technique and applying the set-partitioning principles inherent in TCM. The state reduction in RSSE depends on the code, the channel truncation length, and the depth of set-partitioning of the signal constellation. A family of reduced state sequence estimators can be obtained for a given TCM code and a given ISI channel, offering a wide trade-off between decoding complexity and performance. The complexity of RSSE trellis can range between that of the encoder trellis and the combined MLSE trellis. When the complexity of the RSSE trellis is reduced to that of the TCM encoder trellis, the receiver structure is referred to as the parallel decision feedback decoding (PDFD).

We have considered the study of several RSSE and PDFD receiver structures for the decoding of trellis-coded QAM with different orders of complexity reduction, for various ISI channels. The performance of these structures have been studied by simulation and are compared with the error performance of other receiver structures, considered earlier. The RSSE receiver structures exhibit improved performance over KFE-MLSE receiver structure, but at the cost of increased complexity.

For channel equalization, the optimum combined MLSE receiver structure (implemented by VA) or its sub-optimum variants, require an exact knowledge of the channel characteristics, especially when the channel parameters are time-varying. A wide range of adaptive algorithms for channel estimation have been reported in

the literature, the most common being the LMS algorithm and the RLS algorithm. The decision delay inherent in the VA causes poor tracking performance, particularly when the channel characteristics are rapidly time-varying. To circumvent this problem, a new channel estimation procedure has been reported in recent years, where the adaptive channel estimation is accomplished for each state in the VA, using the zero-delay decisions associated with its survivor path to update the channel coefficients.

We next consider the adaptive implementation of the receiver structures discussed earlier, for the decoding of trellis-coded QAM on time-variant ISI channels. We have implemented various adaptive receiver structures employing LMS and RLS channel estimators, using both delayed-decision updating and delay-free updating of channel coefficients. The tracking characteristics of the adaptive algorithms have been studied for various random time-variant ISI channels. The mean-square error performance of the adaptive channel estimator have been studied by simulation. Also, the error performance of the various adaptive receiver structures have been evaluated through simulation.

In recent years, there has been an increasing interest in high-speed digital transmission over cellular mobile radio, and mobile satellite channels, which are characterized as multipath fading channels with time-dispersion. One of the most efficient technique to reduce the effect of fading is through the use of diversity reception, where the receiver is provided with several replicas of the same information transmitted over  $D$ -independently fading channels.

We have next considered a study on the performance of different trellis-coded QAM schemes over fading dispersive channels. The error performance of the adaptive RSSE, PDFD and KFE-MLSE receiver structures have been studied by simulation for different fade rates. Using  $D$ -diversity reception to combat severe fading, the error performance of the above adaptive receiver structures have been determined for different orders of diversity  $D$ .



## ACKNOWLEDGEMENTS

The author wishes to express his deep sense of gratitude to Dr. D.K. Mehra for his invaluable supervision, constructive criticism and suggestions during the course of work. He has been generous in undertaking comprehensive discussion and painstakingly meticulous reviewing of the thesis, without which the work could not have come to its present shape.

The working facilities provided by the Head, Department of Electronics and Computer Engineering, University of Roorkee, are highly acknowledged. The author wishes to express his special thanks to the non-teaching staff of the department, in particular the staff members of the Communication Lab.

The author express his gratitude to Principal, University B.D.T. College of Engineering for sponsoring him under the Q.I.P. scheme and granting him the necessary leave in this regard.

The author wishes to express his respectful tribute to this father who passed away, six years earlier on this day, during the initial phase of this work. With affection author wishes to dedicate this work in the memory of his father. He also wishes to express his gratitude towards his living mother, for her care and affection. The moral support, encouragement received by his brother and relatives deserves a special mention.

Words do not suffice to express author's feeling towards the members of his family, particular his wife for the hardships she faced during the period of this work. She deserves a special mention. He feels elated to make a special mention of his children Anu, Vinay and Shruthi, whom he missed a lot during the preparation of this thesis. Anything said would be inadequate to compensate for the neglect and hardships they had to face because of his involvement in the research program.

The author is thankful to his fellow research scholars in E & CE Department for their co-operation.

He wishes to express gratitude to his friends K.C. Siddappa and Kamesh Rao for their support and encouragement during the preparation of this thesis.

The author appreciates very much the support and encouragement received by his friend and colleague, T. Veerabhadrappa.

He also wishes to express special thanks to Satish Annigere for his help, support and encouragement during the course of the work.

This acknowledgement would be incomplete without a mention of special thanks to Sunil Deshpande for the help, understanding and support during the preparation of the thesis, without which the author would have been in trouble.

Finally, Raju deserves a word of appreciation for his co-operation and the work of neat typing of the thesis.

Place : Roorkee

**Suresh Chandra Mohan**

Dated : August 28, 1997

# CONTENTS

	<b>Page No.</b>
<i>Candidate's Declaration</i>	
<i>Abstract</i>	i
<i>Acknowledgements</i>	vii
<i>Table of Contents</i>	ix
<i>List of Figures</i>	xiii
<i>List of Tables</i>	xix
<i>List of Acronyms</i>	xxi
<i>List of Notations</i>	xxiii
<b>Chapter 1 : Introduction</b>	
1.1 Review of the earlier work	2
1.2 Statement of the problem	14
1.3 Organization of the thesis	15
<b>Chapter 2 : Trellis-Coded Modulation Over AWGN Channel</b>	
2.1 Introduction	19
2.2 Classical coding schemes	21
2.3 Trellis-coded modulation	22
2.3.1 General Structure	23
2.3.2 Set-partitioning and the TCM Mapping Rules	25
2.3.3 Multi-level Signal Constellations	27
2.4 TCM Code Design	29
2.4.1 The 4-State 16-QAM TCM Scheme	29
2.4.2 The 8-State 64-QAM TCM Scheme	35
2.4.3 The 16-QAM TCM Using Two Rate 1/2 4-State 4-AM TCM Schemes	38
2.5 Maximum-Likelihood Soft-Decision Decoding of TCM	40
2.5.1 Performance Analysis of the Viterbi Algorithm	42
2.5.2 Performance Evaluation Parameters	43
2.5.3 Performance Bounds of TCM on AWGN Channels	46

2.6	Computation of the Distance Spectrum	48
2.6.1	Unidirectional Trellis Search Algorithm to Compute the Distance Spectrum of TCM Code	49
2.6.2	Example:Distance Spectrum of 4-State 16-QAM TCM Code	51
2.7	Results and Discussion	53

### **Chapter 3 : TCM Transmission Over Time-Dispersive ISI Channels**

3.1	Introduction	69
3.2	Time-Dispersive Channel and Equalization Problem	70
3.2.1	Baseband Digital Transmission System	71
3.2.2	Equalizer Structures	74
3.3	Decoding of TCM Signals in the Presence of ISI and AWGN	77
3.3.1	Combined MLSE Equalization and TCM Decoding	77
3.4	Trellis Structures for Combined MLSE Equalization and TCM Decoding	81
3.4.1	The 16-State Combined ISI-Code Trellis for 4-State 4-QAM TCM ( $L=2$ )	81
3.4.2	The 32-State Combined ISI-Code Trellis for 4-state 16-QAM TCM ( $L=1$ )	83
3.4.3	The 128-State Combined ISI-Code Trellis for 4-State 64-QAM TCM ( $L=1$ )	83
3.4.4	The 64-State Combined ISI-Code Trellis for 8-State 16-QAM TCM ( $L=1$ )	85
3.5	Performance Evaluation of MLSE Receiver Using Combined ISI-Code Trellis Through Bounds	87
3.6	Results and Discussion	89

### **Chapter 4 : Reduced Complexity KFE-MLSE Receiver Structure for TCM Decoding on ISI Channels**

4.1	Introduction	109
4.2	Sub-Optimum MLSE Structure With Pre-Filtering	111
4.3	KFE-MLSE Receiver Structure	112
4.4	Kalman-Filter Equalizer	113
4.4.1	Innovations representation of the observation process and computation of the Kalman gains	118
4.4.2	Transformed Kalman gains through spectral factorization	120

4.5	Performance Evaluation of KFE-MLSE Receiver	123
4.6	Results and Discussion	127

**Chapter 5 : Sub-Optimum Reduced State Algorithms for TCM Decoding on ISI Channels**

5.1	Introduction	145
5.2	Reduced State Truncated Combined ISI-Code Receiver	147
5.2.1	The 8-State Truncated Combined ISI-Code Trellis for 4-State 4-QAM TCM Transmission for $L > 2$ and $J = 1$	148
5.2.2	The 32-state Truncated Combined ISI-Code Trellis for 4-state 16-QAM TCM Transmission for $L > 2$ and $J = 1$	151
5.2.3	The 128-State Truncated Combined ISI-Code Trellis for 4-State 64-QAM TCM Transmission for $L > 2$ and $J = 1$	151
5.2.4	The 64-State Truncated Combined ISI-Code Trellis for 8-State 16-QAM TCM Transmission for $L > 2$ and $J = 1$	152
5.3	Reduced State Sequence Estimation	152
5.3.1	The 8-State RSSE Trellis for a 4-State Trellis-Coded QAM and $J = 1$	155
5.3.2	The 16-State RSSE Trellis for 4-State Trellis-Coded QAM and $J = 1$	158
5.3.3	The 32-State RSSE Trellis for 4-State Trellis-Coded QAM and $J = 2$	158
5.3.4	The 32-State RSSE Receiver for 8-State Trellis-Coded QAM and $J = 1$	160
5.4	Parallel Decision Feedback Decoding	162
5.5	Results and Discussion	164

**Chapter 6 : Adaptive Receiver Structures for TCM Transmission Over Time-Dispersive Fading Channels**

6.1	Introduction	177
6.2	Fading Channel Model for TCM Transmission	179
6.3	Channel Estimation	182
6.3.1	Channel Estimation Using LMS Algorithm	185
6.3.2	Channel Estimation Using RLS Algorithm	187
6.3.3	Delay-free Channel Estimation Using Per-Survivor Processing	189

6.4	Decoding of TCM Signals Transmitted Over Time-Dispersive Multi-Path Fading Channel Using D-Diversity Reception	191
6.5	Results and Discussion	195
<b>Chapter 7 : Conclusions</b>		<b>207</b>
<b>Appendix-A</b>	Spectral factorization	213
<b>Appendix-B</b>	Variance of ARMA(P-Q) process	217
<b>Appendix-C</b>	Fading Dispersive Channel	221
	<b>References</b>	<b>225</b>

## LIST OF FIGURES

Fig. No.	Caption	Page No.
2.1	General structure of Ungerboeck's TCM scheme.	24
2.2	Signal sets for one-dimensional Amplitude Modulation and two dimensional Quadrature Amplitude Modulation.	28
2.3	Minimal feedback-free convolutional encoders for M-QAM TCM schemes.	30
2.4	Set-partitioning of 16-QAM signal constellation.	31
2.5	The 4-state 16-QAM TCM scheme.	32
2.6	Uncoded reference systems for 16-QAM and 64-QAM TCM schemes.	34
2.7	Set-partitioning of 64-QAM signal constellation.	36
2.8	The 8-state 64-QAM TCM scheme.	37
2.9	Superposed view of a 16-QAM TCM scheme using two rate-1/2 4-state 4-AM TCM schemes.	39
2.10	Formation of an error event.	43
2.11	The 4-state 16-QAM TCM code trellis and its distance trellis	52
2.12	Error event performance of M-QAM TCM schemes on AWGN channel for different values of decision delay $\delta$ .	54
2.13	Performance comparison of 4-state 16-QAM TCM scheme on AWGN channel with different 8-QAM reference systems	56
2.14	Performance comparison of 8-state 64-QAM TCM scheme on AWGN channel with different 32-QAM reference systems.	56
2.15	The error performance of 16-QAM TCM schemes on AWGN channel.	65
2.16	The error performance of 64-QAM TCM schemes on AWGN channel.	66
2.17	The error performance of 4-state 4-PAM TCM and 4-state 4-QAM TCM schemes on AWGN channel.	67

2.18	Performance comparison among the different 16-QAM TCM schemes and the 64-QAM TCM schemes on AWGN channel.	67
3.1	Baseband digital transmission system	72
3.2	Discrete-time white noise channel model	72
3.3	Maximum-likelihood sequence estimator	76
3.4	Baseband TCM transmission and detection with MLSE	78
3.5	Combined discrete-time white noise model	78
3.6	The 16-state combined ISI-Code trellis structure, for 4-state 4-QAM TCM transmission over an ISI channel of memory length $L=2$	82
3.7	The 32-state combined ISI-Code trellis structure, for 4-state 16-QAM TCM transmission over an ISI channel of memory length $L=1$	84
3.8	Error performance of the combined MLSE receiver which uses an 8-state combined ISI-code trellis structure for the decoding of 4-state 4-QAM TCM signals transmitted over an ISI channel of memory $L=1$	97
3.9	Error performance of the combined MLSE receiver which uses a 16-state combined ISI-code trellis structure for the decoding of 4-state 4-QAM TCM signals transmitted over an ISI channel of memory $L=2$	99
3.10	Error performance of the combined MLSE receiver which uses a 32-state combined ISI-code trellis structure for the decoding of 4-state 4-QAM TCM signals transmitted over an ISI channel of memory $L=3$	100
3.11	Error performance of the combined MLSE receiver which uses a 32-state combined ISI-code trellis structure for the decoding of 4-state 16-QAM TCM signals transmitted over an ISI channel of memory $L=1$	103



3.12	Error performance of the combined MLSE receiver which uses an 128-state combined ISI-code trellis structure for the decoding of 4-state 64-QAM TCM signals transmitted over an ISI channel of memory $L=1$	104
3.13	Error performance of the combined MLSE receiver which uses a 64-state combined ISI-code trellis structure for the decoding of 8-state 16-QAM TCM signals transmitted over an ISI channel of memory $L=1$	105
3.14	Performance comparison of the combined ISI-code trellis structures based on 4-state and 8-state 16-QAM TCM schemes	106
4.1	The sub-optimum KFE-MLSE receiver	112
4.2	The block diagram of ULMMSE estimator	117
4.3	The steady-state structure of ULMMSE Kalman-equalizer	117
4.4	The KFE-VA receiver structure	124
4.5	Combined impulse response of the channel and KFE for the decoding of 4-state 16-QAM TCM signals using the KFE-MLSE receiver structures	130
4.6	The Combined impulse response of the channel and KFE of the different KFE-MLSE receiver structures used for decoding of trellis-coded M-QAM signals	131
4.7	Error performance of the KFE-MLSE receiver structure for 4-state 16-QAM TCM transmission on different ISI channels	132
4.8	Error performance of the KFE-MLSE receiver structure for 8-state 16-QAM TCM transmission on different ISI channels	136
4.9	Error performance of the KFE-MLSE receiver structure for 16-state 16-QAM TCM transmission on different ISI channels	137
4.10	Error performance of the KFE-MLSE receiver structure for 4-state 64-QAM TCM transmission on different ISI channels	139

4.11	Error performance of the KFE-MLSE receiver structure for 8-state 64-QAM TCM transmission on different ISI channels	140
4.12	Error performance of the KFE-MLSE receiver structure for 16-state 64-QAM TCM transmission on different ISI channels	141
4.13	Performance comparison of the KFE-MLSE receiver structures different TCM schemes for 16-QAM transmission on ISI channel	142
4.14	Performance comparison of the KFE-MLSE receiver structures different TCM schemes for 64-QAM transmission on ISI channel	142
5.1	The 8-state truncated combined ISI-Code trellis structure, for 4-state 4-QAM TCM transmission over an ISI channel of memory length $L \geq 2$ , using a truncation length $J=1$	150
5.2	The 8-state RSSE trellis structure, for 4-state M-QAM signal transmission over an ISI channel of memory length $L \geq 2$ , using truncation length $J=1$ , $m_1=1$	157
5.3	The 16-state RSSE trellis structure, for 4-state M-QAM signal transmission over an ISI channel of memory length $L \geq 2$ , using truncation length $J=1$ , $m_1=2$	159
5.4	The 32-state RSSE trellis structure, for 4-state M-QAM signal transmission over an ISI channel of memory length $L \geq 2$ , using truncation length $J=2$ , $m_1=2$ , $m_2=1$	161
5.5	The 32-state RSSE trellis structure, for 8-state M-QAM signal transmission over an ISI channel of memory length $L \geq 2$ , using truncation length $J=1$ $m_1=2$	163
5.6	Error performance of the truncated combined MLSE receiver which employs an 8-state truncated combined ISI-code trellis structure for the detection of 4-state 4-QAM TCM signals over an ISI channel of memory $L > 1$	166

5.7	Error performance of the truncated combined MLSE receiver which employs an 16-state truncated combined ISI-code trellis structure for the detection of 4-state 4-QAM TCM signals over an ISI channel of memory $L > 2$	167
5.8	Error performance of the truncated combined MLSE receiver which employs an 32-state truncated combined ISI-code trellis structure for the detection of 4-state 16-QAM TCM signals over an ISI channel of memory $L > 1$	169
5.9	Error performance of the 128-state truncated combined ISI-code trellis structure used for the detection of 4-state 64-QAM TCM signals over an ISI channel of memory $L > 1$	170
5.10	Error performance of the 64-state truncated combined ISI-code trellis structure used for the detection of 8-state 16-QAM TCM signals over an ISI channel of memory $L > 1$	171
5.11	Error performance of the different RSSE receiver structures used for the detection of the 4-state 16-QAM TCM signals over an ISI channel of memory $L$	173
5.12	Error performance of the different RSSE receiver structures used for the detection of the 4-state 64-QAM TCM signals over an ISI channel of memory $L$	174
5.13	Error performance of the RSSE receiver structure (RSSE-IV) used for the detection of the 8-state 16-QAM TCM signals over an ISI channel of memory $L$	174
5.14	Error performance of the different PDFD receiver structures employed for the detection of M-QAM TCM signals over an ISI channel of memory $L$	175
6.1	The TCM data transmission over a fading channel	180

6.2	The TDL model for TCM transmission over a fading dispersive channel	180
6.3	The general structure of an adaptive MLSE receiver	183
6.4	The steepest-descent LMS channel estimator	183
6.5	Adaptive MLSE structure using per-state processing (PSP) channel estimator	190
6.6	TCM data transmission system over D-diversity fading channel	192
6.7	Discrete-time white noise channel model for baseband TCM transmission over D-diversity fading channel	192
6.8	Convergence Characteristics of the LMS and RLS channel estimators on a time-dispersive fading channel at $BT=10^{-2}$	196
6.9	Tracking Characteristics of RLS and LMS channel estimators	198
6.10	Error performance comparison of the various receiver structures using conventional LMS channel estimator and the PSP channel estimator	200
6.11	Error performance of the PDFD receiver structure employing D-diversity reception for the decoding of 4-state 16-QAM TCM signals transmitted over multi-path (time dispersive) fading channel	201
6.12	Error performance of the RSSE-I receiver structure employing D-diversity reception for the decoding of 4-state 16-QAM TCM signals transmitted over multi-path (time dispersive) fading channel	202
6.13	Error performance of the KFE-MLSE receiver structure using D-diversity reception for the decoding of 4-state 16-QAM TCM signals transmitted over multi-path (time dispersive) fading channel	204
6.14	Error performance of the various receiver structure using D-diversity reception for the decoding of 16-QAM TCM signals transmitted over multi-path (time dispersive) fading channel	204

# LIST OF TABLES

Table No.	Caption	Page No.
2.1	Distance spectrum of 4-state 16-QAM TCM code.	53
2.2	Distance spectrum of 16-QAM TCM codes.	58
2.3	Distance spectrum of 64-QAM TCM codes.	59
2.4	Distance Spectrum of 4-state 4-PAM TCM and 4-state 4-QAM TCM schemes	59
2.5	Error-event performance of 16-QAM TCM schemes on AWGN channel	61
2.6	Error-event performance of 64-QAM TCM schemes on AWGN channel	62
2.7	Error-event performance of 4-state 4-PAM and 4-state 4-QAM TCM schemes on AWGN Channel	63
3.1	Equivalent discrete-time impulse response of the different ISI channels	90
3.2	The different combined ISI-Code MLSE structures and the corresponding reference systems	90
3.3	Computation of $d^2(\epsilon)$ of the output error sequences for some typical TCM codes and ISI channels	93
3.4	Summary of minimum distance calculation for various combined ISI-code trellis structures	94
3.5	Error event performance of the combined ISI-code receivers for some typical ISI channels	95
3.6	Performance gain of combined MLSE structures over uncoded MLSE structures as measured (approx.) from simulation results, at $P_e=10^{-5}$ on different ISI channels	102
4.1	Computed values of the combined impulse response of the channel and the KFE for some of the KFE-MLSE structures at different values of SNR.	126
4.2	Error event performance of the KFE-MLSE receiver structures for some typical ISI channels	128

# LIST OF ACRONYMS

- ACG - Asymptotic Coding Gain
- ARMA - Auto-regressive Moving Average
- AWGN - Additive White Gaussian Noise
- DFE - Decision-feedback Equalizer
- DS - Distance Spectrum
- ED - Euclidean Distance
- EW - Euclidean Weight
- FSM - Finite-state Machine
- iid - independent identically distributed
- ISI - Intersymbol Interference
- KF - Kalman Filter
- KFE - Kalman Filter Equalizer
- LE - Linear Equalizer
- LMS - Least Mean-Square
- ML - Maximum-likelihood
- MLSE - Maximum-likelihood Sequence Estimation
- MMSE - Minimum Mean-square Error
- MPAM - M-ary Pulse Amplitude Modulation
- MPSK - M-ary Phase-shift Keyed (modulation)
- MQAM - M-ary Quadrature Amplitude Modulation
- MTCM - Multiple Trellis-Coded Modulations
- PAM - Pulse Amplitude Modulation
- PDFD - Parallel Decision Feedback Decoding
- PSK - Phase Shift Keyed (modulation)

PSP - Per-state Processing / Per-survivor Processing  
QAM - Quadrature Amplitude Modulation  
QPSK - Quadrature Phase-shift Keyed (modulation)  
RCE - Respective-state Channel Estimation  
RLS - Recursive Least-squares  
RSSE - Reduced State Sequence Estimation  
SNR - Signal-to-noise Ratio  
SNIR - Signal-to-noise Plus Interference Ratio  
TCM - Trellis-coded Modulation  
TDL - Tapped Delay Line  
ULMMSE - Unbiased Linear Minimum Mean-square Error  
VA - Viterbi Algorithm

## LIST OF NOTATIONS

$a(n)$	Data symbol at time instant $n$
$\{a(n)\}$	Sequence of data symbols
$\{\hat{a}(n)\}$	Estimated sequence of data symbols
BT	Fade rate
D	Order of diversity
$d$	Euclidean distance
$d_{\min}$	Minimum Euclidean distance
$d_{\text{free}}$	Minimum free Euclidean distance
$\{g_i\}$	Set of discrete time-invariant channel coefficients (tap gains)
$\{g_k(n)\}$	Set of discrete time-variant channel coefficients
$N_d$	Multiplicity number at distance $d$
$N_{d_{\min}}$	Multiplicity number at distance $d_{\min}$
$N_{d_{\text{free}}}$	Multiplicity number at distance $d_{\text{free}}$
$N_s$	Number of encoder states
$r(n)$	Received waveform / Observation process
$\{r(n)\}$	Sequence of noise-corrupted received waveform
$\gamma$	Encoder Memory
$\delta$	Decision delay of the Viterbi algorithm
L	ISI memory length
M	Constellation size used for coded modulation
$\underline{M}$	Constellation size used for uncoded modulation
$m$	The number of binary inputs
$\tilde{m}$	Number of binary inputs used for encoding
$\tilde{M}_n$	Survivor path metric



$N$	Number of channel coefficient ( $N=L+1$ )
$\alpha_n$	Encoder state
$\mu_n$	Combined ISI-code state
$\lambda_n$	Reduced combined ISI-code state
$\sigma_v$	Noise variance
$\sigma_e$	Innovation noise variance
$\sigma_s$	Signals variance
$\sigma_{v0}$	Overall noise variance
$P_e$	Error event probability
$P_b$	Bit error probability
$Q(\cdot)$	Gaussian error integral function
$\mathbf{g}$	Tap gain vector
$\Phi$	State transition matrix
$V(n/n-1)$	Covariance matrix
$\mathbf{X}$	State vector
$\mathbf{K}$	Kalman gain vector
$\mathbf{I}$	Identity matrix
$h_i$	Combined impulse response of KFE and channel
$X_n$	Binary input sequence to the TCM encoder at time instant $n$
$\{x_n^i\}$	Binary input variables
$x_i$	State vector component
$\{y_n^i\}$	Coded binary input sequence

# INTRODUCTION

---

The tremendous growth in information transmission in recent years, demands the use of coded communication systems having a large spectral efficiency in order to meet the enhanced information rate requirements. This has spurred an active interest in the design and development of reliable digital communication systems that are spectrally-efficient as well as power-efficient. The traditional coding schemes, which treat coding and modulation as two separate entities, trade bandwidth efficiency against power efficiency/coding gain and therefore are considered suitable only for power-limited channels, where bandwidth is abundant [14, 100].

Using random coding bound arguments, Massey [80] suggested that considerable performance improvement could be achieved by treating coding and modulation as a single entity in the design of a coded communication system. This concept was formalized into a rigorous theory by Ungerboeck [126], which culminated in the development of 'Trellis-Coded Modulation' (TCM). It is this work that laid the foundation for an active research in the development of spectrally-efficient and power-efficient coded modulation schemes [19, 22, 30, 51, 127].

Ungerboeck's TCM scheme employs non-binary redundancy modulation in conjunction with a finite-state convolutional encoder that governs the selection of channel signals. The key to this unified design approach is a special mapping technique which ensures that the minimum Euclidean distance (ED) between the coded signal sequences is maximized [127].

The most attractive feature of TCM is its ability to improve the robustness of digital transmission over additive white Gaussian noise (AWGN) channel by 3 to 6 dB relative to an uncoded modulation system without compromising the spectral-efficiency or bandwidth-efficiency [126, 127]. The TCM not only provides an improved performance in the presence of AWGN, but also in the presence of other channel impairments [123]. Thus Ungerboeck's TCM scheme, being the state-of-the-art technique in the coding arena, captured immediate attention and provided the impetus for an intensified research as well as widespread practical applications of the spectrally-efficient coded-modulation schemes [13, 29, 51, 123, 133].

The primary impediments to high speed digital data transmission are the intersymbol interference (ISI) and AWGN [46]. The TCM scheme in combination with an optimum equalizer such as maximum-likelihood sequence estimator (MLSE) has been shown to be an optimum structure to combat the effects of ISI and AWGN [26, 42]. However, due to the reasons of complexity in implementation, the combined MLSE structure tends to be too impractical even for moderate ISI.

The design of the reduced complexity receiver structure for TCM transmission over ISI channels, that maintains some of the performance advantages of the optimum combined MLSE structure, and its performance evaluation is a topic of active research. In the following we present a brief review of the work that has been done in this and the related areas.

## **1.1 REVIEW OF THE EARLIER WORK**

The publication of Shannon's classic paper of 1948 titled 'A Mathematical Theory of Communication' [115] launched the field of error control coding. Using random coding arguments, Shannon established theoretical bounds on the achievable performance of digital coded communication systems and pointed out the 9 dB gap between the rate achievable with uncoded modulation and the channel capacity limit [50, 147]. This immediately inspired a rigorous and intensified research on error control coding aimed at the development of practical coded communication systems

which could approach the channel capacity limit. However, the initial era of excitement was followed by an era of discouragement/disappointment as such practical systems proved to be difficult to find [50].

In the classical coded communication systems, the functions of coding and modulation are treated as two independent operations [126] and a certain coding gain is achieved at the cost of bandwidth expansion. Therefore, practical coding was believed to benefit only power-limited channels, where bandwidth was abundant. Although Shannon's channel capacity theorem [116] predicted data rates exceeding 20,000 bits/sec for typical bandlimited telephone channels, the upper practical limit was considered to be 9600 bits/sec even after 30 years of Shannon's pioneering work. Most of this advance in data transmission was primarily due to advances in the field of adaptive equalization and in fact had nothing to do with Shannon's work [50].

Perhaps the most significant breakthrough in the design of coded communication system, was the development of spectrally-efficient 'Trellis-coded Modulation' (TCM) schemes by Ungerboeck [126] that promised to fill most of the 9 dB gap between rates achievable with the uncoded system and the channel capacity limit. The results on TCM schemes were first published in 1976 [127], followed by a systematic presentation in [126]. Ungerboeck has presented a comprehensive tutorial on TCM schemes in [127].

Ungerboeck's TCM is an integrated design approach that combines the coding and modulation into a single entity. Through the use of optimally designed rate  $(m/m+1)$  trellis codes suitably mapped into an expanded signal constellation of  $2^{m+1}$  points, the TCM scheme could provide a significant coding gain without sacrificing bandwidth or data rate. Thus, Ungerboeck's work captured immediate attention and inspired a rigorous research as well as practical applications of efficient coded-communication systems, both in terms of spectral efficiency and power efficiency.

Around the same time while the TCM schemes were developed [126], Imai and Hirakawa [61] also developed a slightly different integrated design approach called multi-level coding method based on binary block codes and multi-stage decoding procedure. The multilevel coded-modulation scheme of Imai and Hirakawa did not receive the attention it deserved, at the time of publication, due to the lower coding gains relative to Ungerboeck's TCM scheme. Incorporating the use of convolutional coding and soft-decision decoding into Imai-Hirakawa schemes, considerable improvements in the coding gains have been reported in [18, 28, 109, 145]. Following Ungerboeck's integrated encoding and modulation approach, Cusack [28] and Sayegh [109] have constructed a class of optimum signal space block codes using short binary block coding (as opposed to convolutional coding) with performances close to that of Ungerboeck's codes. Pottie and Taylor [96], and Calderbank [18] have presented the construction of several reduced complexity multilevel codes and they give the error performance of several alternative multistage decoding structures. The performance analysis of multilevel coded modulation schemes have been presented by Kofman et al. in [64]. Recently, this approach of multilevel block coding technique has been applied to construct trellis codes for the Rayleigh fading channels [113, 143].

Forney et al. [51] have presented a comprehensive tutorial material on the development of coded-modulation schemes for bandlimited channels and they illustrate the construction of several block-coded and trellis-coded modulation schemes. Calderbank and Mazo [19] have presented an analytical description of trellis codes, that combines the two steps of encoding and mapping into a single operation. This design procedure does not require the exhaustive code search procedure, as in the case of Ungerboeck's design approach, to find a minimal convolutional encoder to suit the mapping operation. In [124], Turgeon and McLane discuss the design of minimal complexity analytical trellis codes and give the rules for conversion from Calderbank-Mazo form to Ungerboeck-form and vice-versa.

A more generalized construction of trellis codes based on lattices and cosets has been proposed by Calderbank and Sloane in [22], as an alternative to Ungerboeck's code design methodology.

The TCM codes are normally not invariant to all phase rotations under which the signal set is phase invariant. This may pose a serious problem in applications where differential encoding/decoding is employed to avoid phase ambiguities [100]. The problem of phase invariance and differential encoding/decoding was solved by Wei [133], who devised several linear and nonlinear codes that are rotationally invariant to 180 or 90 degree phase rotations. Wei's [133] 8-state non-linear trellis code which is invariant to 90 degree phase rotation has been adopted as an international standard for high-speed telephone line modems operating at 9600 bits/sec or 14400 bits/sec [52, 100, 127].

Normally in the design of TCM schemes, symmetric signal constellations with uniform spacing are employed. Although symmetric constellations are optimum for uncoded systems, the same need not be true for TCM schemes. Divsalar et al. [29] have designed TCM schemes with asymmetric signal constellations that achieve a modest performance gain over TCM schemes employing symmetric constellations. These gains, typically around 0.5 dB, disappear with large signal constellation and for codes of higher state complexity. Moreover, in certain cases of asymmetry, the trellis codes tend to become catastrophic. To circumvent the problem of catastrophe in asymmetric TCM code design, Divsalar and Simon [31] have proposed multiple trellis-code modulation (MTCM) scheme, wherein more than one channel symbol per trellis branch is transmitted in order to achieve a modest gain of 1-2 dB for a 2-state MTCM scheme relative to a 2-state TCM scheme. However, it also suffers from the problem of higher code complexity and the use of larger signal constellation.

Forney et al. [51] proposed the idea of designing TCM schemes using constellations with partially overlapped signal points to achieve higher coding gains. While Ungerboeck's TCM schemes require a constellation of  $2^{m+1}$  signal

points to encode  $m$  information bits, the above method re-maps some of the high-power signal points into low power signal points with a subsequent saving in transmitted energy and hence achieve an increase in the coding gain. Soleymani and Kang [121] have investigated the performance of some TCM schemes with partially overlapped signal constellations. Although these schemes achieve marginal gains over Ungerboeck's TCM schemes, they are susceptible to catastrophic error propagation. Moreover, a study of these TCM schemes by Fossorier and Lin [54] indicate that these schemes require large decoding delays and also result in large error coefficients which in turn reduces significantly the achievable coding gain.

An inherent cost of Ungerboeck's two-dimensional (2-D) TCM schemes is that the size of signal constellation is doubled over uncoded modulation, which results in 1-bit redundancy for each signaling interval. Without that cost, the coding gain of the TCM schemes would have been 3 dB higher. Using a multi-dimensional constellation, it is possible to reduce this cost of 3 dB because fewer redundant bits are added for each 2-D signaling interval. The cost is reduced to 1.5 dB or 0.75 dB with the use of 4-dimensional or 8-dimensional signal constellations, respectively [134]. Thus, efforts to achieve higher gains led to the development of multi-dimensional TCM schemes, where multi-dimensional signals are transmitted as sequences of constituent one- or two-dimensional signals, while maintaining the principle of using a signal set of twice the size used for uncoded modulation [100]. In general, a  $2K$ -D TCM scheme employs a  $2^{m+(1/k)}$ -point 2-D signal constellation to transmit  $m$  information bits per symbol. Due to the smaller signal redundancy, the multi-dimensional TCM scheme achieves higher coding gains and sometimes offer better performance/complexity trade-off than a 2-D TCM [134].

Gallager [51] proposed the first multi-dimensional 4-D TCM scheme, while Calderbank and Sloane [20] have also proposed independently a similar 4-D TCM scheme. Wei [134] has developed a class of multi-dimensional TCM schemes that are highly suited for implementation, one of which has been standardized for use in 19.2 kbits/sec modems [48]. Calderbank and Sloane [21] have also developed a

number of multi-dimensional trellis codes. In [135], Wei has presented a class of rotationally invariant MPSK trellis codes. Forney [48] has performed an investigation on the performance/complexity trade-off of the several multi-dimensional TCM schemes described in [22, 51, 127, 134, 135]. In [52], Forney and Wei provide an overview of multidimensional constellations for use with TCM schemes, highlighting some of the important design attributes which are desirable in practice. Based on a new concept of generalized group alphabet-partitioning, Biglieri and Elia [15] have developed some multi-dimensional coded schemes using block codes and trellis codes, for bandlimited digital transmission. While Pietrobon et al [92] have given a comprehensive treatment on a class of Trellis-coded multi-dimensional MPSK modulation schemes, Benedetto [10] presents a procedure for the construction of geometrically uniform multi-dimensional MPSK trellis codes. Pietrobon and Costello [93] have investigated the performance of trellis coding using multi-dimensional QAM signal sets.

Although, the multi-dimensional TCM schemes exhibit larger asymptotic coding gains than 2-D TCM schemes, these gains are compromised by large number of nearest neighbours which subsequently result in the performance degradation at lower SNR [127]. At higher trellis (state) complexities, the 2-D TCM schemes will eventually prevail in performance due to the fact that these schemes have higher signal redundancy available for coding than with the multi-dimensional TCM schemes. The overall difference in real coding gain with multidimensional TCM schemes is not very large, being less than 1 dB for the range of complexities involved. In terms of better performance/complexity trade-off, the Ungerboeck's 4-state and 8-state two dimensional TCM schemes have been considered as benchmark systems for practical use [48, 51, 95].

It is well known that an exact analysis of TCM performance over AWGN channels is difficult to perform and usually one resorts to simulation or evaluation of performance bounds [111]. Simulation is a time consuming process and may not provide realistic estimates of the error performance at higher SNR. The



performance bounds, on the other hand, are quite effective in the evaluation of code performance at moderate to large SNR. The algorithms used, to evaluate the code performance through bounds, need to be fast and efficient. Most of the algorithms proposed in the literature [9, 13, 16, 146] are based on the transfer function approach [59, 129, 130], which when combined with the union bound will yield a tight upper bound on the error event probability. The pair-state transfer function approach, introduced by Biglieri [13], is most general and is applicable to all TCM codes, linear or nonlinear. The approach uses a pair-state diagram and involves a huge computational complexity which thereby limits its practical application. By invoking certain symmetries and uniform properties inherent in the TCM code, it is possible to derive transfer function using a state diagram whose state complexity is equal to that of the TCM encoder [7, 16, 22, 146]. In [22], Calderbank and Sloane introduce the concept of regular codes, which makes it possible to evaluate the code performance by choosing the all-zero information path as the reference path. The ‘superlinearity’ concept introduced by Benedetto et al. [7] is very similar to ‘regularity’ property of [22]. Zehavi and Wolf [146] have exploited the symmetry properties, inherent in the TCM code construction, to evaluate the code performance through bounds by treating the all-zero information path as the reference. Biglieri and McLane [16] have derived a set of sufficient conditions to define a class of uniform TCM schemes and have shown that all Ungerboeck codes are uniform codes. The bidirectional search stack algorithms [108, 111] have also been employed to compute the distance spectrum of TCM codes and hence the evaluation of error performance through bounds. A comprehensive tutorial on the performance evaluation of TCM schemes is presented by Benedetto et al. in [9].

The two primary impediments to reliable high-speed data transmission over a bandlimited channel are AWGN and ISI [46]. The large spectral efficiency and high coding gain achievable with TCM have prompted researchers to investigate its performance and practical application for high-speed data transmission over

bandlimited time-dispersive ISI channels [26, 40, 42, 57, 123, 138, 142, 148]. The TCM scheme in combination with an optimum MLSE equalizer promises to achieve data rates close to channel capacity [40]. The receiver makes use of a combined ISI-Code trellis structure whose state complexity is given by the product of the encoder states and the ISI states [26, 42]. Although this combined MLSE receiver is an optimum structure for bandlimited ISI channels, the fact that its computational complexity grows exponentially with the ISI memory length makes the practical implementation prohibitive even for moderate ISI. This led to an active research to find sub-optimum receiver structures with reduced complexity while maintaining most of the performance advantages of MLSE [26, 42, 138, 142].

The state complexity of the combined MLSE receiver structure can be reduced drastically by employing the prefiltering techniques prior to MLSE, as employed for uncoded transmission [43, 46, 70, 103, 137]. Thapar [123] has proposed the LE-MLSE receiver structure, comprising of a linear equalizer (LE) in cascade with a maximum-likelihood (ML) Viterbi decoder which is often used in practice for high-speed TCM transmission over telephone channels. The LE-MLSE structure performs poorly on channels with in-band nulls due to the fact that LE enhances noise on such channels. With the use of the decision-feedback equalizer (DFE) as prefilter the noise enhancement can be substantially reduced, but for proper operation the DFE requires reliable delay-free data decisions which is not possible with the TCM Viterbi decoder. Thus the DFE-MLSE structure as proposed by Wong and McLane [142], does not perform well, and in fact results in a performance loss as opposed to a gain relative to an uncoded system [26, 42, 84, 94, 138, 142].

As a remedy to the above problem, one approach is the use of interleaving/deinterleaving as proposed by Eyuboglu [40] and Zhou et al. [148]. These methods increase the throughput delays and may be prone to error propagation, and require an interleaver at the transmitter. Forney and Eyuboglu [50] proposed another technique to approach the channel capacity limit, through the use of precoding techniques with spectral shaping. Since precoding is

essentially a transmitter equalization technique, the transmitter needs to know the channel characteristics precisely and hence requires perfect transmitter-receiver co-ordination for proper operation. This may not be possible (and hence applicable) to one-way broadcast or rapidly time-varying channels, unless all the channel characteristics are known apriori. Also, such schemes may not be useful in certain applications due to the existing standards and/or compatability requirements [42]. Thus, there is still a need for a practically viable reduced complexity receiver structure that can approach the performance of an ideal DFE-MLSE receiver for the coded-modulation schemes operating over bandlimited time-dispersive channels.

Lawrence and Kaufman [68] proposed the use of discrete Kalman filter as an equalizer for uncoded binary transmission. Benedetto and Biglieri [6] performed a detailed investigation on the steady-state behaviour of this linear receiver and showed that it as an optimum linear recursive filter/equalizer which performs as a zero forcing equalizer at high SNR. The fact, that the KFE is an optimum linear equalizer whose performance is comparable to that of an ideal DFE (at high SNR) but without error propagation effects, makes the feasibility of KFE-MLSE receiver structure for the detection of TCM signals over time-dispersive ISI channels a topic for further consideration/investigation.

An alternative to the prefiltering technique is the use of reduced complexity sequence estimation algorithms which aim to reduce the state complexity of the combined MLSE receiver structure through channel truncation techniques and/or combining the trellis states into subset states based on the ideas of set-partitioning inherent in TCM. These techniques of channel truncation [43] and the reduced state sequence estimation algorithms have been used extensively for uncoded systems [41, 43, 57].

The state complexity of the combined ISI-Code trellis can be reduced by channel truncation and the residual ISI terms not represented by the truncated combined MLSE trellis structure are cancelled out by an ISI cancellation

mechanism, built within the Viterbi decoder, which makes use of data decisions associated with the survivor path of the truncated trellis state [26, 42]. For TCM schemes employing large signal constellation a further reduction in state complexity is still desired, which can be achieved by incorporating the set-partitioning ideas to define subset states for the truncated combined ISI-Code trellis [42]. This leads to a family of reduced state sequence estimation (RSSE) structures. The state reduction in RSSE depends upon the code, channel truncation length and the depth of set-partitioning employed in the TCM code construction. The state complexity of the RSSE trellis may range between that of encoder trellis and the optimum combined ISI-Code trellis [26, 42]. When the state complexity of the RSSE structure is reduced to that of the TCM encoder, the receiver structure is referred to as parallel-decision feedback decoding (PDFD) and is the simplest form of the reduced state algorithms [42, 57].

Eyuboglu and Qureshi [42], Chevillat and Eleftheriou [26] have presented a study of the RSSE and PDFD structures for the decoding of a 4-state 16-QAM TCM schemes over a limited memory ISI channels. Wesolwski [138], and Hallen and Heegard [57] have also presented independently, the PDFD receiver structures for the decoding of TCM signals over a limited class of ISI channels.

The continuing growth in digital radio communication (digital mobile and digital satellite radio communications) has spurred an active interest in the use of spectrally efficient coded-modulation schemes [13, 25, 30, 32, 35, 82, 110]. The fact that TCM schemes can provide significantly improved performance over bandlimited channels without sacrificing the spectral efficiency or power-efficiency, makes the TCM a potential candidate for application over digital radio channels. These radio channels have been characterized as rapidly time-varying multipath fading channels with time-dispersion [5, 62, 87, 99, 100]. Ungerboeck's work [126] provided the stimulus for a rigorous research aimed at the design and development of spectrally efficient and power efficient coded communication systems for applications on satellite and digital cellular mobile radio channels

[13, 29, 30, 32, 110, 131]. Most of the initial work dealt with the applications of Trellis coded MPSK schemes with interleaving on fading channels and the performance analysis using the pair state approach [13]. The notable contribution in the area are due to Divsalar and Simon [29, 30, 32]. Divsalar and Simon [30] investigated the performance of MPSK TCM schemes with interleaver/deinterleaver using the pair state approach of Biglieri [13, 36, 60, 71, 81] for applications over a fading mobile satellite channel. In a further work on the application of trellis codes (with interleaver/deinterleaver) for fading channels [30], they have shown that for optimum performance the code design guided by other factors such as length of the shortest error event and the product of branch distances. However, they have also pointed out that, with no interleaver/deinterleaver, the design of trellis codes for the fading channels are still governed by the maximization of minimum free distance of the code, as in the case of AWGN channels.

The increasing growth in digital cellular mobile radio communications, in recent years, demands for enhanced data rate requirements which can be accomplished through the bandwidth efficient and power efficient modulations formats such as M-QAM for  $M > 8$  [12, 35, 45, 90, 131, 132]. Feher [45] points out that the next generation modems, for the emerging digital cellular mobile radio systems, are required to be designed with more spectrally efficient coded modulation schemes to achieve a spectral efficiency in the range of 2-5 b/s/Hz.

Although M-QAM modulation schemes achieve higher coding gains on AWGN channels than MPSK schemes ( $M > 4$ ) because of their efficient constellation shaping, they suffer seriously on fading channels due to their non-constant envelope property. However, it has been reported by Moher and Lodge [85] that through the use of pilot sequence for channel state measurement (channel state information), the M-QAM trellis codes does exhibit improved performance over MPSK trellis codes for fading channels. There has been considerable interest in recent years in the application of M-QAM schemes to fading channels [23, 25, 33, 35, 45, 55, 93]. Feher [45] has reported the development of trellis coded 16-QAM modem for

cellular mobile radio with a promising performance in the spectral range of 2.2–3.0 b/s/Hz.

Since the radio channels are time-variant and unknown, the receiver needs to be provided with a means to estimate the time varying channel impulse response. A wide variety of adaptive algorithms are available for channel estimation [38, 74, 76, 85, 86, 101] and the most common being the least-mean squares (LMS) and the recursive least-square (RLS) algorithms. The LMS algorithm [139] although much simpler to implement performs poorly on time-varying channels due to its slow rate of convergence. In contrast the RLS algorithms exhibit faster convergence and better tracking performance and hence are considered for applications on time-varying channels [37]. However, the LMS/RLS channel estimators, employed in the adaptive MLSE receiver structure [78] or its sub-optimum variants, perform a delayed channel estimation due to the decision delay inherent in the Viterbi algorithm, and therefore are considered unsuitable for rapidly time-varying channels. To circumvent this problem, a new channel estimation procedure called per-survivor processing (PSP) channel estimation [105] has been proposed in recent years by Kubo [65] and Seshadri [112] independently. This procedure maintains a separate channel estimator for each state of the VA and the channel adaptation is performed using the zero-delay decisions associated with the survivor path of the state. The PSP channel estimation procedure, although relatively complex, has been shown to be quite effective for the adaptive equalization of the MLSE receiver structures for rapidly time-varying radio channels [66, 105].

In addition to the use of coded-modulations schemes for the multipath fading channels, the use of diversity combining technique has been shown to be quite effective for the multipath fading channels and is normally employed to combat severe fades present on such channels [4, 27, 91, 99, 118, 122]. In diversity reception, the receiver is provided with multiple replicas of the same information transmitted over  $D$ -independent fading channels. The diversity reception is effective since it is based on the notion that the probability of receiving

simultaneously two or more (independently) severely faded signals is very small [117].

## 1.2 STATEMENT OF THE PROBLEM

The present work encompasses a study of bandwidth-efficient and power-efficient Trellis-coded QAM schemes with applications to high-speed data transmission over bandlimited time-dispersive channels of both time-invariant and time-variant nature, and investigates the evaluation of error rate performance of these schemes through bounds and simulation.

The problem as treated in this study may be divided into five main parts as :

- (i) A study of Trellis-coded QAM schemes over AWGN channel and the performance evaluation through bounds using the distance spectrum, and through simulation.
- (ii) A study of Trellis-coded QAM schemes on time-invariant ISI channels using the optimum combined MLSE receiver that employs a combined ISI-Code trellis structure, and the evaluation of error performance through bounds using the error structure of the basic TCM code as well as by simulation.
- (iii) A study of the prefiltering technique that employs the sub-optimum KFE-MLSE structure for the detection of Trellis-coded QAM signals transmitted over ISI channels, and the performance evaluation through bounds and simulation.
- (iv) A study of the reduced complexity sequence estimation algorithms, which incorporate the channel truncation techniques and set-partitioning ideas, for the detection of TCM signals in the presence of ISI and AWGN, and also the evaluation of their error performance through simulation.
- (v) A study of the adaptive receiver structures for TCM transmission over fading time-dispersive channels, through the use of per-state processing channel estimation procedure and the diversity technique.

### **1.3 ORGANIZATION OF THE THESIS**

The work embodied in this thesis has been arranged in seven chapters as detailed below :

#### **Chapter 2 : Trellis-Coded Modulation over AWGN Channel**

We first discuss the drawbacks of classical coding schemes and then present Ungerboeck's TCM design concepts which aim at overcoming these drawbacks. We next present the design of a few TCM schemes employing QAM signal constellations. The performance measures used in the evaluation of error event probability through the union bound are considered next. An algorithm to compute the distance spectrum of Ungerboeck TCM codes is presented. The distance spectrum of the TCM codes so derived has been used in the evaluation of error performance using bounds. The simulation results of the error event probability of TCM schemes over AWGN channel are compared with those obtained through bounds.

#### **Chapter 3 : TCM on Time-dispersive ISI channels**

In this chapter, we first consider the equalization problem for the transmission of digital signals over bandlimited ISI channels and briefly review the equalizer structures normally employed in practice to mitigate the effects of ISI. We next consider an optimum combined MLSE receiver structure, realized by the Viterbi algorithm operating on a combined ISI-Code trellis, for the detection of TCM signals in the presence of ISI and AWGN. We have presented the design of several combined ISI-Code trellis structures for different TCM codes on ISI channels of limited memory. The state complexities of these combined ISI-Code trellis structures, which limits their practical applicability, have been discussed. We present a method, using the error structure of the TCM code, to evaluate the error performance of the combined ISI-Code receiver through bounds. We finally present the results of a study that has been performed to evaluate the performance using bounds and through simulation.



## **Chapter 4 : Reduced complexity KFE-MLSE Receiver Structure for TCM decoding on ISI channels**

We first review the prefiltering techniques employed in practice for both uncoded and coded transmission systems in an effort to reduce the state complexity of the optimum MLSE receiver structure. We then propose the reduced complexity KFE-MLSE structure for the detection of Trellis-coded QAM signals transmitted over a time-dispersive ISI channel. We next present a method to evaluate the error performance of the KFE-MLSE receiver using innovations representation and spectral factorization technique. We then present the results of the study performed for different TCM codes on several ISI channels, and the performance bounds so derived are compared with those of simulation results. We also compare the error performance of the sub-optimum KFE-MLSE receiver with that of the optimum combined ISI-Code receiver structure on different ISI channels.

## **Chapter 5 : Sub-optimum Reduced State Algorithms for TCM Decoding on ISI Channels**

As an alternative to the prefiltering techniques, we first consider the use of channel truncation to reduce the state complexity of the optimum combined ISI-Code trellis structure. Several design examples of the truncated combined ISI-Code trellis structures have been presented. We then consider the use of set-partitioning ideas, in conjunction with channel truncation, to construct several RSSE structures for the decoding of TCM signals in the presence of ISI and AWGN. The simplest form of RSSE namely the PDFD is also considered. The error performance of these reduced state receiver structures for various TCM schemes on different ISI channels have been studied through simulation and results are presented.

## **Chapter 6 : Adaptive Receiver Structure for TCM Transmission over Time-dispersive Fading Channels**

In this chapter, we consider a study on the adaptive receiver using various structures discussed earlier. We first consider the discrete-time model for the

time-variant (fading) channel. We next consider the channel estimators based on LMS/RLS criterion, for use with optimum MLSE structure or its sub-optimum variants on slowly time-varying channels. We then consider a relatively more complex channel estimation procedure called per-state processing (PSP) channel estimation using delay-free decisions for the updating of channel estimates on a rapidly time-varying channel. The error performance and tracking characteristics for these channel estimators have been studied through simulation. The error rate performance of the various adaptive receiver structures, for the decoding of TCM signals transmitted over fading channels, have been studied through simulation and the results are presented. Finally, we consider the use of D-diversity reception technique for the detection of TCM signals transmitted over multi-path fading channels with severe fade. The results of a study on the D-diversity receivers for different orders of D on various multipath fading channels have been presented.

## **Chapter 7 : Conclusions**

We conclude the thesis with a summary of important results and suggestions for further work.

Also included are three appendices. In Appendix-A we present the Cholesky spectral factorization technique which is used in the computation of steady-state Kalman gains and hence the evaluation of combined impulse response of the channel and the KFE. In Appendix-B we present the derivation of the variance of an autoregressive moving average ARMA process, which is used to find the overall noise variance at the output of the channel and the KFE. In Appendix-C the fading dispersive channel model, which is used in the study of adaptive receiver structures in this thesis, has been presented.

# TRELLIS-CODED MODULATION OVER AWGN CHANNEL

---

## 2.1 INTRODUCTION

In recent years the fact that there is a tremendous demand for power-efficient and bandwidth-efficient communication systems for transmission of high-speed digital data over bandlimited channels, has spurred an active interest in the coding arena. In the past, all traditional coded communication systems treated coding and modulation as two separate operations with regard to overall system design and the subsequent results were quite disappointing [127]. Ever-since Massey suggested, in a 1974 seminal paper [80], the notion of improving system performance by looking at modulation and coding as a combined entity, the researchers have been investigating ways of implementing this idea into a reality. The most significant contribution in this direction was the development of ‘Trellis-Coded Modulation’ (TCM) by Ungerboeck [14,126].

Ungerboeck proposed TCM as an integrated system design approach that regards coding and modulation as a single entity. The primary advantage of TCM, over modulation schemes employing error-correction coding, is the ability to achieve increased power efficiency without the need for customary bandwidth expansion introduced by the coding process. Over additive white Gaussian noise (AWGN) channels, for symbol error rates of  $10^{-6}$ , Ungerboeck codes could achieve gains of 3 to 6 dB; thus promising to fill most of the 9 dB gap between the rate achievable with coded-modulation and Shannon’s channel capacity limit [40]. The TCM not only

provides a significantly improved performance in the presence of AWGN, but also in the presence of other channel impairments [123]. Thus Ungerboeck's TCM, representing a significant advance in the state-of-the-art in the coding arena, captured much attention and inspired an intensified research, as well as widespread practical applications of bandwidth-efficient coded-modulation schemes.

The exact analysis of TCM code performance is difficult and in most cases the performance evaluation is carried out either through simulation or using bounds. Simulation is very time-consuming and is applicable for short constraint length codes and at lower SNR. Performance evaluation using union bound gives a better estimate and is applicable over a wide range of SNR of practical interest. In order to determine the upper bound on the error probability, one needs to compute the distance properties of the code. The computation of minimum free distance  $d_{\text{free}}$  and its multiplicity  $N_{d_{\text{free}}}$  enables one to find the optimum code performance at higher SNR. In order to evaluate a tight upper bound on the error performance, the distance spectrum of the code has to be evaluated. We have proposed an unidirectional trellis search algorithm, which can be used to compute the distance spectrum of all Ungerboeck codes, that is fast and efficient.

In this chapter, we begin with a brief discussion on the drawbacks of classical coding schemes, followed by Ungerboeck's TCM design concepts which aims at overcoming these drawbacks. We then present the design of TCM codes using QAM constellations. A number of examples for the above are given. The maximum-likelihood soft-decision Viterbi decoder, which enables one to achieve high coding gains for TCM scheme, and its performance measures are considered next. The use of bounds in the performance evaluation of TCM codes over AWGN channels is considered next. The new algorithm to find the distance spectrum of TCM codes is presented. The distance spectrum so computed has been used to evaluate the performance of TCM codes over AWGN channels. Comparison of simulation result with the bounds evaluated is also considered.

## 2.2 CLASSICAL CODING SCHEMES

In the classical coded communication system, the functions of encoding and modulation are treated as two independent operations at the transmitter, and so also the decoding and detection processes at the receiver [127]. The encoding process provides a forward-error correction capability by introducing additional redundant bits, if the channel permits bandwidth expansion. Thus, bandwidth efficiency is traded for increased power efficiency/coding gain. The additional bandwidth so demanded may not be available, as often is the case with bandlimited telephone and satellite channels.

On such bandlimited channels a certain performance gain with coding is still desired, without expanding the bandwidth. To realize this goal, the redundancy required for coding could be obtained by enlarging the signal-set of the modulation process. This calls for non-binary redundancy for which codes are hard to realize. An increase in signal alphabets by a factor of 2 requires an additional 3 dB signal power to maintain the same error rate relative to an uncoded system. Therefore, if modulation and coding are treated as two independent operations, then very powerful codes are required to offset this 3 dB penalty due to signal-set expansion and still provide a significant coding gain. Normally this is very difficult to realize and such an approach leads to very disappointing results as discussed in [127].

Ungerboeck [127] recognized two drawbacks of the classical approach. Firstly, the received signals are independently demodulated with hard-decisions prior to decoding and thereby incur an irreversible loss of information. A better approach would be the soft-decision decoding, where the decoder operates directly on unquantized 'soft' output samples of the channel. Secondly, the classical approach aims at maximizing the Hamming distance (HD) between the code words, which is not equivalent to maximizing the Euclidean distance (ED), when non-binary modulation (redundancy) is employed. The optimum performance on AWGN channel could only be

attained if the decoding schemes are based on minimum ED between the received waveform and the members of the signaling alphabet. Conversely, good signaling alphabets are those having maximum ED. Therefore, code design must aim at maximizing the minimum ED of the coded signal sequence. This motivated Ungerboeck to look for a new code-design strategy which culminated in the development of ‘Trellis-Coded Modulation’ schemes.

### 2.3 TRELLIS-CODED MODULATION

Ungerboeck proposed, in his 1982 paper [126], an elegant solution to the problems of classical channel coding. If modulation is treated as an integral part of the coding process and is designed in conjunction with the code, so as to increase the minimum ED between pairs of coded sequences, then the loss from signal-set expansion can be overcome and a significant coding gain can still be achieved with relatively simple codes. The key to this integrated design approach, is to devise an effective method of mapping coded bits into channel signals such that the minimum ED is maximized. Such a mapping rule, called mapping by set-partitioning, involves successive partitioning of channel signal-sets into subsets with increasing intra-subset distances. Most of the achievable coding gain can be obtained by doubling the signal alphabet and using an appropriate code.

Ungerboeck’s TCM schemes employ redundant non-binary modulation in combination with a finite-state encoder that governs the selection of modulation signals to generate coded signal sequences. The TCM code can be represented by either a finite-state machine description (state diagram) or by a trellis diagram (state-transition diagram), while the former is more compact, the latter has the advantage of depicting pictorially the time evolution of coded sequences. Often, the TCM codes are also referred to as ‘Trellis Codes’, because the TCM schemes are normally described by the trellis diagram of the encoder.

At the receiver, the noise corrupted TCM signals are decoded by a soft-decision maximum-likelihood (ML) Viterbi decoder. A simple 4-state TCM code

improves the robustness of digital transmission over AWGN channel by 3 dB relative to an uncoded modulation system. With more complex TCM schemes (256-, 512-state), it is possible to achieve coding gains of upto 6 dB relative to uncoded multilevel system [127], without compromising bandwidth efficiency or power efficiency.

In the subsequent sections, we consider the general structure of TCM scheme and the special mapping rule used in TCM code construction.

### 2.3.1 General Structure

Generally, a typical TCM scheme [127] consists of a binary convolutional encoder followed by a signal mapper as shown in Fig.2.1, although several alternative forms have been described in the literature [7, 19, 22, 51].

To transmit  $m$ -information bits per modulation interval,  $\tilde{m} \leq m$  bits are expanded by a rate  $\tilde{m}/(\tilde{m}+1)$  convolutional encoder into  $(\tilde{m}+1)$  coded bits. These  $(\tilde{m}+1)$  bits are used to select one of the possible  $2^{\tilde{m}+1}$  subsets of a redundant signal constellation with  $2^{m+1}$  channel symbols. The remaining  $(m-\tilde{m})$  uncoded bits are used to determine which of the  $2^{m-\tilde{m}}$  signals of the chosen subset is selected for transmission.

During each signaling interval, the subset selection and hence the channel symbol selection depends not only on the incoming information bits, but also on  $\gamma$  past information bits, where  $\gamma$  represents the constraint length of the encoder. These  $\gamma$  bits will define the state of the encoder, and the total number of encoder states is thus  $2^\gamma$ . Therefore a TCM encoder with memory  $\gamma$ , can be represented by a trellis diagram consisting of  $N_s = 2^\gamma$  states (nodes). From each state, there will be  $2^m$  emerging transitions that correspond to  $2^m$  possible values of the  $m$ -bit information input  $X_n$ . The number of states reachable from each state is  $2^{\tilde{m}}$  and corresponds to distinct transitions (branches) of the trellis diagram. The number of parallel transitions associated with each branch is  $2^{m-\tilde{m}}$  and is determined by  $(m-\tilde{m})$  uncoded bits.

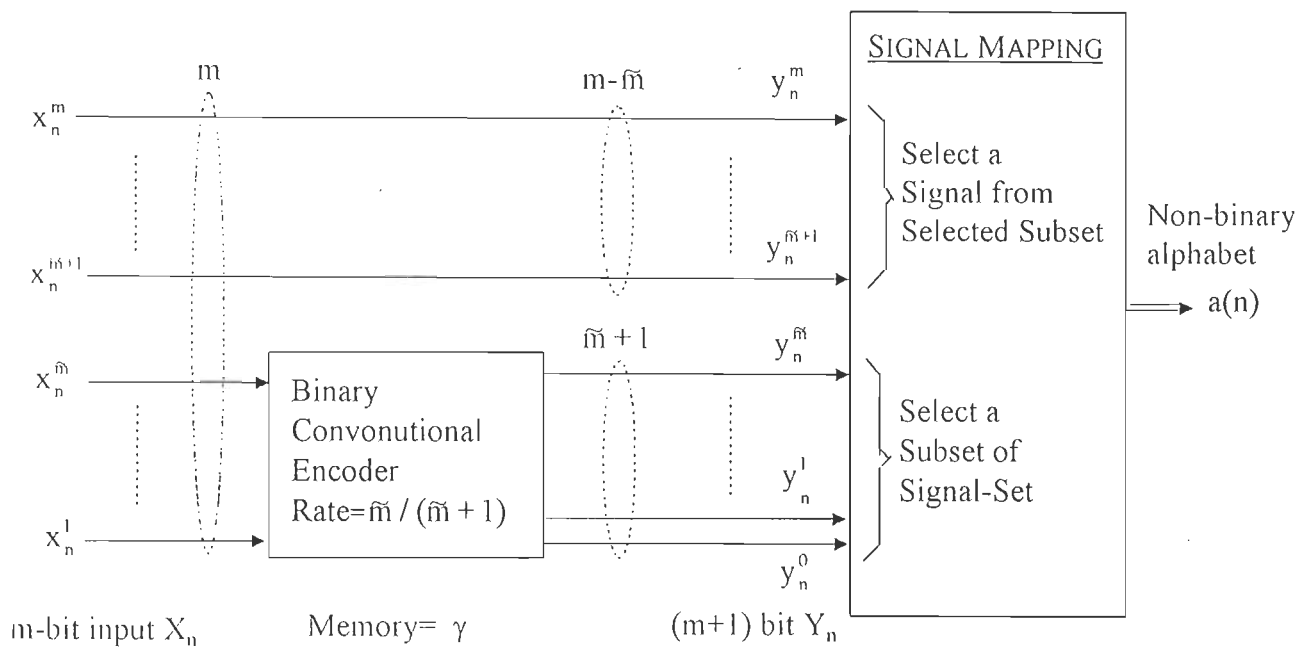


FIG.2.1 GENERAL STRUCTURE OF UNGERBOECK'S TCM SCHEME.



The process of mapping the coded bits into channel symbols involves the signal-set-partitioning concept and TCM mapping rules and is discussed in the following section.

### 2.3.2 Set-partitioning and the TCM Mapping Rules

The TCM uses a design approach, that aims at maximizing the minimum ED of the coded sequence, based on a mapping rule called ‘mapping by set-partitioning’. The concept of set-partitioning plays a pivotal role in the TCM code construction. Set-partitioning divides a signal constellation into smaller subsets with increasing intra-subset distances. Each partition is a binary partition. The subsets can themselves be partitioned further in the same manner. This is explained in detail with the TCM code design examples in the following section. A signal constellation of  $2^p$  points can be partitioned upto  $n$  levels where  $n \leq p$ . At each stage, the number of points is halved and the minimum distance of the subset increases (by a factor of  $\sqrt{2}$  for QAM signals). The degree to which a given signal-set is partitioned depends on the code. With a rate  $\tilde{m}/(\tilde{m}+1)$  convolutional encoder, the  $(\tilde{m}+1)$  coded bits will dictate the depth of partitioning. This method of set-partitioning, although not proved to be an optimal scheme [123], does provide an improved performance over uncoded system.

The TCM encoder being represented by a trellis diagram, the state transitions are assigned the channel signals from the partitioned signal-constellation in accordance with the following mapping rules [126] :

- (1) The  $2^m$  transitions diverging from (or merging into) a single state must be assigned signals from one of the two subsets at the partition level-1.
- (2) The parallel transitions, defined by  $(m-\tilde{m})$  uncoded bits, must be assigned signals from one of the subset belonging to the partition at  $(\tilde{m}+1)$ -level, that is from a subset having the largest intra-subset distance.
- (3) All signals must occur with equal frequency and with a fairly good symmetry.

Rules (1) and (2) guarantee that the ED associated with a single- or multiple-transition paths will exceed that of the uncoded system. Rule (3) ensures that the code trellis will have a regular structure.

The very rationale behind the set-partitioning concept and hence TCM design, is that the coded signal sequences are impervious to noise-induced detection errors if they are very different from each other [127]. This translates into the requirement that the signal sequences must have a large ‘free distance’ in the Euclidean signal space. The mapping by set-partitioning rule, in combination with a convolutional encoder, achieves this goal of maximizing the minimum squared ED between coded signal sequences. Thus, TCM design concept enables to realize codes whose free-distance significantly exceeds that of uncoded modulation system, for a given data rate, bandwidth, and signal power.

The squared free-distance of the code is the minimum squared ED between all possible code sequences, and is defined by [126],

$$d_{\text{free}}^2 = \min_{\{a(n)\} \neq \{a'(n)\}} \left[ \sum_n |a(n) - a'(n)|^2 \right] \quad \dots(2.1)$$

for all pairs of channel signal sequences  $\{a(n)\}$  and  $\{a'(n)\}$  which the encoder can produce.

The effectiveness of a coded system over an uncoded system can then be measured in terms of free-distances normalized with respect to signal energy. Thus, the achievable coding gain of a TCM scheme at high SNR, also called as asymptotic coding gain (ACG), relative to an uncoded modulation (reference) system at the same data rate and bandwidth, is given by the ratio of normalized squared free-distance of the code to that of the uncoded system. Expressed in decibels, the asymptotic coding gain is

$$\text{ACG} = 10 \log_{10} \left[ \left( \frac{d_{\text{free-c}}^2}{E_{s-c}} \right) / \left( \frac{d_{\text{free-u}}^2}{E_{s-u}} \right) \right] \text{ dB} \quad \dots(2.2)$$

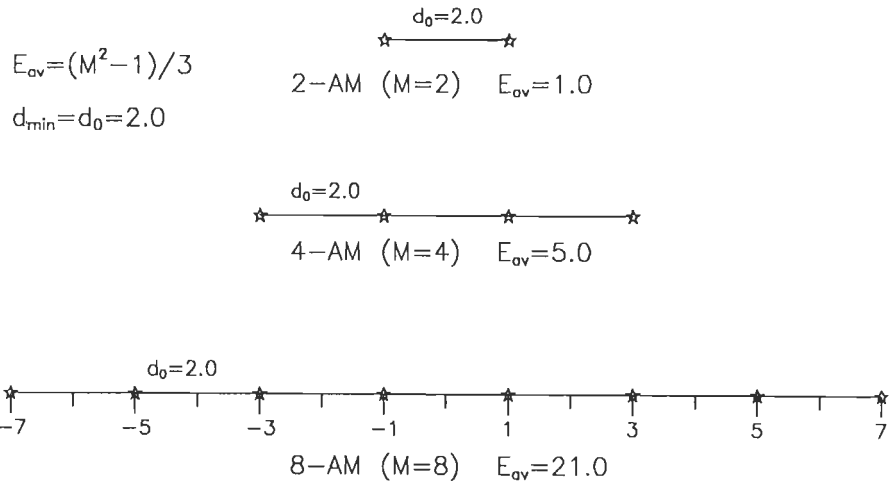
where  $d_{\text{free-c}}^2$  and  $d_{\text{free-u}}^2$  are the squared free Euclidean distances, and  $E_{\text{s-c}}$  and  $E_{\text{s-u}}$  denote the average signal energies of the coded and uncoded schemes respectively. The free distance  $d_{\text{free-u}}$  of the uncoded system represents the minimum ED between the adjacent signal points of the constellation.

Before presenting the design examples for TCM, we consider below the multi-level signal constellations.

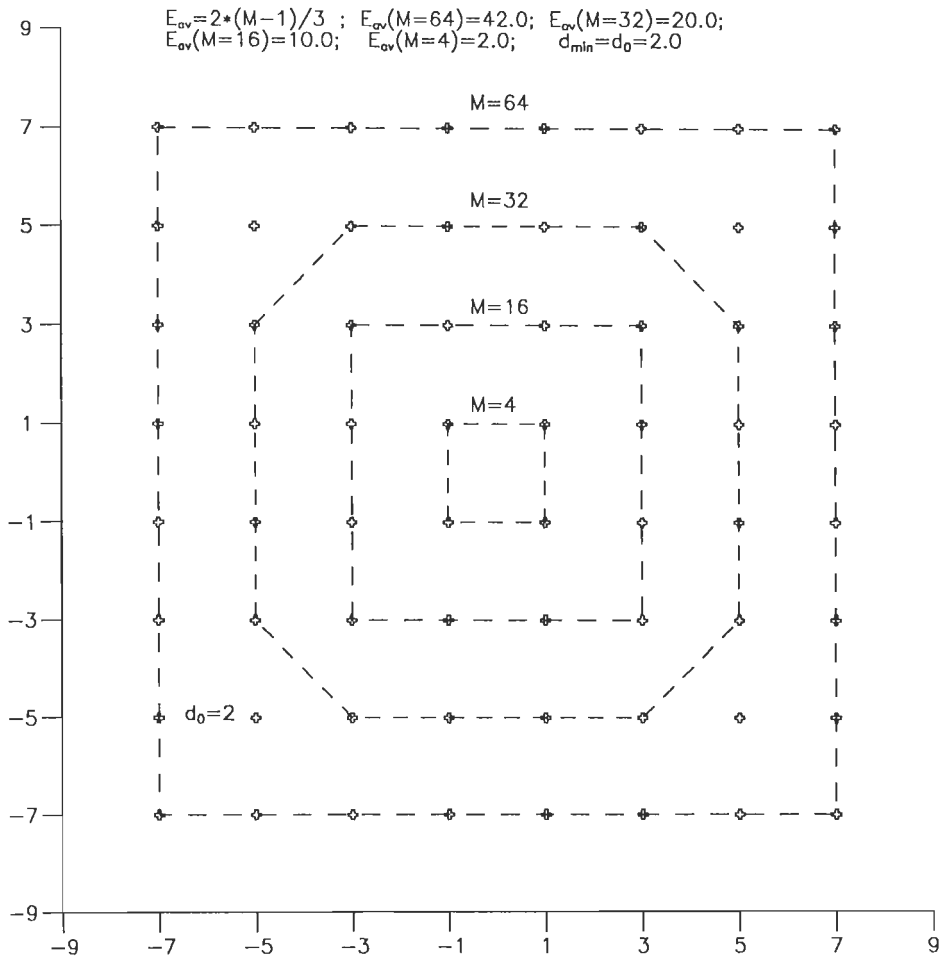
### 2.3.3 Multi-level Signal Constellations

The digital signaling schemes can be compared on the basis of SNR required to achieve a specific probability of error at a fixed data rate and/or bandwidth.

The two-dimensional M-ary modulation systems require a Nyquist bandwidth of  $1/T$  Hz around the carrier frequency to transmit signals at a baud rate of  $1/T$  symbols/sec. Therefore, the two-dimensional  $2^m$ -ary modulation schemes (such as M-QAM or M-PSK where  $M=2^m$ ), achieve a spectral efficiency of about  $m$  bits/sec/Hz. The M-ary PAM also exhibits the same spectral efficiency. Although the M-QAM and M-PSK exhibit the same spectral efficiency, on AWGN channels M-QAM outperforms M-PSK in error rate performance because of its efficient constellation shaping. To maintain the same error rate performance, the M-PSK requires an additional  $(3M^2/2(M-1)\pi)$  signal energy over that of M-QAM [100]. The M-QAM rectangular signal sets ( $M=2^m$  for  $m=2, 4, 6, \dots$ ) have the distinct advantage of being easily generated as two m-PAM signals superposed upon phase quadrature carriers forming a signal space of M-points arranged on a square grid (eg.  $\pm 1, \pm 3, \pm 5, \dots$ ). Also, they can easily be demodulated to yield two quadrature components. Moreover, the superposed view of modulation/demodulation process leads to a modular implementation. Although many other types of rectangular signal constellations have been investigated and reported in the literature [51, 53], very few outperform with a marginal gain in terms of energy efficiency, which is often offset by the complexity in implementation.



(a) ONE-DIMENSIONAL M-AM SIGNAL CONSTELLATIONS



(b) TWO-DIMENSIONAL M-QAM SIGNAL CONSTELLATIONS

FIG.2.2 SIGNAL SETS FOR ONE-DIMENSIONAL AMPLITUDE MODULATION AND TWO-DIMENSIONAL QUADRATURE AMPLITUDE MODULATION.

The signal sets for one-dimensional amplitude modulation and two-dimensional amplitude/phase modulation are shown in Fig.2.2. The average signal energy  $E_{av}$  is also indicated for each signal set.

For applications on time-variant channels, the constant-amplitude M-PSK signal sets are being used extensively, particularly 4-PSK in satellite communications. However, in recent years, M-QAM has received much attention for its application in high-speed data transmission over telephone network, digital satellite/radio communications, mobile and cellular communications [23, 35, 55, 93, 131, 132].

## 2.4 TCM CODE DESIGN

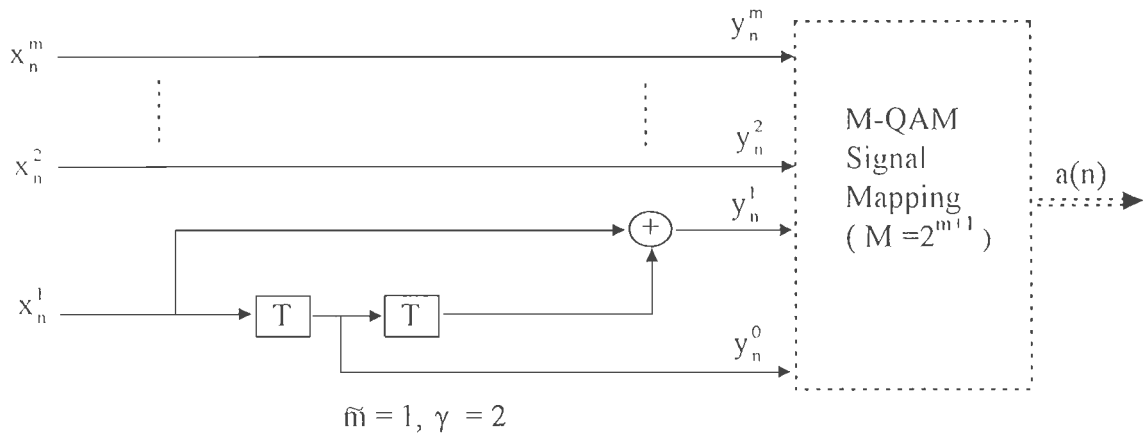
In the following, based upon Ungerboeck's design procedure [126, 127] several TCM schemes for M-QAM constellations have been considered. The convolutional encoders employed in the code design are minimal feedback-free convolutional encoders of [126] and are shown in Fig.2.3.

### 2.4.1 The 4-State 16-QAM TCM Scheme

The 16-QAM signal constellation as shown in Fig.2.4 is partitioned into two subsets B0 and B1. Further partitioning leads to a larger separation between signal points of the subset.

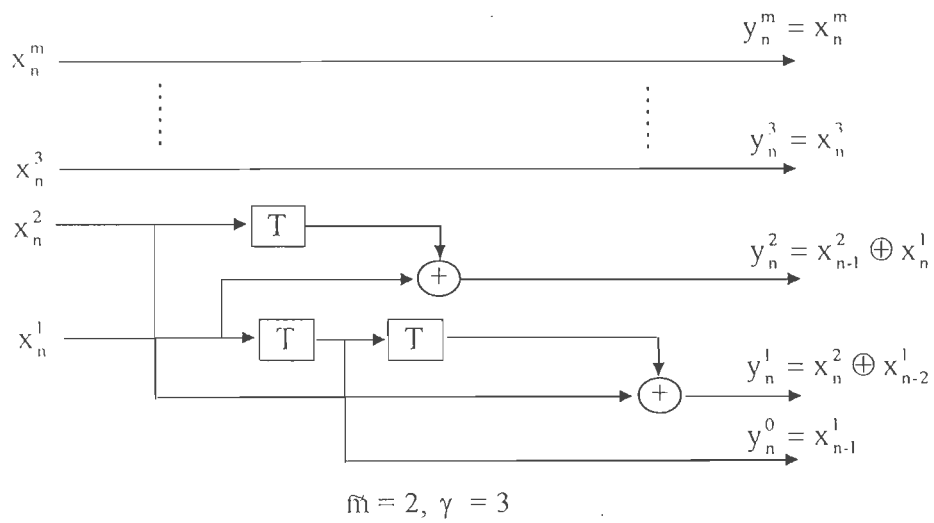
In the code design, a 4-state rate 1/2 convolutional encoder as shown in Fig.2.5(a) is employed. Following the usual notation,  $m=3$ ,  $\tilde{m}=1$  and  $\gamma=2$ . Since  $\tilde{m}=1$ , the 16-QAM signal constellation is required to be partitioned into  $\tilde{m}+1=2$  levels that results in four subsets C0, C1, C2 and C3, each consisting of four signal points as shown in Fig.2.4.

For performance comparison, an uncoded 8-QAM scheme is used as the reference system. This uncoded system employs signal points of either B0 or B1 for which the minimum ED is  $d_1=2\sqrt{2}$ , and corresponds to a 1-state trellis with 8-parallel transitions as depicted in Fig.2.5(b). The labels on the trellis transitions correspond to signal points of the subset B0.

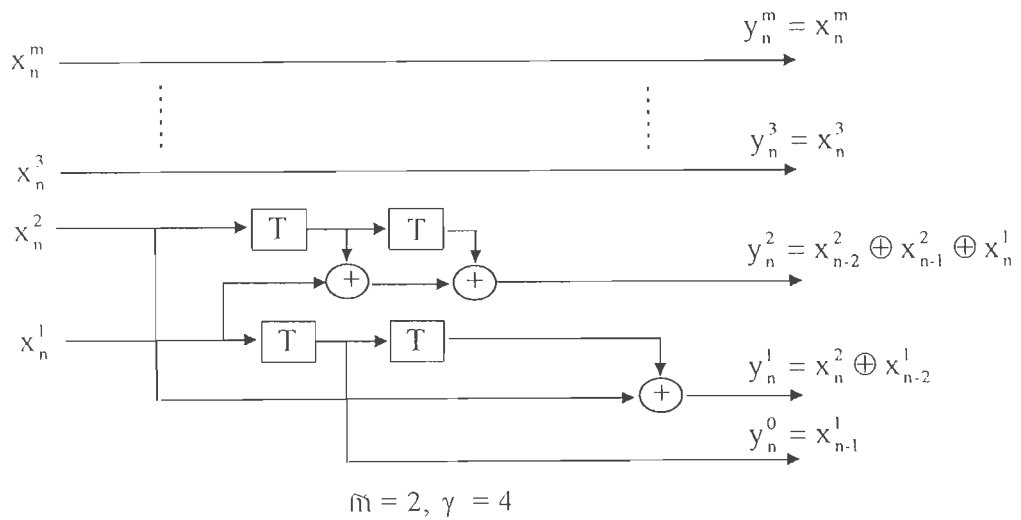


Note:  $y_n^0 = x_{n-1}^1$ ,  $y_n^1 = x_n^1 \oplus x_{n-2}^1$ , and  $y_n^j = x_n^j$  for  $2 \leq j \leq m$

(a) 4-State Encoder.



(b) 8-State Encoder.



(c) 16-State Encoder.

NOTE: NUMBER OF ENCODER STATES,  $N_s = 2^\gamma$

FIG.2.3 MINIMAL FEEDBACK-FREE CONVOLUTIONAL ENCODERS FOR M-QAM TCM SCHEMES.

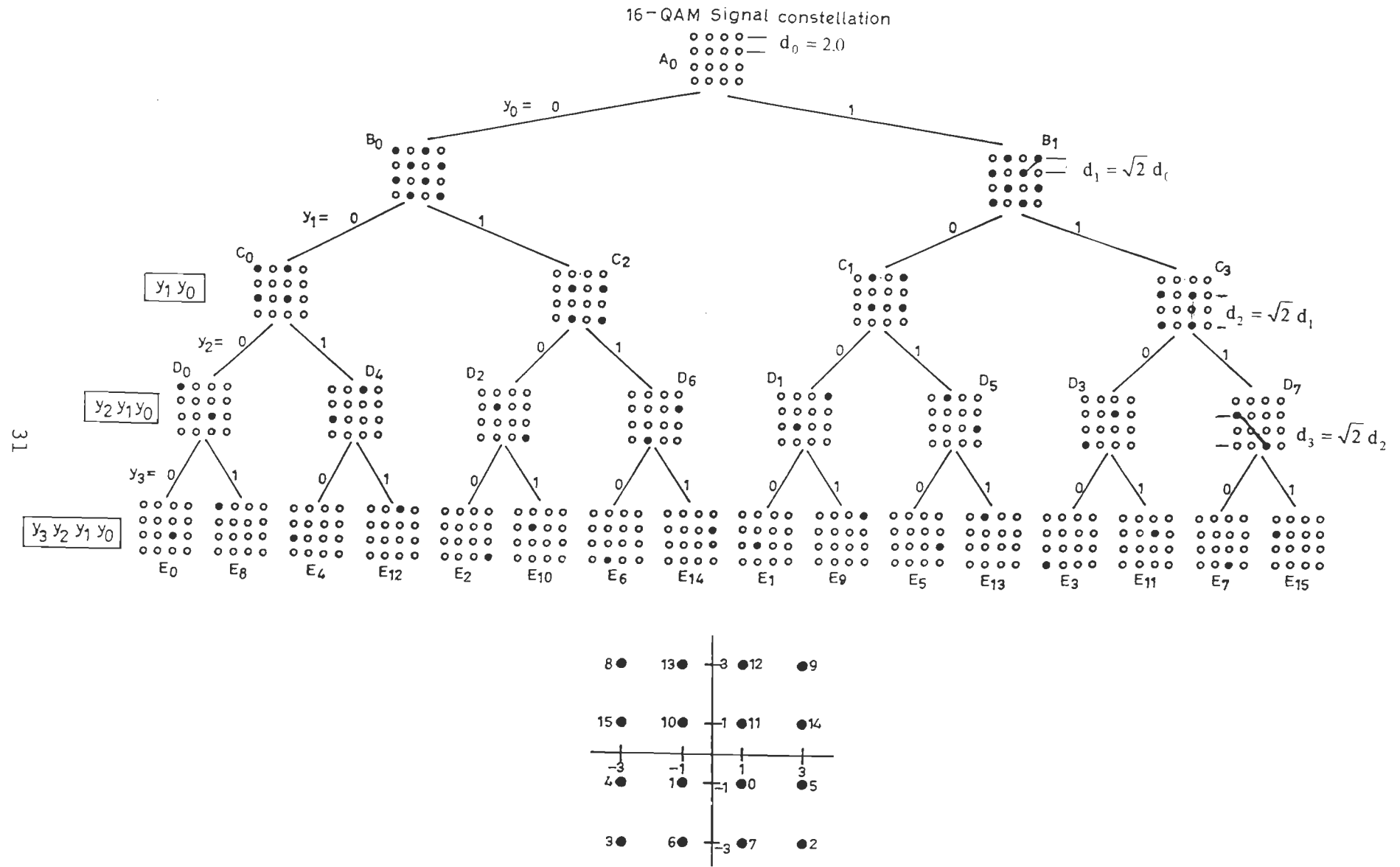
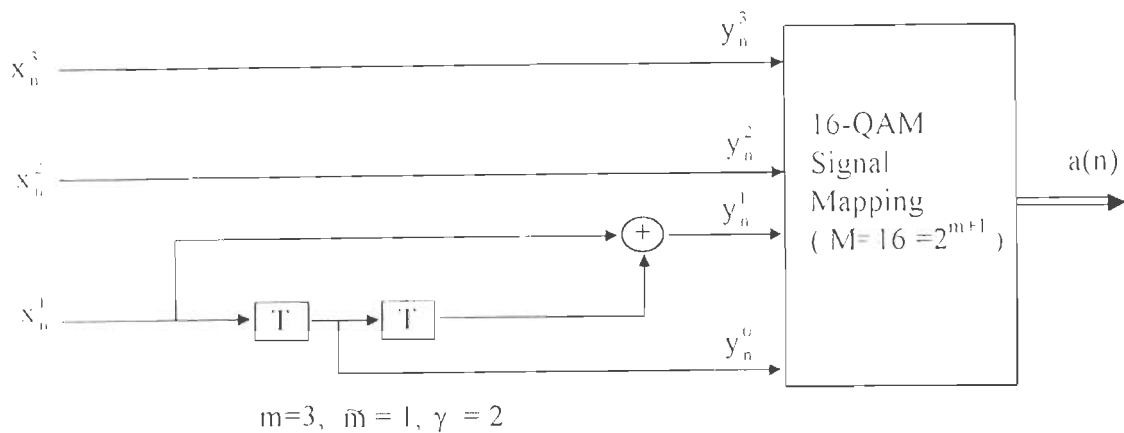
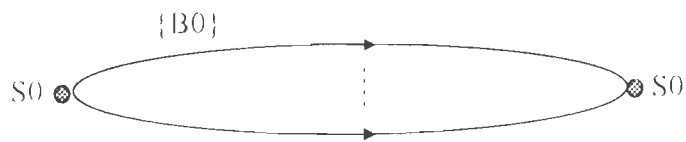


FIG.2.4 SET-PARTITIONING OF 16-QAM SIGNAL CONSTELLATION.

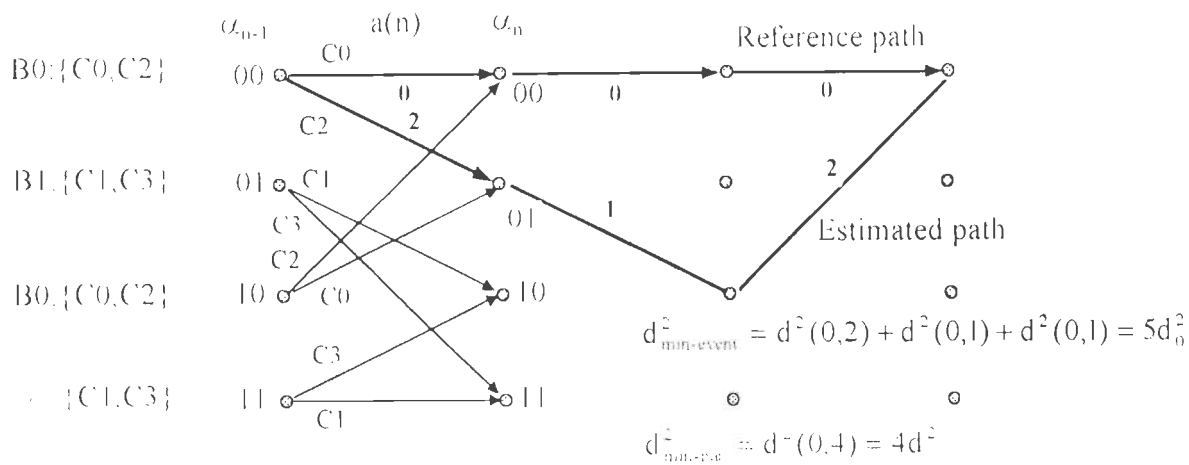


Note:  $y_n^0 = x_{n-1}^1$ ,  $y_n^1 = x_n^1 \oplus x_{n-2}^1$ , and  $y_n^j = x_n^j$  for  $2 \leq j \leq 3$

(a) 4-State 16-QAM TCM Encoder/Modulator.



(b) 1-State Trellis for Uncoded 8-QAM System.



(c) The 4-state Trellis for 16-QAM TCM

FIG.2.5 THE 4-STATE 16-QAM TCM SCHEME.

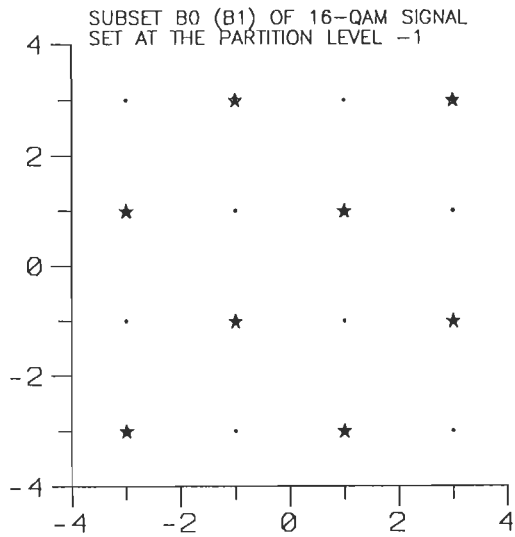


We next consider the use of partitioned 16-QAM signal constellation in conjunction with the 4-state convolutional encoder. The encoder is represented by a 4-state trellis diagram as shown in Fig.2.5(c). From each state there are  $2^m=8$  transitions corresponding to  $2^m=8$  possible input combinations. Since  $\tilde{m}=1$ , there are  $2^{\tilde{m}}=2$  distinct transitions (branches) from each state, each representing 4 parallel transitions corresponding to  $m-\tilde{m}=2$  uncoded bits of the encoder. The trellis branches are assigned channel signals from the partitioned constellation of Fig.2.4, in accordance with TCM mapping rules and the resulting branch labelling are indicated in the Fig.2.5(c). Each branch representing 4 parallel transitions is assigned signals from the subset C0, C1, C2 or C3, while each state is associated with signals of subset B0 or B1. As can be seen, all channel signals occur with equal frequency, and the trellis exhibits regularity and symmetry.

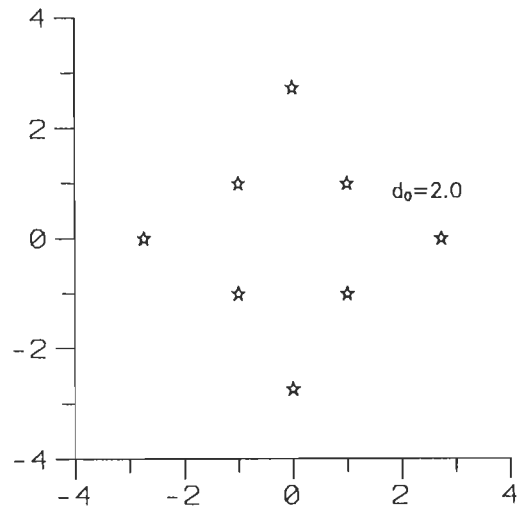
The minimum squared ED between parallel transitions, represents the minimum ED of the C-type subset and is given by  $d_{\text{min-par}}^2 = d_2^2 = 16.0$ . On the trellis diagram of Fig.2.5(c), we consider two distinct paths emerging from state 0 and merging into the same state after three transitions, forming an error event, as highlighted by the signal paths (0,0,0) and (2,1,2). This is a minimum length signal sequence and has a minimum squared ED of  $d_{\text{min-event}}^2 = (d_1^2 + d_0^2 + d_1^2) = 20.0$ . Hence the squared free distance of this code, by definition, is  $d_{\text{free-c}}^2 = \min(16, 20) = 16.0$ . The average signal energy for 16-QAM signal set is  $E_{s-c} = 10.0$ .

For the uncoded 8-QAM reference system, represented by the subset B0 of 16-16-QAM as shown in Fig.2.6(a), we have  $d_{\text{free-u}}^2 = 8.0$  and  $E_{s-u} = 10.0$ . Therefore, the asymptotic coding gain of this code is

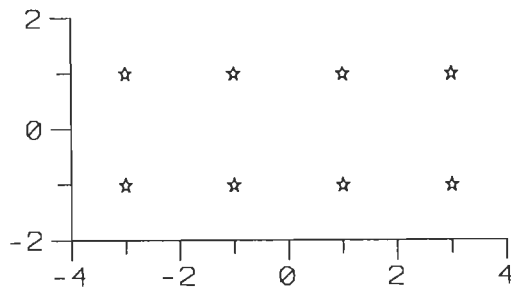
$$\begin{aligned} \text{ACG} &= 10 \log_{10} \left[ \left( d_{\text{free-c}}^2 / E_{s-c} \right) / \left( d_{\text{free-u}}^2 / E_{s-u} \right) \right] \\ &= 10 \log_{10} \left[ \left( 16/10 \right) / \left( 8/10 \right) \right] = 3.01 \text{ dB}. \end{aligned}$$



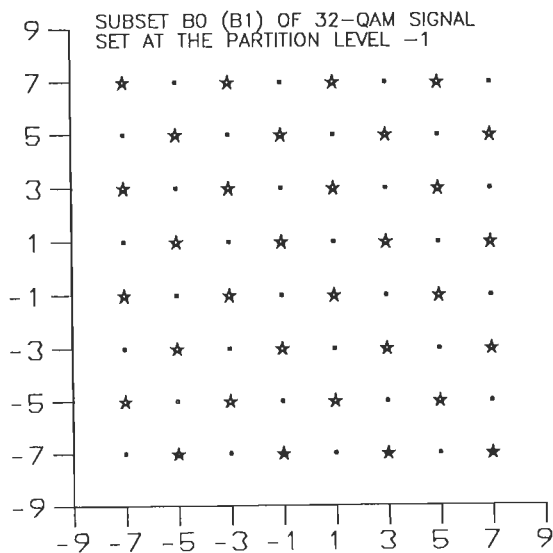
(a) UNCODED 8-QAM REFERENCE SYSTEM  
Ref-(i) WITH  $E_{av}=10.0$



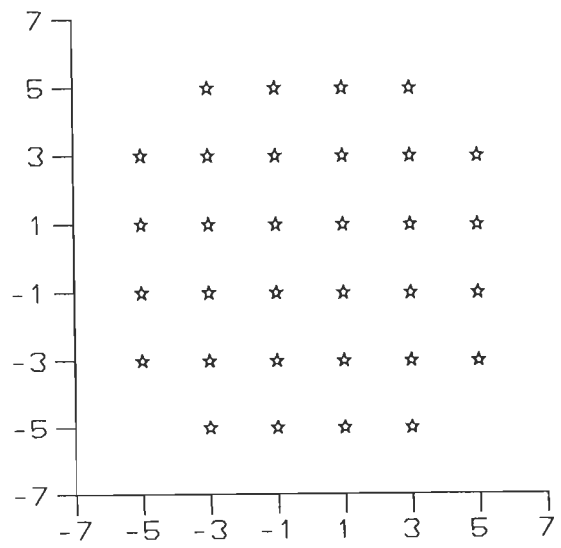
(b) UNCODED 8-QAM REFERENCE SYSTEM  
Ref-(ii) WITH  $E_{av}=4.732$



(c) UNCODED 8-QAM REFERENCE SYSTEM  
Ref-(iii) WITH  $E_{av}=10.0$



(d) UNCODED 32-QAM REFERENCE SYSTEM  
Ref-(i) WITH  $E_{av}=42.0$



(e) UNCODED 32-QAM REFERENCE SYSTEM  
Ref-(ii) WITH  $E_{av}=20.0$

FIG.2.6 UNCODED REFERENCE SYSTEMS FOR 16-QAM AND 64-QAM TCM SCHEMES

Thus, we find that the 4-state 16-QAM TCM code achieves a gain of 3 dB over uncoded 8-QAM reference system, for the same information rate, bandwidth, and signal energy.

For the 16-QAM TCM code, the coding gain depends on the uncoded modulation system being considered as the reference. To illustrate this, we consider two other 8-QAM signal constellations [100] as shown in Fig.2.6 as the reference systems for the 4-state 16-QAM TCM scheme. For the 8-QAM reference system of Fig.2.6(b), we find  $d_{\text{free-u}}^2 = 4.0$  and  $E_{\text{s-u}} = 4.73$ . With this 8-QAM system as the reference, the ACG of the TCM code is 2.77 dB. For the other 8-QAM reference system of Fig.2.6(c),  $d_{\text{free-u}}^2 = 4.0$ ,  $E_{\text{s-u}} = 6.0$  and  $\text{ACG} = 3.8$  dB. Thus, we find that ACG of this 4-state 16-QAM TCM varies between 2.77 dB and 3.8 dB depending upon the reference system being considered.

#### 2.4.2 The 8-State 64-QAM TCM Scheme

The set-partitioning of the 64-QAM signal set is shown in Fig.2.7. An 8-state rate 2/3 convolutional encoder employed in the code construction is as shown in Fig.2.8(a), with  $m=5$ ,  $\tilde{m}=2$  and  $\gamma=3$ . Since  $\tilde{m}+1=3$ , the signal set is required to be partitioned into three levels, which results in 8 subsets  $D_0, D_1, \dots, D_7$ , each consisting of 8 signal points. The encoder is represented by an 8-state trellis diagram as shown in Fig.2.8(b). From each state 4 distinct transitions (branches) emerge, each representing 8 parallel transitions. The channel mapping, assigning channel symbols to code trellis, is carried out in accordance with TCM mapping rules. That is, each branch is assigned signals from one of the D-type subset and each state is assigned signals belonging to either  $B_0$  or  $B_1$  in a symmetric manner, as depicted in Fig. 2.8(b).

The two non-parallel paths  $(0,0,0)$  and  $(6,5,2)$ , as shown in Fig.2.8(b) form an error event with minimum squared ED  $d_{\text{min-event}}^2 = 5d_0^2 = 20.0$ . The minimum squared ED among parallel transitions is  $d_{\text{min-par}}^2 = 8d_0^2 = 32.0$ . Therefore the squared free

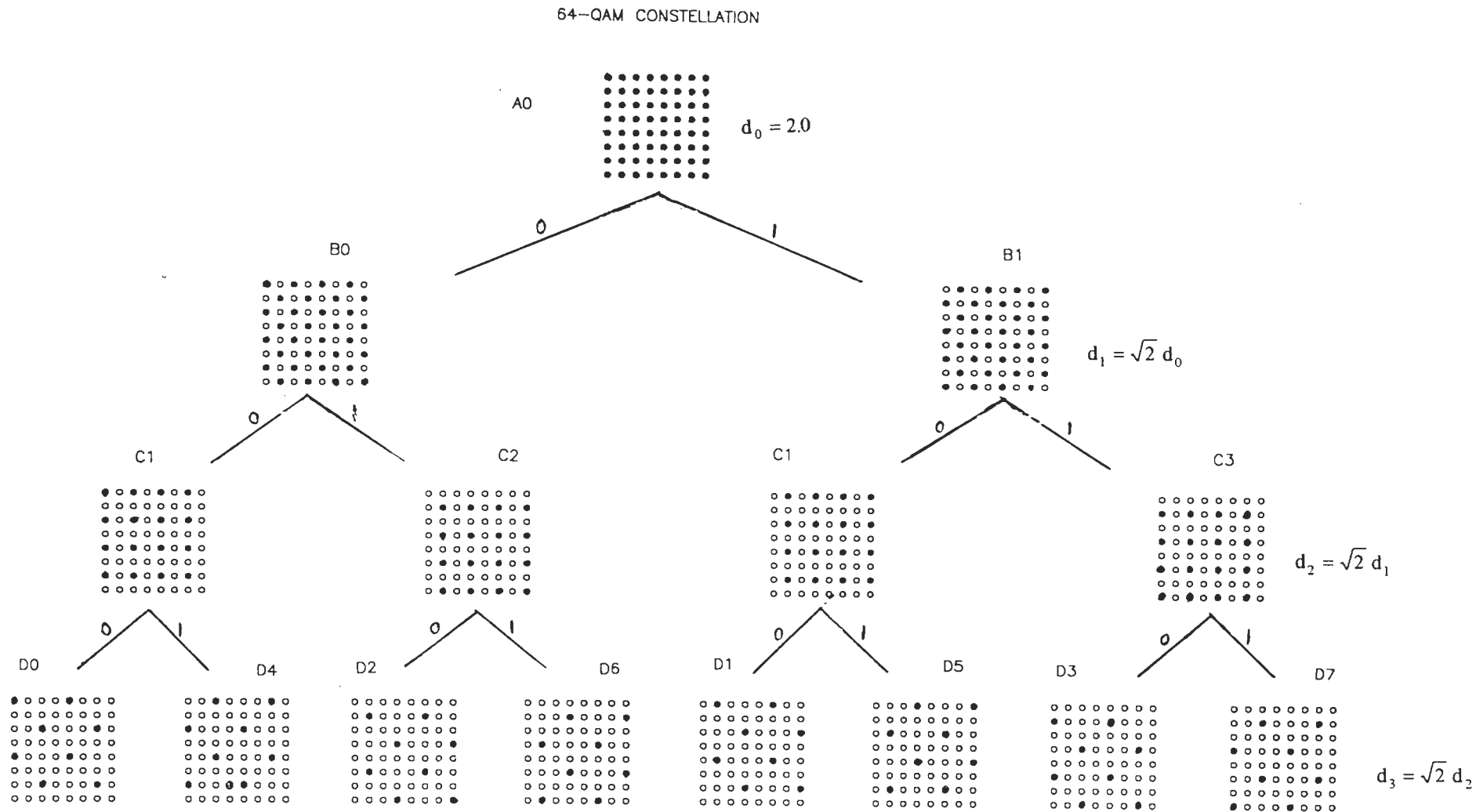
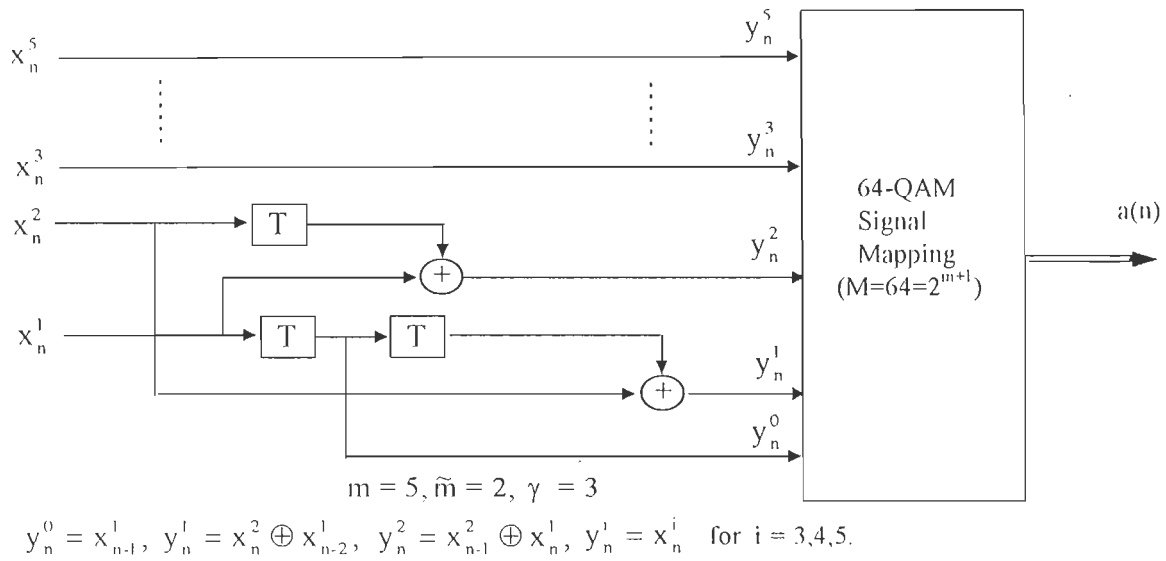
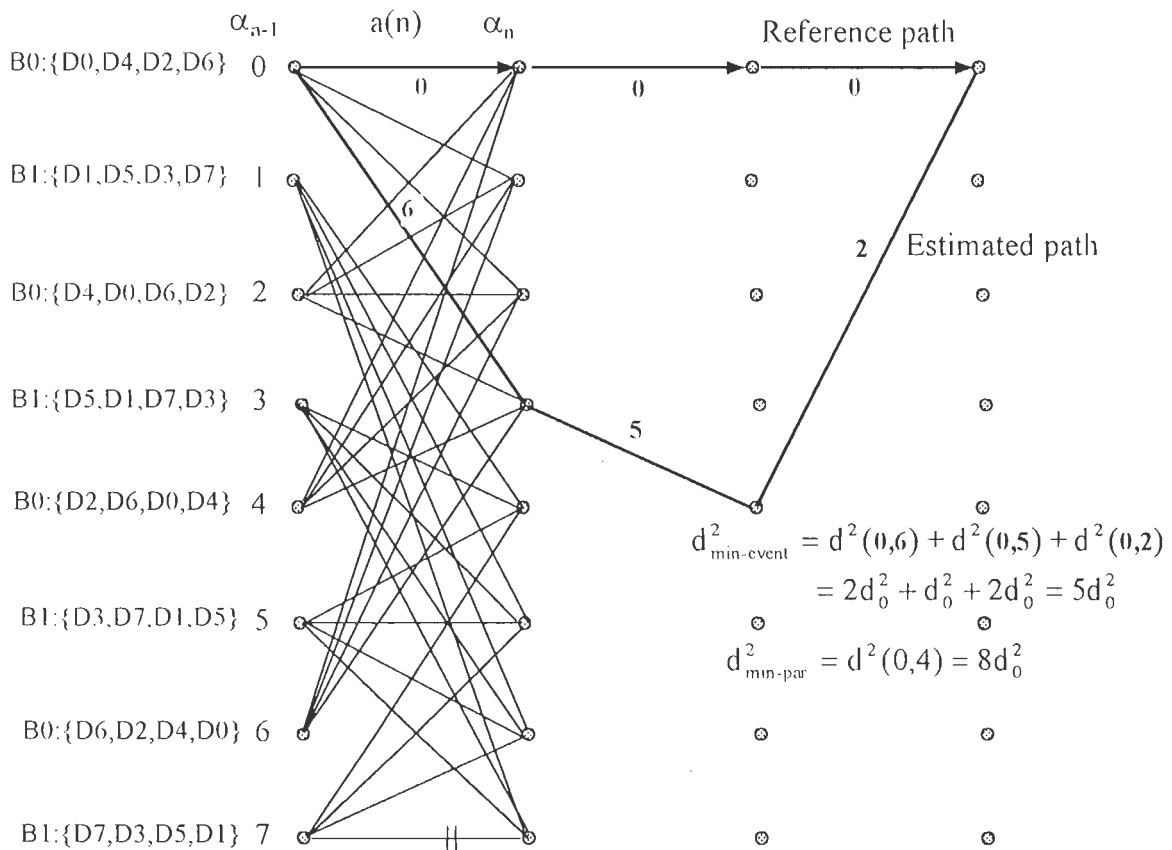


FIG.2.7 SET-PARTITIONING OF 64-QAM SIGNAL CONSTELLATION.



(a) 8-State 64-QAM TCM Encoder/Modulator.



Note: Each branch represents 8 parallel transitions.

(b) The 8-state Trellis for 64-QAM TCM.

FIG. 2.8 THE 8-STATE 64-QAM TCM SCHEME.

distance of the code is  $d_{\text{free-c}}^2 = \min(20,32)=20.0$ . For 64-QAM signal constellation the average signal energy is  $E_{\text{s-c}} = 42.0$ .

For the uncoded 32-QAM reference system, the signals of subset B0 (or B1) of 64-QAM constellation as shown in Fig.2.6(d) are being used. For this uncoded system, we find that minimum ED is  $d_1=2\sqrt{2}$ , and the average signal energy is 42.0. Thus  $d_{\text{free-u}}^2 = d_1^2=8.0$ , and  $E_{\text{s-u}}=42.0$ . Therefore, the ACG of 8-state 64-QAM TCM is 3.98 dB with reference to uncoded 32-QAM of subset B0 of Fig.2.7.

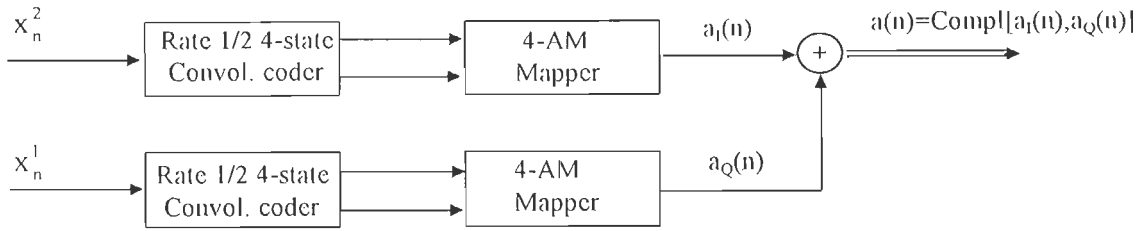
We next consider a 32-QAM cross signal constellation of Fig.2.6(e) as the reference system. This signal set has  $d_{\text{free-u}}^2=4.0$  and  $E_{\text{s-u}}=20.0$ . Hence ACG of 8-state 64-QAM TCM is 3.77 dB. Thus, we find that there is a degradation of 0.2 dB indicating that signal set of the latter reference system has a better constellation shaping compared to the first reference system.

### 2.4.3 The 16-QAM TCM Using Two Rate 1/2 4-State 4-AM TCM Schemes

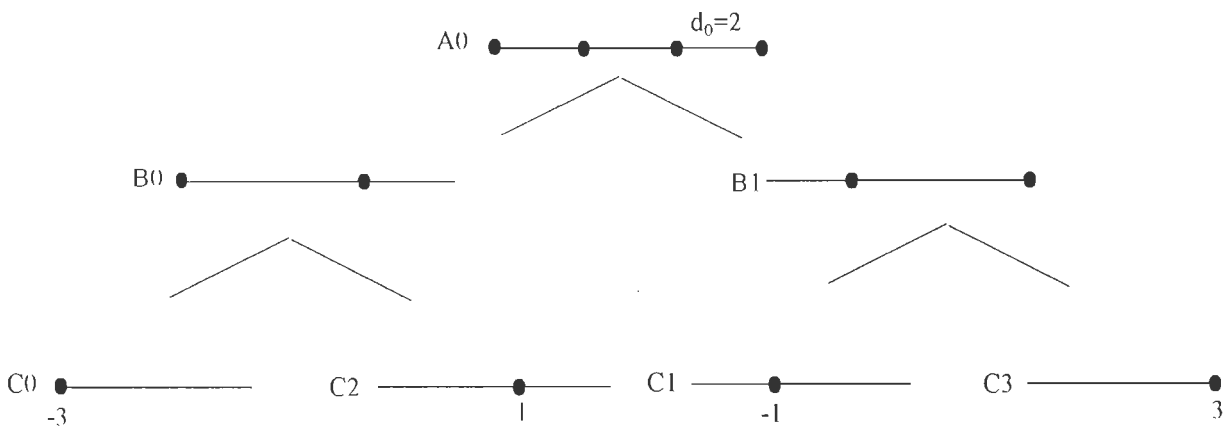
Since a rectangular M-QAM system can be viewed as two-AM systems superposed on quadrature carriers, we adopt two rate 1/2 4-state 4-AM TCM schemes to realize a 16-QAM TCM code. The structure is shown in Fig.2.9(a).

Now consider the design of rate 1/2 4-state 4-AM TCM scheme. Here  $m=\tilde{m}=1$ ,  $\gamma=2$ . The 4-AM signal constellation and its set partitioning are shown in Fig.2.9(b). The signal set is partitioned into  $(\tilde{m}+1)=2$  levels with the result that each subset of the last partition contains only one signal point, and hence no parallel transitions along trellis branch. The rate 1/2 4-state convolutional, encoder of Fig.2.3(a) is employed and the corresponding trellis diagram is shown in Fig.2.9(c).

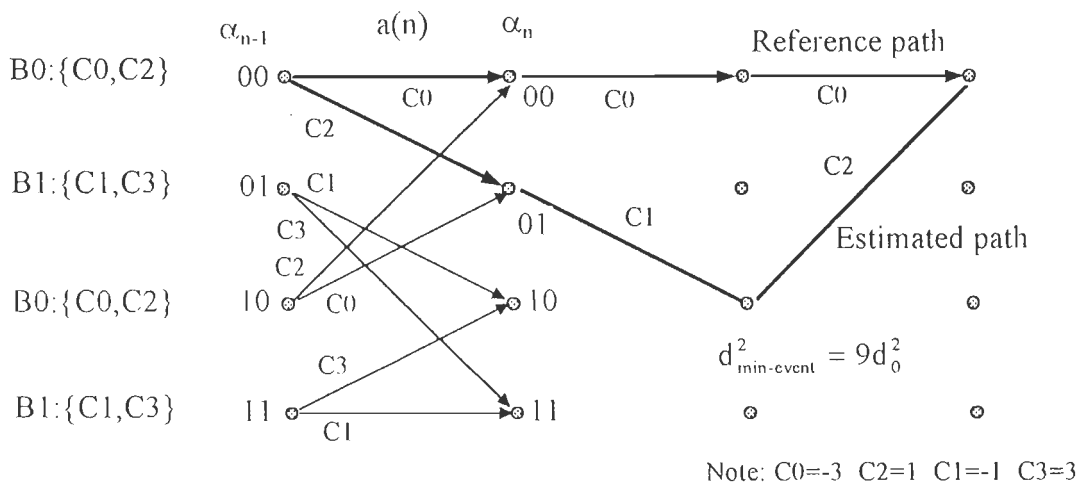
For the code under consideration, we find that  $d_{\text{free-c}}^2=9d_0^2=36.0$  by considering the error event as highlighted in the trellis diagram of Fig.2.9(c). Also, the average signal energy  $E_{\text{s-c}}=5.0$ . Considering a 2-AM uncoded system as the reference, we find  $d_{\text{free-u}}^2=4.0$  and  $E_{\text{s-u}}=1.0$ . With this as the reference system, the ACG of the 4-state 4-AM TCM scheme is 2.55 dB.



(a) STRUCTURE OF 16-QAM TCM USING TWO RATE OF 1/2 4-AM TCM SCHEMES.



(b) Set-partitioning of 4-AM Signal Constellation.



(c) The 4-state 4 AM Trellis with channel signals.

FIG.2.9 SUPERPOSED VIEW OF 16-QAM TCM USING TWO RATE 1/2 4-STATE 4-AM TCM SCHEMES.

## 2.5 MAXIMUM-LIKELIHOOD SOFT-DECISION DECODING OF TCM

Assume that the TCM signals are transmitted over an AWGN channel. Let the discrete channel output be  $r(n)=a(n)+v(n)$ , where  $a(n)$  is the discrete complex-valued signal sent by the TCM transmitter and  $v(n)$  represents the complex sampled value of the AWGN process. Because of the dependency introduced by the convolutional encoder between the successive transmitted symbols, the minimum distance between the two signal points is no longer a measure of the decoder performance. But it is the minimum distance between the allowed sequences of symbols that determines the system performance [123]. Therefore hard-decision decoding, if employed, causes an irreversible loss of information resulting in performance degradation. A better approach would be soft-decision decoding. The optimum decision rule for the sequence decoder is to determine among all possible signal sequences, a sequence with minimum squared ED from the received sequence.

The Viterbi algorithm (VA), originally proposed for the decoding of convolutional codes [128], has been shown to be an attractive solution to a variety of digital estimation problems. The VA tracks the state of a stochastic process with a recursive method that is optimum, and lends itself readily for implementation and analysis [47].

The VA is a maximum-likelihood sequence estimation (MLSE) technique that finds among the set of all coded signal sequences which the TCM encoder can produce, a sequence  $\{\hat{a}(n)\}$  which is closest to the received sequence  $\{r(n)\}$  in the sense of ED. This recursive decoding procedure involves a search for the most likely path in the code trellis based on the received sequence. The received signal sequence  $R \equiv \{r(n)\} = \{r(1), r(2), \dots, r(n)\}$  is decoded into one of the allowed signal sequences in the set  $\{A(i)\}$ , where  $A(i) = \{a_i(1), a_i(2), \dots, a_i(n)\}$ , based on the optimum decision rule that selects  $A(k)$  if  $\text{Prob}(R/A(k)) > \text{Prob}(R/A(j))$  for all  $j \neq k$  [123]. For an AWGN channel, this translates to computing the squared ED between  $A(i)$  and  $R$ , and selecting the signal sequence  $A(k)$  for which



$|R - A(k)|^2 < |R - A(j)|^2$  for all  $j \neq k$ , where  $|R - A(i)|^2 \equiv \sum_{p=1}^n |r(p) - a_i(p)|^2$  and  $|r(p) - a_i(p)|^2$  represents the branch metric.

The soft-decision Viterbi decoding for TCM is accomplished in two-steps [100, 127]. Note that each branch of TCM code trellis corresponds to a signal subset assigned to parallel transitions. The first step called subset decoding, determines the best signal point from among the subset points of the trellis branch, that is closest to the received signal. These branch signals are stored along with their branch metric. In the second step, the selected branch signal points and their corresponding branch metrics are used in the Viterbi algorithm to find a signal path through the code trellis that has the minimum cumulative squared distance from the sequence of noisy channel outputs being received.

The essential features of VA are summarized as follows [73, 123, 127]: Starting from infinite past upto the present time  $n$  the optimal signal path, called the survivor, entering into each state of the code trellis is assumed to be known. To proceed from  $n$  to  $n+1$ , all the survivor paths are extended and the total path metric is computed by adding extended branch metric to the already known best path metric of the state (node). The total path metric of all extended paths merging into each state are then compared, and the shortest among them is retained as the survivor and the rest are discarded. The total path metric of the survivor path is called the best path metric. Note that for each state of the code trellis, there will be one survivor path and correspondingly the best path metric. The procedure is repeated iteratively. It can be observed that the VA requires three basic operations namely add, compare and select.

Looking backwards in time, all the surviving paths tend to merge into the same history path at some time  $n-\tau$ . With a sufficient decoding delay  $\delta > \tau$ , the information associated with a state transition on the common history path at time  $n-\delta$  can be selected as the decoder output (estimate). In practice, a decoding delay of  $\delta \geq 5\tau$  will suffice most of the applications, where  $\tau$  is the constraint

length of the code.

### 2.5.1 Performance Analysis of the Viterbi Algorithm

An important feature of VA is the straight-forwardness with which its performance can be analysed [47, 73, 89]. In many cases tight upper and lower bounds to error probability can be derived.

The VA seeks the most likely path through the trellis based upon the received sequence. Due to the presence of noise and other (imperfections) disturbances on the channel, the estimated sequence (path) may not coincide with the actual transmitted sequence (path) at all times, but typically diverge and remerge a number of times. Each distinct separation is called an error event. Thus an error event is formed by a pair of distinct sequences that depart from a single state and then merge into a single state some steps later, but does not simultaneously occupy the same state in between. Mathematically, an error event of length  $k$  ( $k \geq 2$ ) can be defined by two sequences as

$$\begin{aligned} \{a\} &= (a(n), a(n+1), \dots, a(n+k-1)) \\ \{\hat{a}\} &= (\hat{a}(n), \hat{a}(n+1), \dots, \hat{a}(n+k-1)) \end{aligned} \quad \dots(2.3)$$

and

$$\begin{aligned} \alpha_n &= \hat{\alpha}_n ; & \alpha_{n+k} &= \hat{\alpha}_{n+k} \\ \alpha_i &\neq \hat{\alpha}_i & \text{for } i &= n+1, n+2, \dots, n+k-1 \end{aligned} \quad \dots(2.4)$$

where  $\{a\}$  corresponds to correct (transmitted) sequence

$\{\hat{a}\}$  corresponds to the estimated (received) sequence,

$\alpha_j$  denotes the transmitter (encoder) state at time  $j$

and  $\hat{\alpha}_j$  denotes the receiver (estimator) state time  $j$ .

An error event is shown in Fig.2.10 for illustration. The error event concept plays an important role in the performance analysis of VA. The basic property of error events is that they are probabilistically independent of each other. The

error events in general may be of unbounded length, but the probability of such occurrences is nearly zero [47].

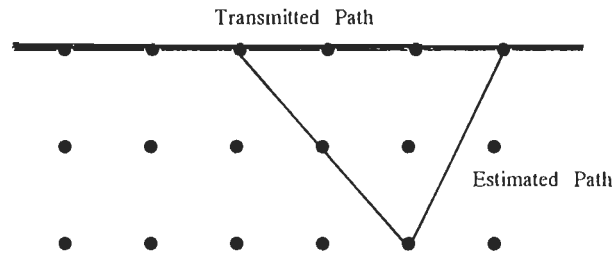


**Fig.2.10 Formation of error event**

Let  $\epsilon_k$  be the set of all possible error events starting at some time  $k$ . The probability  $P(\epsilon_k)$  of occurrence of any error event in  $\epsilon_k$  can be upper bounded by a union bound, that is by the sum of probabilities of all error events in  $\epsilon_k$ . This sum may be infinite, but is typically dominated by one or a few leading terms representing the most likely error events, which then forms a good approximation to  $P(\epsilon_k)$ . On the otherhand, a lower bound to the event error probability can be obtained by a particular error event that has the greater probability of occurrence among all the error events of the set  $\epsilon_k$ , and hence determines the asymptotic behaviour at high SNR.

The important parameters desired in the evaluation of code performance are discussed in the following section.

### 2.5.2 Performance Evaluation Parameters

When the VA is used for decoding of TCM, it is possible to compute the performance provided some important parameters for TCM can be specified. To define these parameters, we shall assume that the TCM encoded sequence  $\{a(n)\}$  is transmitted over AWGN channel with a double-sided spectral noise  $N_0/2$ , and the receiver performs a maximum-likelihood soft-decision decoding. For the two dimensional QAM signal constellations under consideration, the noise variance in each dimension is  $\sigma_v^2 = N_0/2$ .

The important parameters used for the performance evaluation of a TCM scheme operating over an AWGN channel are as follows:

(i) *Signal-to-noise ratio, SNR*

The signal-to-noise ratio is defined by

$$\text{SNR} \equiv \frac{E\{|a(n)|^2\}}{2\sigma_v^2} \quad \dots(2.5)$$

where  $E\{|a(n)|^2\}$  denotes the average signal energy.

(ii) *Minimum free Euclidean distance,  $d_{\text{free}}$*

The  $d_{\text{free}}$  is the smallest of the minimum ED due to either parallel transitions or non-parallel paths that lead to an error event.

(iii) *Number of nearest neighbours,  $N_d$*

The  $N_d$  is a multiplicity number corresponding to the average number of nearest neighbour signal sequences of minimum ED  $d$ , for  $d \geq d_{\text{free}}$

(iv) *Distance Spectrum, DS*

A spectral line defines the minimum ED  $d$  and the multiplicity  $N_d$  of an error event. The collection of all spectral lines of the code is called the distance spectrum.

(v) *Event-Error Probability,  $P_e$*

The probability that at any given time, the decoder makes a wrong decision among signals associated with parallel transitions or starts to make a sequence of wrong decisions along some path that diverges from the correct path for more than one transition, is called the error event probability  $P_e$ .

A union bound on the error event probability  $P_e$  may be obtained by summing the error event probability over all possible incorrect paths [130]. Thus, at any

time  $P_e$  is upper bounded by

$$P_e \leq \sum_{d=d_{\text{free}}} N_d \cdot Q(d/2\sigma_v) \quad \dots(2.6)$$

where  $d$  is the minimum ED of the error event,  $N_d$  is its multiplicity number,  $d_{\text{free}}$  is the minimum free ED of the code,  $\sigma_v^2$  is the noise variance in each dimension, and  $Q(\cdot)$  is the Gaussian error integral defined by

$$Q(x) = \frac{1}{\sqrt{2\pi}} \int_x^\infty \exp(-y^2/2) dy \leq \frac{1}{2} \exp(-x^2/2) \quad \dots(2.7)$$

Because of the exponential decrease of  $Q(x)$  with increasing  $x$ , the error event probability  $P_e$  is dominated, at high SNR, by the term involving the minimum value of  $d$ , that is  $d_{\text{free}}$ . Therefore, at high SNR, the  $P_e$  is approximated by the lower bound as [46, 127]

$$P_e \approx N_{d_{\text{free}}} \cdot Q(d_{\text{free}}/2\sigma_v) \quad \dots(2.8)$$

Thus, the performance of a code at high SNR can be roughly estimated only in terms of  $d_{\text{free}}$  and  $N_{d_{\text{free}}}$  of the code.

(vi) *Bit-Error Probability,  $P_b$*

The bit error probability  $P_b$  is the average number of bit errors per decoded information symbol. Similar to  $P_e$ , an upper bound on the bit error probability  $P_b$  can be obtained through union bound as [108]

$$P_b \leq \sum_{d=d_{\text{free}}} B_d \cdot Q(d/2\sigma_v) \quad \dots(2.9)$$

where  $B_d$  represents the average number of information bits on all paths at distance  $d$  from the correct path.

The lower bound on error probability gives the optimum code performance at high SNR, and is mainly dependent on  $d_{\text{free}}$  and  $N_{d_{\text{free}}}$ . On the otherhand, the upper

bound on the error probability gives a better estimate of the code performance applicable at lower and moderate SNR, but requires a knowledge of the distance spectrum of the code.

### 2.5.3 Performance Bounds of TCM on AWGN Channels

Since the publication of spectrally efficient TCM schemes by Ungerboeck [126], there has been considerable interest in the computational techniques for the evaluation of their performance. The exact analysis of TCM performance is difficult and usually one resorts to either simulation or the evaluation of performance bounds [111]. While simulation is useful only for short constraint length codes and at lower SNR, the bounds are most effective for the estimation of system performance at moderate to large SNR.

The two important parameters normally employed in the performance evaluation of TCM are free ED and error event probability. The algorithms used for the computation of these parameters assume significant importance, because of the fact that the design of an optimum TCM scheme is based on a search among a class of possible candidates, for all of which the performance must be evaluated. Therefore, it is essential that these algorithms be fast and efficient.

Most of the algorithms for computation of the above are based on the generating (transfer) function approach [91, 128, 130], that has been extensively applied in the performance evaluation of linear convolutional codes, which when combined with a union bound gives the upper bound on the error event probability. The generating function enumerates the distance, length and number of errors on any incorrect path with reference to a correct path. When the code is linear/regular, the distance between the correct path and incorrect path does not depend on the transmitted sequence. Therefore, normally all-zero information path is assumed to be the reference in the derivation of the transfer function [146]. The complication arises in TCM due to the fact that, in general, the distance between any incorrect path and correct path is dependent upon data sequence being

transmitted, and hence averaging over all correct and incorrect paths is necessary. This requires the derivation of the transfer function by a pair-state approach that uses a 'pairwise-state diagram' with  $N_s^2$  states, where  $N_s$  is the number of encoder states. The method is quite involved with a large computational complexity that limits its applicability to TCM codes with large  $N_s$ . However in certain cases, by taking advantage of the linearity property of the convolutional code on which TCM design is based, as well as 'symmetries' and 'regularity' of signal constellations used and the way it is partitioned, it is possible to derive the transfer function from a modified-state diagram having only  $N_s$  states.

Thus, the algorithms presently available can be broadly classified into two categories. The first approach is based on the pair-state diagram and is most general in applications but has a complexity proportional to  $N_s^2$ . Biglieri [13] has applied this pair-state approach to evaluate the performance of TCM schemes over linear and non-linear channels. The second approach uses a modified-state diagram with only  $N_s$  states and has a complexity proportional to  $N_s$ . But this approach is applicable only to a certain class of trellis codes namely symmetric trellis codes [146], regular trellis codes [22], superlinear trellis codes [7], quasi-regular trellis codes [108], and uniform trellis codes [16]. Biglieri and McLane [16] have shown that all Ungerboeck codes are uniform codes. For a uniform code, the free distance does not depend upon the transmitted sequence [49]. A tutorial material on the performance evaluation of TCM schemes is available in [9].

However, as pointed out by Ungerboeck [127], it is not necessary to compute distance between every pair of TCM signal sequences, and the free ED can be determined by treating the all-zero information sequence as the reference path, even though linearity does not hold for TCM signal sequences. Henceforth in our analysis, we use this argument to compute the distance properties of the code. We have proposed an algorithm to compute the distance spectrum of TCM code, using an  $N_s$ -state trellis where the all-zero information path is regarded as the reference in the computation of the minimum ED  $d$  and the nearest neighbours  $N_d$  of all the

error-events of the code. Once we compute  $d$  and  $N_d$  for all possible error-events of the code, the error event probability can be computed.

## 2.6 COMPUTATION OF THE DISTANCE SPECTRUM

The computation of minimum free distance is equivalent to finding the lowest-weight non-trivial closed path in the state diagram. A large number of unidirectional and bidirectional algorithms have been employed in various network problems to find the lowest-weight paths. A collection of such algorithms can be found in a comprehensive tutorial paper by Drefus [34]. According to Drefus, bidirectional search algorithms are much inferior over unidirectional search algorithms. However, by making use of the symmetries inherent in the code trellis structure, the bidirectional search algorithms tend to become more efficient [3].

Bahl et al. [3] proposed an efficient bidirectional search algorithm to compute  $d_{\text{free}}$  of convolutional codes. Larsen [67] observed certain flaws in that algorithm and introduced the corrected version, which is still regarded as the most efficient bidirectional search algorithm that computes  $d_{\text{free}}$  of binary convolutional codes using Hamming weights. Ungerboeck [126] used the Larsen algorithm to compute the minimum free ED  $d_{\text{free}}$  of TCM code by replacing Hamming weights with Euclidean weights and treating the all-zero information path as the reference.

The distance spectrum computing algorithms require more storage and computation than the conventional  $d_{\text{free}}$  computing algorithms, because here no paths are discarded. Rouanne and Costello [108] used a bidirectional stack algorithm to compute the distance spectrum of TCM codes by assuming that all-zero information sequence is sent. The complexity of the stack algorithm depends on the number of paths to be extended, but not on the constraint length of the code, thereby making it attractive for codes having large constraint length. The stack algorithm requires dynamic storage allocation which is computationally intensive but saves on total memory required for computation. On the other hand,



unidirectional Viterbi-like trellis search algorithms are well suited for distance spectrum calculation, although they require large memory, they are computationally efficient.

In the following, we propose a unidirectional trellis-search distance spectrum computing algorithm based on the shortest-route principle used in graph theory [72]. Following the above approach, the algorithm computes the minimum ED of all error events of the TCM code, in the order of increasing distance together with their multiplicities, by treating the all-zero information path as the reference. This algorithm is simple to implement as it requires only an  $N_s$ -state distance trellis for a  $N_s$ -state code and is applicable to all Ungerboeck codes.

### 2.6.1 Unidirectional Trellis Search Algorithm to Compute the Distance

#### Spectrum of TCM Code

Assume that the states of the code trellis are numbered as 1, 2, ..., N. An error event starts with a diverging transition from state 1 and ends with a transition merging into the same state 1 after two or more transitions, while making transitions in between through states other than state 1. Therefore, to find error events of length  $k \geq 2$ , transition from state 1 to state 1 in a single-step is disallowed by treating it as non-connected. All minimum distance paths starting from node 1 at trellis depth  $n=0$  and ending at some node  $j$  for all  $j \neq 1$ , after a certain depth  $n=k$ , will represent unmerged paths and must be retained, as they are still contenders for the formation of higher order error-events.

Given the  $N_s$ -state code trellis with channel symbols as branch labels and the connectivity between the states, derive an  $N_s$ -state distance trellis that defines the minimum squared ED associated with a branch transition with respect to the all-zero information path represented by the channel symbol labelled as 0. If parallel transitions exist, then retain the least distance path and also record the number of such paths along that branch. From the  $N_s$ -state distance trellis, derive a distance matrix  $D(N_s \times N_s)$ , whose element  $D_{ij}$  represents the minimum

squared ED of the branch connecting states  $i$  and  $j$ , with respect to the reference branch (transition from state 1 to state 1). The states which are non-connected are represented by a large distance, say  $D_{ij}=1000.0$  if states  $i$  and  $j$  are non connected in the code trellis. Since transition from state 1 to state 1 is disallowed in a single-hop, set  $D_{11}=1000.0$ . Also, let  $\xi^k$  be  $N \times N$  matrix whose element  $\xi_{ij}^k$  gives the cumulative (total) ED along a path that starts from state  $i$  at  $n=0$  and ends in a state  $j$  at  $n=k$ . Initially set  $\xi_{11}^0=0.0$  and  $\xi_{ij}^0=1000.0$  for all the other values of  $i$  and  $j$ . Then the total accumulated distance along a path of the trellis is computed by [72].

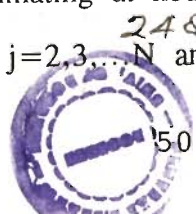
$$\xi^k = \xi^{k-1} * D \quad \dots(2.10)$$

where the matrix operation  $*$  is in fact a minimum distance search operation, defined as  $\sum_{\min}$ , that corresponds to adding all branch (squared) distances with the cumulative distance and choosing the minimum among them as the new cumulative distance. Thus an entry  $\xi_{ij}^k$  of  $\xi^k$  can be defined as

$$\xi_{ij}^k = \min\{(\xi_{ip}^{k-1} + D_{pj})\} \quad \text{for } p=2,3,\dots,N \quad \dots(2.11)$$

Each matrix operation  $*$  extends the trellis search by one depth. After each extension, check for the occurrence of an error event. An error event occurs if  $\xi_{11}^k < 1000.0$ . Then set  $d_{\min\text{-event}}^2 = \xi_{11}^k$ . After the occurrence of an error event, for the next extension reset  $\xi_{11}^k = 1000.0$

To compute the multiplicity number, define an  $N \times N$  matrix  $M$  such that each element  $M_{ij}$  represents the number of minimum distance parallel transitions along the branch  $ij$  with reference to the all-zero information path. For all non-connected transitions  $ij$  (including the transition 1-1) set  $M_{ij}=0$ . Define also  $N \times N$  matrix  $Q^k$  whose element  $Q_{ij}^k$  denotes total multiplicity of that path starting from node  $i$  at depth  $n=0$  and terminating at node  $j$  at depth  $n=k$ . Initially set  $Q_{ij}^0=1$  if  $ij$  is an allowed transition for  $j=2,3,\dots,N$  and  $Q_{ij}^0=0$  for  $i$  and  $j$  except  $i=1$ .  $Q^k$  is



updated after trellis extension using the relation,

$$Q^k = Q^{k-1} \otimes M \quad \dots(2.12)$$

where  $\otimes$  is a multiplicity search operation and is defined as

$$Q_{ij}^k = \sum (Q_{ip}^{k-1} * M_{pj}) \quad \dots(2.13)$$

if  $(\xi_{ip}^{k-1} + D_{pj})$  results in a minimum during the operation  $\xi^k = \xi^{k-1} * D$ . Upon the occurrence an error event at depth  $n=k$  set  $N_d = Q_{11}^k$  and then reset  $Q_{11}^k = 0$ .

To start with, specify the maximum length of the error event upto which the distance parameters  $(d, N_d)$  are desired to be computed. Also compute, from the code trellis, the minimum squared ED among the parallel transitions of the branch  $d_{\min\text{-par}}^2$ . If  $d_{\min\text{-event}}^2$  represents the minimum squared ED of all the error events under consideration, then

$$d_{\text{free}}^2 = \min (d_{\min\text{-par}}^2, d_{\min\text{-event}}^2) \quad \dots(2.14)$$

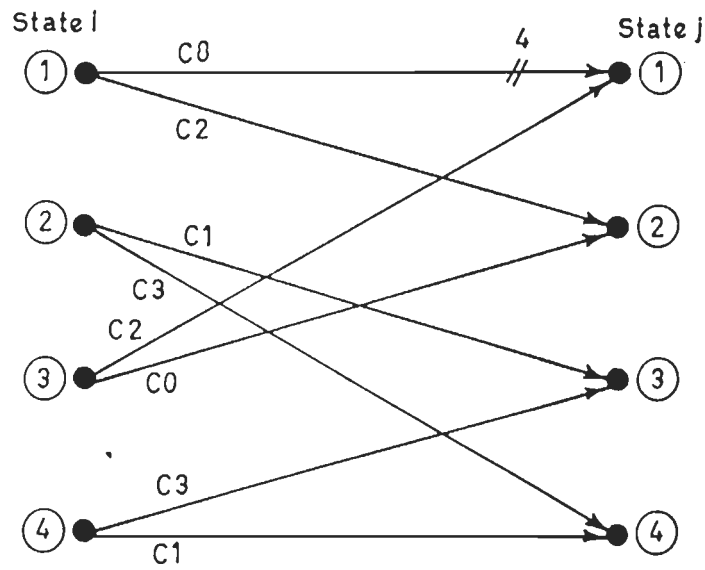
and the corresponding multiplicity number (averaged) will be  $N_{d_{\text{free}}}$ . For each  $d_{\min\text{-event}}^2$ , there will be a corresponding multiplicity number  $N_d$ .

The distance spectrum trellis reach algorithm is illustrated with an example as given below.

### 2.6.2 Example : Distance Spectrum of 4-State 16-QAM TCM Code

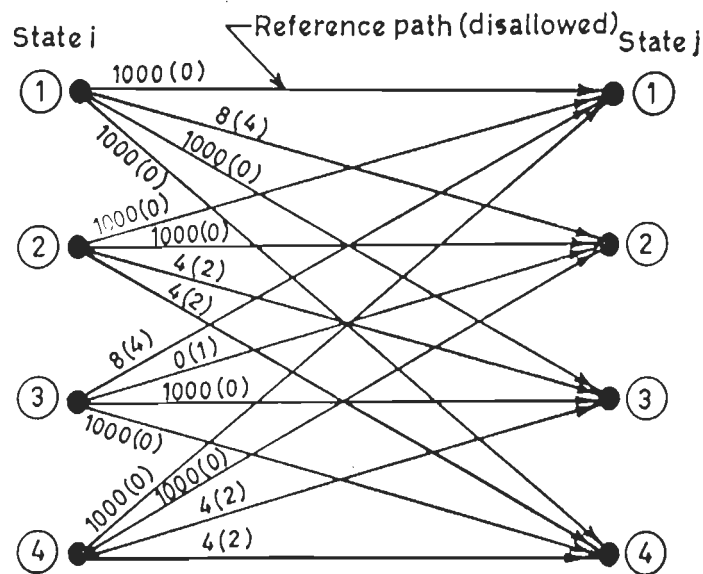
The encoder trellis with channel symbol assignment is shown in Fig.2.11(a) and its corresponding distance trellis is shown in Fig.2.11(b). The minimum squared ED and its multiplicity with reference to the all-zero information path are labelled along each transition. The distance matrix  $D$  and the branch multiplicity matrix  $M$  are also indicated in Fig.11(b).

The minimum squared Euclidean distance among the parallel transitions of the code trellis is  $d_{\min\text{-par}}^2 = 16.0$ . By recursive application of (2.10) and (2.12), we



$C_0 = \{0, 4, 8, 12\}$ ;  $C_2 = \{2, 10, 6, 14\}$ ;  $C_1 = \{1, 9, 5, 13\}$ ;  
 $C_3 = \{3, 11, 7, 15\}$

(a) 4-State 16 QAM Code trellis.



$$D = \begin{bmatrix} 1000 & 8 & 1000 & 1000 \\ 1000 & 1000 & 4 & 4 \\ 8 & 0 & 1000 & 1000 \\ 1000 & 1000 & 4 & 4 \end{bmatrix} ; M = \begin{bmatrix} 0 & 4 & 0 & 0 \\ 0 & 0 & 2 & 2 \\ 4 & 1 & 0 & 0 \\ 0 & 0 & 2 & 2 \end{bmatrix}$$

(b) Distance trellis defining D & M matrices.

FIG.2.11 THE 4-STATE 16-QAM TCM CODE TRELLIS AND ITS DISTANCE TRELLIS.

can find the error events of length  $k$ , their minimum squared ED and the multiplicity number. The results of this computation for the above are given in the Table 2.1

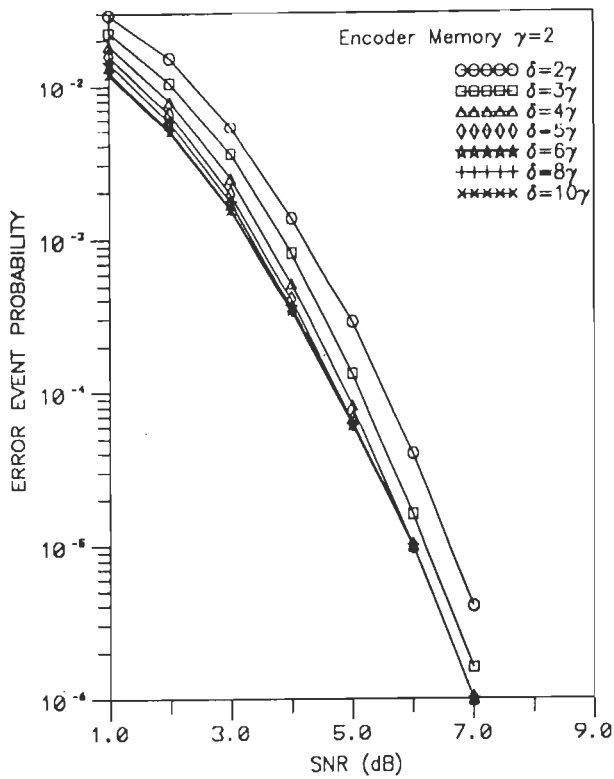
**Table 2.1 Distance Spectrum of 4-State 16-QAM TCM CODE**

Error event length (Depth $k$ )	$d_{\min}^2$	$N_d$
3	20.0	4
4	24.0	12
5	24.0	12
6	28.0	36
7	28.0	16
8	32.0	80

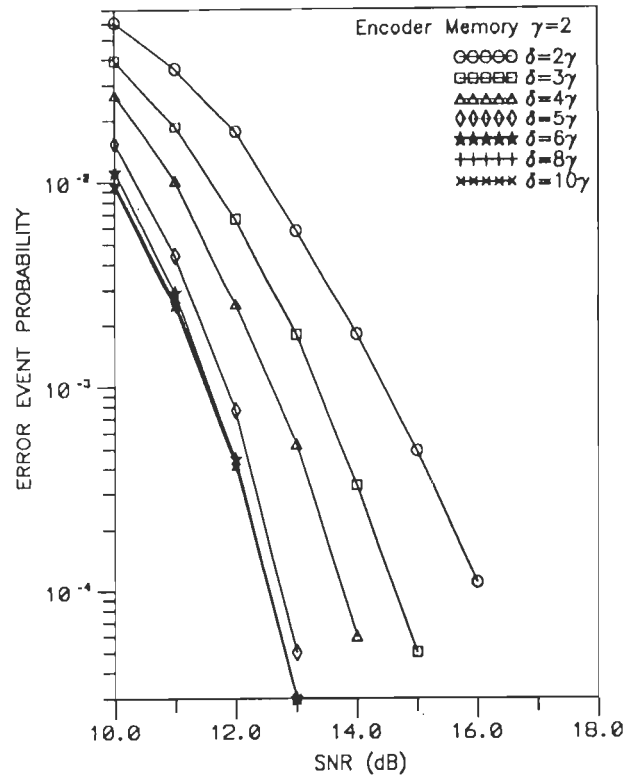
## 2.7 RESULTS AND DISCUSSION

In this section, we give the error performance of the TCM schemes over AWGN channels through the evaluation of bounds and simulation.

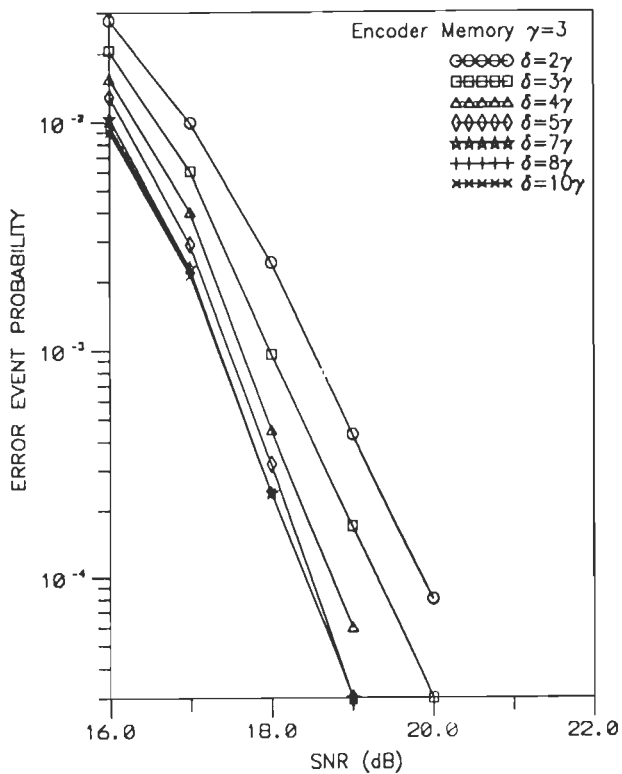
For the simulation of TCM data transmission over AWGN channel, as considered in section 2.5, the following comments are in order. For the generation of an independent identically distributed (i.i.d.) sequence of TCM symbols, we employ a uniformly distributed random binary sequence generator which outputs  $m$ -bits per baud interval. The TCM encoder/modulator transforms these  $m$ -bits into a complex-valued channel signal  $a(n)$  (a member of the  $M$ -QAM signal constellation) in accordance with the TCM coding rules. The channel signal is corrupted by the complex-valued additive white Gaussian noise process  $v(n)$ . For the generation of AWGN process, we consider the use of two Gaussian random variables defined as  $v_I(n) = \sigma_v \sqrt{-2 \ln R1} \cos(2\pi R2)$  and  $v_Q(n) = \sigma_v \sqrt{-2 \ln R1} \sin(2\pi R2)$  where  $R1$  and  $R2$  are



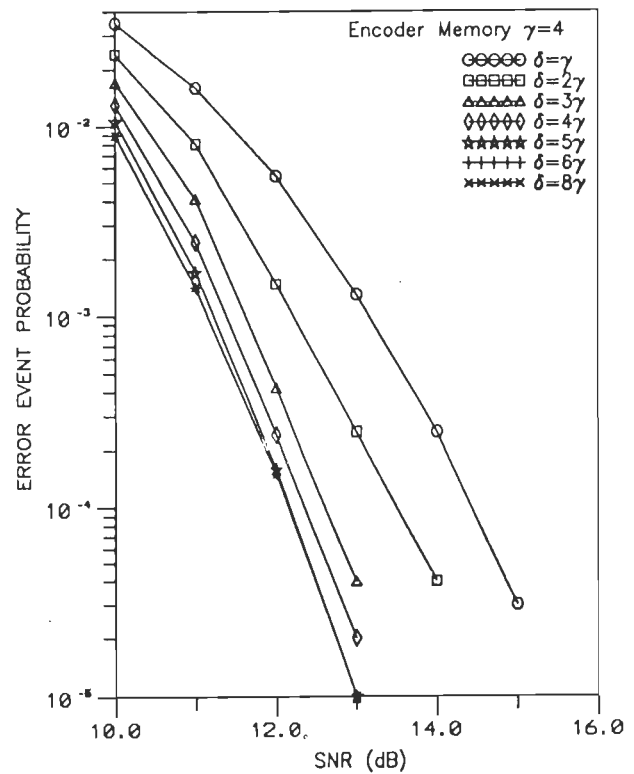
(a) 4-STATE 4-QAM TCM SCHEME



(b) 4-STATE 16-QAM TCM SCHEME



(c) 8-STATE 64-QAM TCM SCHEME



(d) 16-STATE 16-QAM TCM SCHEME

FIG.2.12 ERROR EVENT PERFORMANCE OF THE M-QAM TCM SCHEMES ON AWGN CHANNEL FOR DIFFERENT VALUES OF DECISION DELAY  $\delta$ .

uniformly distributed random variables,  $\sigma_v^2$  is the noise variance in each dimension, and  $v_I(n)$  and  $v_Q(n)$  are the in-phase and quadrature components of the complex AWGN process  $v(n)$ . Thus the received signal  $r(n)$  is given by  $r(n)=a(n)+v(n)$ .

At the receiver, the sequence of received signals  $\{r(n)\}$  are applied to a maximum-likelihood sequence detector implemented through the Viterbi algorithm. The VA performs a minimum cost search on the code trellis to find an estimated data sequence  $\{\hat{a}(n)\}$  which is closest to the received sequence  $\{r(n)\}$ . The VA employs a decision delay of  $\delta \geq 6\gamma$  for the decoding of a trellis with  $2^\gamma$  states.

The effect of decision delay  $\delta$  of the VA on the error event probability of TCM schemes have been studied. Fig.2.12 illustrates the error performance characteristics of different M-QAM TCM schemes for different values of the decision delay  $\delta$ , as given in the legend. It may be observed from Fig.2.12 that an increase in decision delay beyond  $6\gamma$  does not result in a significant improvement in the performance. Thus, most of the performance gain for a TCM code could be obtained through the Viterbi algorithm using a decision delay of  $6\gamma$  to decode a trellis structure with  $2^\gamma$  states, and we follow this logic in all our subsequent simulation work.

As discussed in section 2.4, the achievable coding gain with a TCM scheme depends upon uncoded system that is being used as the reference. To illustrate the gain achievable (asymptotically) with a 4-state 16-QAM TCM scheme, we consider the use of three different 8-QAM signal sets, of Fig.2.6 (a)-(c), as the reference systems. Fig.2.13 shows the error performance of 4-state 16-QAM TCM scheme and that of the three uncoded 8-QAM reference systems labelled as Ref.-(i), Ref.-(ii) and Ref.-(iii) respectively. The reference system Ref.-(i) corresponds to the uncoded modulation employing the signals of subset B0 (or B1) of the partitioned 16-QAM signal constellation as shown in Fig.2.6(a), while Ref.-(ii) and Ref.-(iii) corresponds to uncoded reference systems employing 8-QAM signal sets of Fig.2.6(b) and Fig.2.6(c) respectively. It may be noted that all the three reference systems

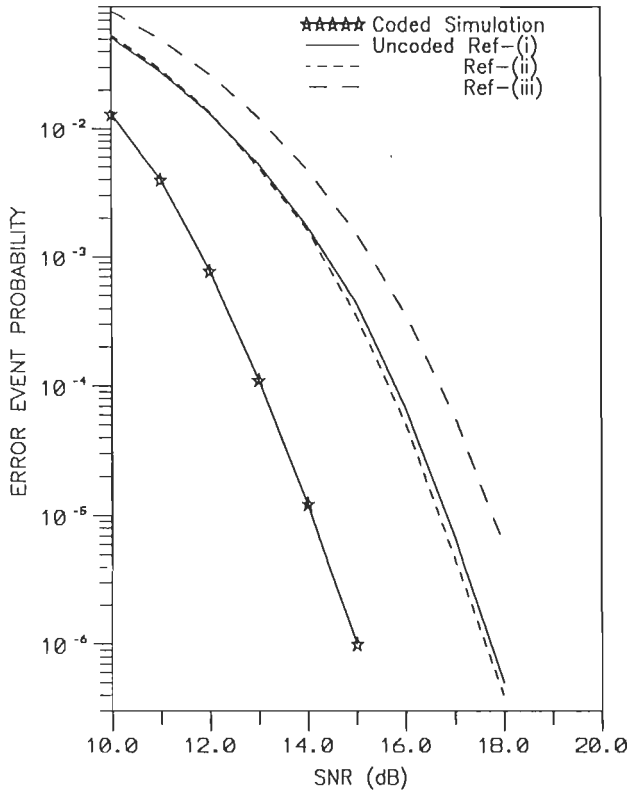


FIG.2.13 PERFORMANCE COMPARISON OF THE 4-STATE 16-QAM TCM SCHEME ON AWGN CHANNEL FOR DIFFERENT 8-QAM REFERENCE SYSTEMS.

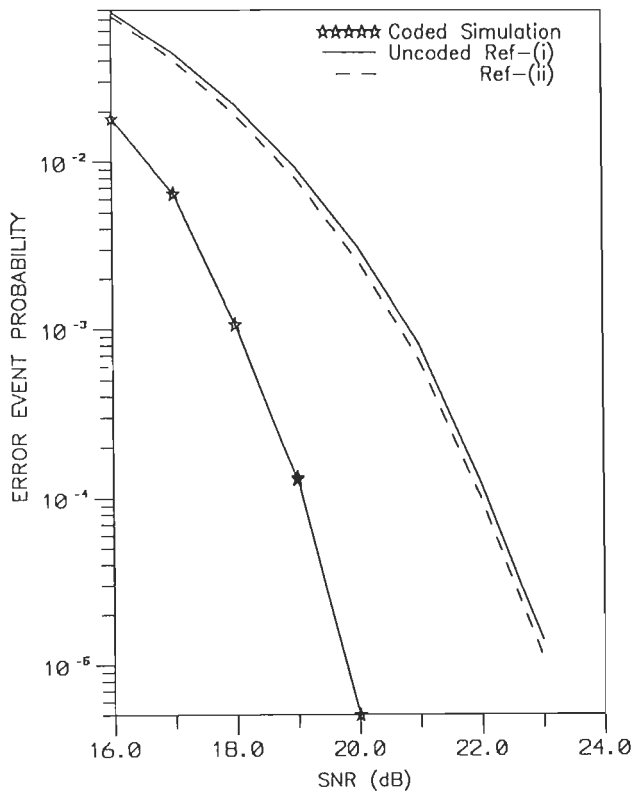


FIG.2.14 PERFORMANCE COMPARISON OF THE 8-STATE 64-QAM TCM SCHEME ON AWGN CHANNEL FOR DIFFERENT 32-QAM REFERENCE SYSTEMS.



have the same data rate and bandwidth as the coded scheme but with different average symbol energies. While Ref.-(i) has the same signal energy ( $E_{av}=10.0$ ) as that of the coded system, the reference systems Ref.-(ii) and Ref.-(iii) have average signal energies of  $E_{av}=4.73$  and  $E_{av}=6.0$  respectively. From the error performance characteristics of Fig.2.13, it can be observed that the gain achievable with the 4-state 16-QAM TCM scheme, at high SNR, is about 3 dB relative to Ref.-(i), while it is nearly 2.8 dB and 3.8 dB with reference to uncoded systems Ref.-(ii) and Ref.-(iii) respectively.

We have shown, earlier in section 2.4.1, that the asymptotic coding gain (ACG) achievable with a 4-state 16-QAM TCM varies between 2.77 dB and 3.8 dB for the use of three 8-QAM reference systems of Fig.2.6(a)-(c). The simulation results of Fig.2.13 are in agreement with the theoretical calculations of section 2.4.1.

Similarly, Fig.2.14 depicts the variations in the coding gain achievable with an 8-state 64-QAM TCM using two different uncoded 32-QAM signal constellations. In Fig. 2.14, Ref.-(i) refers to the uncoded 32-QAM system employing the subset B0 of the partitioned 64-QAM signal constellation with an average signal energy  $E_{av}=42.0$  as shown in Fig.2.6(d), while Ref.-(ii) refers to the 32-QAM cross signal constellation with  $E_{av}=20.0$  as shown in Fig.2.6(e). Both Ref.-(i) and Ref.-(ii) have the same data rate and bandwidth as the coded system, but with different signal energies. With the reference system Ref.-(i) having the same energy as that of the coded system we find, from Fig. 2.14, that at high SNR the coding gain achievable is nearly 4 dB, while for the reference system Ref.-(ii) the gains drops to about 3.8 dB. The simulation results of Fig.2.14 are in close conformity with theoretical calculations of the ACG of the 8-state 64-QAM TCM scheme of section 2.4.2.

The uncoded reference system employed in the performance study of a TCM scheme is normally based on the criterion of equal data rate, bandwidth and signal energy as that of the coded system. Henceforth, in all further analysis, we consider the use of subset B0 (or B1) of the partitioned signal constellation,

Table 2.2 Distance Spectrum of 16-QAM TCM Codes

TCM Scheme	Length of error event								Coded		8-QAM uncoded	ACG dB
	3	4	5	6	7	8	9	10	$d_{free}^2$	$N_{d_{free}}$	$d_{min}^2$	
(a) 4-state 16-QAM TCM	$d^2=20.0$	24.0	24.0	28.0	28.0	32.0	32.0	36.0	16.0	2	8.0	3.0
	$N_d=4$	12	12	36	16	80	162	240				
(b) 8-state 16-QAM TCM	$d^2=20.0$	20.0	24.0	24.0	24.0	28.0	28.0	28.0	20.0	8	8.0	4.0
	$N_d=4$	4	16	48	16	72	64	192				
(c) 16-state 16-QAM TCM	$d^2=24.0$	24.0	28.0	28.0	28.0	32.0	32.0	32.0	24.0	32	8.0	5.0
	$N_d=8$	8	16	36	64	32	112	48				

Table 2.3 Distance Spectrum of 64-QAM TCM Codes

TCM Scheme	Length of error event								Coded		32-QAM uncoded	ACG dB
	3	4	5	6	7	8	9	10	$d_{free}^2$	$N_{d_{free}}$	$d_{min}^2$	
(a) 4-state 64-QAM TCM	$d^2=20.0$ $N_d=12$	24.0 48	24.0 48	28.0 172	28.0 84	32.0 446	32.0 146	36.0 1034	16.0	3	8.0	3.0
(b) 8-state 64-QAM TCM	$d^2=20.0$ $N_d=8$	20.0 8	24.0 32	24.0 16	24.0 16	28.0 64	28.0 24	28.0 24	20.0	16	8.0	4.0
(c) 16-state 64-QAM TCM	$d^2=24.0$ $N_d=12$	24.0 12	28.0 24	28.0 56	28.0 96	32.0 72	32.0 196	32.0 112	24.0	48	8.0	5.0

59

Table 2.4 Distance Spectrum of 4-state 4-PAM TCM and 4-state 4-QAM TCM schemes

TCM Scheme	Length of error event								Coded		Uncoded Reference	ACG dB
	3	4	5	6	7	8	9	10	$d_{free}^2$	$N_{d_{free}}$	$d_{min}^2$	
(a) 4-state 4-PAM TCM	$d^2=36.0$ $N_d=4$	40.0 4	40.0 8	44.0 8	44.0 24	48.0 48	48.0 24	52.0 64	9.0	2	5.0 (2-PAM)	2.55
(b) 4-state 4-QAM TCM	$d^2=20.0$ $N_d=4$	20.0 4	24.0 8	24.0 8	28.0 12	28.0 12	32.0 4	32.0 16	16.0	2	8.0 (2-QAM)	3.0

that is Ref.-(i) as the reference system for performance comparison.

We next consider the performance evaluation of TCM schemes operating over AWGN channel using bounds and give its comparison with simulation results. For each TCM code, the distance spectrum has been computed using the algorithm given in section 2.6. For illustration, the first few spectral lines of the distance spectrum for each of the TCM codes considered in the present study are presented in Tables 2.2–2.4. The Table 2.2 gives the distance spectrum of 4-state, 8-state, and 16-state Trellis codes employing 16-QAM signal constellations, while Table 2.3 gives correspondingly results for those of 64-QAM TCM codes. The Table 2.4 gives the distance spectrum of 4-state 4-PAM and 4-state 4-QAM TCM codes. Also included in these tables are the squared minimum ED between the parallel transitions  $d_{\text{min-par}}^2$ , the squared free ED of the code  $d_{\text{free-c}}^2$ , the squared free distance of the uncoded system  $d_{\text{free-u}}^2$  and the asymptotic coding gain ACG of the TCM code, which is computed using relation (2.2) under the assumption of equal signal energy ( $E_{s-c} = E_{s-u}$ ).

In the performance evaluation of TCM scheme over AWGN channel with spectral noise power  $N_0$ , we use the following definitions of bounds [13, 100]:

The lower bound (LB) on the error event probability is given by

$$P_{e,\text{LB}} = (1/2) \cdot \text{erfc} (d_{\text{free}} / \sqrt{4N_0}) \quad \dots(2.15)$$

At high SNR, the first error event is well approximated by an asymptotic estimate (AE) as given by

$$P_{e,\text{AE}} = (1/2) N_{d_{\text{free}}} \cdot \text{erfc} (d_{\text{free}} / \sqrt{4N_0}) \quad \dots(2.16)$$

and the error event probability is upper bounded by

$$P_{e,\text{UB}} = (1/2) \sum_{d=d_{\text{free}}} N_d \cdot \text{erfc} (d / \sqrt{4N_0}) \quad \dots(2.17)$$

where  $d_{\text{free}}$  is the free distance of the code and  $N_{d_{\text{free}}}$  its multiplicity number,

Table 2.5 Error-event performance of 16-QAM TCM schemes on AWGN Channel

TCM Scheme	SNR (dB)	$\sigma_v$	Coded System Error event Probability				8-QAM uncoded system
			Lower bound $P_{e,LB}$	Asymptotic estimate $P_{e,AE}$	Upper bound $P_{e,UB}$	Simulation $P_e$	Probability of symbol error
(a) 4-state 16-QAM TCM (Table 2.2a) (Fig. 2.15a)	10.0	0.7071	0.234E-02	0.468E-02	0.618E-01	0.153E-01	0.513E-01
	11.0	0.6302	0.753E-03	0.151E-02	0.133E-01	0.389E-02	0.279E-01
	12.0	0.5617	0.185E-03	0.370E-03	0.207E-02	0.613E-03	0.133E-01
	13.0	0.5006	0.323E-04	0.646E-04	0.221E-03	0.710E-04	0.532E-02
	14.0	0.4462	0.368E-05	0.737E-05	0.159E-04	0.700E-05	0.172E-02
	15.0	0.3976	0.246E-06	0.491E-06	0.735E-06	0.500E-06	0.443E-03
(b) 8-state 16-QAM TCM (Table 2.2b) (Fig. 2.15b)	10.0	0.7071	0.783E-03	0.313E-02	0.457E-01	0.104E-01	0.513E-01
	11.0	0.6302	0.194E-03	0.776E-03	0.788E-02	0.225E-02	0.279E-01
	12.0	0.5617	0.343E-04	0.137E-03	0.920E-03	0.291E-03	0.133E-01
	13.0	0.5006	0.397E-05	0.159E-04	0.677E-04	0.230E-04	0.532E-02
	14.0	0.4462	0.270E-06	0.108E-05	0.291E-05	0.100E-05	0.172E-02
	15.0	0.3976	0.936E-08	0.374E-07	0.673E-07	-	0.443E-03
(c) 16-state 16-QAM TCM (Table 2.2c) (Fig. 2.15c)	10.0	0.7071	0.266E-03	0.213E-02	0.177E-01	0.423E-02	0.513E-01
	11.0	0.6302	0.508E-04	0.406E-03	0.232E-02	0.714E-03	0.279E-01
	12.0	0.5617	0.647E-05	0.518E-04	0.195E-03	0.540E-04	0.133E-01
	13.0	0.5006	0.496E-06	0.397E-05	0.980E-05	0.300E-05	0.532E-02
	14.0	0.4462	0.201E-07	0.161E-06	0.274E-06	-	0.172E-02
	15.0	0.3976	0.363E-09	0.291E-08	0.379E-08	-	0.443E-03

Table 2.6 Error-event performance of 64-QAM TCM schemes on AWGN Channel

TCM Scheme	SNR (dB)	$\sigma_v$	Coded System Error event Probability				32-QAM uncoded system
			Lower bound $P_{e,LB}$	Asymptotic estimate $P_{e,AE}$	Upper bound $P_{e,UB}$	Simulation $P_e$	Probability of symbol error
(a) 4-state 64-QAM TCM (Table 2.3a) (Fig. 2.16a)	16.0	0.7263	0.295E-02	0.884E-02	0.821E-01	0.216E-01	0.783E-01
	17.0	0.6473	0.100E-02	0.301E-02	0.191E-01	0.706E-02	0.444E-01
	18.0	0.5769	0.263E-03	0.790E-03	0.324E-02	0.171E-02	0.221E-01
	19.0	0.5141	0.502E-04	0.151E-03	0.404E-03	0.220E-03	0.924E-02
	20.0	0.4583	0.637E-05	0.191E-04	0.343E-04	0.200E-04	0.312E-02
	21.0	0.4084	0.487E-06	0.146E-05	0.196E-05	0.100E-05	0.812E-03
(b) 8-state 64-QAM TCM (Table 2.3b) (Fig. 2.16b)	16.0	0.7263	0.104E-02	0.624E-02	0.565E-01	0.14E-01	0.783E-01
	17.0	0.6473	0.276E-03	0.165E-02	0.106E-01	0.343E-02	0.444E-01
	18.0	0.5769	0.531E-04	0.319E-03	0.135E-02	0.644E-03	0.221E-01
	19.0	0.5141	0.684E-05	0.411E-04	0.119E-03	0.610E-04	0.924E-02
	20.0	0.4583	0.532E-06	0.319E-05	0.629E-05	0.400E-05	0.312E-02
	21.0	0.4084	0.219E-07	0.131E-06	0.191E-06	-	0.812E-03
(c) 16-state 64-QAM TCM (Table 2.3c) (Fig. 2.16c)	16.0	0.7263	0.372E-03	0.298E-02	0.175E-01	0.643E-02	0.783E-01
	17.0	0.6473	0.771E-04	0.617E-03	0.266E-02	0.103E-02	0.444E-01
	18.0	0.5769	0.109E-04	0.871E-04	0.268E-03	0.110E-03	0.221E-01
	19.0	0.5141	0.949E-06	0.759E-05	0.167E-04	0.700E-05	0.924E-02
	20.0	0.4583	0.452E-07	0.36E-06	0.588E-06	-	0.312E-02
	21.0	0.4084	0.100E-08	0.802E-08	0.104E-07	-	0.812E-03

Table 2.7 Error-event performance of 4-state 4-PAM and 4-state 4-QAM TCM schemes on AWGN Channel

TCM Scheme	SNR (dB)	$\sigma_v$	Coded System Error event Probability				Uncoded system
			Lower bound $P_{e,LB}$	Asymptotic estimate $P_{e,AE}$	Upper bound $P_{e,UB}$	Simulation $P_e$	Probability of symbol error
(a) 4-state 4-PAM TCM (Table 2.4a) (Fig. 2.17a)	3.0	0.7080	0.290E-01	0.116E+00	0.140E+00	0.425E-01	0.103E+00
	5.0	0.5623	0.852E-02	0.341E-01	0.388E-01	0.279E-01	0.559E-01
	7.0	0.4467	0.133E-02	0.534E-02	0.584E-02	0.662E-02	0.228E-01
	9.0	0.3548	0.780E-04	0.312E-03	0.332E-03	0.400E-03	0.581E-02
	11.0	0.2818	0.966E-06	0.387E-05	0.402E-05	0.400E-05	0.744E-03
	13.0	0.2239	0.103E-08	0.413E-08	0.423E-08	-	0.327E-04 (2-PAM uncoded)
(b) 4-state 4-QAM TCM (Table 2.4b) (Fig. 2.17b)	2.0	0.8516	0.948E-03	0.217E-02	0.742E-02	0.488E-02	0.231E-01
	3.0	0.7088	0.324E-03	0.725E-03	0.178E-02	0.152E-02	0.126E-01
	4.0	0.6317	0.650E-04	0.187E-03	0.306E-03	0.335E-03	0.615E-02
	5.0	0.5630	0.815E-05	0.296E-04	0.346E-04	0.610E-04	0.244E-02
	6.0	0.5018	0.120E-05	0.473E-05	0.231E-05	0.100E-04	0.822E-03
	7.0	0.4472	0.113E-06	0.451E-06	0.794E-06	0.100E-05	0.197E-03 (2-QAM uncoded)

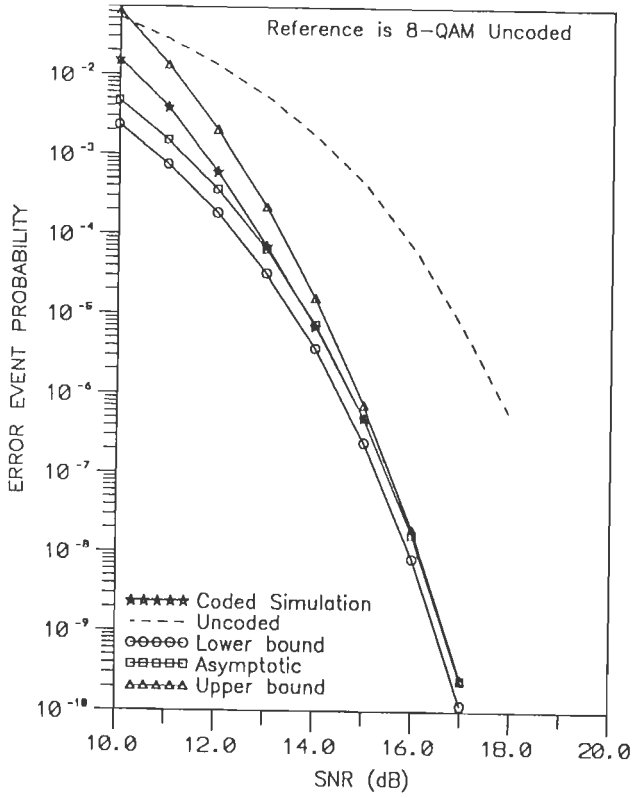
$N_d$  is the multiplicity number of error events with minimum ED  $d$ ,  $N_0$  is the noise energy given as  $N_0=2\sigma_v^2$  for two dimensional transmission and  $N_0=\sigma_v^2$  for one dimensional transmission, and  $\text{erfc}(\cdot)$  is the complementary error function. It can be verified that the error event probability  $P_e$  is bounded by  $P_{e,LB} \leq P_e \leq P_{e,UB}$ , and at high SNR  $P_e \approx P_{e,AE}$ .

To compute the upper bound  $P_{e,UB}$ , we use the first few terms of the distance spectrum of the code, since the contribution of the higher order terms on  $P_{e,UB}$  of (2.17) becomes insignificant due to the exponentially decreasing nature of  $\text{erfc}(x)$  with increasing values of  $x$ .

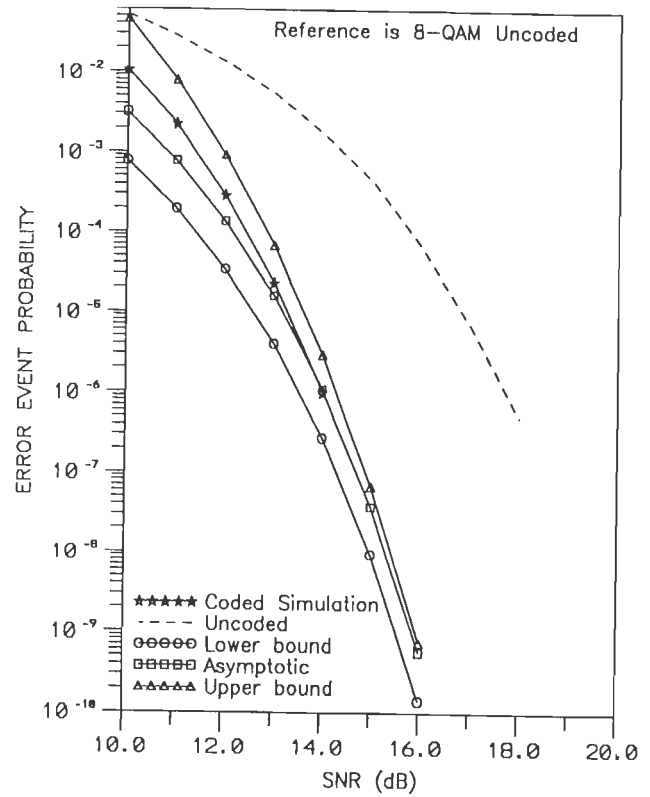
The error performance of the TCM codes have been evaluated through the bounds (2.15)-(2.17) using the distance spectrum given in Tables 2.2-2.4 and the computed values of the error event probability are given correspondingly in Tables 2.5-2.7. The Table 2.5 gives the error performance parameters such as lower bound  $P_{e,LB}$  asymptotic estimate  $P_{e,AE}$ , upperbound  $P_{e,UB}$ , which are evaluated for the 4-state, 8-state, and 16-state 16-QAM TCM schemes, using the data given in Table 2.2. Similarly, Table 2.6 gives the error performance of 4-state, 8-state, and 16-state 64-QAM TCM scheme evaluated through (2.15)-(2.17) using the distance spectrum given in Table 2.3. The Table 2.7 gives the performance of of 4-state 4-PAM and 4-state 4-QAM TCM schemes computed through the use of data given in Table 2.4. These Tables 2.5-2.7 also include the results obtained through simulation. The number of symbols employed in the simulation run varies from  $10^5$  to  $10^7$  depending upon the state complexity of the trellis structure and we have used a decision delay  $\delta = 6\gamma$  for the VA.

The error performance characteristics of the 4-state 16 QAM TCM scheme, as given in Table 2.5(a) have been shown in Fig.2.15(a). The legend 'Lower bound', 'Asymptotic' and 'Upper bound' correspond respectively to the bounds  $P_{e,LB}$ ,  $P_{e,AE}$  and  $P_{e,UB}$  of the error event probability as defined by (2.15)-(2.17). 'Coded simulation' refers to the error event probability of the 4-state 16-QAM TCM code obtained through simulation and 'uncoded' refers to the 8-QAM uncoded reference

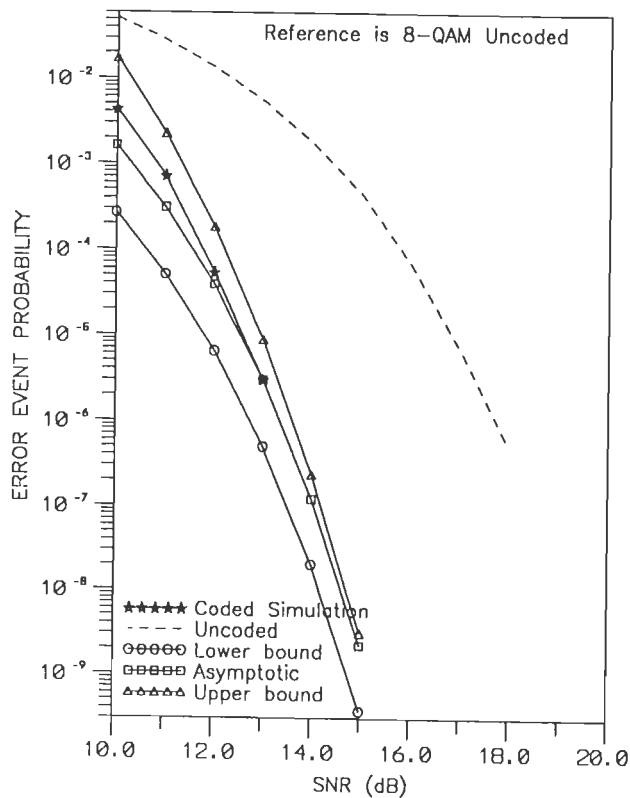




(a) 4-STATE 16-QAM TCM

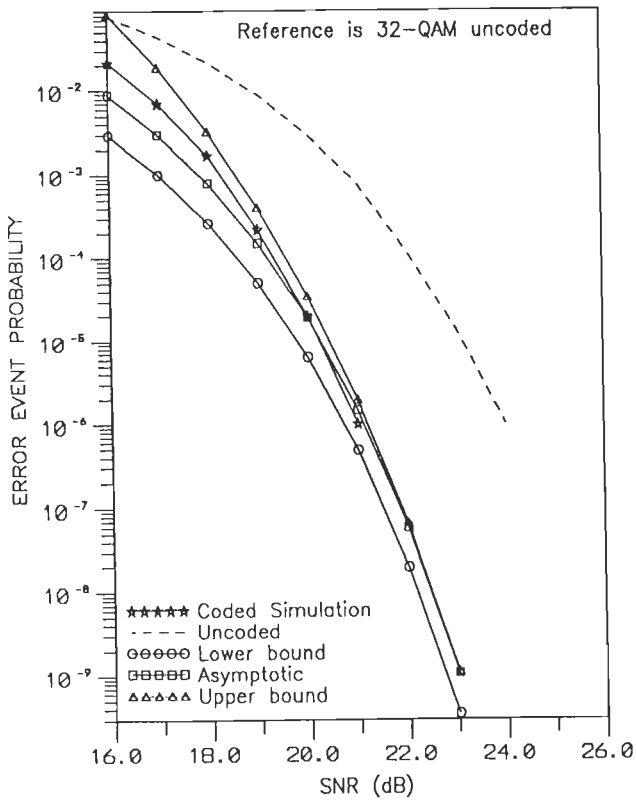


(b) 8-STATE 16-QAM TCM

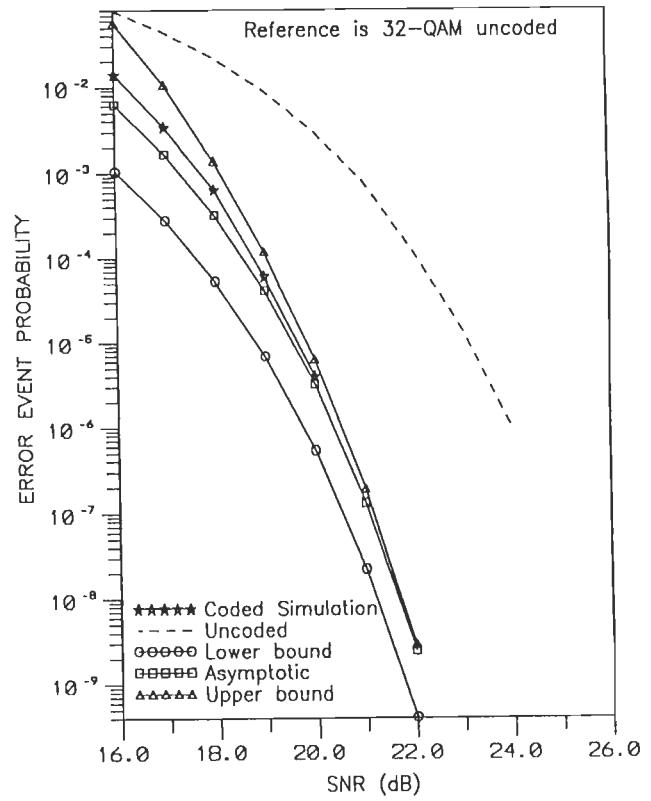


(c) 16-STATE 16-QAM TCM

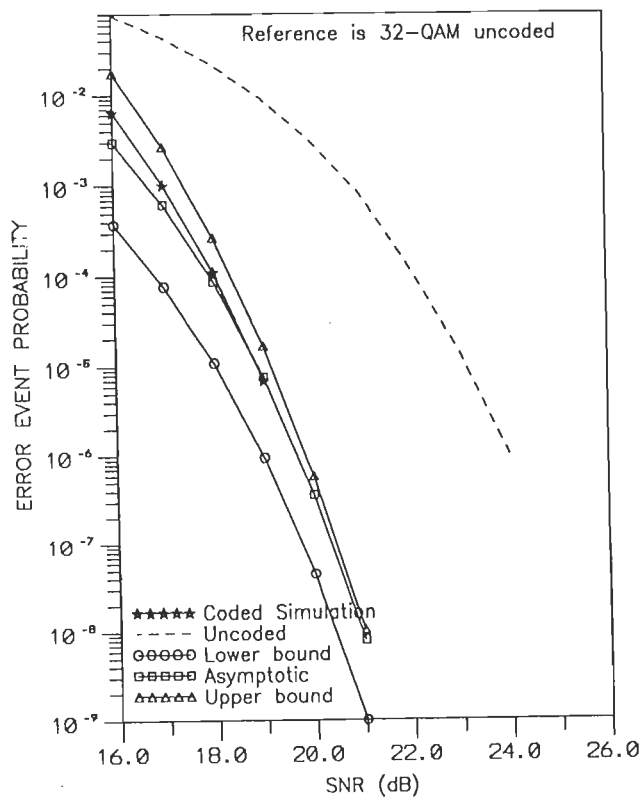
FIG.2.15 THE ERROR PERFORMANCE OF 16-QAM TCM SCHEMES ON AWGN CHANNEL.



(a) 4-STATE 64-QAM TCM

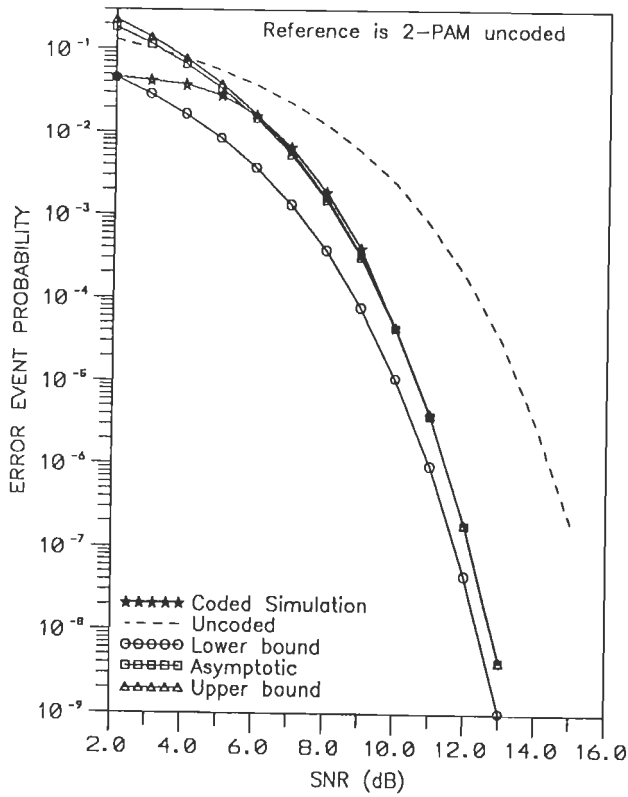


(b) 8-STATE 64-QAM TCM

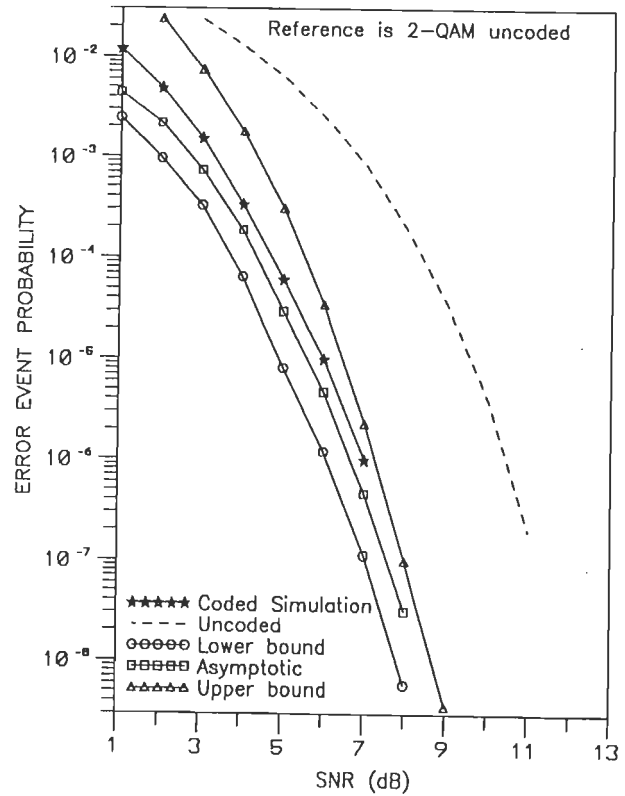


(c) 16-STATE 64-QAM TCM

FIG.2.16 THE ERROR PERFORMANCE OF 64-QAM TCM SCHEMES ON AWGN CHANNEL.

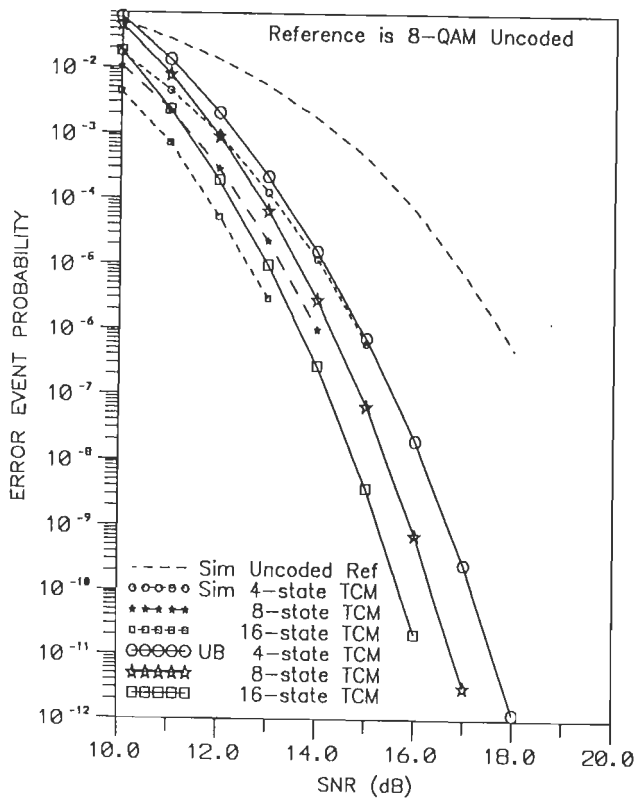


(a) 4-STATE 4-PAM TCM

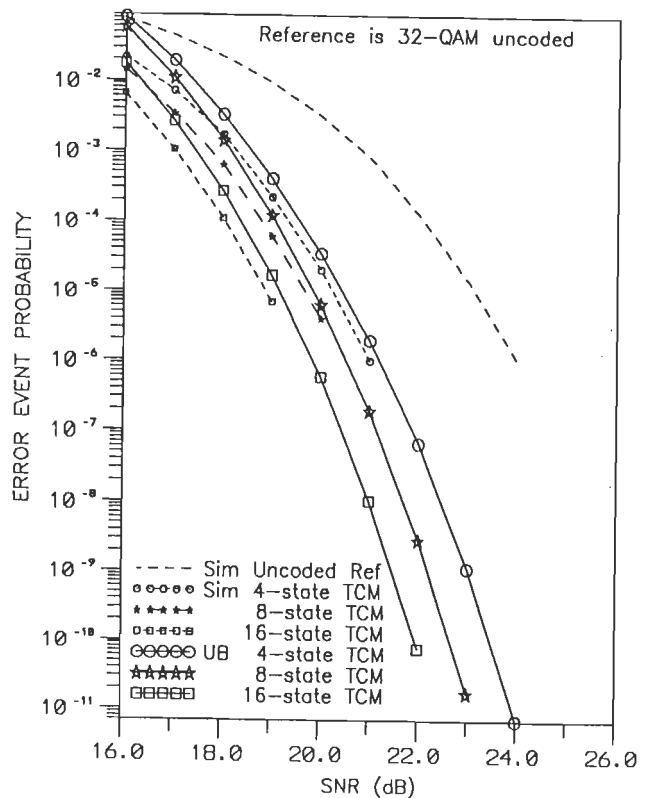


(b) 4-STATE 4-QAM TCM

FIG.2.17 ERROR PERFORMANCE OF 4-STATE 4-PAM TCM AND 4-STATE 4-QAM TCM SCHEMES ON AWGN CHANNEL.



(a) 16-QAM TCM SCHEMES



(b) 64-QAM TCM SCHEMES

FIG.2.18 PERFORMANCE COMPARISON AMONG THE DIFFERENT 16-QAM TCM SCHEMES AND THE 64-QAM TCM SCHEMES ON AWGN CHANNEL.

system. Fig.2.15(b) and Fig.2.15(c) depict the error performance of 8-state and 16-state 16-QAM TCM schemes respectively corresponding to the computations given in Table 2.5(b)-(c). Similarly, the error performance characteristics of 4-state, 8-state, and 16-state 64-QAM TCM schemes, corresponding to computations given in Table 2.6(a)-(c), have been shown in Fig.2.16(a) to Fig.2.16(c) respectively. Also the error performance of the 4-state 4-PAM and 4-state 4-QAM TCM codes, corresponding to computations given in Table 2.7(a)-(b), have been shown in Fig.2.17(a) and Fig.2.17(b).

Fig.2.18 shows the summary of the error performance of the 16-QAM and 64-QAM TCM schemes derived through the use of the computed upper bounds and simulation results. We can note from their performance characteristics that larger coding gain is achievable with the use of 8-state and 16-state TCM schemes, which is respectively about 1 dB and 2 dB relative to the 4-state TCM scheme.

We note, from the error performance characteristics as shown in Fig.2.15-Fig.2.17 that the simulation result is well within the bounds computed and at high SNR, the asymptotic estimate and the upper bounds follow closely the simulation result. In all fairness it can be said that the upper bound, derived from the use of the distance spectrum computing algorithm of section 2.6, gives a nearly tight estimate of the error event probability and hence we may conclude that the proposed algorithm can be applied effectively in the performance evaluation of all Ungerboeck TCM codes over additive white Gaussian noise channels.

# TCM TRANSMISSION OVER TIME-DISPERSIVE ISI CHANNELS

---

## 3.1 INTRODUCTION

With the growth in information technology, there is an ever increasing demand for bandwidth-efficient digital communication systems. The two major impediments to the reliable high-speed data transmission over a bandlimited channel are the additive white Gaussian noise (AWGN) and the intersymbol interference (ISI). The conventional coding schemes increase the reliability at the cost of bandwidth. The coded-modulation schemes, such as TCM, can effectively enhance noise immunity without increasing the bandwidth. To mitigate the effects of ISI, a powerful equalization technique such as the maximum-likelihood sequence estimation (MLSE) is required. Thus for the bandlimited time-dispersive ISI channels, a TCM scheme in combination with an optimum MLSE equalizer promises to achieve data rate close to channel capacity [15].

The cascade of a TCM encoder and the ISI channel can be viewed as a combined finite-state machine, and hence as a combined ISI-Code trellis whose states are given by the product of the TCM encoder states and the ISI states. Consequently, the resulting receiver performs a maximum-likelihood sequence estimation of the data sequence using the Viterbi algorithm that searches for a minimum cost path in the ISI-Code trellis. This combined ISI-Code receiver (also called the combined equalization/TCM decoding receiver) structure is optimum and treats the functions of equalization and TCM decoding as a single entity.

The error rate performance of the optimum combined ISI-Code receiver can be evaluated through bounds, by making use of the error structure of the TCM encoder and the ISI channel characteristics. We present a new method for the performance evaluation of TCM scheme on ISI channels, following the approach adopted by Magee and Proakis [79] to evaluate the performance of MLSE receiver for uncoded transmission over time-dispersive channels. Since the ISI channel is linear, the output error sequence can be uniquely related to the input error sequence using the discrete channel impulse response. From the output error sequence, the Euclidean weight (squared ED) of the output error event can be computed. Making use of the distance spectrum computing algorithm (of section 2.6), it is possible to obtain a set of input error sequences of the TCM encoder. Accordingly, we get a set of output error sequences and correspondingly their Euclidean weights. The minimum of Euclidean weights then represents the minimum squared ED of the combined ISI-Code structure and hence the performance bounds can be evaluated.

In this chapter, we first consider the equalization problem for the transmission of digital signals over time-dispersive channels and the different equalizer structures used in practice to combat the effects of ISI. We next consider the decoding of TCM signals in the presence of ISI and AWGN, using the optimum combined ISI-Code receiver structures employing the maximum-likelihood Viterbi decoder. We then present the new approach that makes use of the error structure of the TCM scheme to evaluate the performance of the combined ISI-Code receiver using bounds. We also present, the results of a study that has been performed to evaluate the error rate performance of some combined ISI-Code receiver structures for the decoding of Trellis-coded QAM signals, using bounds and through simulation.

### **3.2 TIME-DISPERSIVE CHANNEL AND EQUALIZATION PROBLEM**

In a bandwidth-efficient digital communication system, the effects of each symbol transmitted over a time-dispersive channel extend beyond the time allowed

to represent that symbol [46]. Consequently, this overlapping of received symbols results in a linear distortion called the intersymbol interference (ISI), which turns out to be the primary obstacle to high-speed data transmission over bandlimited channels. The minimization of probability of error in the presence of ISI, constitutes the equalization problem. In a broad sense, the term equalizer refers to any signal processing technique/device designed to mitigate the effects of ISI.

Besides telephone channels, there are other physical channels that exhibit some form of time dispersion and thereby introduce ISI distortion. The digital mobile channels and other radio channels such as shortwave ionospheric (HF) propagation and tropospheric scatter are classified as time-dispersive channels. In these, time dispersion and hence ISI arises due to the multiple propagation paths of different path delays. These digital radio channels are normally called as the time-variant multipath fading channels, since their channel characteristics vary with time [100].

In addition to linear ISI distortion, the signals transmitted over a bandlimited channel are subject to other impairments such as nonlinear distortion, frequency offset, phase jitter, impulse noise, and thermal noise. Unfortunately, a channel model encompassing all these impairments is most difficult to analyze [100]. Therefore, for mathematical tractability, the channel model that is normally adopted for a bandlimited channel is a linear time-invariant filter that introduces the ISI and adds white noise that is Gaussian in nature.

### 3.2.1 Baseband Digital Transmission System

The model for a typical baseband digital transmission system which is subjected to ISI is shown in Fig.3.1.

Consider the transmission of a data sequence  $\{a(k)\}$  at a rate of one symbol every  $T$  seconds over a baseband channel whose impulse response is  $g(t)$ . Carrier modulated data transmission systems such as quadrature amplitude modulation (QAM)

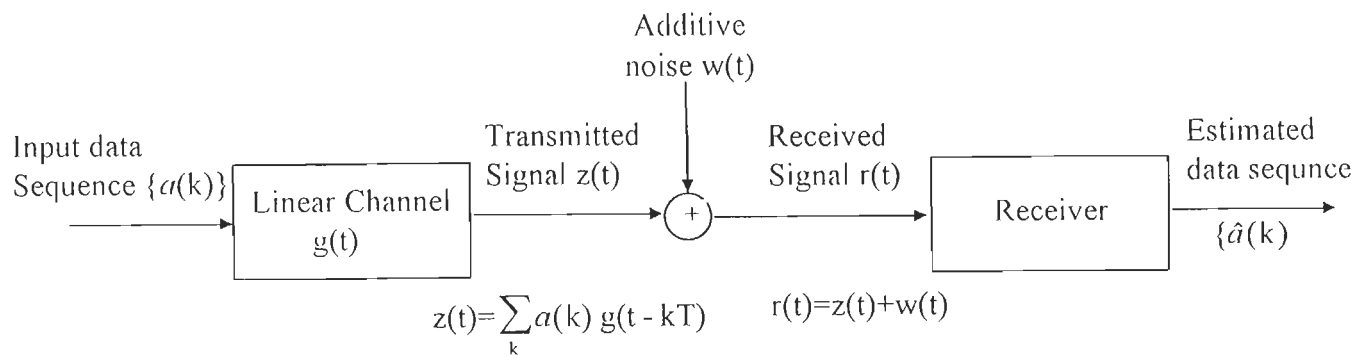


FIG.3.1 BASEBAND DIGITAL TRANSMISSION SYSTEM MODEL.

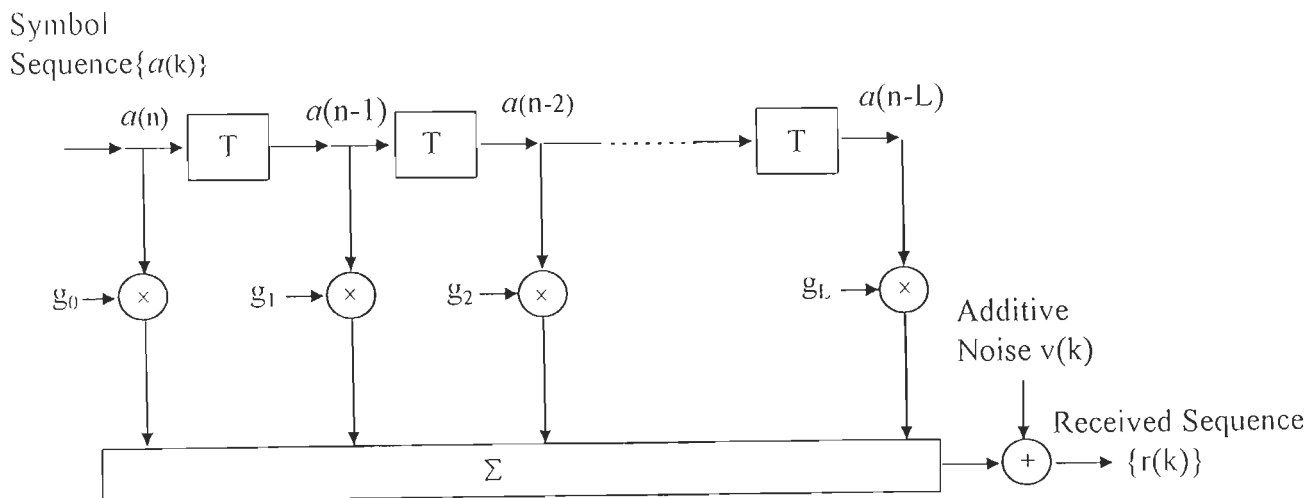


FIG. 3.2 DISCRETE-TIME WHITE NOISE CHANNEL MODEL.



and quadrature phase shift keyed (QPSK) system can be represented by an equivalent linear baseband model that differs from the real baseband system by the fact the symbol  $a(k)$  and the channel impulse response  $g(t)$  are complex-valued [125]. The channel is assumed to be linear and time-invariant, and delivers to the receiver a distorted time-smeared version of the transmitted signal. In this model, the channel may represent the effect of the modulator, transmitter filter and the transmission medium (the actual channel) in cascade. The channel output is corrupted by the complex additive white Gaussian noise  $w(t)$ . Thus, the received waveform is given by

$$r(t) = \sum_k a(k) \cdot g(t-kT) + w(t) \quad \dots(3.1)$$

Thus, the instantaneous value of the received waveform depends on several transmitted symbols, giving rise to the problem of ISI. The ISI arises due to the fact that  $g(t)$  remains non-vanishing over several symbol durations. Therefore, the linear channel may be assumed to have a finite memory of  $L$  symbols, and can be represented by a finite-state machine. The received waveform is processed by a receiver that may be linear or nonlinear which is optimized with respect to certain performance measure to combat the effects of the ISI and AWGN.

The optimum sequence estimator requires the entire received waveform before a decision can be made. Forney [46] has shown that the samples of a whitened matched filter form sufficient statistics for the detection of the transmitted sequence  $\{a(n)\}$ . Thus the cascade of the linear channel representing the modulator, the transmitter filter and the actual channel and the receiver filter consisting of a whitened matched filter and a symbol rate sampler, can be modeled as a discrete-time white noise channel as shown in Fig.3.2. It may be noted that  $T$  is the symbol signaling interval.

Using the above model, the received signal at the time instant  $nT$  is given by

$$r(n) = \sum_{i=0}^L g_i \cdot a(n-i) + v(n) \quad \dots(3.2)$$

where  $g_i$ 's are complex tap gains, and correspond to the sampled channel impulse response, and  $v(n)$  are samples of i.i.d complex-valued Gaussian noise with zero mean and variance  $2\sigma_v^2$ . The noise and data sequences are assumed to be uncorrelated. The number of taps are  $(L+1)$ , where  $L$  represents the channel memory.

If the signal constellation used for the transmission of  $a(i)$ 's has an alphabet size of  $M$  symbols and the channel memory is of  $L$  symbols, then the discrete-time channel can be represented by either an  $M^L$ -state finite state machine [46] or an  $M^L$ -state trellis diagram. The system state (ISI state) at any time instant  $n$  is defined by  $L$  previous symbols as

$$s_n = (a(n-1), a(n-2), \dots, a(n-L)) \quad \dots(3.3)$$

where  $s_n$  may assume one of the  $M^L$  possible values represented by  $\{a(n-i)\}$  for  $1 \leq i \leq L$ .

### 3.2.2 Equalizer Structures

To combat the effects of ISI, a variety of receiver equalizer structures have been proposed in the literature [56, 77, 104]. Although the exact nature of the optimum receiver depends upon the problem formulation, the general form remains the same in almost all approaches; namely a matched filter followed by a suitable equalizer algorithm. While the matched filter reduces the errors due to AWGN, the equalizer minimizes the error due to ISI. The nature of the equalizer may vary from simple transversal filter through nonlinear decision-feedback equalizer structures to the more sophisticated MLSE algorithms like the Viterbi algorithm. For a comprehensive tutorial coverage on equalizer structures see [104]. In the following, we consider the salient features of some basic equalizer structures, for the received sequence given by (3.2).

#### (i) Linear Equalizer (LE)

An optimum linear equalizer consists of an infinite length transversal filter

which minimizes the errors due to ISI. The LE finds wide applications in practice, because of its simplicity in implementation. It provides satisfactory performance in most of the applications. However, on channels with severe amplitude distortion, it enhances and correlates noise which results in performance degradation, especially on multipath fading channels [11].

### **(ii) Decision-Feedback Equalizer (DFE)**

The nonlinear DFE, as compared to LE, uses the information provided by the estimates of the previous symbols. If the past decisions are assumed correct, then the ISI caused by them can be subtracted from the received signal in arriving at a correct decision about the present symbol, provided the channel response is known exactly. The concept of using previous decisions to cope with the ISI problem was first introduced by Austin [11], and Mosen [86] proposed the first DFE receiver structure for time-dispersive channels.

The DFE structure consists of two filter sections, the feed-forward filter (FFF) and the feed-back filter (FBF) which mitigate the effect of ISI due to precursor and post cursor symbol respectively. On severely distorted channels the DFE provides an improved performance as compared to an LE. However, the DFE suffers from severe error propagation due to the FBF section. An incorrect decision fed into the FBF results in error bursts, as if an impulsive noise has been injected into the decoder.

### **(iii) Kalman Filter Equalizer (KFE)**

The KFE is based on discrete Kalman filter and uses a state-variable representation of the channel model. The KFE which is an optimum unbiased linear minimum mean-square error (ULMMSE) estimator, provides the best linear estimate of the transmitted symbol when the channel response is known. The use of the discrete Kalman filter for the equalization of a binary transmission channel was first proposed by Lawrence and Kaufman [68]. Benedetto and Biglieri [6] have investigated the steady-state behaviour of such receiver structures.

Under steady-state this optimum linear receiver turns out to be a time-invariant, stable recursive filter. In the absence of channel noise (at very high SNR), the KFE behaves as a zero-forcing equalizer. Since the KFE utilizes the estimates of the past symbols, in form it is similar to a DFE. But in a KFE the estimates of the symbols are fed back before a decision is made on them, and thus the receiver is linear and the effect of decision-error propagation is thereby eliminated [6]. The performance attainable with a steady-state KFE is superior to that of a conventional LE, for a given complexity of the receiver structure. However for implementation, the KFE needs an exact knowledge of the channel tap-gains and a mismatch in tap setting may lead to performance degradation.

**(iv) Maximum-Likelihood Sequence Estimation (MLSE)**

Forney [46] introduced an optimum receiver structure that performs maximum-likelihood sequence estimation by implementation through the Viterbi algorithm (VA), as shown in Fig.3.3.

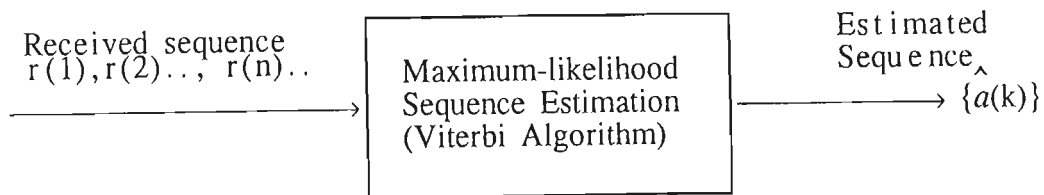


**Fig.3.3 Maximum-likelihood sequence estimator**

Like the Kalman filter, the VA tracks the state of a stochastic process with a recursive method that is optimum in a certain sense. Forney [46] has shown that the VA indeed is a maximum-likelihood sequence estimation technique, and therefore is always optimum. Assume that an ISI channel is represented by an  $\underline{M}^L$ -state trellis structure, where  $L$  is ISI memory length and  $\underline{M}=2^m$  is the constellation size of an uncoded modulation system. Then the Viterbi algorithm by a recursive procedure searches the trellis to find, among all sequences, a sequence which is closest to the received sequence in the sense of maximum-likelihood. The VA is therefore an optimum maximum-likelihood (ML) decoder.

Although MLSE is an optimum solution, its computational complexity and storage requirements grow exponentially with memory length  $L$  and thereby limits its practical use.

### 3.3 DECODING OF TCM SIGNALS IN THE PRESENCE OF ISI AND AWGN

As mentioned earlier, the two primary impediments to reliable high-speed transmission of digital data are the ISI and AWGN. In practice, bandwidth-efficient coded modulation schemes and adaptive equalization techniques have proved to be extremely efficient in overcoming the effects of AWGN and ISI, respectively. Therefore, TCM schemes in combination with an optimum MLSE equalization technique may be employed to realize reliable digital transmission at rates close to channel capacity [40].

Recently, Chevillat and Eleftheriou [26], and Eyuboglu and Qureshi [42] have independently proposed a new integrated approach to the TCM receiver design, wherein the previously separated functions of equalization and TCM decoding are combined into a single entity. Based on this approach, we now consider the combined equalization and TCM decoding scheme for linear ISI channels corrupted with AWGN.

#### 3.3.1 Combined MLSE Equalization and TCM Decoding

Consider the transmission of TCM signals over a time-dispersive ISI channel with AWGN. The communication system comprises a TCM encoder/modulator, a linear channel filter followed by an ML sequence estimator as shown in Fig.3.4. The TCM encoder/modulator, and the channel filter can be represented by an equivalent combined discrete-time white noise channel model as shown in Fig.3.5 [26].

The TCM encoder generates a sequence  $\{a(n)\}$  in response to an input sequence  $\{X_n\}$ , where  $X_n$  is a  $m$ -bit input stream defined by  $X_n = (x_n^1, x_n^2, \dots, x_n^m)$ . The linear channel filter transforms  $\{a(n)\}$  into a channel output sequence  $\{b(n)\}$ .

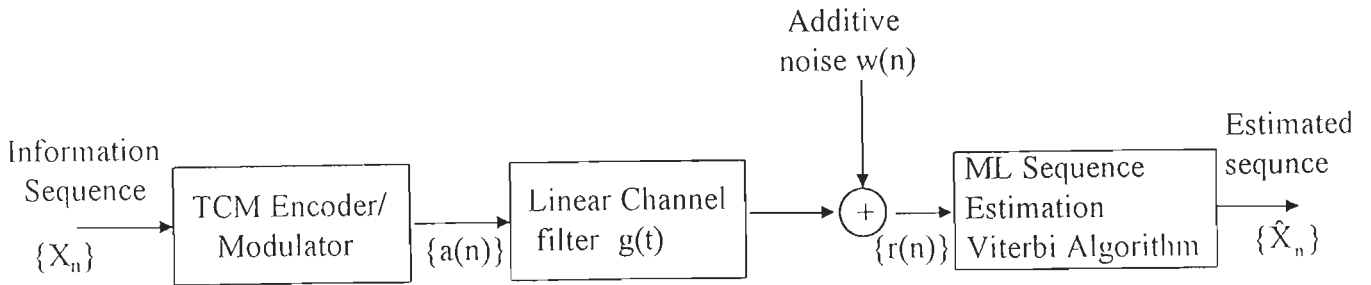


FIG.3.4 BASEBAND TCM TRANSMISSION AND DETECTION WITH MLSE.

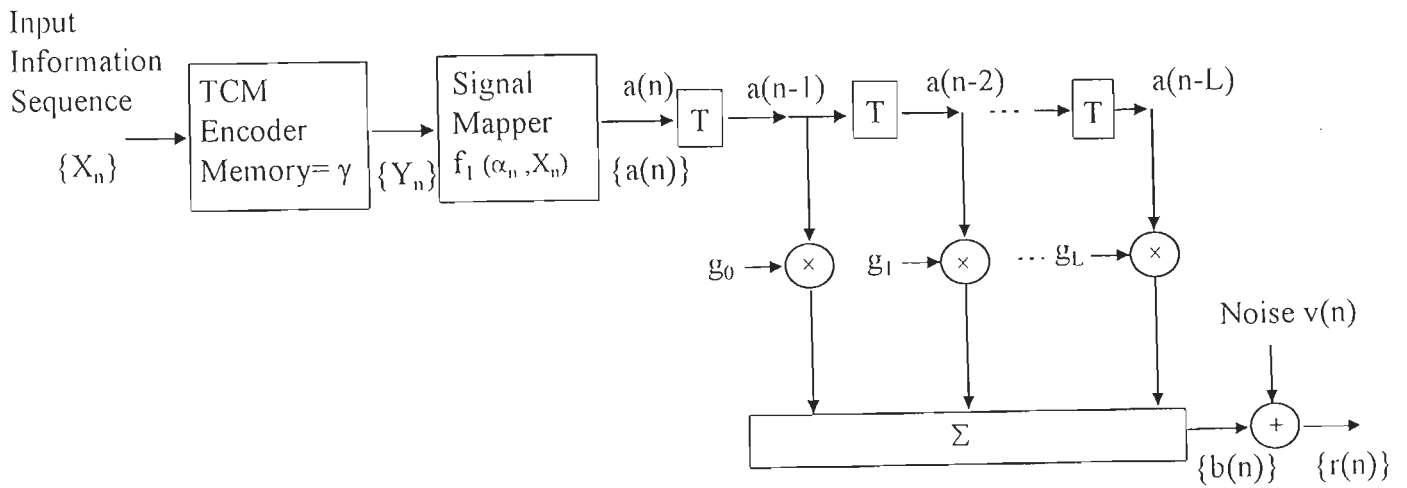


FIG. 3.5 THE COMBINED DISCRETE-TIME WHITE NOISE CHANNEL MODEL.

The TCM encoder being a finite-state machine, the output associated with the next state transition depends on the present state  $\alpha_n$  of the encoder and the input  $X_n$ . Thus the encoder output can be described as

$$a_n = f_1(\alpha_n, X_n) \quad \dots(3.4)$$

Also, the next state of the encoder can be expressed as

$$\alpha_{n+1} = f_2(\alpha_n, X_n) \quad \dots(3.5)$$

The output of the discrete-time model can be expressed as

$$r(n) = b(n) + v(n)$$

$$\text{or} \quad r(n) = g_0 \cdot a(n) + \sum_{i=1}^L g_i \cdot a(n-i) + v(n) \quad \dots(3.6)$$

where the second term represents the ISI and  $v(n)$  is the sampled value of complex additive white Gaussian noise with zero mean and variance  $\sigma_v^2$  in each dimension.

The discrete-time model of Fig.3.5 comprises of two finite-state machines namely the TCM encoder and the ISI channel. This discrete-time model can therefore be viewed as a combined finite-state machine (FSM) that represents the effect of the two individual FSMs. Consequently, a TCM scheme operating over a time-dispersive ISI channel can be modeled as a combined FSM, and correspondingly can be represented by a trellis structure called combined ISI-Code trellis. The states of this combined ISI-Code trellis are defined by [26],

$$\mu_n = (\alpha_n; a(n-1), a(n-2), \dots, a(n-L)) \quad \dots(3.7)$$

where the symbol sequence  $\{a(n-1), a(n-2), \dots, a(n-L)\}$  corresponds to a path which takes the TCM encoder from a previous state  $\alpha_{n-L}$  to the present state  $\alpha_n$  in accordance with the TCM coding rule. The next state transition of the combined ISI-Code trellis is defined by

$$\mu_{n+1} = f(\mu_n, a(n)) \quad \dots(3.8)$$

where  $a(n)$  denotes the symbol allowed by the TCM coding rule along the transition

$$\mu_n \longrightarrow \mu_{n+1}$$

The states of the combined FSM can be expressed in terms of the symbol label sequence  $\{Y_{n-i}\}$  instead of  $\{a(n-i)\}$  in (3.7) as

$$\mu_n = (\alpha_n; Y_{n-1}, Y_{n-2}, \dots, Y_{n-L}) \quad \dots(3.9)$$

or equivalently, in terms of the input information sequence  $\{X_{n-i}\}$  as,

$$\mu_n = (\alpha_{n-L}; X_{n-1}, X_{n-2}, \dots, X_{n-L}) \quad \dots(3.10)$$

Since  $X_{n-i}$  can assume  $2^m$  possible values for a  $m$ -bit input, there will be  $(2^m)^L$  ISI states for each code state. Therefore, for an  $N_s$ -state TCM encoder, the combined FSM and hence the corresponding combined ISI-Code trellis will represent  $N_s \cdot (2^m)^L$  or  $N_s \cdot (M/2)^L$  states, where  $M=2^{m+1}$  represents the size of the signal constellation employed in the TCM scheme. From each state there will be  $(M/2)$  distinct transitions. Thus, the combined ISI-Code trellis represents all possible sequences of  $\{b(n)\}$ .

In the presence of ISI and AWGN, the optimum ML sequence estimator searches among all possible sequences  $\{b(n)\}$  of the combined ISI-Code trellis to find the sequence  $\{\hat{a}(n)\}$  which is closest to the noise corrupted received sequence  $\{r(n)\}$ , in the sense of Euclidean distance. This is accomplished by a soft-decision Viterbi decoder which operates on the combined trellis to determine  $\{\hat{a}(n)\}$  by recursively minimizing the survivor path metric as [26].

$$\tilde{M}_n(\mu_{n+1}) = \min_{\{\mu_n\} \rightarrow \mu_{n+1}} \left\{ \tilde{M}_{n-1}(\mu_n) + \left| r(n) - \sum_{i=0}^L g_i a(n-i) \right|^2 \right\} \quad \dots(3.11)$$

where the minimization is taken over all the trellis branch transitions originating from states  $\{\mu_n\}$  and merging into the successor state  $\mu_{n+1}$ . The second term represents the branch metric which takes into account the ISI cancellation due to the past symbols  $\{a(n-i)\}$ . The computations and storage requirements of the decoder is dependent on the state complexity of the combined ISI-Code trellis which is  $N_s \cdot (M/2)^L$ , for a constellation of size  $M$  and ISI of memory length  $L$ .



### 3.4 TRELLIS STRUCTURES FOR COMBINED MLSE EQUALIZATION AND TCM DECODING

In the following, we present several combined ISI-Code trellis structures for the decoding of Trellis-coded QAM signals transmitted over an ISI channel of memory length  $L$ .

#### 3.4.1 The 16-State Combined ISI-Code Trellis for 4-State 4-QAM TCM ( $L=2$ )

Consider the transmission of 4-state 4-QAM TCM signals over an ISI channel of memory length  $L=2$ . For the TCM encoder of Fig.2.3(a), with a constellation size of  $M=2^{m+1}=4$ , we have  $N_s=4$  and  $m=1$ . For each code state there will be  $(M/2)^L=2^{mL}=4$  ISI states and thus number of states in the combined ISI-Code trellis is  $N_s \cdot 2^{mL}=16$ .

The present state and the next state of the combined ISI-Code trellis, using (3.7), are given by

$$\mu_n = (\alpha_n; a(n-1), a(n-2)) \quad \dots(3.12)$$

and 
$$\mu_{n+1} = (\alpha_{n+1}; a(n), a(n-1)) \quad \dots(3.13)$$

where  $\alpha_n$  and  $\alpha_{n+1}$  are the states of the 4-state TCM encoder defined by  $\alpha_n = x_{n-2}^1 x_{n-1}^1$  and  $\alpha_{n+1} = x_{n-1}^1 x_n^1$ , and  $a(n-2)$ ,  $a(n-1)$  are the two previous symbols represented by the combined state  $\mu_n$  at time  $n$ , and  $a(n)$  is the data symbol allowed by the TCM coding rule along the transition  $\mu_n \rightarrow \mu_{n+1}$ . For the 4-state 4-QAM TCM, we can write  $a(n-i)$  in terms of symbol label  $Y_{n-i} = (y_{n-i}^1, y_{n-i}^0)$ , where  $y_{n-i}^1 = x_{n-i}^1 \otimes x_{n-i-2}^1$  and  $y_{n-i}^0 = x_{n-i-1}^1$  for  $0 \leq i \leq 2$ . Therefore upon substitution and simplification, (3.12) and (3.13) can be expressed as

$$\mu_n = (x_{n-4}^1, x_{n-3}^1, x_{n-2}^1, x_{n-1}^1) \quad \dots(3.14)$$

and 
$$\mu_{n+1} = (x_{n-3}^1, x_{n-2}^1, x_{n-1}^1, x_n^1) \quad \dots(3.15)$$

It can easily be verified that use of (3.10) will also result in the form of (3.14) and (3.15). Realization of (3.14) and (3.15) results in a 16-state combined

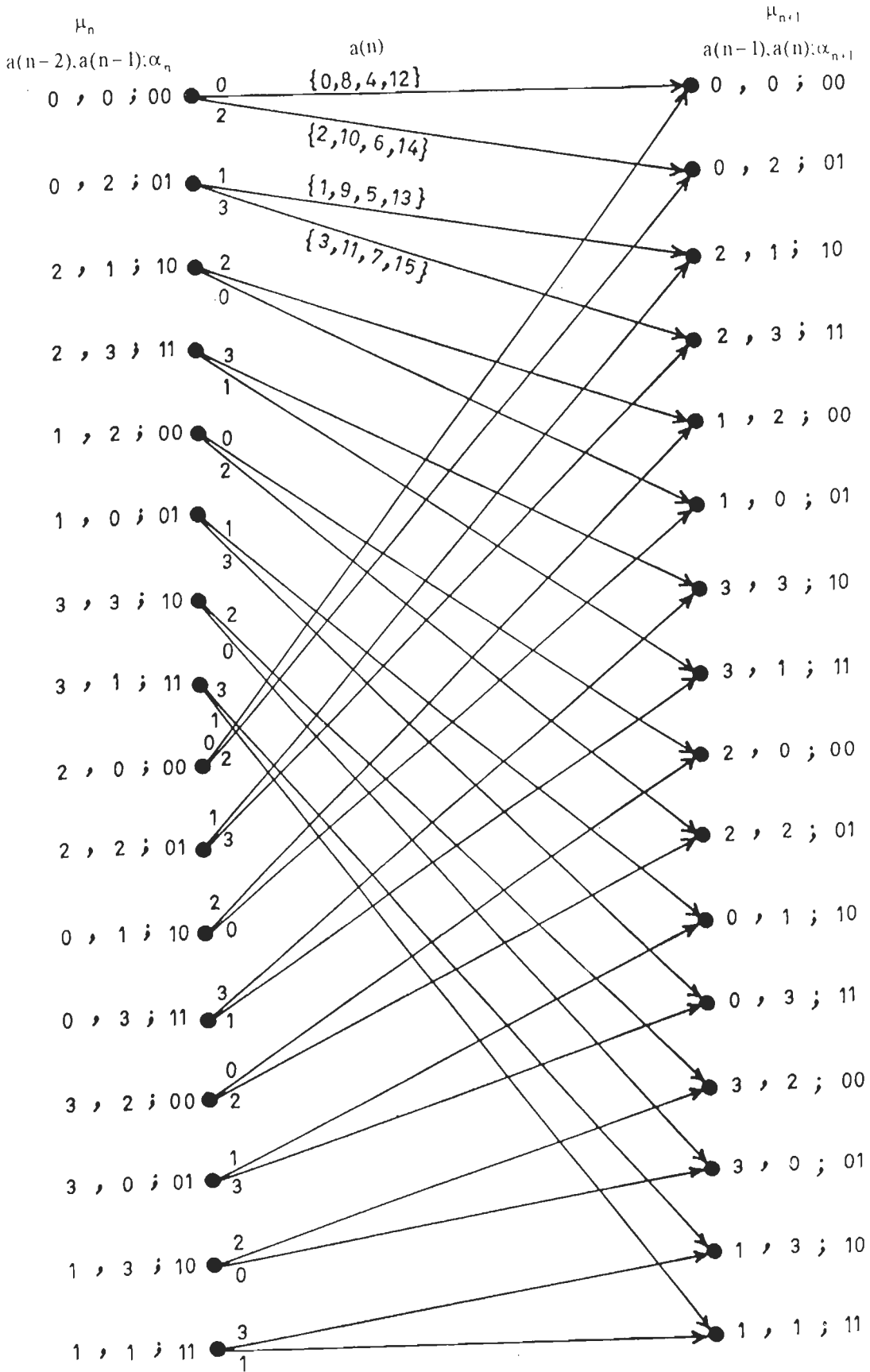


FIG.3.6 THE 16-STATE COMBINED ISI-CODE TRELLIS STRUCTURE, FOR 4-STATE 4-QAM TCM TRANSMISSION OVER AN ISI CHANNEL OF MEMORY LENGTH  $L=2$

ISI-Code trellis structure as shown in Fig.3.6. It may be noted that each state represents two previous symbols associated with it and each transition is a distinct transition.

### 3.4.2 The 32-State Combined ISI-Code Trellis for 4-state 16-QAM TCM (L=1)

We next consider 4-state 16-QAM TCM transmission over an ISI channel of memory length L=1. For the TCM encoder of Fig.2.3(a), with a constellation size of  $M=2^{m+1}=16$ , we have  $N_s=4$ , and  $m=3$ . Since each code state is associated with  $(M/2)^L=2^{mL}=8$  ISI states, the number of states in the combined ISI-Code trellis is  $N_s.(M/2)^L=32$ . With the use of (3.7), the present state and the next state are given by

$$\mu_n = (\alpha_n; a(n-1)) \quad \dots(3.16)$$

and 
$$\mu_{n+1} = (\alpha_{n+1}; a(n)) \quad \dots(3.17)$$

With  $\alpha_n = (x_{n-2}^1, x_{n-1}^1)$ ,  $\alpha_{n+1} = (x_{n-1}^1, x_n^1)$  and  $a(n) = (y_n^3, y_n^2, y_n^1, y_n^0)$  where  $y_n^3 = x_n^3$ ,  $y_n^2 = x_n^2$ ,  $y_n^1 = x_{n-2}^1 \oplus x_n^1$  and  $y_n^0 = x_{n-1}^1$ , we can write  $\mu_n$  and  $\mu_{n+1}$  upon simplification as

$$\mu_n = (x_{n-3}^1, x_{n-2}^1, x_{n-1}^1, x_{n-1}^2, x_{n-1}^3) \quad \dots(3.18)$$

and 
$$\mu_{n+1} = (x_{n-2}^1, x_{n-1}^1, x_n^1, x_n^2, x_n^3) \quad \dots(3.19)$$

The realization of (3.18) and (3.19) leads to a 32-state trellis structure as shown in Fig.3.7.

### 3.4.3 The 128-State Combined ISI-Code Trellis for 4-State 64-QAM TCM (L=1)

We next consider the transmission of 4-state 64-QAM TCM signals over a time-dispersive channel of memory length L=1. The TCM encoder is the same as in the previous examples, with the exception that  $m=5$  as the constellation size is  $M=2^{m+1}=64$ . Each code state has  $2^{mL}=32$  ISI states and the number of states in the combined ISI-Code trellis is  $N_s.(M/2)^L=128$ . Again, the states of this combined

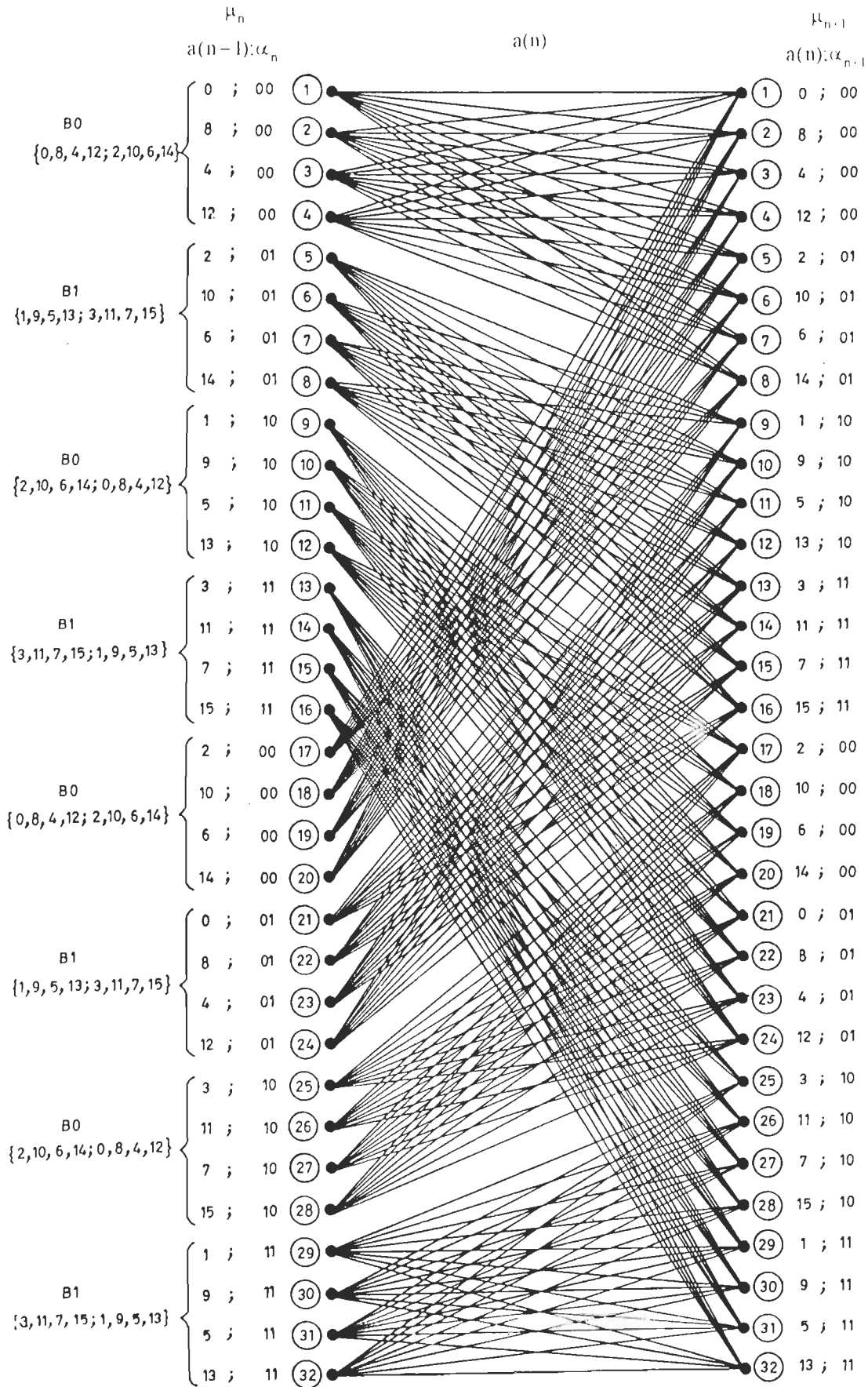


FIG.3.7 THE 32-STATE COMBINED ISI-CODE TRELLIS STRUCTURE, FOR 4-STATE 16-QAM TCM TRANSMISSION OVER AN ISI CHANNEL OF MEMORY LENGTH L=1

trellis are as defined by (3.16) and (3.17), where  $a(n)$  corresponds to a signal point of the 64-point QAM constellation. From each state of the combined ISI-Code trellis there will be  $2^m=32$  distinct transitions. Each of the combined state  $\mu_n$  provides information about the previous symbol  $a(n-1)$ , as depicted in (3.16). Note that the data symbol  $a(n-1)$  can equivalently be expressed in terms of the input  $X_{n-1}$  as  $X_{n-1}=(x_{n-1}^1, x_{n-1}^2, x_{n-1}^3, x_{n-1}^4, x_{n-1}^5)$  and similarly  $a(n)$  by the input  $X_n=(x_n^1, x_n^2, x_n^3, x_n^4, x_n^5)$ . For the 4-state TCM encoder of Fig.2.3(a), we have  $\alpha_n=x_{n-2}^1 x_{n-1}^1$  and therefore we can write  $\alpha_{n-1}=x_{n-3}^1 x_{n-2}^1$ . Making use of the state definition (3.10), the present state and the next state of the combined ISI-Code trellis are given by the simplified expressions as,

$$\mu_n=(x_{n-3}^1, x_{n-2}^1, x_{n-1}^1, x_{n-1}^2, x_{n-1}^3, x_{n-1}^4, x_{n-1}^5) \quad \dots(3.20)$$

and 
$$\mu_{n+1}=(x_{n-2}^1, x_{n-1}^1, x_n^1, x_n^2, x_n^3, x_n^4, x_n^5) \quad \dots(3.21)$$

The input  $(x_n^1, x_n^2, x_n^3, x_n^4, x_n^5)$  determines the symbol  $a(n)$  associated with the transition  $\mu_n \rightarrow \mu_{n+1}$ . Realization of (3.20) and (3.21) leads to a 128-state combined ISI-Code trellis structure for the decoding of 4-state 64-QAM TCM signals operating over an ISI channel of length  $L=1$ . Due to reasons of complexity in sketching the trellis structure is not shown.

### 3.4.4 The 64-State Combined ISI-Code Trellis for 8-State 16-QAM TCM ( $L=1$ )

We next consider the transmission of 8-state 16-QAM TCM signals over a time-dispersive channel of memory length  $L=1$ . The TCM encoder is the same as that shown in Fig.2.3(b), with  $m=3$  and  $M=16$ . Each code state has  $2^{mL}=8$  ISI states and the number of states in the combined ISI-Code trellis is  $N_s(M/2)^L=64$ . Again, the states of this combined trellis are as defined by (3.16) and (3.17), where  $a(n)$  corresponds to a signal point of the 16-point QAM constellation. From each state of the combined ISI-Code trellis there will be  $2^m=8$  distinct transitions. Each of the combined state  $\mu_n$  provides information about one previous symbol  $a(n-1)$ , as

depicted by (3.16). Note that the data symbol  $a(n-1)$  can equivalently be expressed in terms of the input  $X_{n-1}$  as  $X_{n-1}=(x_{n-1}^1, x_{n-1}^2, x_{n-1}^3)$  and similarly  $a(n)$  by  $X_n=(x_n^1, x_n^2, x_n^3)$ . Also, for a 8-state TCM encoder we have  $\alpha_{n-1}=x_{n-3}^1 x_{n-2}^2 x_{n-2}^1$  and therefore we can write  $\alpha_n=x_{n-2}^1 x_{n-1}^2 x_{n-1}^1$ . Making use of the state definition (3.10), the present state and the next state of the combined ISI-Code trellis are given by the simplified expressions as,

$$\mu_n=(x_{n-3}^1, x_{n-2}^2, x_{n-2}^1, x_{n-1}^2, x_{n-1}^1, x_{n-1}^3) \quad \dots(3.22)$$

and 
$$\mu_{n+1}=(x_{n-2}^1, x_{n-1}^2, x_{n-1}^1, x_n^2, x_n^1, x_n^3) \quad \dots(3.23)$$

The input  $(x_n^1, x_n^2, x_n^3)$  determines the symbol  $a(n)$  associated with the transition  $\mu_n \rightarrow \mu_{n+1}$ . Realization of (3.22) and (3.23) leads to a 64-state combined ISI-Code trellis structure for the decoding of 8-state 16-QAM TCM signals operating over an ISI channel of length  $L=1$ . Due to reasons of complexity in sketching, the trellis structure is not shown.

From the above examples, we observe that the state complexity of the combined ISI-Code trellis structure increases with an increase in constellation size  $M$  and/or memory length  $L$ . In particular, the complexity grows exponentially with  $L$  because of the relation  $N_s \cdot (M/2)^L$ . To illustrate the increase in state complexity with  $L$ , consider a combined ISI-Code trellis for 4-state 16-QAM TCM ( $N_s=4, M=16$ ) and an ISI channel of memory length  $L=3$ . The number of states in the combined ISI-Code trellis is  $N_s \cdot (M/2)^L=2048$ . For a 4-state 64 QAM TCM ( $N_s=4, M=64$ ) and  $L=3$ , the number of states in the combined ISI-Code trellis is  $N_s \cdot (M/2)^L=2^{17}$ . Thus with a 4-state TCM employing 16-QAM, the state complexity of the combined ISI-Code trellis increases from 32 for  $L=1$  to 2048 for  $L=3$ , while for the same TCM employing 64 QAM it increases from 128 for  $L=1$  to  $2^{17}$  for  $L=3$ . Therefore, the combined ISI-Code trellis structure, although optimum, becomes unrealistic even for moderate ISI ( $L \leq 3$ ).

In all the above examples, the decoding is accomplished by the implementation of (3.11) through the Viterbi algorithm which operates on the combined ISI-Code trellis, and the resulting receiver structure is optimum. Since the performance of the optimum MLSE (VA) for uncoded systems can be analyzable through bounds [46, 79], we consider below a method for evaluating the performance of the combined ISI-Code receiver structures through bounds.

### 3.5 PERFORMANCE EVALUATION OF MLSE RECEIVER USING COMBINED ISI-CODE TRELLIS THROUGH BOUNDS

It is possible to predict the performance of the combined MLSE receiver, which employs the Viterbi algorithm on the combined ISI-Code trellis structure, by computing the minimum ED  $d_{\min}$  and its multiplicity number  $N_{d_{\min}}$  of the minimum distance error event. For a given channel impulse response, the error probability can be computed by analyzing the error structure of the channel [79].

Let  $g_0, g_1, \dots, g_L$  be the discrete-time channel tap gains and the ISI memory length be  $L$ . Using the delay operator  $D$ , the channel response can be expressed as

$$g(D) = g_0 + g_1 D + g_2 D^2 + \dots + g_L D^L \quad \dots(3.24)$$

Consider an input error sequence of length  $k$ , defined by

$$\epsilon_1(D) = e_{10} + e_{11} D + e_{12} D^2 + \dots + e_{1(k-1)} D^{k-1} \quad \dots(3.25)$$

where

$$e_{1j} = a(j) - \hat{a}(j), \quad \dots(3.26)$$

with  $a(j)$  = transmitted (encoded) symbol, and  $\hat{a}(j)$  = estimated (decoded) symbol, under ISI-free condition.

Since the ISI channel is linear, the channel output error sequence  $\epsilon_0(D)$  is related to  $\epsilon_1(D)$  and  $g(D)$  by

$$\begin{aligned} \epsilon_0(D) &= \epsilon_1(D) \cdot g(D) \\ &= e_{00} + e_{01} D + e_{02} D^2 + \dots + e_{0(n-1)} D^{n-1} \quad \dots(3.27) \end{aligned}$$

where  $n=k+L$  represents the length of the error event at the channel output, for an input error event of length  $k$  and ISI channel for memory length  $L$ .

The Euclidean weight  $d^2(\epsilon)$  of an output error event is defined as the energy associated with the output error sequence of the channel, and is given by

$$d^2(\epsilon) = \|\epsilon_o\|^2 = \sum_{i=0}^{n-1} e_{oi}^2 \quad \dots(3.28)$$

The error rate performance of the VA receiver depends upon  $d_{\min}^2$ , the minimum weight of any error event. If the channel is known, then  $d_{\min}^2$  can be determined by considering all possible error sequences and computing the resultant error weights of the corresponding output error sequences. Then the performance of the VA receiver operating on the combined ISI-Code trellis can be evaluated using an upper bound estimate given by [46, 79].

$$P_e \leq N_{d_{\min}} Q(d_{\min}/2\sigma_v) \quad \dots(3.29)$$

where  $\sigma_v^2$  is the variance of the AWGN process in each dimension,  $d_{\min}^2$  the minimum weight of all possible output error events,  $N_{d_{\min}}$  multiplicity number and  $Q(\cdot)$  is the Gaussian error integral function, as defined earlier in section 2.6.

In order to compute  $d_{\min}$  for the combined ISI-Code trellis, we consider all possible error events of the TCM scheme. For each error event we can define an input error sequence  $\epsilon_i(D)$  from which the corresponding output error sequence  $\epsilon_o(D)$  and its weight  $d^2(\epsilon)$  can be determined. For a given set of error events of the TCM scheme employed, we obtain correspondingly a set of output error sequences and hence a set of Euclidean weight  $\{d^2(\epsilon)\}$ . The minimum weight in the set  $\{d^2(\epsilon)\}$  then represents the  $d_{\min}^2$  of the combined ISI-Code trellis.

The distance spectrum computing algorithm (of section 2.6) has been employed to determine the input error sequences of the first few error events of the TCM scheme. For a given channel response  $g(D)$ , the corresponding output error sequences and their weights are computed, and hence  $d_{\min}^2$ . Therefore, an asymptotic



upper bound on the error event probability  $P_e$  can be estimated by considering the error events of the basic TCM scheme and the discrete channel response. The bounds so evaluated to determine the MLSE performance of the combined ISI-Code trellis are presented in the following section along with the simulation results.

### 3.6 RESULTS AND DISCUSSION

In this section, we present the error performance of the optimum combined MLSE receiver structure, that makes use of the combined ISI-code trellis, for the decoding of trellis-coded QAM signals in the presence of ISI and AWGN. The error performance of the various combined MLSE structures are evaluated through bounds and simulation. The reference system employed for the performance comparison is an uncoded MLSE structure having the same data rate, bandwidth and signal energy. The ISI channel is assumed to be time-invariant and its discrete-time impulse response is known at the receiver.

For the performance study of the baseband TCM data transmission system of Fig.3.4, we consider the implementation of its equivalent combined discrete-time white noise model shown in Fig.3.5. Following the simulation procedure as detailed earlier in section 2.7, we generate an i.i.d. sequence of trellis-coded QAM data symbols. The sequence of TCM data symbols  $\{a(n)\}$  is convolved with the discrete-time impulse response  $\{g_i\}$  of the ISI channel to arrive at the filtered output  $b(n)$ . The discrete complex-valued AWGN  $v(n)$  is then added to  $b(n)$  to obtain the received signal  $r(n)=b(n)+v(n)$ .

The sequence of noise corrupted received signals  $\{r(n)\}$  is then applied to a maximum-likelihood Viterbi decoder, which searches for a minimum cost path along the combined ISI-code trellis to find a sequence of estimated data symbols which is closest to the received sequence.

The discrete-time impulse response of the different ISI channels considered on this study have been given in Table 3.1. It may be noted that  $L$  represents the

**Table 3.1 Equivalent discrete-time impulse response of the different ISI channels**

ISI memory length	Channel label	Channel Coefficients			
		$g_0$	$g_1$	$g_2$	$g_3$
L=1	CH11	0.7746	0.6325	-	-
	CH12	0.8367	0.5477	-	-
	CH13	0.8944	0.4472	-	-
	CH14	0.7071	0.7071	-	-
L=2	CH21	0.7746	0.5000	0.3873	-
	CH22	0.8367	0.4472	0.3162	-
	CH23	0.8944	0.3873	0.2236	-
	CH24	0.4070	0.8170	0.4070	-
	CH25	0.2600	0.9300	0.2600	-
	CH26	0.3040	0.9030	0.3040	-
L=3	CH31	0.6325	0.5477	0.4472	0.3162
	CH32	0.7746	0.5000	0.3162	0.2246
	CH33	0.8367	0.3873	0.2739	0.1581

**Table 3.2 The different combined ISI-Code MLSE structures and the corresponding reference systems**

Sl. No.	ISI Length	Coded System		Uncoded Reference		Reference
		TCM Scheme	Combined MLSE structure	Uncoded system	Uncoded MLSE trellis	
1	1	4-state 4-QAM	8-state combined ISI-Code trellis	2-QAM	2-state ISI trellis	-
2	2	4-state 4-QAM	16-state combined ISI-Code trellis	2-QAM	4-state ISI trellis	Section 3.4.1
3	3	4-state 4-QAM	32-state combined ISI-Code trellis	2-QAM	8-state ISI trellis	-
4	1	4-state 16-QAM	32-state combined ISI-Code trellis	8-QAM	8-state ISI trellis	Section 3.4.2
5	1	4-state 64-QAM	128-state combined ISI-Code trellis	32-QAM	32-state ISI trellis	Section 3.4.3
6	1	8-state 16-QAM	64-state combined ISI-Code trellis	8-QAM	8-state ISI trellis	Section 3.4.4

memory length of the ISI channel and for each channel  $\sum_{k=0}^L |g_k|^2 = 1$ . The choice of the channel is somewhat arbitrary except that all the zeroes of the transfer function are limited to within the unit circle and thus the channel has the minimum phase property [117]. The channels shown in Table 3.1 are also employed in our further study, in Chapters 4 and 5, on the performance of the various receiver structures for the decoding of TCM signals transmitted over time-invariant known ISI channels in the presence of additive white Gaussian noise.

The reference system employed for the performance comparison is an uncoded MLSE receiver structure [46] implemented through the Viterbi algorithm. The VA operates on an  $\underline{M}^L$ -state ISI trellis structure, the states of which are as defined by (3.3), where  $\underline{M}$  corresponds to the size of signal constellation used for the uncoded transmission and  $L$  is the ISI memory length. To illustrate, we consider the design of an MLSE structure for the uncoded 8-QAM transmission system over an ISI channel of memory length  $L=1$ . With  $\underline{M}=8$  and  $L=1$ , the number of states in the ISI trellis structure is  $\underline{M}^L=(8)^1=8$ . The present state and the next state, using (3.3), are given respectively as

$$s_n = a(n-1) \quad \dots(3.30)$$

and  $s_{n+1} = a(n) \quad \dots(3.31)$

where  $a(n)$  is the uncoded data symbol transmitted at time instant  $n$  and corresponds to a signal point of the 8-QAM constellation as determined by the 3-bit binary input  $X_n=(x_n^1 \ x_n^2 \ x_n^3)$ . From each state of the ISI trellis, there will be  $\underline{M}=8$  distinct transections that corresponds to the 8-possible values of the input binary sequence  $(x_n^1 \ x_n^2 \ x_n^3)$ . The decoding is accomplished through the implementation of the Viterbi algorithm on the 8-state ISI trellis.

The performance of this uncoded MLSE structure is then employed as the reference to compute the gain achieved with the use of the combined ISI-code trellis structures for the decoding of 16-QAM TCM schemes over an ISI channel of memory length  $L=1$  (namely the combined MLSE structures of sections 3.4.2 and

3.4.4). The Table 3.2 gives the list of coded MLSE receiver structures and the corresponding uncoded MLSE reference systems used in this study.

The procedure as detailed in section 3.5 is made use of in computing the error performance through bounds. Table 3.3 gives the result of the computations of the Euclidean weight  $d^2(\epsilon)$  of the output error sequences for a given channel impulse response and the TCM scheme considered. The Table 3.3 also shows, for each code considered, the minimum squared distance  $d_{\min}^2$  and its multiplicity number  $N_d$ . Table 3.4 gives the summary of distance computation for the various combined ISI-code trellis structures considered in this study.

An estimate of the upper bound on the error event probability of the combined ISI-code trellis structure is then evaluated using the relation (3.26) or equivalently [7],

$$P_{e,UB} \approx (1/2) \cdot N_{d_{\min}} \cdot \text{erfc} (d_{\min} / \sqrt{8} \sigma_v) \quad \dots(3.32)$$

where  $\sigma_v^2$  represents the variance of the AWGN process in each dimension. The lower bound on the error event probability is computed using the relation,

$$P_{e,LB} \approx (1/2) \cdot \text{erfc} (d_{\min} / \sqrt{8} \sigma_v) \quad \dots(3.33)$$

The Table 3.5 gives the results of the error performance computations for some of the combined MLSE receiver structures for trellis-coded M-QAM signal transmission over ISI channels of limited memory length ( $L \leq 3$ ). The error event probability has been evaluated through bounds using the parameters given in Table 3.4, and also through simulation. Table 3.5 includes also the simulation results on the performance of the uncoded MLSE structure which is used as the reference system for comparison. In the decoding of the combined ISI-code trellis structure with  $2^\gamma$ -states, a decision delay of  $\delta = 6 \cdot \gamma$  has been employed in the implementation of the Viterbi algorithm. Due to huge computational burdens involved in the decoding of the 64-state and 128-state combined ISI-code trellis structures of section 3.4.3 and 3.4.4, the simulation runs were limited to data symbol

Table 3.3 Computation of  $d^2(\epsilon)$  of the output error sequences for some typical TCM codes and ISI channels

Basic TCM Scheme	ISI Channel		Error sequences and their corresponding Euclidean weights										Minimum distance Parameters		
	Length	Type												$d_{\min}^2$	$N_d$
4-State 4-QAM TCM	L=1	CH12	ISL	3	4	5	6	7	8	9	10	11			
			EW	20.0	24.0	24.0	28.0	28.0	32.0	32.0	36.0	36.0			
			OSL	4	5	6	7	8	9	10	11	12			
			EW	12.67	13.0	16.67	17.00	20.67	21.00	24.67	25.00	28.67	12.67	8	
4-State 4-QAM TCM	L=2	CH23	OSL	5	6	7	8	9	10	11	12	13			
			EW	13.35	13.48	16.81	16.94	21.35	21.48	25.89	26.02	30.43	13.35	8	
4-State 4-QAM TCM	L=3	CH31	OSL	6	7	8	9	10	11	12	13	14			
			EW	14.56	18.16	20.88	19.68	25.76	24.56	30.63	29.43	32.31	14.56	8	
4-State 16-QAM TCM	L=1	CH11	ISL	3	4	5	6	7	8	9	10	11			
			EW	20.0	24.0	24.0	28.0	28.0	32.0	32.0	36.0	36.0			
			OSL	4	5	6	7	8	9	10	11	12			
			EW	12.16	35.76	16.16	31.92	20.16	35.92	24.16	39.92	28.16	12.16	8	
4-State 64-QAM TCM	L=1	CH13	ISL	3	4	5	6	7	8	9	10	11			
			EW	20.0	24.0	24.0	28.0	28.0	32.0	32.0	36.0	36.0			
			OSL	4	5	6	7	8	9	10	11	12			
			EW	13.0	14.1	16.8	20.4	24.7	29.2	23.2	27.6	31.8	12.0	32	
8-State 16-QAM TCM	L=1	CH13	ISL	3	4	5	6	7	8	9	10	11			
			EW	20.0	24.0	24.0	24.0	28.0	28.0	28.0	32.0	32.0			
			OSL	4	5	6	7	8	9	10	11	12			
			EW	14.6	23.2	27.2	20.8	27.2	31.2	24.8	31.2	35.2	14.6	16	

Note : ISL - Input sequence length. OSL-Output sequence length. EW-Euclidean weight

Table 3.4 Summary of minimum distance calculation for various combined ISI-code trellis structures

Sl. No.	TCM Scheme	ISI length	Combined ISI-code trellis	Minimum distance parameters											
				Channel type		$d_{\min}^2$	$N_d$								
1	4-state 4-QAM TCM	a) L=1	8-state combined MLSE	CH11 12.2	12	CH12 12.67	8	CH13 13.67	8	CH14 12.0	12	-	-		
		b) L=2	16-state combined MLSE	CH21 12.08	8	CH22 12.4	8	CH23 12.7	8	CH24 10.7	12	CH25 13.35	8	CH26 12.3	8
		c) L=3	32-state combined MLSE	CH31 14.56	8	CH32 15.3	8	CH33 13.52	8	-	-	-	-	-	
2	4-state 16-QAM TCM	L=1	32-state combined MLSE	CH11 12.16	8	CH12 12.67	8	CH13 13.6	8	CH14 12.0	12	-	-		
3	4-state 64-QAM TCM	L=1	128-state combined MLSE	CH11 12.16	32	CH12 12.67	32	CH13 13.6	32	CH14 12.0	48	-	-		
4	8-state 16-QAM TCM	L=1	64-state combined MLSE	CH11 13.67	16	CH12 12.67	16	CH13 14.6	16	CH14 13.2	32	-	-		

Table 3.5 Error event performance of the combined ISI-code receivers for some typical ISI channels

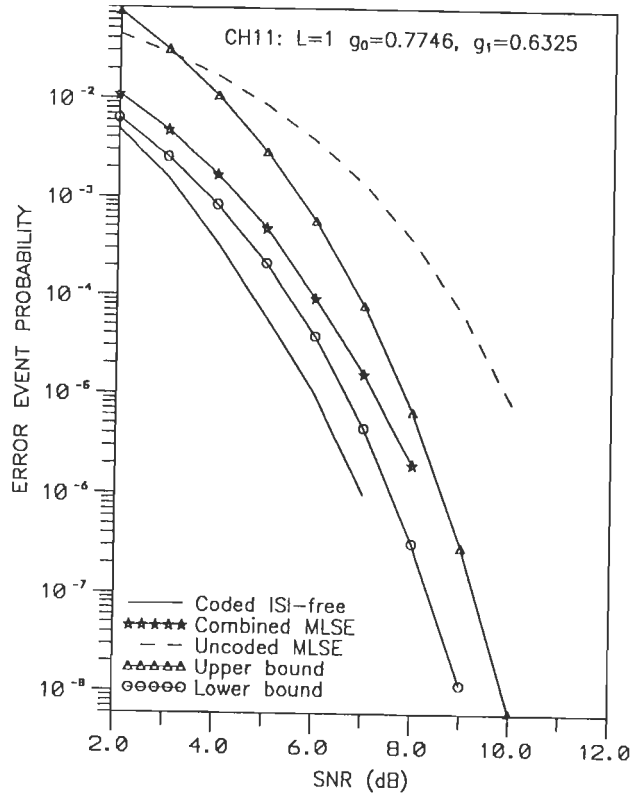
Sl. No.	Combined MLSE structures	ISI channel	SNR dB	$\sigma_v$	Error event Probability (Coded)			Uncoded MLSE structure (simulation)
					Lower bound $P_{e, LB}$	Upper bound $P_{e, UB}$	Simulation $P_e$	
1	8-state combined ISI-code trellis (4-state 4-QAM TCM; L=1) Fig. 3.8(b)	CH12 (L=1)	2.0	0.7943	0.808E-02	0.368E-01	0.142E-01	0.419E-01
			4.0	0.6310	0.123E-02	0.538E-02	0.215E-02	0.156E-01
			6.0	0.5012	0.689E-04	0.293E-03	0.770E-04	0.328E-02
			8.0	0.3981	0.797E-05	0.332E-05	0.900E-05	0.282E-03
2	16-state combined ISI-code trellis (4-state 4-QAM TCM; L=1) Fig. 3.9(c)	CH23 (L=2)	2.0	0.7943	0.107E-01	0.493E-01	0.103E-01	0.223E-01
			4.0	0.6310	0.189E-02	0.833E-02	0.169E-02	0.817E-02
			6.0	0.5012	0.134E-03	0.570E-03	0.154E-03	0.173E-02
			8.0	0.3981	0.128E-05	0.510E-05	0.200E-05	0.146E-03
3	32-state combined ISI-code trellis (4-state 4-QAM TCM; L=1) Fig. 3.10(a)	CH32 (L=3)	2.0	0.7943	0.105E-01	0.418E-01	0.151E-01	0.164E-01
			4.0	0.6310	0.170E-02	0.747E-02	0.300E-02	0.721E-02
			6.0	0.5012	0.113E-04	0.483E-03	0.218E-03	0.144E-02
			8.0	0.3981	0.173E-05	0.721E-05	0.500E-05	0.130E-03
4	32-state combined ISI-code trellis (4-state 16-QAM TCM; L=1) Fig. 3.11(a)	CH11 (L=1)	10.0	0.7071	0.676E-02	0.184E+00	0.287E-01	0.635E-01
			12.0	0.5613	0.938E-03	0.245E-01	0.577E-02	0.206E-01
			14.0	0.4462	0.453E-04	0.115E-02	0.222E-03	0.307E-02
			16.0	0.3544	0.416E-06	0.104E-04	0.100E-05	0.139E-03
5	128-state combined ISI-code trellis (4-state 64-QAM TCM; L=1) Fig. 3.12(c)	CH13 (L=1)	16.0	0.7263	0.556E-02	0.150E+00	0.368E-01	0.829E-01
			18.0	0.5769	0.696E-03	0.180E-01	0.783E-02	0.277E-01
			20.0	0.4583	0.286E-04	0.726E-03	0.280E-04	0.428E-02
			22.0	0.3640	0.204E-06	0.506E-05	-	0.240E-03
6	64-state combined ISI-code trellis (8-state 16-QAM TCM; L=1) Fig. 3.13(b)	CH12 (L=1)	10.0	0.7071	0.592E-02	0.107E+00	0.206E-01	0.597E-01
			12.0	0.5613	0.766E-03	0.133E-01	0.245E-02	0.179E-01
			14.0	0.4462	0.332E-05	0.561E-03	0.510E-05	0.248E-02
			16.0	0.3544	0.256E-06	0.424E-05	-	0.107E-03

transmission length of the order of  $10^5$ , where as for other systems the simulation run length is of the order of  $10^6$ - $10^7$  symbols.

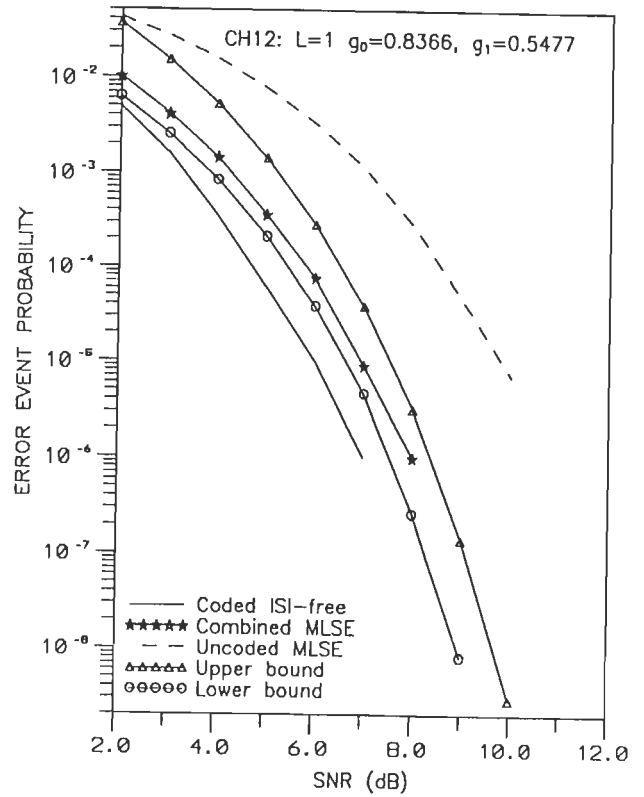
The error performance characteristics of the combined MLSE receiver structures considered in this study are given in Fig.3.8-3.13, for which the following comments are in order. For each case considered, we have given the error event performance of the combined MLSE structure obtained through simulation under an ISI-free environment as well as in the presence of ISI, which have been marked respectively as 'ISI-free' and 'Combined MLSE' in the legend of the figure. Also, we have given the error event performance of the uncoded MLSE reference system obtained through simulation which is marked as 'Uncoded MLSE' in the legend. The upper and lower bounds on the error event probability have been computed through the use of distance parameters, given in Table 3.4, using (3.32) and (3.33) respectively and have been marked accordingly in the legend as 'Upper bound' and 'Lower bound'.

The Fig.3.8 shows the error performance characteristics of the combined MLSE structure that uses an 8-state combined ISI-code trellis for the decoding of 4-state 4-QAM TCM signals transmitted over an ISI channel of memory length  $L=1$ , for 4 different values of channel coefficients (CH11-CH14). From the performance characteristics of Fig.3.8(a) for channel CH11, we note that the combined MLSE structure achieves a coding gain of nearly 2.75 dB at  $P_e=10^{-5}$ , although its performance is about 1.25 dB degraded with respect to ISI-free AWGN performance. Similarly we observe that the coded MLSE structure achieves a gain of nearly 2.9 dB, 3.0 dB and 2.7 dB at  $P_e=10^{-5}$  relative to uncoded MLSE respectively, on channels CH12, CH13 and CH14, while the performance loss correspondingly is about 1 dB, 0.75 dB and 1.25 dB relative to the coded ISI-free performance. From Fig. 3.8(a)-(c) , we can note that CH13 gives the best performance, followed by CH12, CH11 and CH14 in that order. It may also be noted that the simulation results lie within the performance bounds evaluated through the use of procedure given in section 3.5.

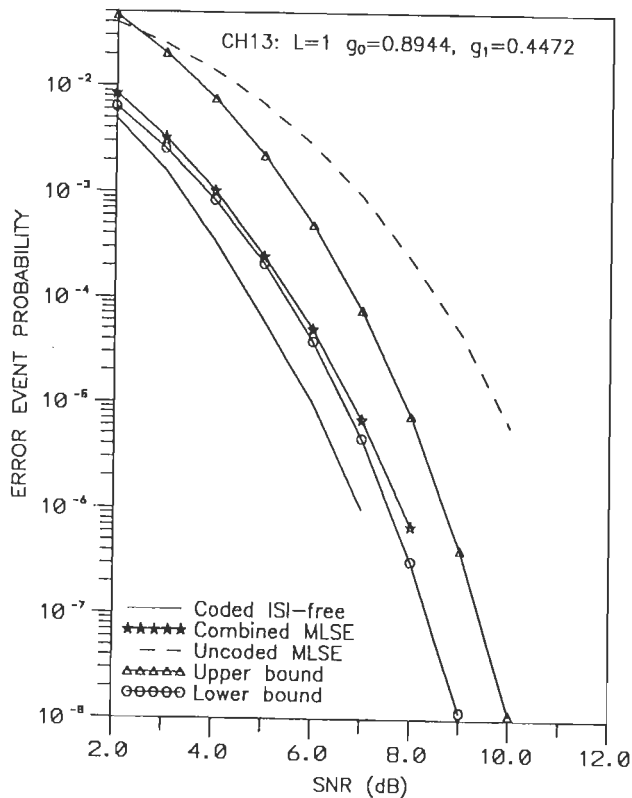




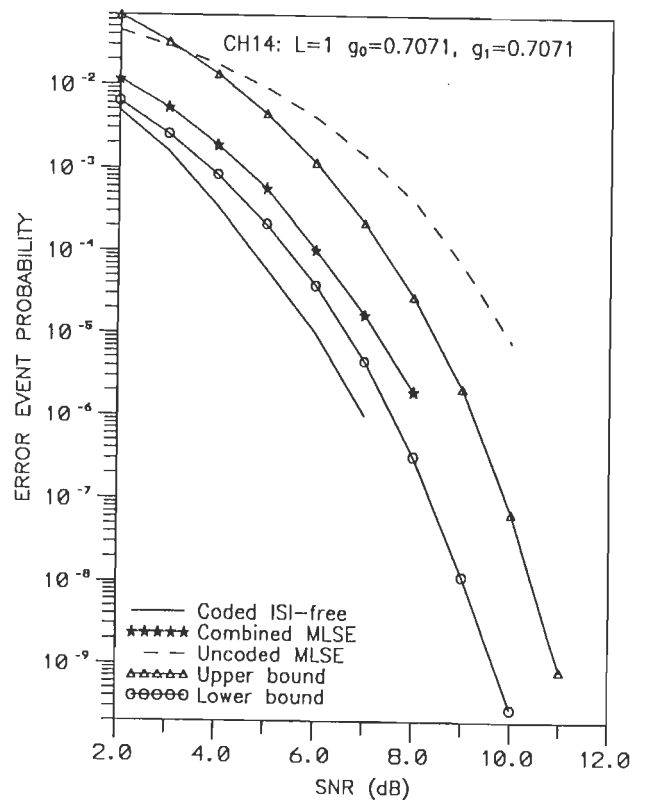
(a) ISI CHANNEL CH11:  $L=1$



(b) ISI CHANNEL CH12:  $L=1$



(c) ISI CHANNEL CH13:  $L=1$



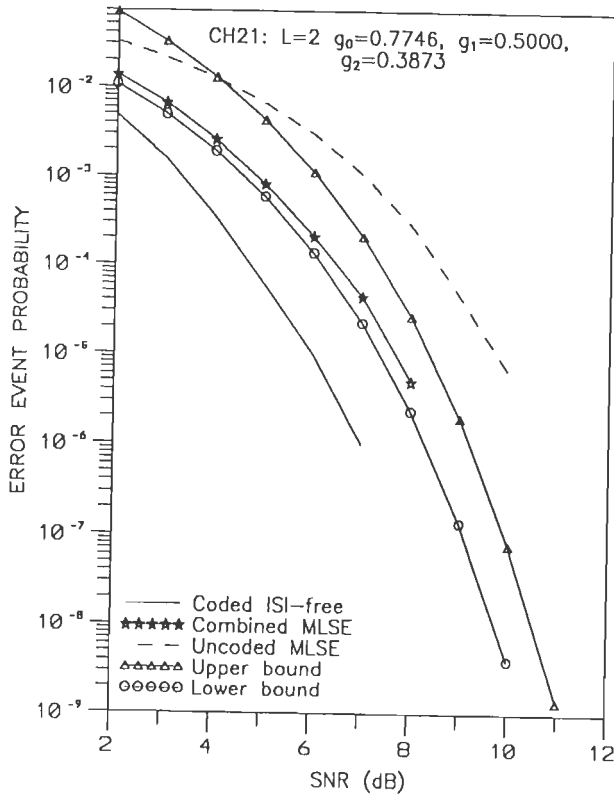
(d) ISI CHANNEL CH14:  $L=1$

FIG.3.8 ERROR PERFORMANCE OF THE COMBINED MLSE RECEIVER WHICH USES AN 8-STATE COMBINED ISI-CODE TRELLIS STRUCTURE FOR THE DECODING OF 4-STATE 4-QAM TCM SIGNALS TRANSMITTED OVER AN ISI CHANNEL OF MEMORY  $L=1$ .

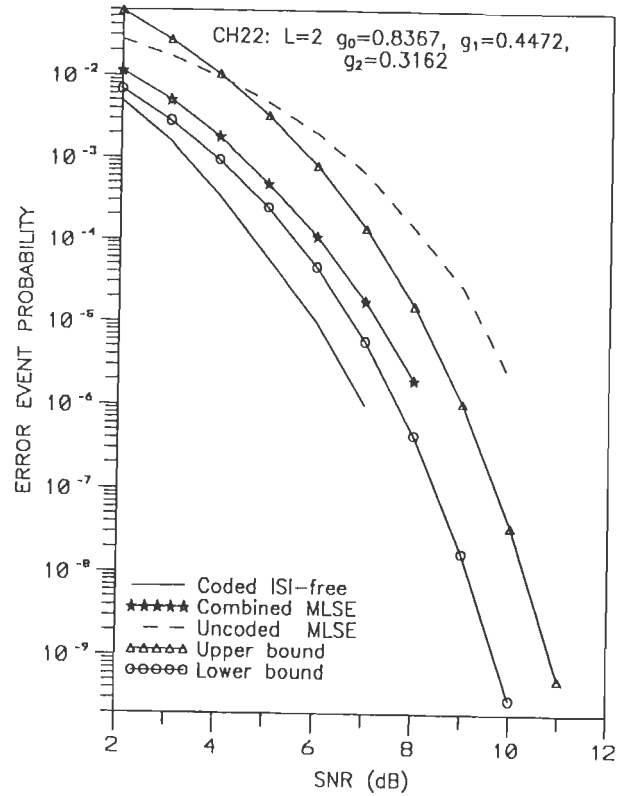
Fig.3.9 gives the performance of the combined MLSE receiver, that uses the 16-state combined ISI-Code trellis of section 3.4.1, for the decoding of 4-state 4-QAM TCM over an ISI channel of length  $L=2$ . From the performance characteristics given in Fig.3.9(a)–(f) for the 6 different channels considered, CH21–CH26, we note that the combined MLSE structure achieves a gain of about 2 – 3 dB at  $P_e=10^{-5}$  over uncoded MLSE structure, the details of which are listed in Table 3.6. Although the combined MLSE structure achieves a gain of 3 dB over uncoded MLSE on channel CH24 (Fig.3.9(d)), it exhibits a loss of 2dB over ISI-free condition. The performance on channel Ch23, as shown in Fig. 3.9(c), rather appears to be optimum with a gain of 2.75 dB over uncoded MLSE reference system while being nearly ISI-free with a degradation of only about 0.75 dB. In most cases, we may note that the performance degradation relative to the coded ISI-free performance is about 1.25–1.5 dB. Almost in all cases, the simulation results are well within the computed upper and lower bounds.

Fig.3.10 gives the performance characteristics of the combined MLSE structure, that employs a 32-state combined ISI-code trellis, for the decoding of 4-state 4-QAM TCM signals transmitted over an ISI channel of memory length  $L=3$ . For the ISI channel CH31, the combined MLSE structure achieves a gain of about 1.75 dB over uncoded MLSE, although it is degraded by about 1.7 dB relative to its ISI-free performance. On channel CH32, the coded MLSE structure achieves a gain of 2.25 dB relative to the uncoded MLSE, but with a performance loss of about 1.25 dB over its ISI-free performance.

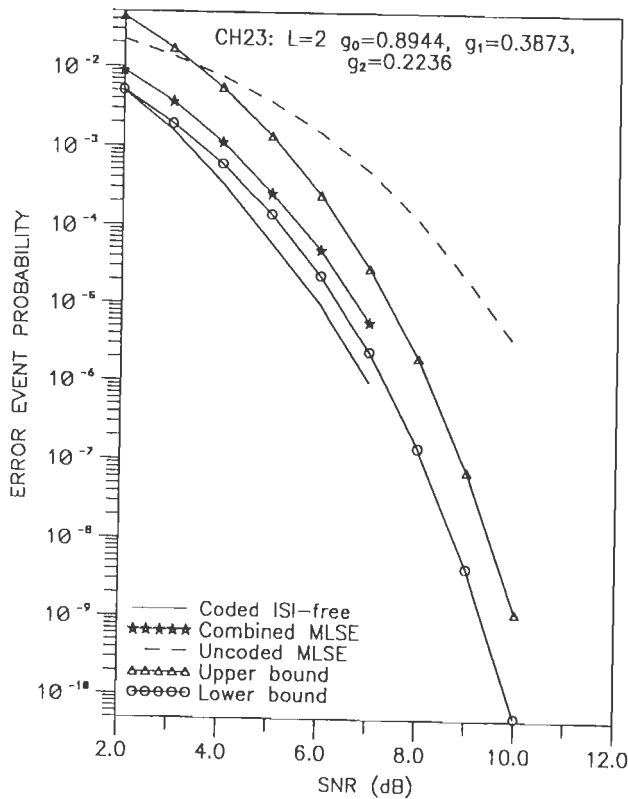
We consider next, the performance characteristics of the combined MLSE structure that makes use of the 32-state combined ISI-code trellis, as discussed earlier in section 3.4.2, for the decoding for 4-state 16-QAM TCM signals transmitted over an ISI channel of memory length  $L=1$ . Shown in Fig.3.11(a)-(d) are the characteristics of the receiver structure for 4 different ISI channels of memory length  $L=1$ . Although it suffers a performance degradation of 1 – 1.9 dB relative to its ISI-free performance at  $P_e=10^{-5}$  the coded combined MLSE structure



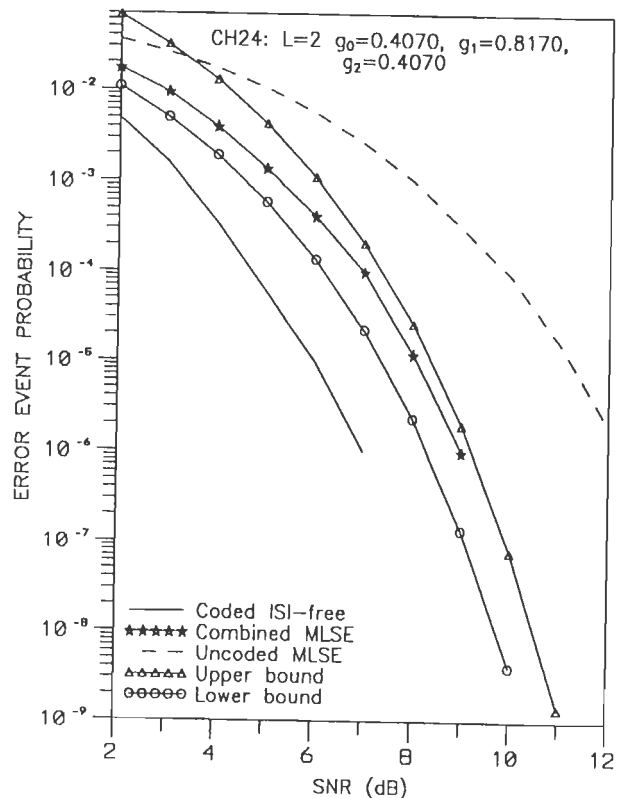
(a) ISI CHANNEL CH21:  $L=2$



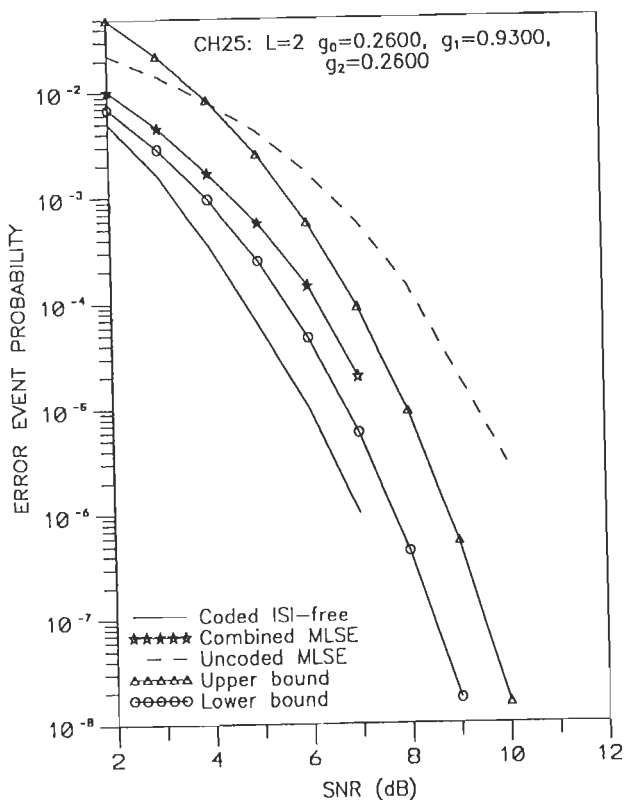
(b) ISI CHANNEL CH22:  $L=2$



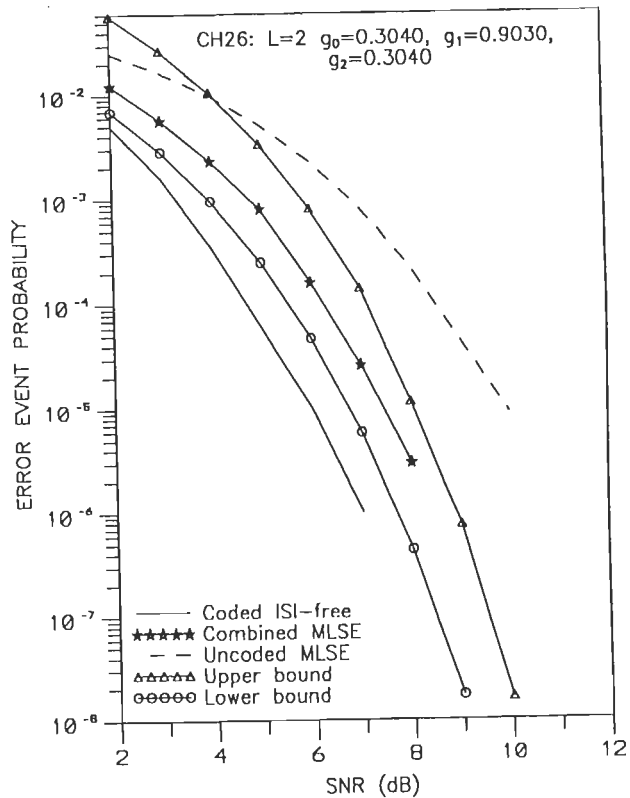
(c) ISI CHANNEL CH23:  $L=2$



(d) ISI CHANNEL CH24:  $L=2$

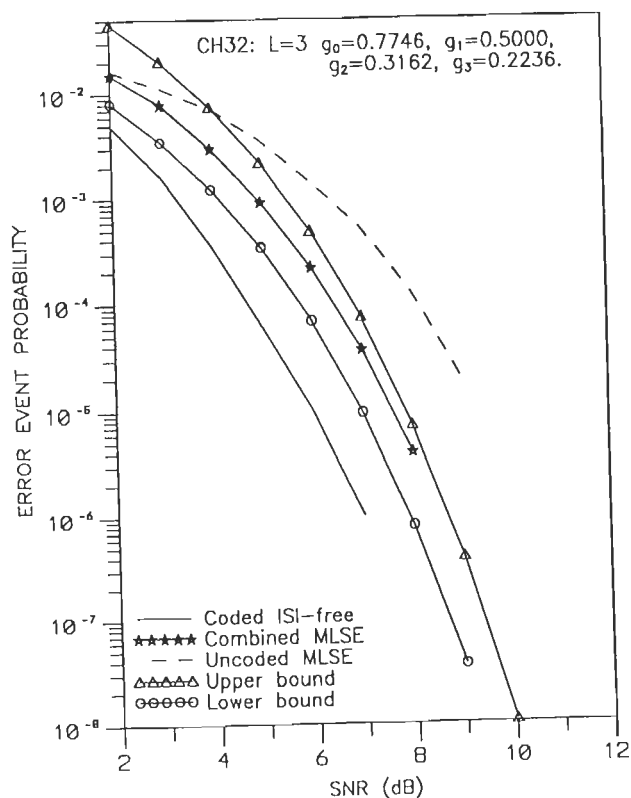


(e) ISI CHANNEL CH25:  $L=2$

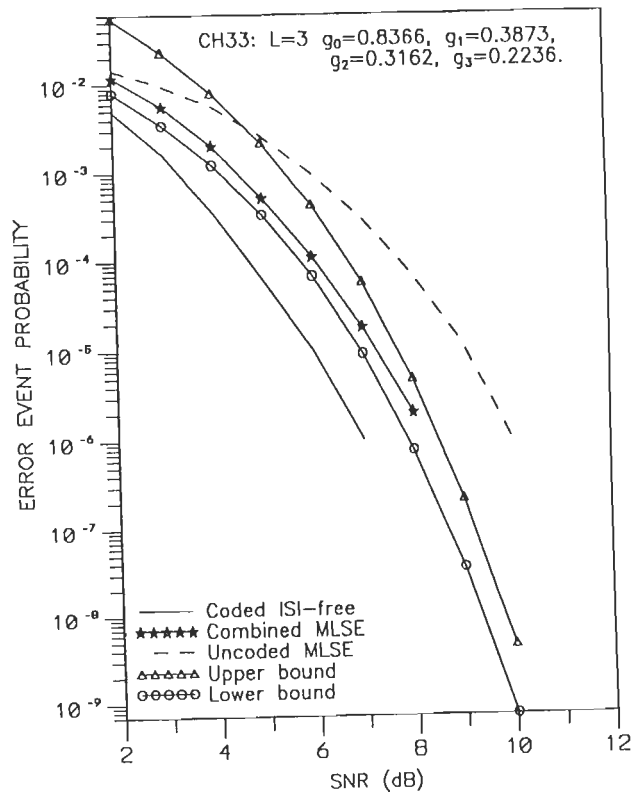


(f) ISI CHANNEL CH26:  $L=2$

FIG.3.9 ERROR PERFORMANCE OF THE COMBINED MLSE RECEIVER WHICH USES A 16-STATE COMBINED ISI-CODE TRELLIS STRUCTURE FOR THE DECODING OF 4-STATE 4-QAM TCM SIGNALS TRANSMITTED OVER AN ISI CHANNEL OF MEMORY  $L=2$ .



(a) ISI CHANNEL CH32:  $L=3$



(b) ISI CHANNEL CH32:  $L=3$

FIG.3.10 ERROR PERFORMANCE OF THE COMBINED MLSE RECEIVER WHICH USES A 32-STATE COMBINED ISI-CODE TRELLIS STRUCTURE FOR THE DECODING OF 4-STATE 4-QAM TCM SIGNALS TRANSMITTED OVER AN ISI CHANNEL OF MEMORY  $L=3$ .

achieves a gain of about 2.5 - 3 dB relative to an uncoded 8-QAM MLSE receiver structure. The combined ISI-code structure suffers a loss of about 1 - 1.75 dB over its ISI-free performance. The performance of the coded MLSE structure is found to be best on CH13 to be followed by CH12, CH11 and CH14 in that order.

The fact that the 8-state TCM scheme activates a coding gain of 1 dB higher than that of 4-state TCM scheme (over AWGN channel) has been reflected in the performance characteristics of the combined MLSE structures of Fig.3.11–3.13. It is clearly evident, from Fig.3.13(c) that the combined MLSE structure based on 8-state TCM schemes achieves a gain of nearly 3 dB over uncoded MLSE, as compared to the performance gain achieved by the combined MLSE structures based on 4-state TCM schemes which is around 2.25–2.5 dB as can be seen from Fig.3.10 and Fig.3.11.

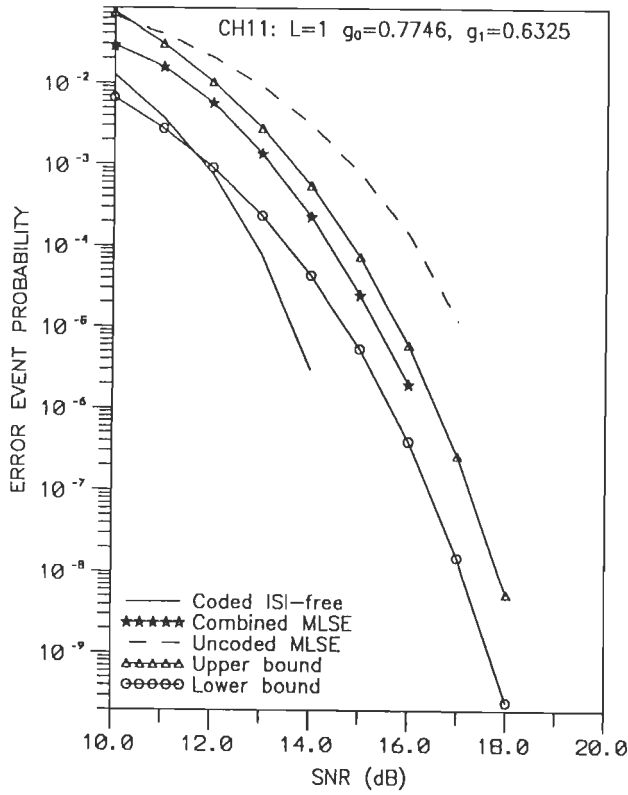
From the performance characteristics of the combined MLSE structures as shown in Fig.3.8-3.13, we note that the simulation result is well bounded by the upper and lower bounds evaluated through the use of computed distance parameters given in Table 3.4. Therefore, we may conclude that the proposed method for the computation of upper bound of the combined MLSE structures as discussed in section 3.5, is quite applicable for all ISI channels. The combined MLSE structure for a 4-state 16-QAM TCM for  $L=1$  achieves a gain of about 1.6 - 2.5 dB over uncoded 8-QAM MLSE receiver structure. The channel CH13 yields the best performance with a coding gain for 2.5 dB over uncoded MLSE reference system at  $P_e=10^{-5}$ . This is followed by those of CH12, CH11 and CH14 in order, as can be observed from the entries of Table 3.6. Again we note, from each of the performance characteristics of Fig.3.11, that the simulation results is well within the computed bounds.

The performance characteristics of the 128-state combined ISI-code trellis structure, for the decoding of 4-state 64-QAM TCM over an ISI channel of length  $L=1$  as discussed in section 3.4.3, have been given in Fig.3.12 for 4 different channels CH11-CH14. The performance gain achieved over uncoded 32-QAM MLSE structure varies between 1.5–2.25 dB at  $P_e=10^{-4}$  while the performance degradation is about 1.25–2 dB relative to its ISI-free performance. The performance isoptimum

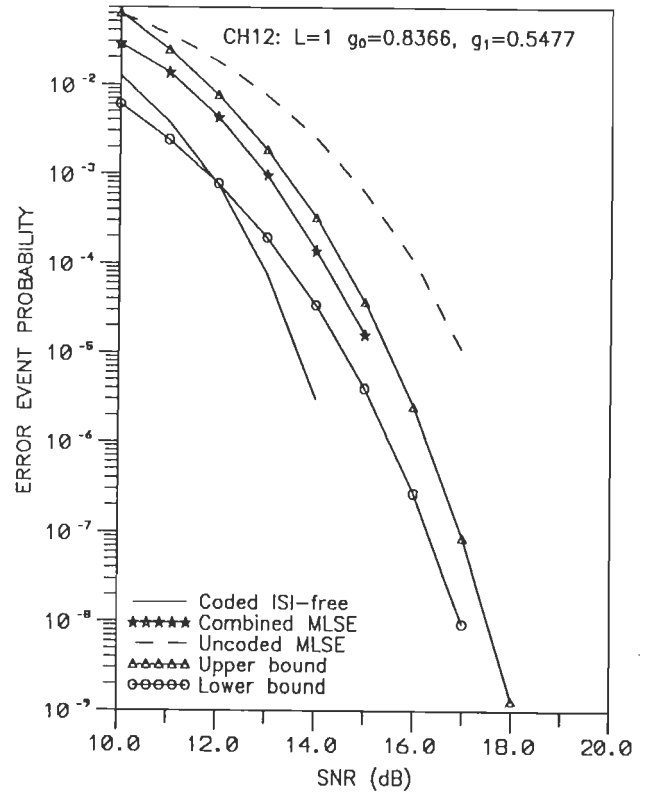
**Table 3.6 Performance gain of combined MLSE structures over uncoded MLSE structures as measured (approx.) from simulation results, at  $P_e = 10^{-5}$  on different ISI channels**

Sl. No.	Structure	Coding gain on ISI channel relative to uncoded system, in dB						Performance loss relative to its ISI-free performance, in dB					
		CH11	CH12	CH13	CH14	-	-	CH11	CH12	CH13	CH14	-	-
1	8-state combined ISI-code trellis (4-state 4-QAM TCM; L=1) Fig. 3.8	CH11 +2.75	CH12 +2.90	CH13 +3.00*	CH14 +2.70	-	-	CH11 -1.25	CH12 -1.00	CH13 -0.75	CH14 -1.25	-	-
2	16-state combined ISI-code trellis (4-state 4-QAM TCM; L=2) section 3.4.1; Fig. 3.9	CH21 +2.25	CH22 +2.25	CH23 +2.75*	CH24 +3.00	CH25 +2.00	CH26 +2.50	CH21 -1.50	CH22 -1.25	CH23 -0.75	CH24 -2.00	CH25 -1.50	CH26 -1.50
3	32-state combined ISI-code trellis (4-state 4-QAM TCM; L=3) Fig. 3.10	CH31 +1.75	CH32 +2.25*	-	-	-	-	CH31 -1.75	CH32 -1.25	-	-	-	-
4	32-state combined ISI-code trellis (4-state 16-QAM TCM; L=1) section 3.4.2; Fig. 3.11	CH11 +1.70	CH12 +2.00	CH13 +2.50*	CH14 +1.90	-	-	CH11 -1.70	CH12 -1.50	CH13 -1.00	CH14 -1.90	-	-
5	128-state combined ISI-code trellis (4-state 64-QAM TCM; L=1) section 3.4.3; Fig. 3.12 Note : at $P_e = 10^{-4}$	+1.50	+1.75	+2.25*	+2.00	-	-	-1.75	-1.50	-1.25	-2.00	-	-
6	64-state combined ISI-code trellis (8-state 16-QAM TCM; L=1) section 3.4.4; Fig. 3.13	+2.50	+2.75	+2.90*	+2.75	-	-	-1.75	-1.40	-1.00	-1.50	-	-

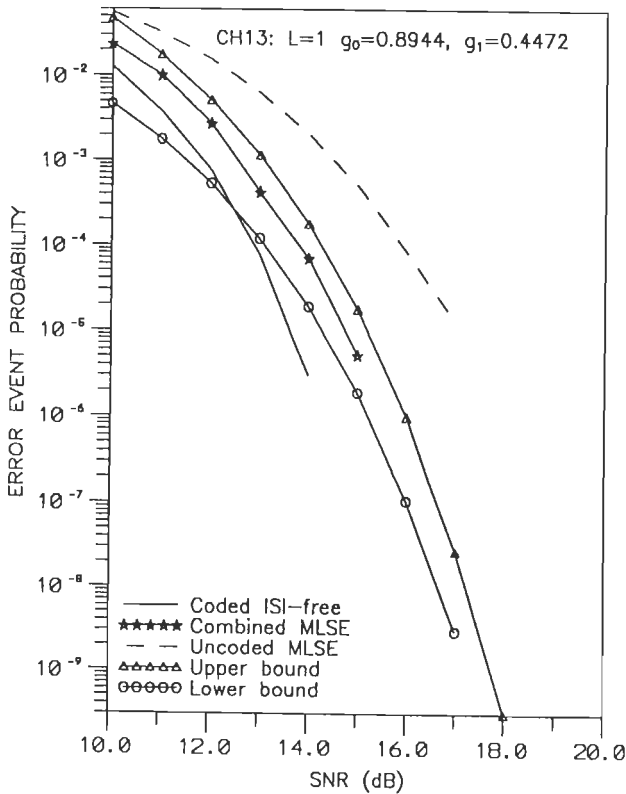
Note : \* Indicates the best performance



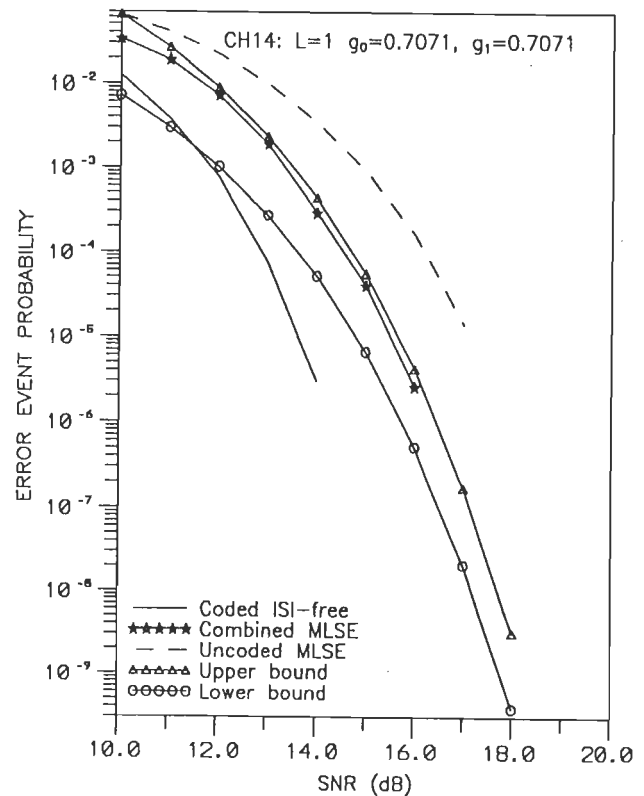
(a) ISI CHANNEL CH11:  $L=1$



(b) ISI CHANNEL CH12:  $L=1$

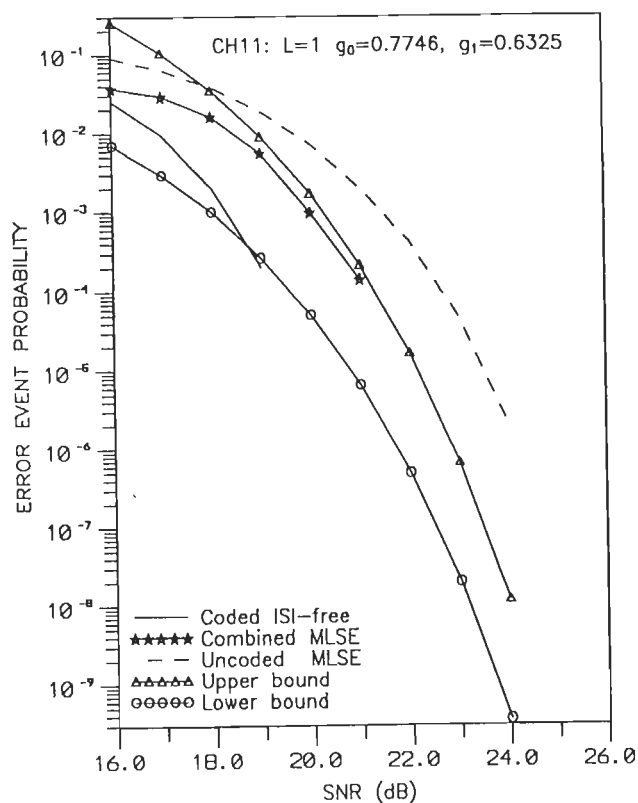


(c) ISI CHANNEL CH13:  $L=1$

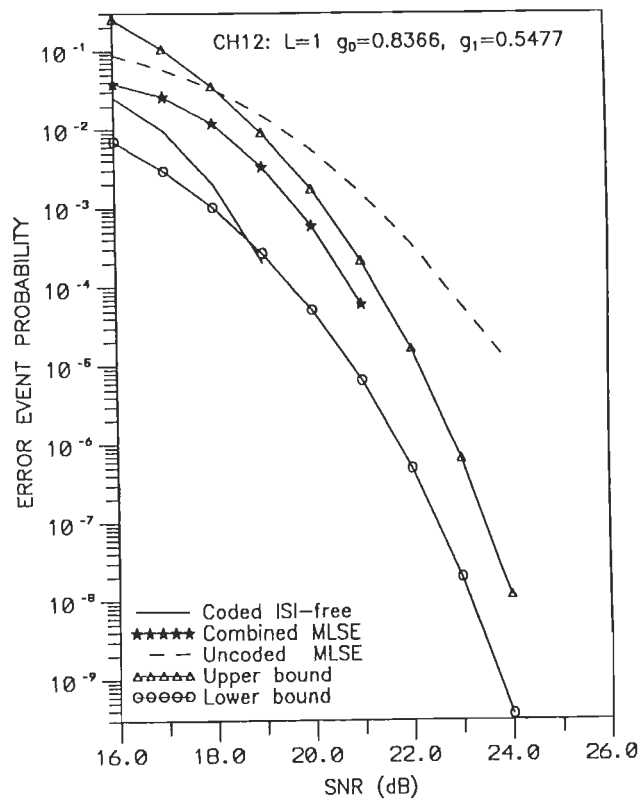


(d) ISI CHANNEL CH14:  $L=1$

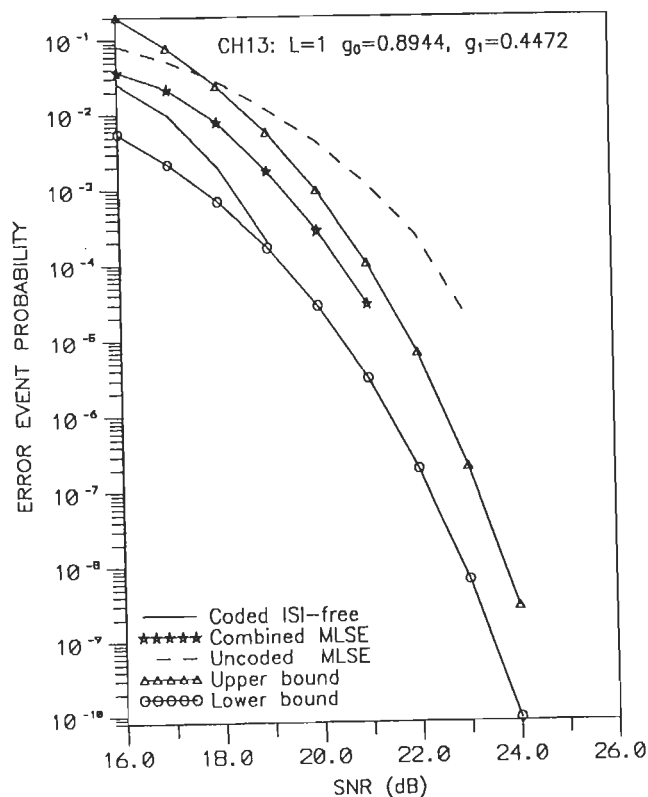
FIG.3.11 ERROR PERFORMANCE OF THE COMBINED MLSE RECEIVER WHICH USES A 32-STATE COMBINED ISI-CODE TRELLIS STRUCTURE FOR THE DECODING OF 4-STATE 16-QAM TCM SIGNALS TRANSMITTED OVER AN ISI CHANNEL OF MEMORY  $L=1$ .



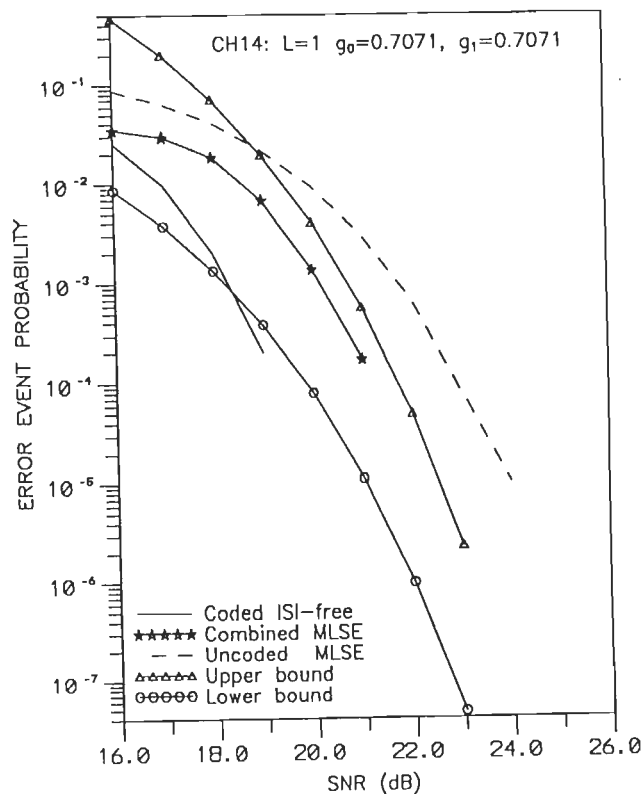
(a) ISI CHANNEL CH11:  $L=1$



(b) ISI CHANNEL CH12:  $L=1$



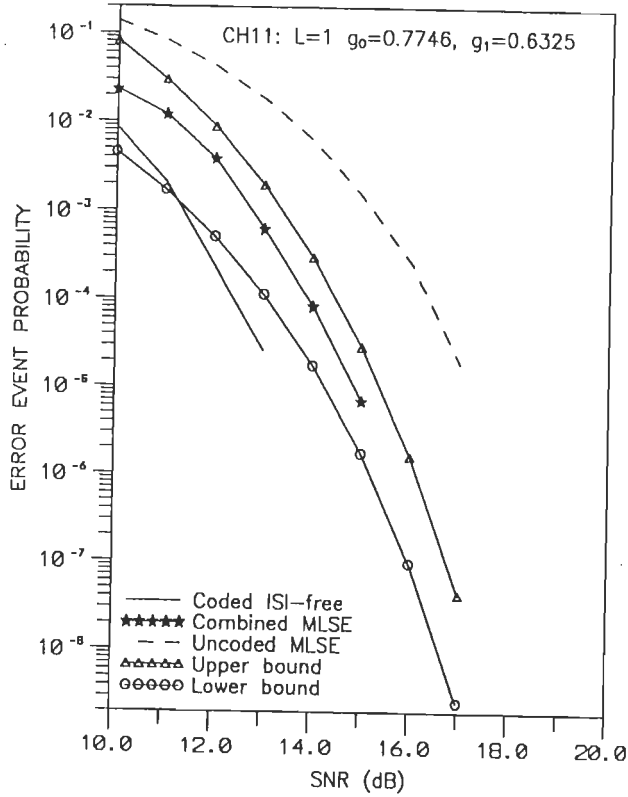
(c) ISI CHANNEL CH13:  $L=1$



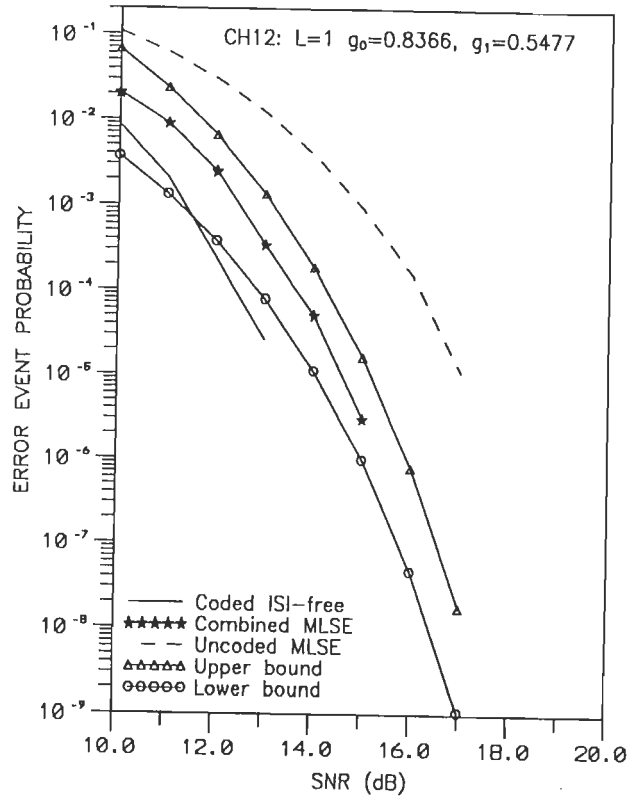
(d) ISI CHANNEL CH14:  $L=1$

FIG.3.12 ERROR PERFORMANCE OF THE COMBINED MLSE RECEIVER WHICH USES AN 128-STATE COMBINED ISI-CODE TRELLIS STRUCTURE FOR THE DECODING OF 4-STATE 64-QAM TCM SIGNALS TRANSMITTED OVER AN ISI CHANNEL OF MEMORY  $L=1$ .

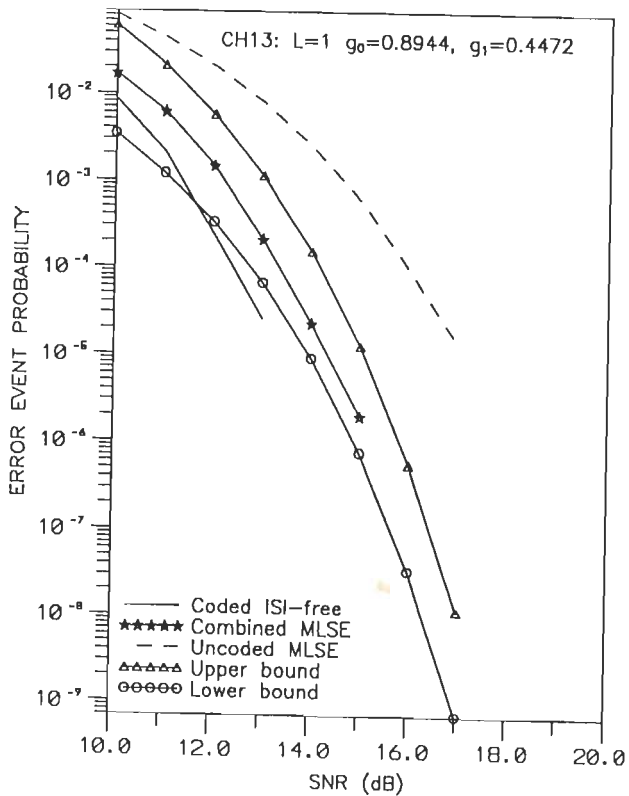




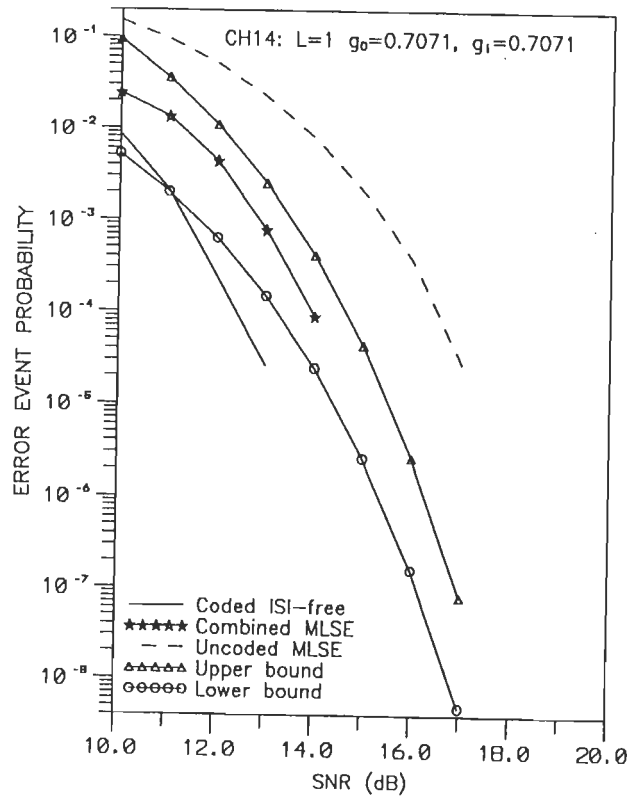
(a) ISI CHANNEL CH11:  $L=1$



(b) ISI CHANNEL CH12:  $L=1$

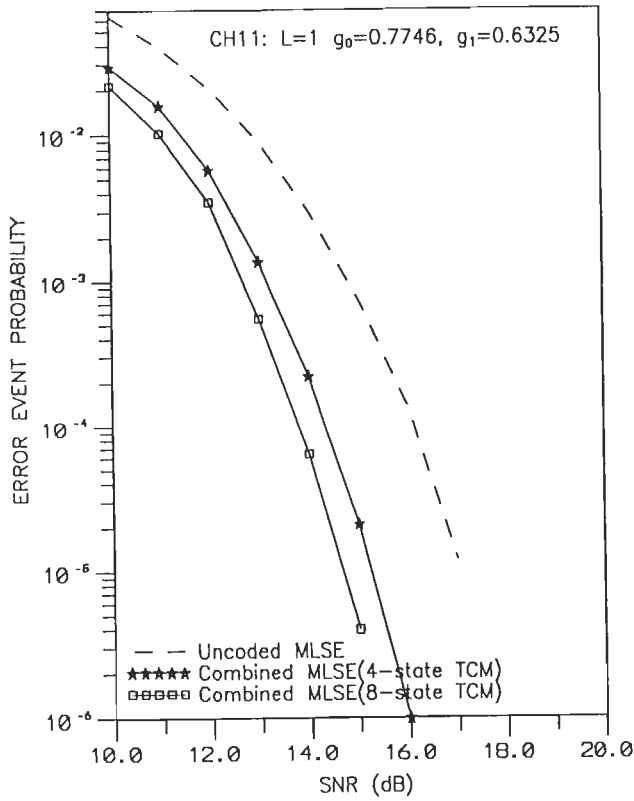


(c) ISI CHANNEL CH13:  $L=1$

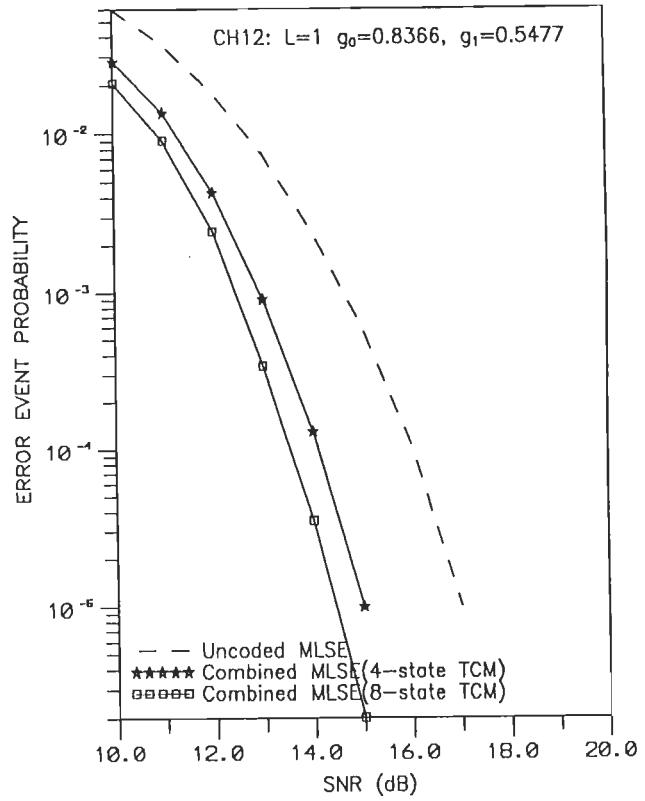


(d) ISI CHANNEL CH14:  $L=1$

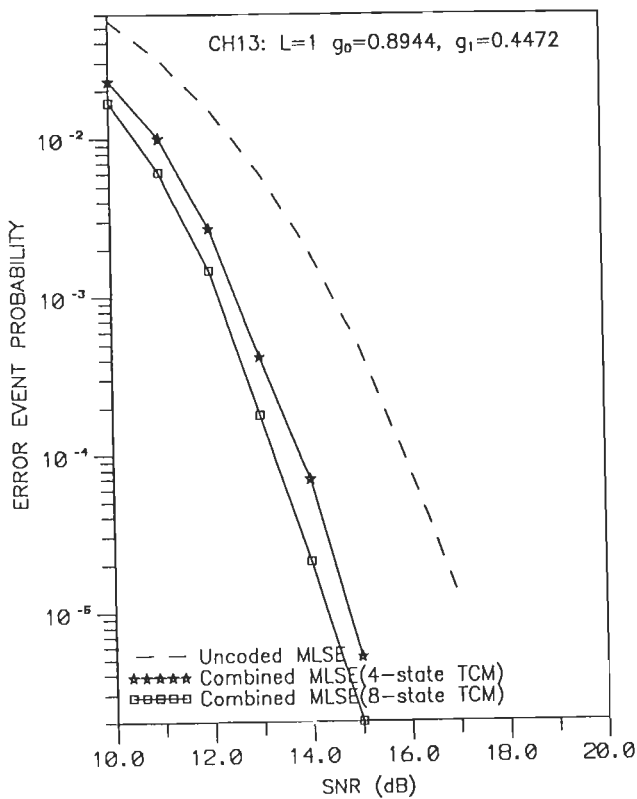
FIG.3.13 ERROR PERFORMANCE OF THE COMBINED MLSE RECEIVER WHICH USES A 64-STATE COMBINED ISI-CODE TRELLIS STRUCTURE FOR THE DECODING OF 8-STATE 16-QAM TCM SIGNALS TRANSMITTED OVER AN ISI CHANNEL OF MEMORY  $L=1$ .



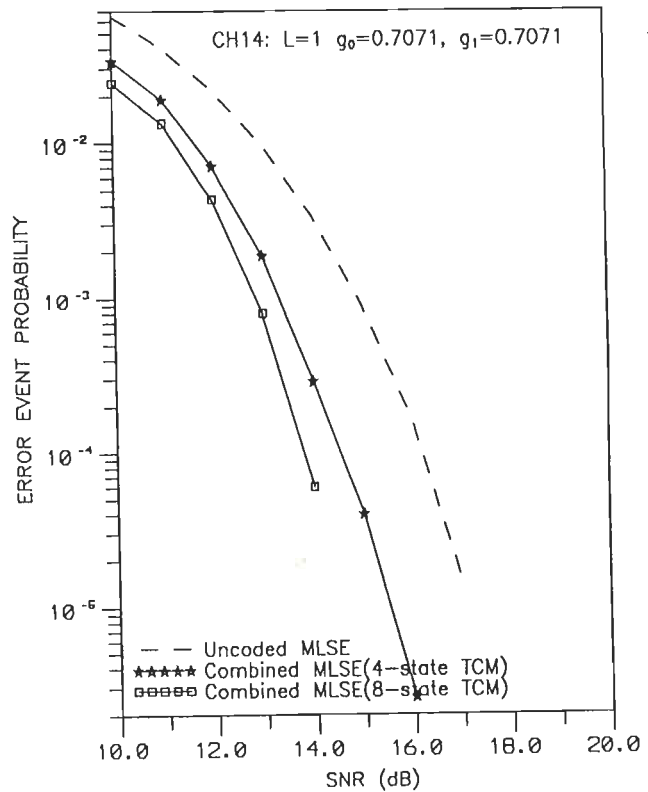
(a) ISI CHANNEL CH11:  $L=1$



(b) ISI CHANNEL CH12:  $L=1$



(c) ISI CHANNEL CH13:  $L=1$



(d) ISI CHANNEL CH14:  $L=1$

FIG.3.14 PERFORMANCE COMPARISON OF THE COMBINED ISI-CODE TRELLIS STRUCTURES BASED ON 4-STATE AND 8-STATE 16-QAM TCM SCHEMES

on CH13, to be followed by CH12, CH11 and CH14 in that order. It may be noted that the simulation results of the coded MLSE structure could not be obtained for  $P_e < 10^{-4}$  due to the computation complexity involved.

Fig.3.13 gives the performance characteristics of the 64-state combined MLSE receiver structure of section 3.4.4, for the decoding of 8-state 16-QAM TCM over an ISI channel of memory length  $L=1$ , and the ISI channels considered are CH11-CH14. Again we note that the coded combined MLSE structure achieves a gain of 2.5 dB to nearly 3 dB at  $P_e \leq 10^{-4}$  relative to uncoded 8-QAM MLSE receiver structure. The combined ISI-code structure suffers a loss of about 1–1.75 dB over its ISI-free performance. Again we find that performance of the coded combined MLSE structure is superior on channel CH13, to be followed by those on channels CH12, CH11 and CH14 in that order.

The fact that the 8-state TCM scheme activates an additional gain of 1 dB over 4-state TCM scheme (on AWGN channel) has been reflected in the error performance characteristics of the combined MLSE structure, shown in Fig.3.11–3.13. From Fig.3.13(c) we find that the combined MLSE structure (of section 3.4.4), which is based on the 8-state TCM scheme, achieves a gain of nearly 3 dB on channel CH13 over uncoded MLSE, while a performance gain of about 2.25–2.5 dB is achieved with the use of combined MLSE structures (of section 3.4.2 and 3.4.3) that are based on 4-state TCM scheme, as is evident from the characteristics of Fig.3.10(c) and 3.11(c).

In summary, the combined MLSE receiver structures (using the combined ISI-code trellis) achieve a coding gain in the range of 2-3 dB over uncoded MLSE receiver structures, although they suffer a loss of about 0.75 dB to 1 dB relative to this ISI-free performance. The performance characteristics show clearly, that the simulation result is well within the computed performance bounds. Therefore, we may conclude that the method employed to compute the performance bound is quite effective.

# REDUCED COMPLEXITY KFE-MLSE RECEIVER STRUCTURE FOR TCM DECODING ON ISI CHANNELS

---

## 4.1 INTRODUCTION

In the previous chapter we have seen that the computational complexity of the MLSE receiver grows exponentially with the channel memory length, thereby making the implementation of the optimum combined ISI-Code receiver prohibitively too complex even for moderate ISI, particularly with QAM signaling at high data rates. This has motivated an active research to find sub-optimum TCM receiver structures with reduced complexity, while maintaining most of the performance advantages of MLSE.

The complexity of the optimum receiver can be reduced by employing prefiltering techniques prior to MLSE. In practice, the LE-MLSE structure comprising of a linear equalizer (LE) in cascade with the ML Viterbi decoder is often used for high-speed TCM transmission over telephone channels [123]. However, the fact that LE enhances noise on channels with in-band nulls results in the performance degradation of LE-MLSE receiver structures. With a decision-feedback equalizer (DFE), the noise enhancement is substantially less but it requires reliable delay-free decisions for proper operation, which is not possible with a TCM Viterbi decoder. Consequently, a tandem combination of DFE and MLSE for TCM schemes does not perform well and results in a performance loss as opposed to a gain [138]. Thus, there is still a need for a feasible reduced complexity receiver

structure that can approach the performance of an ideal DFE-MLSE structure for coded-modulation.

We propose a suboptimum KFE-MLSE receiver structure comprising of the Kalman filter equalizer (KFE) followed by the ML Viterbi decoder for the decoding of TCM signals in the presence of ISI and AWGN. The KFE is known to be an optimum linear structure in the sense of minimum mean-square error (MMSE) and is realizable as a finite dimensional recursive filter [6]. Also under stable conditions, it behaves as a zero-forcing equalizer at high SNR.

The performance of the proposed sub-optimum KFE-MLSE receiver structure can be evaluated by finding its performance degradation relative to the performance of the ML Viterbi decoding under ISI-free environment. The performance degradation can be evaluated by assuming that the Viterbi algorithm still operates with a white noise process, whose variance is the overall variance of the correlated noise and the residual ISI present at the KFE output. By finding the combined impulse response of the channel and the KFE, through the use of innovations representation and the spectral factorization technique, it is possible to determine the effect of KFE prefiltering on the free distance of the TCM code and hence the performance evaluation of the KFE-MLSE structures using bounds.

In this chapter, we first discuss the various pre-filtering techniques which are normally employed to reduce the complexity of the receiver structure for both uncoded and coded-modulation systems. We then present, the reduced complexity KFE-MLSE structure for the decoding of Trellis-coded QAM signals transmitted over a time-dispersive channel. We next present the results of a study that has been performed, using innovations representation of the processes involved and the spectral factorization technique, to compute the performance of the proposed KFE-MLSE structure for several Trellis-coded QAM schemes. The performance bounds so derived are compared with the simulation results. Also, the performance of the proposed suboptimum KFE-MLSE receiver is compared with that of the optimum combined ISI-Code receiver structure for ISI channels of short memory length.

## 4.2 SUB-OPTIMUM MLSE STRUCTURE WITH PRE-FILTERING

Although, MLSE is implementable by the virtue of recursive nature of VA, the combined ISI-Code trellis structure becomes too complex for most of the channels of practical interest. The practical limitations of the optimum combined MLSE receiver structure prompted researchers to find sub-optimum MLSE receiver structures of reduced complexity.

One such approach, as suggested by Forney [46] in his original paper on MLSE for uncoded transmission, is to employ a linear equalizer as a prefilter to shape the channel into a short desired impulse response channel and then apply VA to this partially equalized channel. Qureshi and Newhall [113] proposed such an LE-MLSE receiver structure for uncoded binary transmission over a time-dispersive telephone channel, while Falconer and Magee [43] proposed an adaptive LE-MLSE structure using MMSE criterion. The fact that DFE provides a much better performance over LE on channels having severe amplitude distortion (in-band nulls), prompted researchers to employ DFE as a prefilter instead of LE. Lee and Hill [70] proposed a reduced complexity sub-optimum DFE-MLSE receiver structure for uncoded binary transmission, while Weslowski [137] presented a similar DFE-MLSE structure for uncoded QAM data transmission. The pre-filtering technique reduces considerably the complexity of the MLSE receiver structure for uncoded transmission and as a consequence also find applications in coded-modulation systems.

Much prior to the invent of coded-modulation schemes, using channel capacity arguments Price [40, 42] made an important observation. At a sufficiently high SNR if a coded modulation scheme can approach channel capacity on an ISI-free channel, then the same scheme can also approach that capacity on channels with ISI, provided the receiver uses an ideal DFE-MLSE structure [42].

Wong and McLane [142] proposed such a pre-filtering technique employing a DFE-MLSE receiver structure for transmission of TCM signals over multipath HF channels. But the performance of this DFF-MLSE receiver for TCM transmission was

observed to be no better than that of an uncoded DFE receiver [138, 142].

For proper operation a DFE requires reliable and delay-free decisions, and with TCM schemes employing ML Viterbi decoder such reliable delay-free decisions are not available. Thus, the potential benefits of cascading a DFE with MLSE for TCM decoding can not be realized in a straight-forward manner.

Thapar [123] has shown that an LE in cascade with a ML Viterbi decoder, the LE-MLSE structure, is a good solution for high-speed TCM transmission over voice-grade telephone channels. However, on channels with in-band nulls the LE-MLSE structure exhibits poor performance due to noise enhancement.

Thus, for coded-modulation schemes there is still a need for reduced complexity receiver structure which can approach the performance of an ideal DFE-MLSE receiver. Since the KFE is an optimum linear equalizer which behaves as a zero-forcing equalizer at high SNR (ideal DFE), we propose to investigate the viability of a KFE-MLSE receiver structure for the decoding of Trellis-coded QAM signals in the presence of ISI and AWGN.

### 4.3 KFE-MLSE RECEIVER STRUCTURE

Consider the baseband TCM communication system of section 3.3.1 (Fig. 3.4), with the receiver portion being replaced by KFE-MLSE structure consisting of Kalman-filter equalizer in cascade with the maximum-likelihood Viterbi decoder as shown in Fig. 4.1

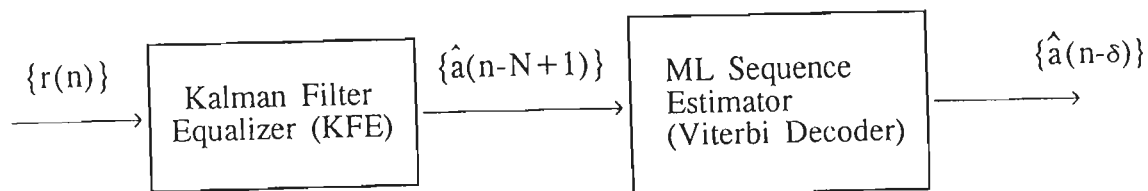


**Fig.4.1 The Sub-optimum KFE-MLSE Receiver**

The TCM encoder/modulator transforms the i.i.d information sequence into a stream of complex data symbol sequence  $\{a(n)\}$ . The data symbols are assumed to be

uncorrelated complex random variables whose mean and variance are given by

$$E[a(n)] = 0; \quad E[a(n) a^*(k)] = \sigma_s^2 \delta_{nk} \quad \dots(4.1)$$

The transmission channel is assumed to be linear, causal and time-invariant with a finite duration impulse response  $g(t)$  such that  $g(t) = 0$  for  $t < 0$  and  $t \geq NT$ , where  $N$  represents the number of channel tap-gains, and the ISI memory length  $L$  is related to  $N$  by  $L = N - 1$ . The channel output being perturbed by AWGN, the received samples are given by

$$r(n) = \sum_{i=0}^{N-1} g_i a(n-i) + v(n) \quad \dots(4.2)$$

where  $g_i$ 's represent the sampled channel impulse response and  $v(n)$  is the sampled complex additive white Gaussian noise with mean and variance given by

$$E[v(n)] = 0; \quad E[v(n) v^*(k)] = 2\sigma_v^2 \delta_{nk} \quad \dots(4.3)$$

The data sequence  $\{a(n)\}$  and noise sequence  $\{v(n)\}$  are assumed to be uncorrelated.

If the input data sequence  $\{a(n)\}$  is characteristically similar to a white noise process, then the channel model can be formulated using a state variable representation of the discrete Kalman filter. The state variables are the successive transmitted symbols. The complex envelope of the received waveform can then be expressed in terms of a discrete-time dynamic system driven by a white process. Under a known channel condition the Kalman filter, which is dual to the channel model, represents an optimum linear equalizer in the sense of MMSE [6].

The output of the KFE, representing nearly an ISI-free signal, is then processed by a soft-decision ML sequence estimator (Viterbi algorithm) in order to decode the TCM signals.

#### 4.4 KALMAN-FILTER EQUALIZER

Lawrence and Kaufmann [68] posed the equalization problem as one of obtaining



MMSE estimate of the transmitted symbol  $a(n)$ . Thus, it is required to obtain the unbiased linear minimum error variance estimate  $\hat{a}(i)$  of each transmitted symbol  $a(i)$ , such that  $E[|a(i)-\hat{a}(i)|^2]$  is a minimum. The only constraints being imposed on the estimator sequence are linearity and stability [6].

For the channel equalization, we make use of the state variable representation of the message process and the observation sequence at the channel output, and a discrete Kalman filter as considered by Lawrence and Kaufman [68]. Thus, the dynamics of the message process and the observation process at the channel output can be described by

$$\mathbf{X}(n+1) = \Phi \mathbf{X}(n) + \Gamma u(n+1) \quad \dots(4.4)$$

$$r(n) = \mathbf{g} \mathbf{X}(n) + v(n) \quad \dots(4.5)$$

where  $\mathbf{X}(n)$  is a  $N$ -state vector at time  $n=NT$ ,

$\Phi$  is a  $N \times N$  state transition matrix with elements  $\Phi(i+1,i)=1$  for  $i=1,2,\dots, N-1$  and  $\Phi(i,j)=0$  for all other values of  $i,j$ ,

$\Gamma$  is a  $N$  column vector defined by  $\Gamma = [1,0,0,\dots,0]^T$ ,

$\mathbf{g}$  is a  $N$  row vector defined by  $\mathbf{g} = [g_0 g_1 \dots g_{N-1}]$

$u(n)$  is the plant noise having the statistics as those of  $a(n)$  that is  $u(n)=a(n)$ , and  $v(n)$  is the observation noise which is white, and  $\tau$  represents the transpose.

The state vector components represent the  $N$  consecutive transmitted symbols as

$$\mathbf{X}(n) = \begin{bmatrix} x_1(n) \\ x_2(n) \\ \vdots \\ x_i(n) \\ \vdots \\ x_N(n) \end{bmatrix} \stackrel{\Delta}{=} \begin{bmatrix} a(n) \\ a(n-1) \\ \vdots \\ a(n-i+1) \\ \vdots \\ a(n-N+1) \end{bmatrix} \quad \dots(4.6)$$

The discrete Kalman filter operates on the sampled baseband signals  $r(n)$  to estimate the channel state  $\hat{\mathbf{X}}(n)$ , that is to yield  $\hat{a}(n), \hat{a}(n-1), \dots, \hat{a}(n-N+1)$ . It is a well established fact that the Kalman filter provides the mean-sequence optimum linear estimate of  $\mathbf{X}(n)$ . The discrete Kalman filter minimizes not only the trace of the error covariance matrix, but any linear combinations of main diagonal elements [6]. Therefore, due to the choice of (4.6) of the state vector, the Kalman filter also minimizes  $E[|a(i)-\hat{a}(i)|^2]$ .

The unbiased linear minimum mean-square error (ULMMSE) estimator for the discrete system (4.4)-(4.6) is described by the following equations [6, 69];

The state estimation filter algorithm:

$$\hat{\mathbf{X}}(n/n) = \phi \hat{\mathbf{X}}(n-1/n-1) + \mathbf{K}(n) [r(n) - \mathbf{g} \phi \hat{\mathbf{X}}(n-1/n-1)] \quad \dots(4.7)$$

The Kalman gain equation:

$$\mathbf{K}(n) = \mathbf{V}(n/n-1) \mathbf{g}^* [\mathbf{g} \mathbf{V}(n/n-1) \mathbf{g}^* + 2 \sigma_v^2]^{-1} \quad \dots(4.8)$$

The apriori error variance algorithm:

$$\mathbf{V}(n/n-1) = \phi \mathbf{V}(n-1/n-1) \phi^T + \sigma_s \Gamma \Gamma^T \quad \dots(4.9)$$

The aposteriori error variance algorithm

$$\mathbf{V}(n/n) = [\mathbf{I} - \mathbf{K}(n) \mathbf{g}] \mathbf{V}(n/n-1) \quad \dots(4.10)$$

The implementation of the above system of (4.7)-(4.10) require initial values of  $\hat{\mathbf{X}}(0/0)$  and  $\mathbf{V}(0/0)$ . This is done by setting

$$\hat{\mathbf{X}}(0/0) = E[\mathbf{X}] = \mathbf{0} \quad \dots(4.11)$$

$$\text{and } \mathbf{V}(0/0) = E[\mathbf{X} \mathbf{X}^*] = \sigma_s^2 \mathbf{I} \quad \dots(4.12)$$

where  $\mathbf{I}$  is  $N \times N$  identity matrix

From (4.7) it can be observed that the estimator utilizes the estimates of past symbols in arriving at the present estimate, which is analogous to DFE operation. The operation of ULM MSE estimator can be described by a block diagram as shown in Fig.4.2. The current (present) estimate  $\hat{\mathbf{X}}(n/n)$  is formed by predicting forward the previous estimate  $\hat{\mathbf{X}}(n-1/n-1)$  and correcting it with the observation error, weighted by  $\mathbf{K}(n)$ . The observation error  $\varepsilon(n)=r(n)-\hat{r}(n/n-1)$  is usually called as 'innovation'.

Under steady-state, the ULM MSE estimator becomes a time-invariant stable linear filter [6]. Therefore in practice, the filter can be implemented as a recursive digital filter as shown in Fig.4.3, which is quite suitable for digital implementation.

For any observation instant, the N estimates of the consecutive transmitted symbols are available at the output of the Kalman filter. As each component of the state vector  $\mathbf{X}(n)$  is the time translate of the message sequence, we have from (4.6),

$$x_{\beta}(n) = a(n-\beta+1) \quad \dots(4.13)$$

where  $x_{\beta}(n)$  is the  $\beta^{\text{th}}$  component of the state vector  $\mathbf{X}(n)$ . Thus the estimate of the transmitted symbol may be obtained as

$$\hat{a}(n-\beta) = \hat{x}_{\beta+1}(n) \quad 0 \leq \beta \leq N-1 \quad \dots(4.14)$$

Although N estimates are available at each instant, it is better to estimate just one symbol in order to achieve the minimum error variance. It is shown in [6] that a good estimation of the transmitted symbol is possible for  $d=N-1$ . Thus while receiving  $r(n)$  the best estimate is  $\hat{x}_N(n)=\hat{a}(n-N+1)$ , which represents the estimate of  $a(n)$  transmitted (N-1) time instants earlier.

From (4.8)-(4.10), it can be observed that the error variance equations and Kalman gain equation are independent of the observation sequence  $\{r(n)\}$ . Hence, for the case of known channel tap gains, the quantities can be precomputed, if

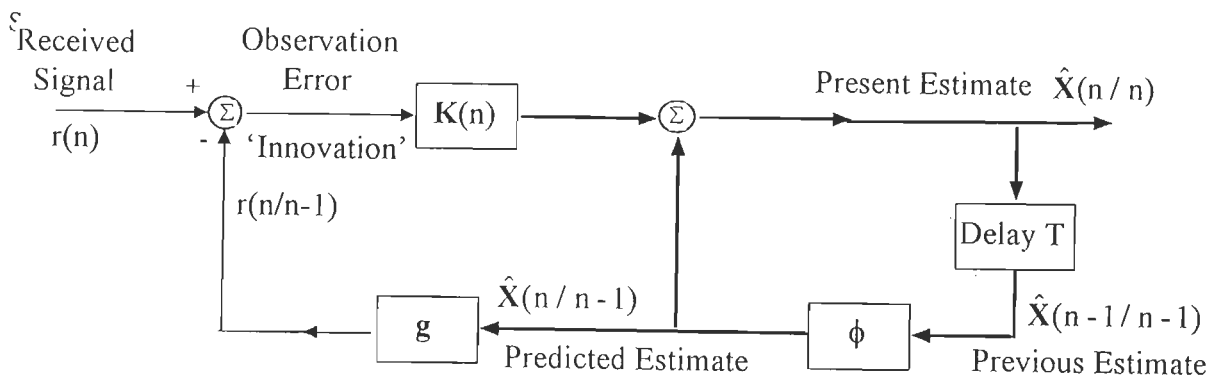


Fig.4.2. BLOCK DIAGRAM OF ULM MSE ESTIMATOR.

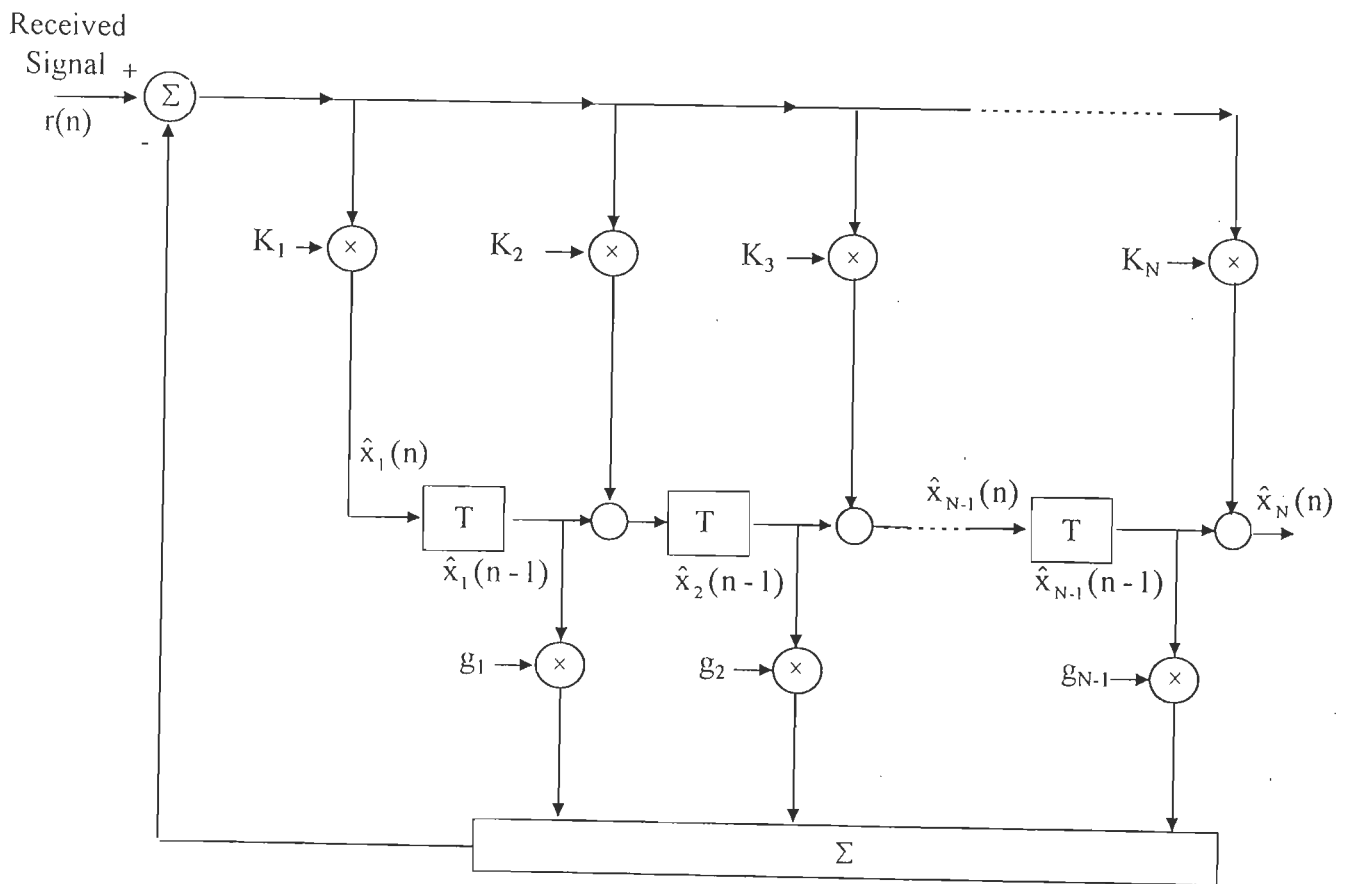


FIG.4.3 THE STEADY-STATE STRUCTURE OF ULM MSE KALMAN EQUALIZER.

desired. Also, under steady-state the Kalman gain matrix  $K(n)$  becomes independent of  $n$  for sufficiently large  $n$ . That is, in the limit as  $n \rightarrow \infty$ ,  $K(n) \equiv K$ .

It would be of interest to compute the steady-state Kalman gains  $K$  from the observation sequence  $r(n)$ , using the innovations representation of the observation process, through a non-singular transformation as discussed below.

#### 4.4.1 Innovations representation of the observation process and computation of the Kalman gains

Consider the transformation of the system defined by

$$\mathbf{X}(n+1) = \phi \mathbf{X}(n) + \Gamma u(n+1) \quad \dots(4.15)$$

$$r(n) = \mathbf{g} \mathbf{X}(n) + v(n) \quad \dots(4.16)$$

into a standard canonical form through a non-singular transformation [83],

$$\mathbf{X}^*(n) = \mathbf{Q} \mathbf{X}(n) \quad \dots(4.17)$$

where

$$\mathbf{Q} = \begin{bmatrix} \mathbf{g}_{N-1} & & & 0 \\ \mathbf{g}_{N-2} & \mathbf{g}_{N-1} & & \\ \cdot & & & \\ \cdot & & & \\ \cdot & & & \\ \mathbf{g}_0 & \mathbf{g}_1 & \dots & \mathbf{g}_{N-1} \end{bmatrix} \quad \dots(4.18)$$

The transformed system is then given by

$$\mathbf{X}^*(n+1) = \phi^* \mathbf{X}^*(n) + \Gamma^* u(n+1) \quad \dots(4.19)$$

$$r(n) = \mathbf{g}^* \mathbf{X}^*(n) + v(n) \quad \dots(4.20)$$

where  $\phi^* = \phi$

$$\Gamma^* = [\mathbf{g}_{N-1}, \mathbf{g}_{N-2}, \dots, \mathbf{g}_0]^T$$

$$\mathbf{g}^* = [0, 0, \dots, 1]$$

The algorithm in the steady-state, for the MMSE state estimate  $\hat{\mathbf{X}}^*(n)$  of system (4.19) - (4.20) may be written as

$$\hat{\mathbf{X}}^*(n) = \Phi \hat{\mathbf{X}}^*(n-1) + \mathbf{K}^* \varepsilon(n) \quad \dots(4.21)$$

where  $\mathbf{K}^* = [K_1^* K_2^* \dots K_N^*]^T \quad \dots(4.22)$

is the steady-state transformed Kalman gain vector and  $\varepsilon(n)$  is the innovation process given by

$$\varepsilon(n) = r(n) - \mathbf{g}^* \Phi \hat{\mathbf{X}}^*(n-1)$$

that is  $\varepsilon(n) = r(n) - \hat{x}_{N-1}^*(n-1) \quad \dots(4.23)$

Rewriting (4.23), we have

$$r(n) = \varepsilon(n) + \hat{x}_{N-1}^*(n-1) \quad \dots(4.24)$$

From (4.21), we can write

$$\hat{x}_{N-1}^*(n-1) = \hat{x}_{N-2}^*(n-2) + K_{N-1}^* \varepsilon(n-1)$$

Substituting this in (4.24), we get

$$r(n) = \varepsilon(n) + K_{N-1}^* \varepsilon(n-1) + \hat{x}_{N-2}^*(n-2)$$

Repeating the above procedure (N-2) times, we obtain

$$r(n) = \varepsilon(n) + K_{N-1}^* \varepsilon(n-1) + \hat{x}_{N-2}^* \varepsilon(n-2) + \dots + K_1^* \varepsilon(n-N+1) \quad \dots(4.25)$$

This is the moving average representation of the observation sequence  $r(n)$  in terms of the innovations and the transformed Kalman gains. The Kalman gains  $K_1^*$ ,  $K_2^*$ , ...,  $K_{N-1}^*$ , and the variance  $\sigma_\varepsilon^2$  of the innovation process can be estimated from the observation sequence  $r(n)$  through spectral factorization. Then  $K_N^*$  can be determined using the relation [63, 83],

$$K_N^* = 1 - (\sigma_v^2 / \sigma_\varepsilon^2) \quad \dots(4.26)$$

Once the transformed Kalman gains are determined, the steady-state Kalman gains of the untransformed system are derived from [83],

$$\mathbf{K} = \mathbf{Q}^{-1} \mathbf{K}^* \quad \dots(4.27)$$

In the following section, we consider the evaluation of transformed Kalman gains using spectral factorization.

#### 4.4.2 Transformed Kalman gains through spectral factorization

Consider the observation process defined by

$$r(n) = \sum_{i=0}^{N-1} g_i a(n-i) + v(n) \quad \dots(4.28)$$

and

$$r(n) = \varepsilon(n) + K_{N-1}^* \varepsilon(n-1) + \dots + K_1^* \varepsilon(n-N+1) \quad \dots(4.29)$$

Defining the shift operator  $z$  as

$$z.r(n) = r(n-1)$$

we can write (4.28) and (4.29) as,

$$r(n) = \mathbf{G}(z) u(n) + v(n) \quad \dots(4.30)$$

$$r(n) = \mathbf{K}^*(z) \varepsilon(n) \quad \dots(4.31)$$

where  $\mathbf{G}(z) = g_0 + g_1 z + g_2 z^2 + \dots + g_{N-1} z^{N-1} \quad \dots(4.32)$

$$\mathbf{K}^*(z) = 1 + K_{N-1}^* z + K_{N-2}^* z^2 + \dots + K_1^* z^{N-1} \quad \dots(4.33)$$

Since the correlation statistics of the process  $r(n)$  in both representations (4.30) and (4.31) must be the same, we can write

$$\sigma_s^2 \mathbf{G}(z) \mathbf{G}(z^{-1}) + \sigma_v^2 = \sigma_\varepsilon^2 \mathbf{K}^*(z) \mathbf{K}^*(z^{-1}) \quad \dots(4.34)$$

where  $\sigma_s^2$  is the variance of the symbol sequence  $\{a(n)\}$ ,

$\sigma_v^2$  is the variance of the observation noise process  $v(n)$ ,

and  $\sigma_\varepsilon^2$  is the variance of the innovation process  $\varepsilon(n)$ .

Given the tap gain vector  $g$ , the evaluation of the transformed Kalman gain vector  $\mathbf{K}^*$  corresponds to finding the solution for the polynomial  $\mathbf{K}^*(z)$  and  $\sigma_\varepsilon^2$  from (4.34), with the knowledge of  $\sigma_s^2$ ,  $\sigma_v^2$  and  $\mathbf{G}(z)$ . This is the spectral factorization problem considered by Rissanen [106] and Rissanen and Kailath [107], and is outlined in Appendix A.

Writing the left hand side of (4.34) as

$$\sigma_s^2 \mathbf{G}(z) \mathbf{G}(z^{-1}) + \sigma_v^2 = \sum_{i=-(N-1)}^{N-1} p_i z^i \quad \dots(4.35)$$

we form the following infinite dimensional symmetric Toeplitz matrix  $\mathbf{P}$  of the correlation coefficient  $p_i$  as

$$\mathbf{P} = \begin{bmatrix} p_0 & p_1 & \dots & p_{N-1} & 0 & \dots & \dots \\ p_{-1} & p_0 & p_1 & \dots & \dots & p_{N-1} & 0 & \dots \\ \vdots & \vdots & \vdots & \vdots & \vdots & \vdots & \vdots & \vdots \\ p_{-(N-1)} & p_{-(N-2)} & \dots & p_0 & p_1 & \dots & p_{N-1} & 0 \\ 0 & \dots & \dots & \dots & p_0 & \dots & \dots & \dots \\ \vdots & \vdots & \vdots & \vdots & \vdots & \vdots & \vdots & \vdots \\ \dots & \dots & \dots & \dots & \dots & \dots & \dots & p_0 \end{bmatrix} \quad \dots(4.36)$$

The positive definite matrix  $\mathbf{P}$  through a congruent transformation can be written as

$$\mathbf{P} = \mathbf{F} \lambda \mathbf{F}^{*\tau} \quad \dots(4.37)$$

where  $\mathbf{F}$  is the unit lower triangular matrix given by

$$\mathbf{F} = \begin{bmatrix} 1 & & & \\ f_{10} & 1 & & 0 \\ f_{20} & f_{21} & 1 & \\ & & & 1 \end{bmatrix} \quad \dots(4.38)$$





Then it can be shown that the MMSE estimate  $\hat{a}(n)$  of the transmitted symbol  $a(n)$  is given by [83],

$$\hat{u}(n) = \sum_{i=-(N-1)}^{-\infty} h_i u(n-i) + v_0(n+N-1) \quad \dots(4.43)$$

where  $h_i$ 's are the samples of the combined impulse response of the channel and the KFE given by

$$h_i = \frac{\sigma_\epsilon^2}{\sigma_s^2} \left[ \sum_{j=1}^N K_{j+i} K_j \right] \quad \dots(4.44)$$

for  $i = -(N-1), -(N-2) \dots 0 \dots \infty$ , and  $K_v = 0, \quad v \leq 0$

The correlated noise sequence  $v_0(n)$  at the output of the equalizer in (4.43) is the solution of the auto-regressive moving average series given by

$$\begin{aligned} v_0(n) + K_{N-1}^* v_0(n-1) + K_{N-2}^* v_0(n-2) + \dots + K_1^* v_0(n-N+1) \\ = K_N v(n) + K_{N-1} v(n-1) + \dots + K_1 v(n-N+1) \end{aligned} \quad \dots(4.45)$$

The variance of the correlated output noise  $\sigma_{v_0}^2$  can be computed by a procedure given in [17], and as detailed in Appendix B.

With a knowledge of the combined impulse response  $\{h_i\}$ , it is possible to determine the effect of KFE-prefiltering on the free distance of the TCM code, and hence on the performance of the ML Viterbi decoder.

#### 4.5 PERFORMANCE EVALUATION OF KFE-MLSE RECEIVER

Consider the receiver structure as shown in Fig.4.4, where the VA operates on the partially equalized signal available at the output of the KFE. Let  $\{h_i\}$  represent the combined impulse response of the channel and the equalizer.

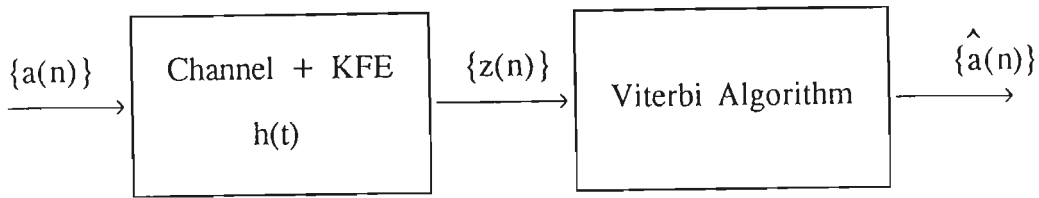


**Fig.4.4 The KFE-VA Receiver Structure**

The equalizer output  $z(n)$  can be expressed in terms of the combined impulse response  $\{h_i\}$  as

$$z(n) = a(n) h_0 + \sum_{\substack{i=-N+1 \\ i \neq 0}}^{\infty} h_i a(n-i) + v_0(n) \quad \dots(4.46)$$

The first term is the desired output and the second term represents the residual ISI components and  $v_0(n)$  is the correlated output noise whose variance is  $\sigma_{v_0}^2$ .

The measure of the equalizer performance is expressed by the signal to noise plus interference ratio (SNIR) defined by [142].

$$\text{SNIR} = \frac{|h_0|^2 \sigma_s^2}{2\sigma_{v_0}^2 + \sum_{i \neq 0} |h_i|^2 \sigma_s^2} = \frac{|h_0|^2 \sigma_s^2}{2\sigma^2} \quad \dots(4.47)$$

where  $\sigma_s^2$  is the signal variance and  $\sigma^2 = \sigma_{v_0}^2 + 0.5 \sum_{i \neq 0} |h_i|^2 \sigma_s^2$

We shall assume that the equalizer output noise is a white noise sequence, so that the performance of VA can be assumed optimum. With this assumption, the probability of minimum distance error event can be expressed as

$$P_e \sim Q \left[ \sqrt{\frac{|h_0|^2 d_{\min}^2}{4\sigma^2}} \right] \quad \dots(4.48)$$

where  $Q(\cdot)$  stands for Gaussian error integral, as defined in section 2.5.

For an ideal channel,  $|h_0|=1.0$ ,  $|h_n|=0$  for all  $n$  except  $n=0$ . Thus for ideal channel (ISI-free channel) the probability of error event is given by

$$P_e \sim Q \left[ \sqrt{\frac{d_{\min}^2}{4\sigma_v^2}} \right] \quad \dots(4.49)$$

where  $\sigma_v^2$  is the variance of additive white Gaussian noise in each dimension.

Thus the degradation in performance of the sub-optimum KFE-MLSE receiver structure relative to an ISI-free channel is given as

$$\text{degradation in performance} = 10\log_{10} \left[ \sqrt{\frac{|h_0|^2 \sigma_v^2}{\sigma^2}} \right] \text{ dB} \quad \dots(4.50)$$

$$= 10\log_{10} \left[ \sqrt{\frac{|h_0|^2 \sigma_v^2}{2\sigma_{v0}^2 + \sum_{i \neq 0} |h_i|^2 \sigma_s^2}} \right] \text{ dB}$$

For a given ISI channel response  $\{g_i\}$ , we can compute the combined impulse response  $\{h_i\}$ , by using the innovations representation and the spectral factorization technique as described in the previous sections. The overall variance  $\sigma_{v0}^2$  of the correlated noise at the output of KFE can be computed by the procedure as detailed in Appendix B [17]. Hence, we can determine the error performance of the sub-optimum KFE-MLSE structure by finding the degradation in performance relative to the optimum MLSE receiver operating under an ISI-free environment through the use of (4.48) and (4.49). The combined impulse response and the overall variance  $\sigma_{v0}^2$  have been determined for various ISI channels and are presented in the next section. Also we have presented in the following, the performance of KFE-MLSE receiver structures evaluated through bounds together with the simulation results.

Table 4.1 Computed values of the combined impulse response of the channel and the KFE for some of the KFE-MLSE structures at different values of SNR.

Sl. No.	TCM scheme employed	ISI channel	SNR dB	Combined impulse response coefficients	Overall noise variance $\sigma_{vo}^2$
1	4-state TCM 16-QAM	CH13	10.0	0.0348, 0.9261, 0.0342, -0.158, 0.0073, -0.0034, 0.0016, -0.0007, 0.0003, -0.0002, 0.0001	0.6573
			12.0	0.234, 0.9514, 0.231, -0.0110, 0.0052, -0.0025, 0.0012, -0.0006, 0.0003, -0.0001, 0.0001	0.4501
			14.0	0.0154, 0.9685, 0.0153, -0.0074, 0.0036, -0.0017, 0.0008, -0.0004, 0.0002, -0.0001	0.3001
			16.0	0.0100, 0.9797, 0.0099, -0.0049, 0.0024, -0.0012, 0.0006, -0.0003, 0.0001, -0.0001	0.1961
2	8-state TCM 16-QAM	CH22	10.0	0.0143, 0.0323, 0.9138, 0.0320, 0.0138, -0.0179, 0.0042, 0.0041, -0.0035, 0.0003, 0.0001, -0.0006	0.7597
			12.0	0.0096, 0.0216, 0.9431, 0.0215, 0.0093, -0.0124, 0.0031, 0.0029, -0.0025, 0.0003, 0.0008, -0.0005	0.5240
			14.0	0.0062, 0.0141, 0.9630, 0.0141, 0.0061, -0.0083, 0.0021, 0.0019, -0.0018, 0.0002, 0.0005, -0.0004	0.3508
			16.0	0.0040, 0.0114, 0.9703, 0.0114, 0.0050, -0.0068, 0.0017, 0.0016, -0.0015, 0.0002, 0.0004, -0.0003	0.2300
3	8-state TCM 64-QAM	CH23	16.0	0.0019, 0.0064, 0.9814, 0.0064, 0.0018, -0.0023, 0.0005, 0.0003, -0.0003, 0.0000, 0.0001	0.7619
			17.0	0.0012, 0.0041, 0.9882, 0.0011, 0.0012, -0.0015, 0.0004, 0.0002, -0.0002, 0.0000	0.4892
			18.0	0.0009, 0.0032, 0.9906, 0.0032, 0.0009, -0.0012, 0.0003, 0.0002, -0.0001	0.2315
			19.0	-0.0006, 0.002, 0.9921, 0.0028, 0.0006, -0.0009, 0.0002, 0.0001, -0.0001	0.1127
4	16-state TCM 64-QAM	CH32	16.0	0.003, 0.0134, 0.9705, 0.0134, 0.0004, 0.0032, -0.0056, 0.0024, -0.0002, 0.0007, -0.0011	1.1860
			17.0	0.0026, -0.0004, 0.0108, 0.9763, 0.0108, -0.0004, 0.026, -0.0045, 0.0019, -0.0001, 0.0006	0.7729
			18.0	0.0021, -0.0003, 0.0087, 0.9811, 0.0087, -0.0003, 0.0021, -0.0036, 0.0016, -0.0001, 0.0005	0.5314
			19.0	0.0017, -0.0003, 0.0069, 0.9849, 0.0069, -0.0003, 0.0017, -0.0029, 0.0013, -0.0001, 0.0004	0.3372

## 4.6 RESULTS AND DISCUSSION

In this section, we present the error performance of the KFE-MLSE receiver structure employed for the sub-optimum detection of trellis-coded QAM signals in the presence of ISI and AWGN. The error event probability of the KFE-MLSE structure is computed through the evaluation of bounds as discussed in section 4.5 and also through simulation. The reference system employed is an uncoded KFE receiver structure having the same data rate, bandwidth and energy as that of the coded KFE-MLSE structure. The performance of the sub-optimum KFE-MLSE structure is compared with that of the optimum combined MLSE receiver structure for a limited variety of ISI channels ( $L=1$ ). The ISI channels considered in this study are same as those considered earlier in section 3.6 and listed in the Table 3.1.

The baseband TCM data transmission system considered in this study has been implemented in the same manner as detailed in section 3.6. The receiver structure, as shown in Fig.4.1, is a cascade of the KFE and the maximum-likelihood Viterbi decoder. Representing the message process and the observations process in the form of (4.4) and (4.5) respectively, the KFE is realized through the implementation of (4.7)-(4.10) and subjected to the initial conditions (4.11) and (4.12). The output of the KFE, representing nearly an ISI-free signal sequence, is then applied to the maximum-likelihood Viterbi decoder which operates on the encoder trellis to determine a sequence of estimated TCM data symbols.

For the performance evaluation of the KFE-MLSE receiver structure through the use of bounds, we consider the estimation of steady-state Kalman gains and hence the combined impulse response of the channel and the KFE. Through the use of innovations representation of the processes involved and the Cholskey Spectral factorization technique as detailed in Appendix A, the combined impulse response of the channel and the KFE is derived for the given ISI channel. Table 4.1 gives the computed values of the combined impulse response for some typical cases. The table also includes the overall noise variance  $\sigma_{v_0}^2$ , which is computed using the method of Box and Zenkins [17], as explained in Appendix B.

Table 4.2 Error event performance of the KFE-MLSE receiver structures for some typical ISI channels

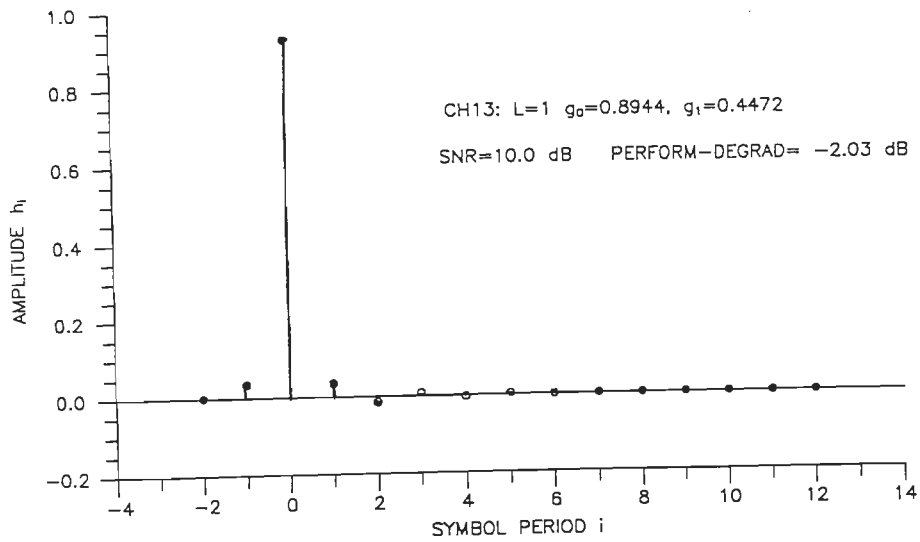
Sl. No.	TCM Scheme employed	ISI channel	SNR dB	$\sigma_v$	Coded KFE-MLSE Structure. Error Event Probability, Pe			Uncoded KFE reference	$h_0$	Performance degradation
					Lower bound	Upper bound	Simulation	Simulation		
1	4-state 16-QAM TCM	CH13	10.0	0.7071	0.214E-01	0.129E+00	0.433E-01	0.127E+00	0.9261	-2.03
			12.0	0.5613	0.539E-02	0.324E-01	0.161E-01	0.550E-01	0.9514	-2.09
			14.0	0.4462	0.665E-03	0.399E-02	0.236E-02	0.643E-02	0.9685	-2.14
			16.0	0.3544	0.266E-04	0.160E-03	0.100E-03	0.680E-03	0.9797	-2.17
2	8-state 16-QAM TCM	CH22	10.0	0.7071	0.195E-01	0.468E+00	0.372E-01	0.193E+00	0.9138	-2.76
			12.0	0.5613	0.468E-02	0.112E+00	0.269E-01	0.106E+00	0.9431	-2.82
			14.0	0.4462	0.515E-03	0.129E-01	0.977E-02	0.452E-01	0.9630	-2.86
			16.0	0.3544	0.191E-04	0.458E-03	0.114E-02	0.137E-01	0.9762	-2.88
3	8-state 64-QAM TCM	CH23	16.0	0.7263	0.102E-01	0.203E+00	0.329E-01	0.169E+00	0.9814	-1.77
			18.0	0.5669	0.175E-02	0.349E-01	0.163E-01	0.708E-01	0.9882	-1.78
			20.0	0.4583	0.118E-03	0.236E-02	0.163E-02	0.189E-01	0.9920	-1.78
			22.0	0.3640	0.184E-05	0.367E-04	0.200E-04	0.304E-02	0.9950	-1.79
4	16-state 64-QAM TCM	CH32	16.0	0.7263	0.208E-01	0.867E+00	0.206E-01	0.307E+00	0.9705	-3.84
			18.0	0.5669	0.516E-02	0.289E+00	0.162E-01	0.176E+00	0.9831	-3.87
			20.0	0.4583	0.621E-03	0.348E-01	0.938E-02	0.743E-01	0.9814	-3.92
			22.0	0.3640	0.240E-04	0.144E-02	0.910E-03	0.207E-01	0.9806	-3.98

The combined impulse response characteristics of the KFE-MLSE receiver structure, employed for the decoding of 4-state 16-QAM TCM signals transmitted over an ISI channel CH13 ( $L=1$ ), have been shown in Fig.4.5 for different values of SNR and corresponds to the entries at Sl. No. 1 of Table 4.1. The Fig.4.6 shows the combined impulse response characteristics of some of the KFE-MLSE receiver structures corresponding to the data given in Table 4.1 at SNR=10.0 dB. For a given ISI channel, the degradation in the performance of the KFE-MLSE receiver structure relative to its ISI-free performance has been computed using the discrete combined impulse response and the output noise variance  $\sigma_{v0}^2$ , as discussed in section 4.5. The computed value of performance degradation has been given, for each set of the combined impulse responses, in Fig.4.5 and Fig.4.6.

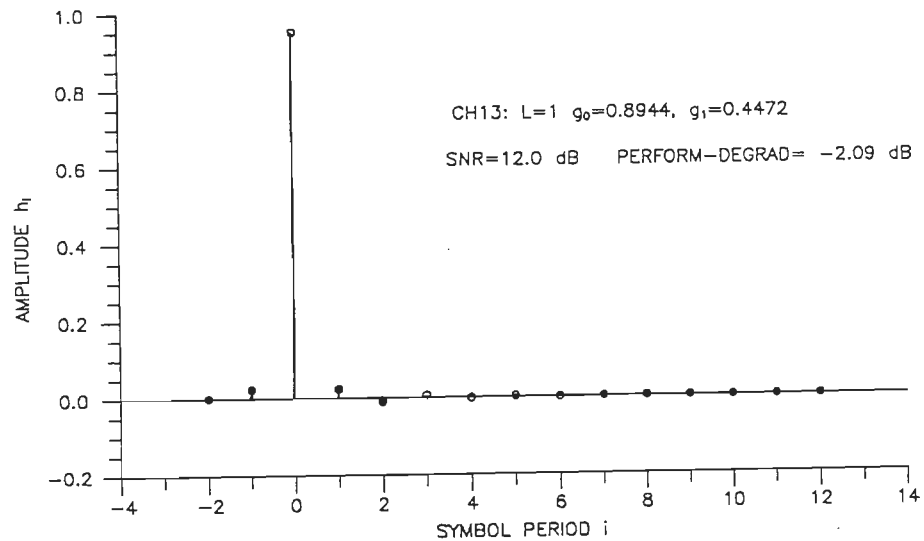
The performance of the KFE-MLSE structure under an ISI-free environment corresponds to that of the basic TCM scheme on AWGN channel, as discussed in section 4.5. For a given ISI channel, the performance degradation of the KFE-MLSE structure has been computed for different SNR using the combined impulse response and the overall noise variance. Since the performance bounds of the structure under an ISI-free environment are known, the performance bounds under an ISI environment can be computed using the performance degradation. The error performance so derived have been given in Table 4.2 for some typical cases. The table also includes the simulation results on the error performance of the coded KFE-MLSE structure and correspondingly those of the uncoded KFE receiver which is used as the reference system.

The error performance characteristics of the various KFE-MLSE receiver structures used in this study have been shown in Fig.4.7-4.14. The performance characteristics of the KFE-MLSE receiver structure used for the detection of 4-state 16-QAM TCM signals in the presence of ISI and AWGN have been shown in Fig.4.7 for a variety the ISI channels (of memory length  $L=1$  to  $L=3$ ) as listed in Table 3.1. For ISI memory length  $L=1$ , the KFE-MLSE performance is compared with that of the combined MLSE receiver that makes use of the combined ISI-Code trellis

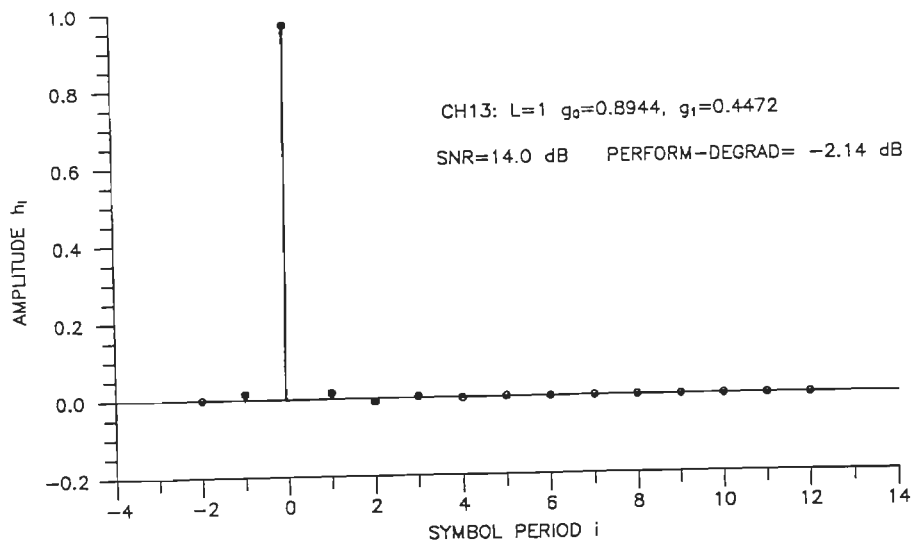




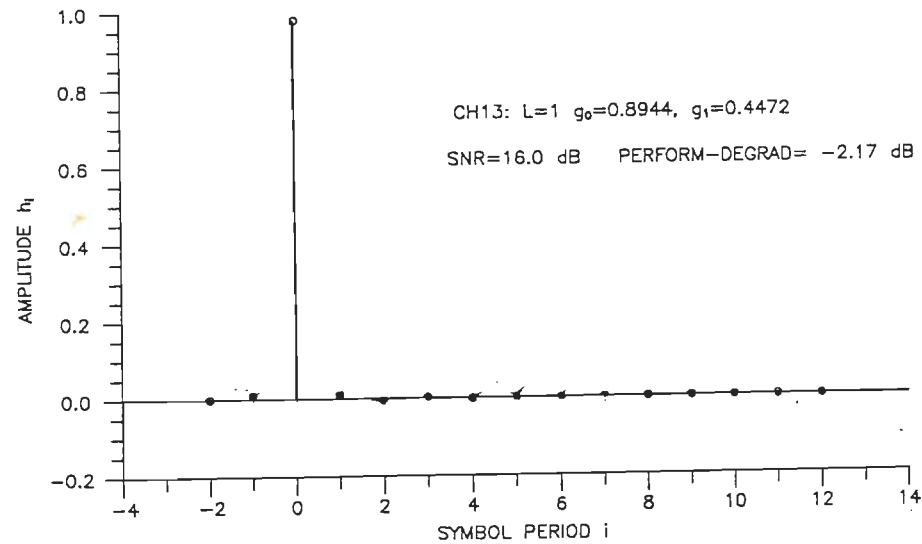
(a) ISI CHANNEL CH13 ; SNR=10.0 dB



(b) ISI CHANNEL CH13 ; SNR=12.0 dB



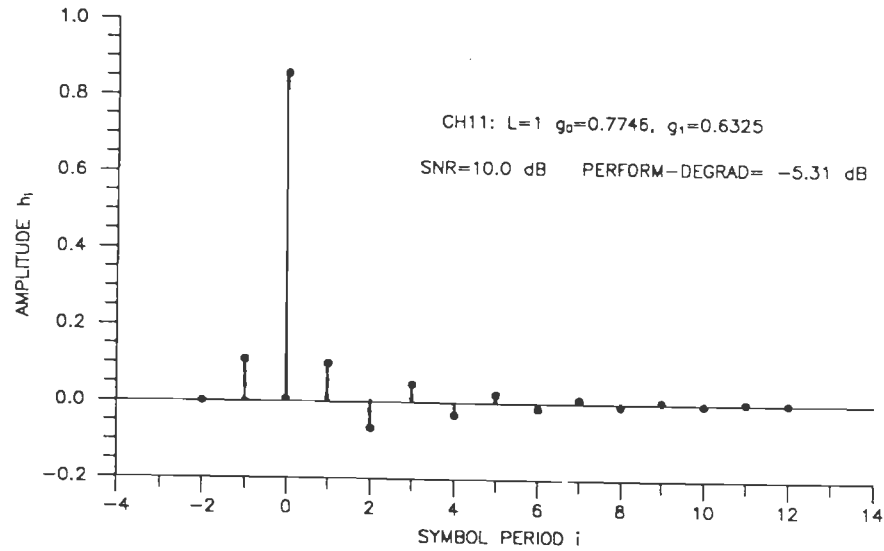
(c) ISI CHANNEL CH13 ; SNR=14.0 dB



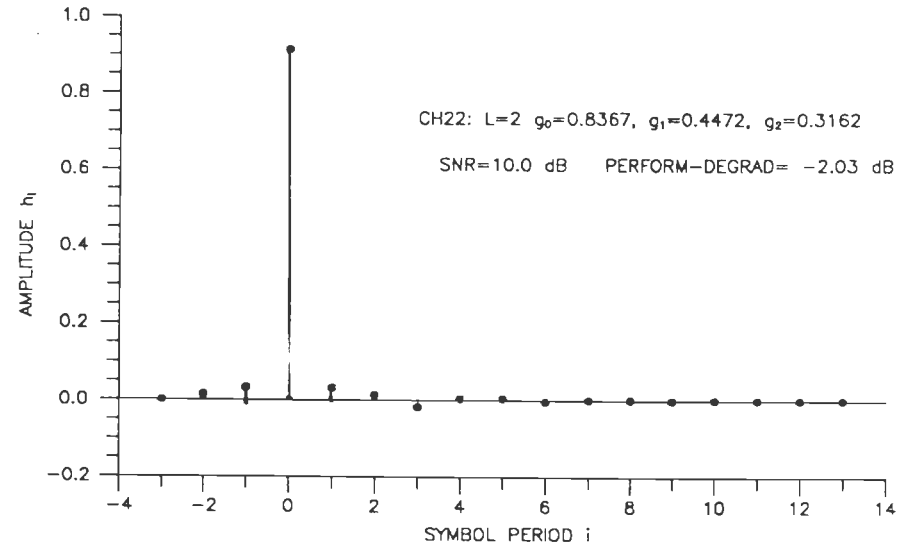
(d) ISI CHANNEL CH13 ; SNR=16.0 dB

FIG.4.5 THE COMBINED IMPULSE RESPONSE OF THE CHANNEL AND KFE FOR THE DECODING OF 4-STATE 16-QAM TCM SIGNALS THROUGH THE USE OF KFE-MLSE RECEIVER STRUCTURE.

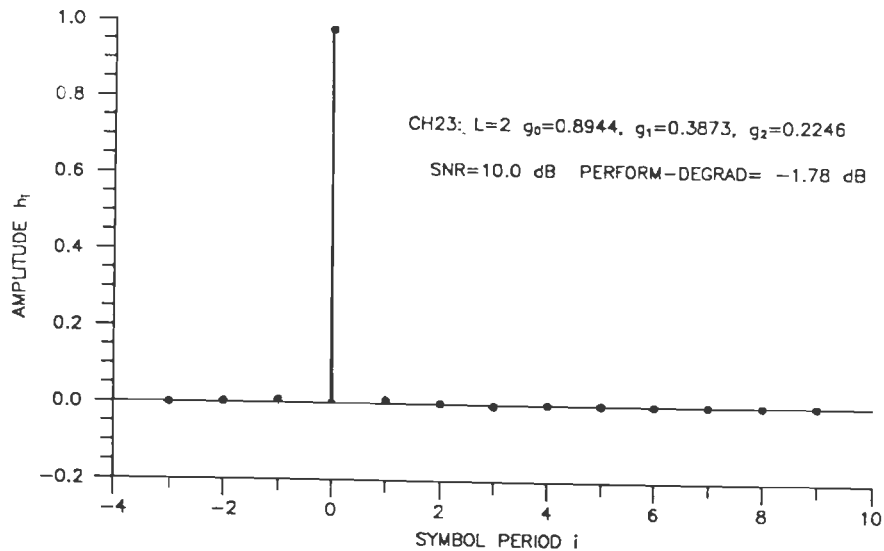
130



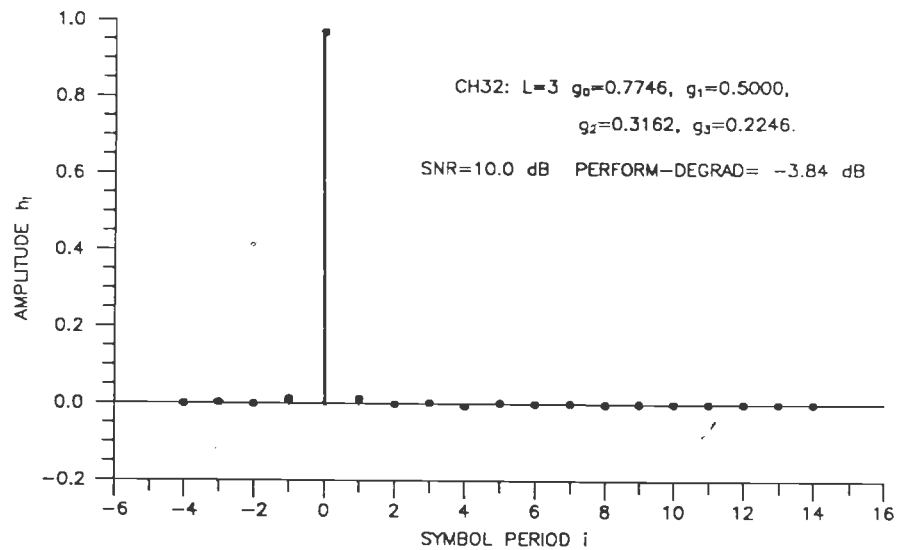
(a) 4-STATE 16-QAM TCM ON ISI CHANNEL CH11 AT SNR= 10.0 dB



(b) 8-STATE 16-QAM TCM ON ISI CHANNEL CH22 AT SNR= 10.0 dB

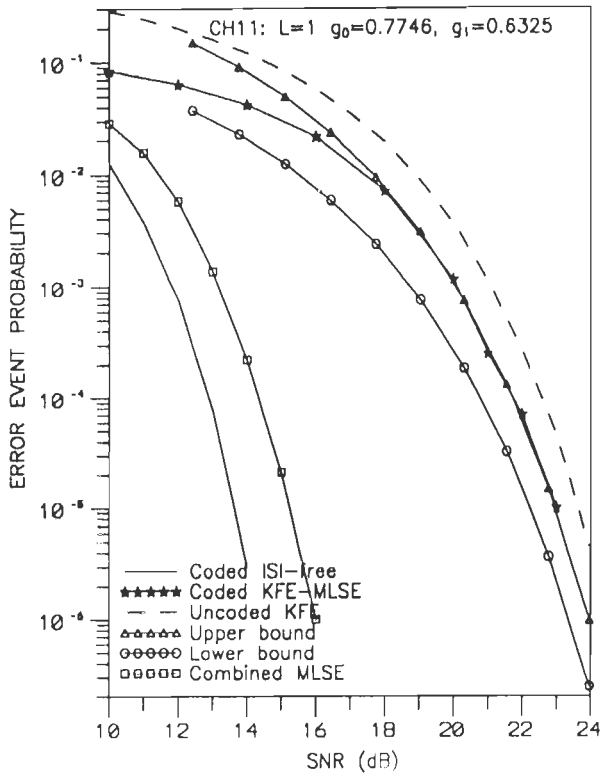


(c) 8-STATE 64-QAM TCM ON ISI CHANNEL CH23 AT SNR= 10.0 dB

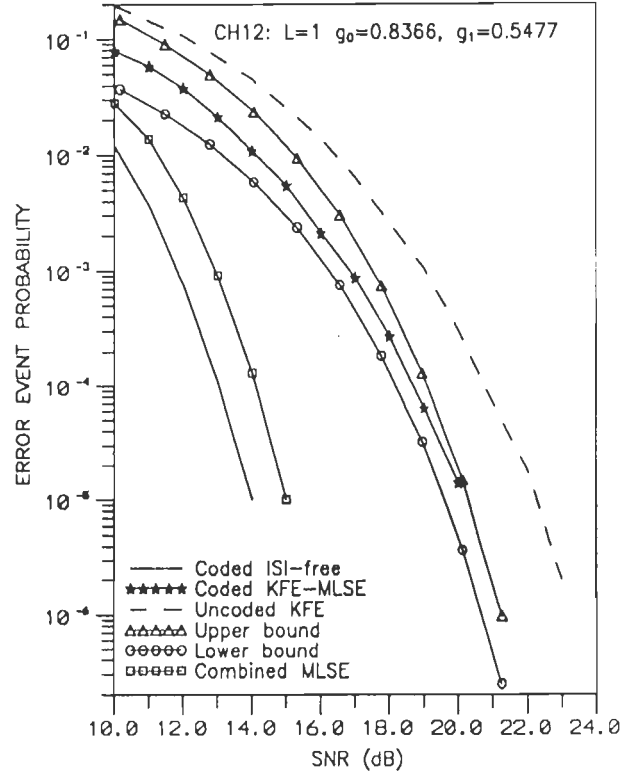


(d) 16-STATE 64-QAM TCM ON ISI CHANNEL CH32 AT SNR= 10.0 dB

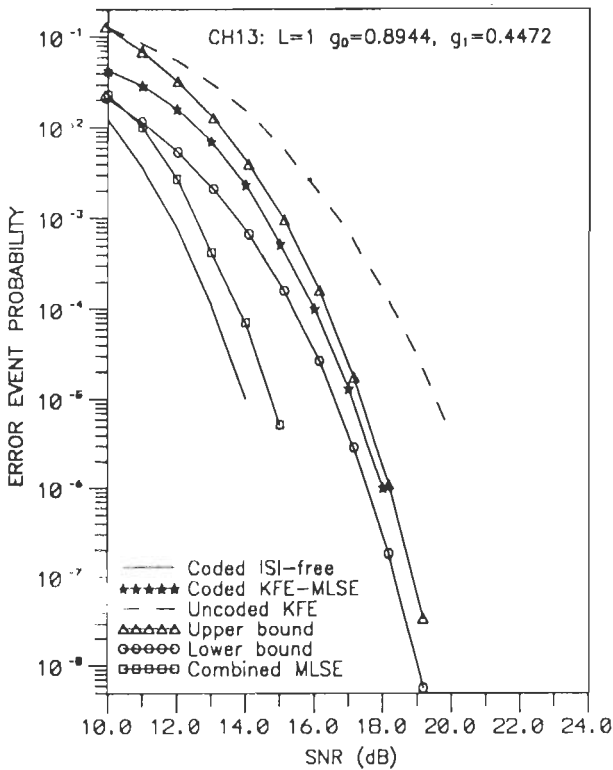
FIG.4.6 THE COMBINED IMPULSE RESPONSE OF THE CHANNEL AND KFE OF THE DIFFERENT KFE-MLSE RECEIVER STRUCTURES USED FOR DECODING OF TRELLIS-CODED M-QAM SIGNALS.



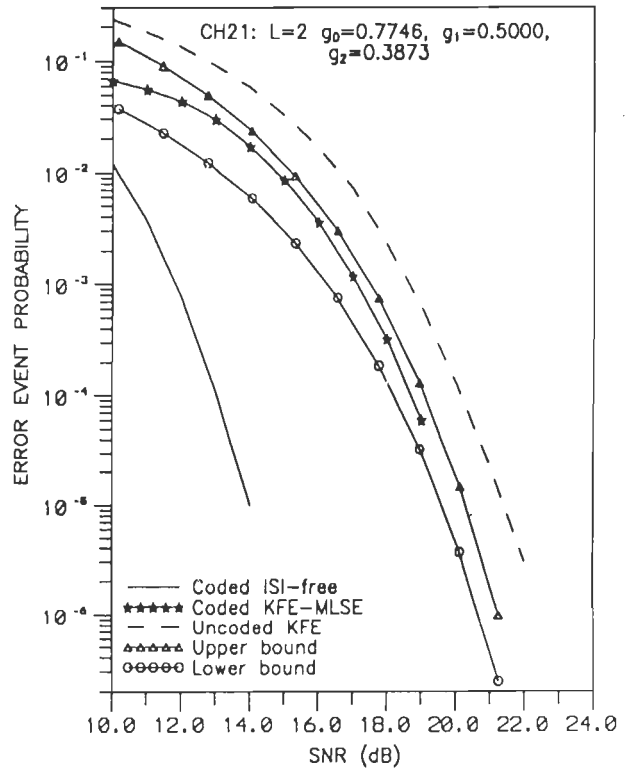
(a) 4-STATE 16-QAM TCM ON ISI CHANNEL CH11



(b) 4-STATE 16-QAM TCM ON ISI CHANNEL CH12

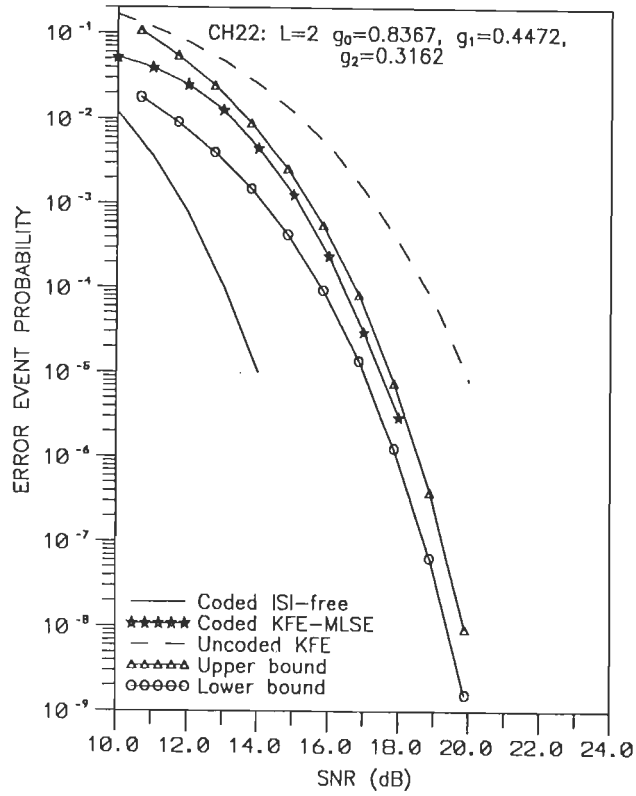


(c) 4-STATE 16-QAM TCM ON ISI CHANNEL CH13

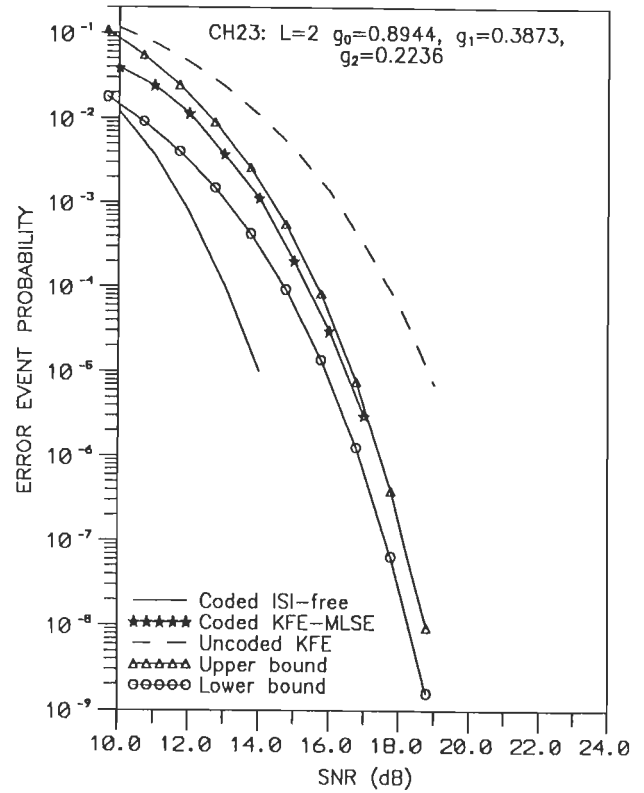


(d) 4-STATE 16-QAM TCM ON ISI CHANNEL CH21

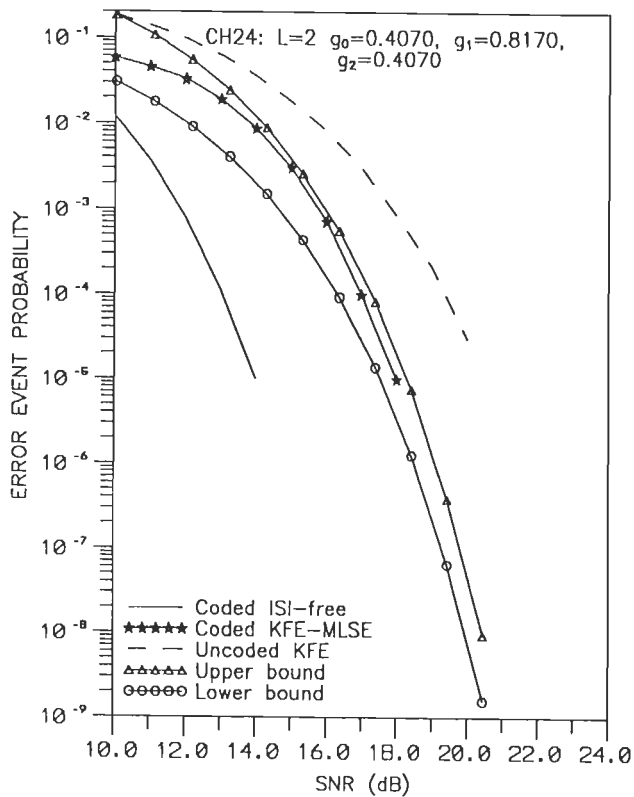
FIG.4.7 (Continued)



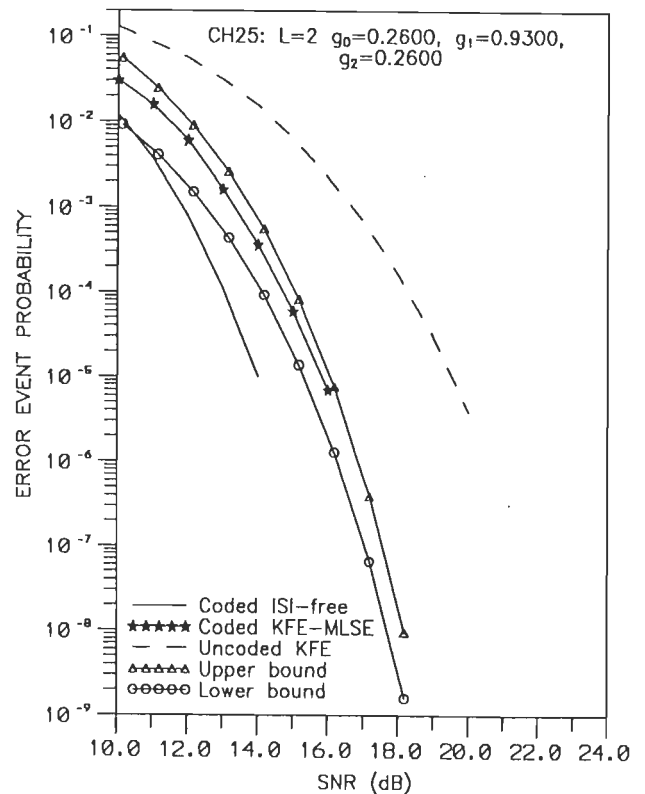
(e) 4-STATE 16-QAM TCM ON ISI CHANNEL CH22



(f) 4-STATE 16-QAM TCM ON ISI CHANNEL CH23

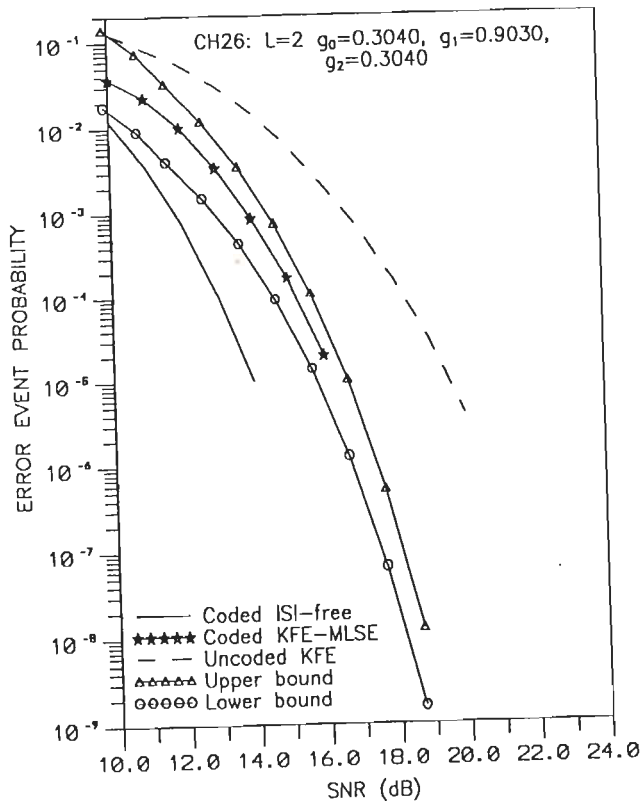


(g) 4-STATE 16-QAM TCM ON ISI CHANNEL CH24

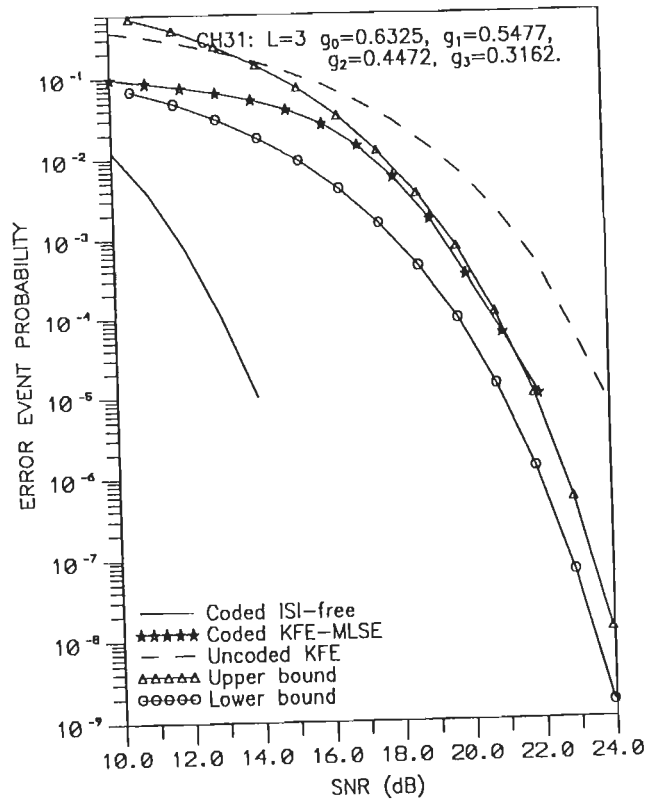


(h) 4-STATE 16-QAM TCM ON ISI CHANNEL CH25

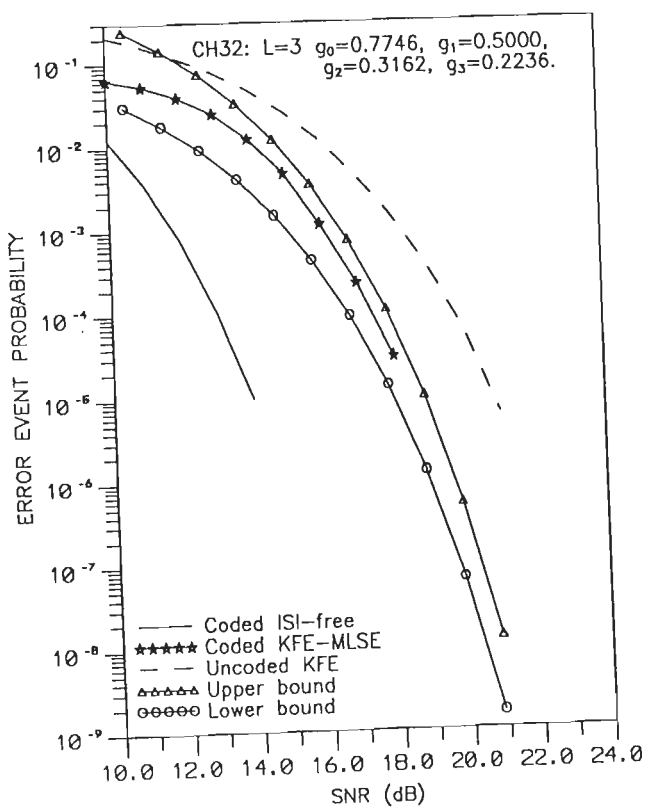
FIG.4.7 (Continued)



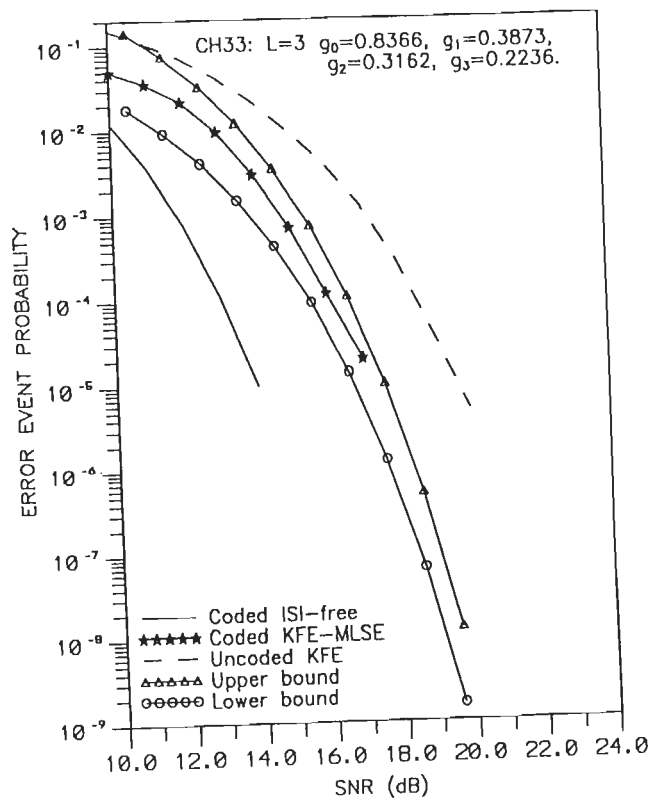
(j) 4-STATE 16-QAM TCM ON ISI CHANNEL CH26



(i) 4-STATE 16-QAM TCM ON ISI CHANNEL CH31



(k) 4-STATE 16-QAM TCM ON ISI CHANNEL CH32



(l) 4-STATE 16-QAM TCM ON ISI CHANNEL CH33

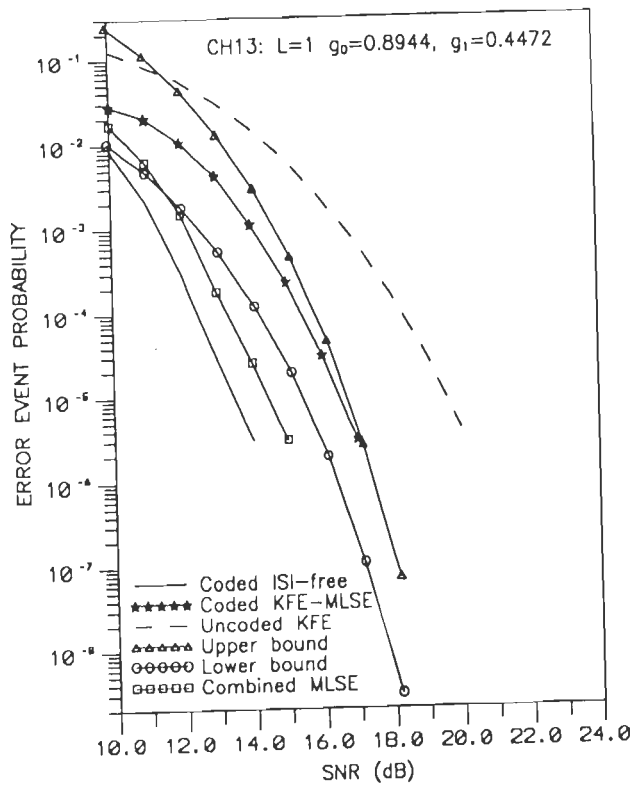
FIG.4.7 ERROR PERFORMANCE OF THE KFE-MLSE RECEIVER STRUCTURE FOR 4-STATE 16-QAM TCM TRANSMISSION ON DIFFERENT ISI CHANNELS.

for the detection of TCM signals in the presence of ISI and AWGN. From Fig.4.7(a)-(c) we note that the KFE-MLSE structure, although sub-optimum relative to the 32-state coded combined MLSE structure (of section 3.4.2), achieves a considerable coding gain of 2.25–3 dB at  $P_e=10^{-5}$  relative to the uncoded KFE reference system without the compromising bandwidth efficiency or power efficiency. We may recall that the coded combined MLSE receiver structure had maintained almost the same gain margin over its uncoded MLSE reference structure.

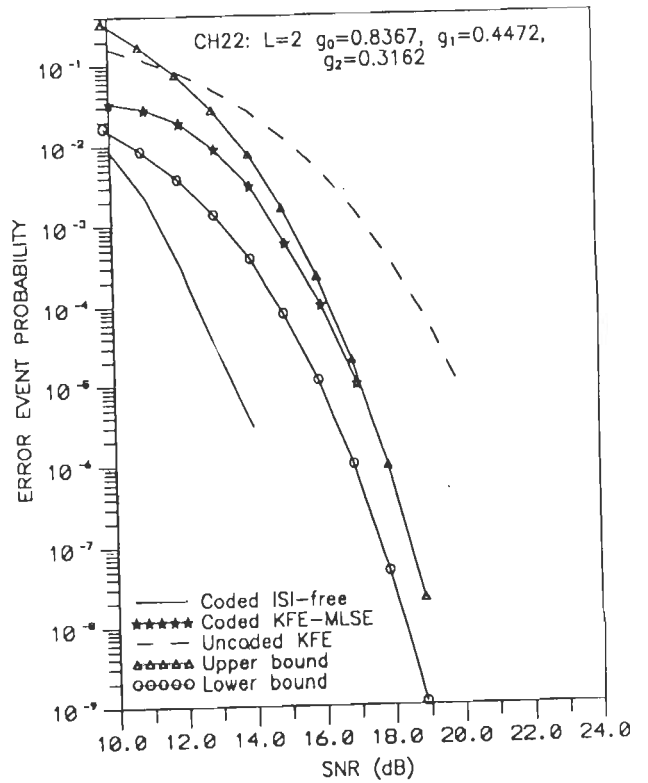
The characteristics shown in Fig.4.7(d)-(i) correspond to the performance of the coded KFE-MLSE structure used for the detection of 4-state 16-QAM TCM signals transmitted over ISI channels of memory length  $L=2$ , while the characteristics of Fig.4.7(j)-(l) correspond to that of channels with memory  $L=3$ . Also shown in Fig.4.7 are the performance bounds evaluated through the procedure of section 4.5. We observe that, in each case, the simulation result on the error performance of the coded KFE-MLSE structure lies well within the computed upper and lower bounds on the error event probability.

Fig.4.8 shows the error performance characteristics of the 8-state 16-QAM TCM based KFE-MLSE receiver structure for 4 different ISI channels CH13, CH22, CH24 and CH33 of Table 3.1. From the simulation results, we note that the KFE-MLSE structure achieves a coding gain of about 2.75 – 3.0 dB over the uncoded KFE reference system. The computed upper and lower bounds on the error event probability are quite tight, in the sense that the simulation result lies well within the bounds.

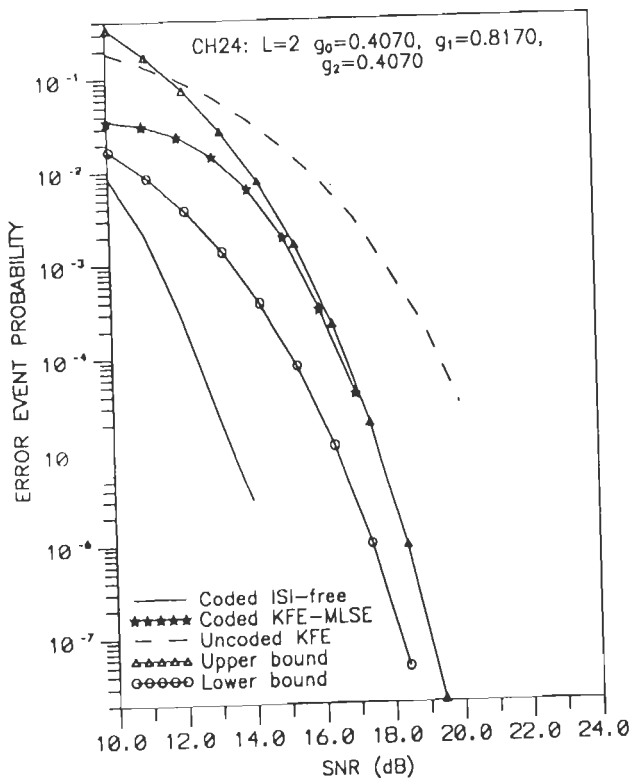
Similarly, Fig.4.9 shows the error performance of the 16-state 16-QAM TCM based KFE-MLSE receiver for 4 different ISI channels CH13, CH21, CH26 and CH32. The coded KFE-MLSE structure achieves a significant coding gain in the range of 3.0 – 4.0 dB (approx.) over the uncoded KFE reference system for the same data rate, bandwidth and signal energy. Again we observe that the simulation result is well bounded by the computed upper and lower bounds on the error event probability.



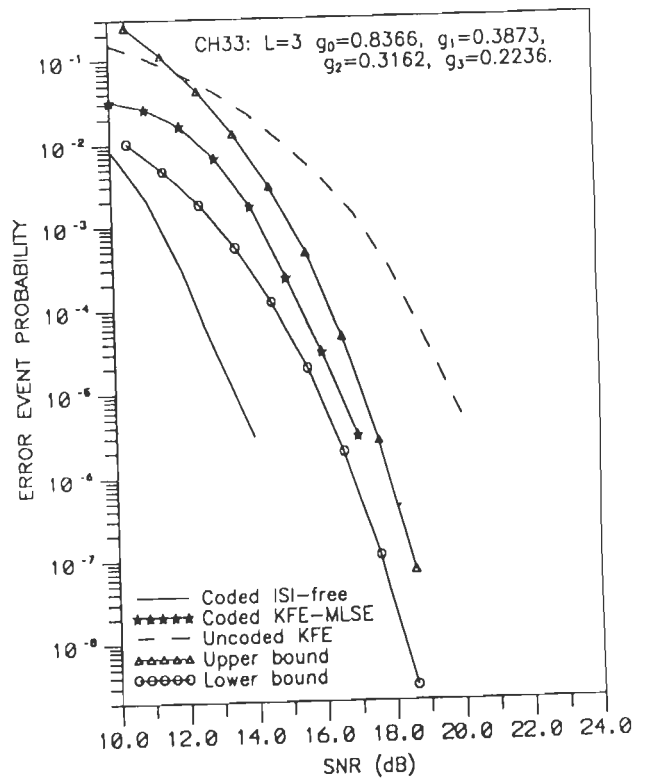
(a) 8-STATE 16-QAM TCM ON ISI CHANNEL CH13



(b) 8-STATE 16-QAM TCM ON ISI CHANNEL CH22

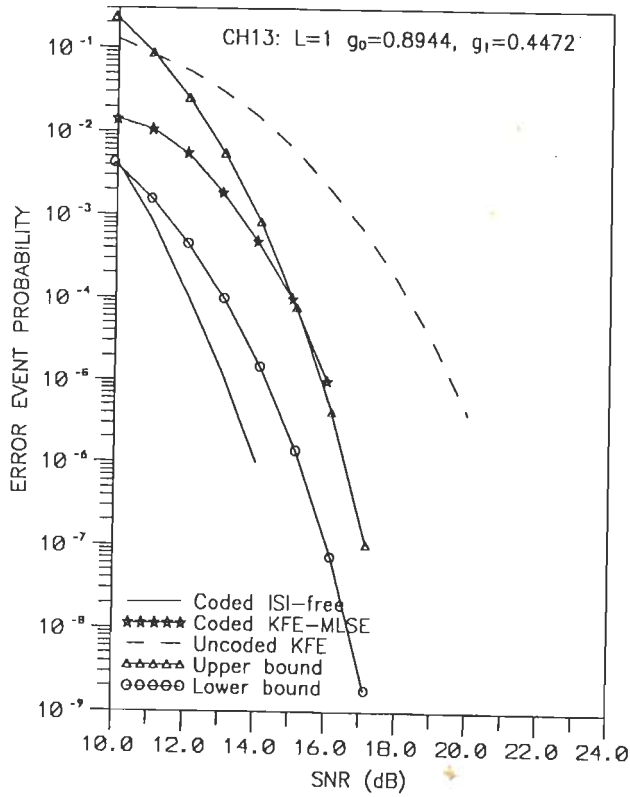


(c) 8-STATE 16-QAM TCM ON ISI CHANNEL CH24

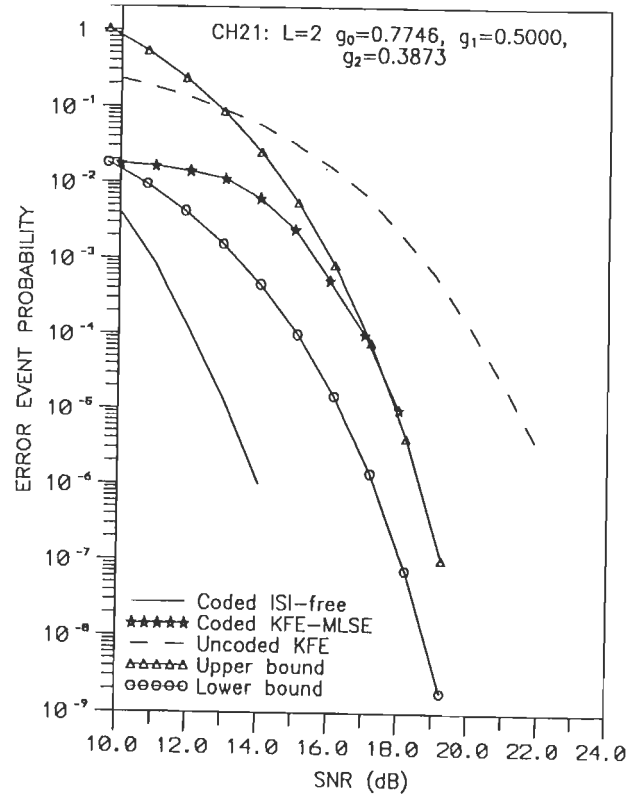


(d) 8-STATE 16-QAM TCM ON ISI CHANNEL CH33

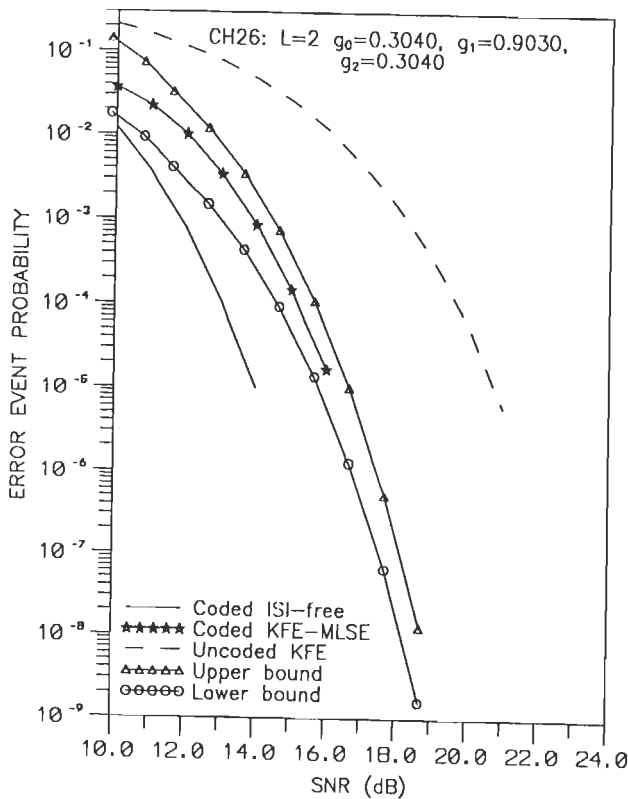
FIG.4.8 ERROR PERFORMANCE OF THE KFE-MLSE RECEIVER STRUCTURE FOR 8-STATE 16-QAM TCM TRANSMISSION ON DIFFERENT ISI CHANNELS.



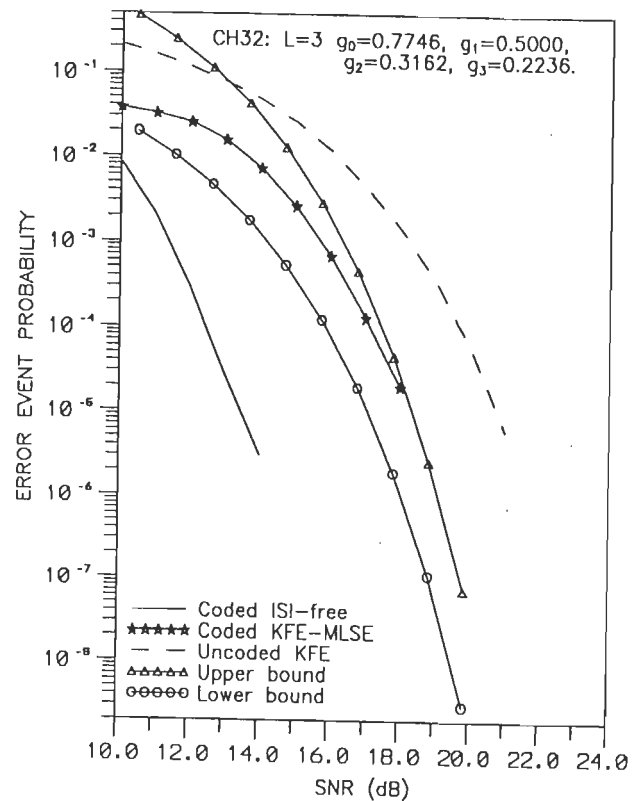
(a) 16-STATE 16-QAM TCM ON ISI CHANNEL CH13



(b) 16-STATE 16-QAM TCM ON ISI CHANNEL CH21



(c) 16-STATE 16-QAM TCM ON ISI CHANNEL CH26



(d) 16-STATE 16-QAM TCM ON ISI CHANNEL CH32

FIG.4.9 ERROR PERFORMANCE OF THE KFE-MLSE RECEIVER STRUCTURE FOR 16-STATE 16-QAM TCM TRANSMISSION ON DIFFERENT ISI CHANNELS.

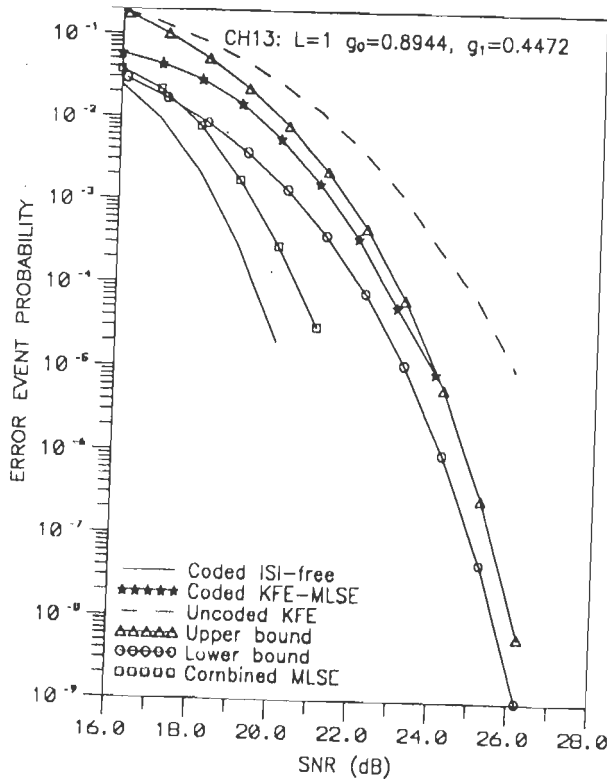


Fig.4.10-4.12 show respectively the error performance characteristics of the KFE-MLSE structures for the 4-state, 8-state and 16-state trellis-coded 64-QAM signal transmissions over different ISI channels. From the characteristics of Fig.4.10-4.12, we note that the coding gain of the KFE-MLSE structure for the 4-state 64-QAM TCM transmission is in the range of 2-2.5 dB, while it ranges between 2.5-3.0 dB and 2.5-4.0 dB respectively for the 8-state and 16-state 64-QAM TCM schemes. In Fig.4.11 and Fig.4.12, we find that the simulation result in most cases does agree with the computed bounds.

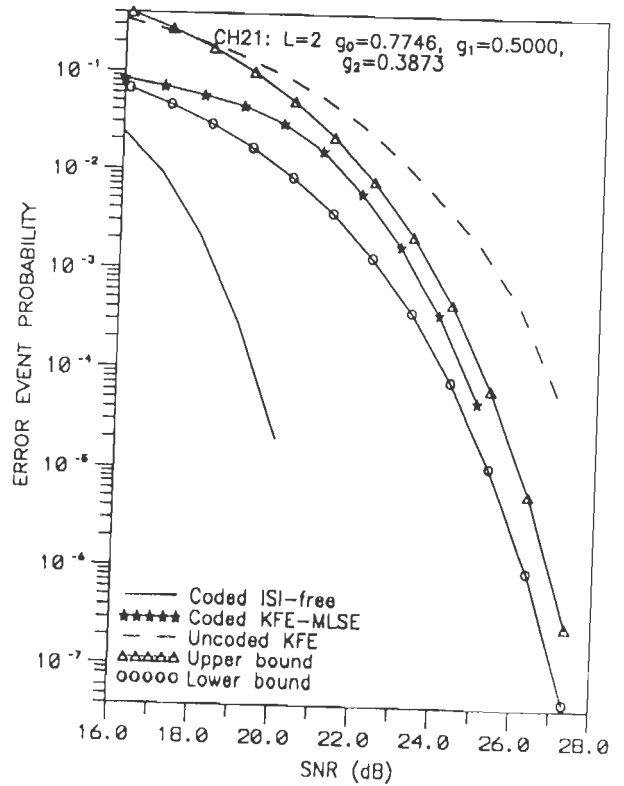
The performance comparison of the different KFE-MLSE receiver structures used for the 16-QAM TCM transmission have been presented in Fig.4.13. From the performance characteristics, we can observe that there is an increase in the coding gain with the use of 8-state or 16-state TCM schemes relative to that achievable with the 4-state TCM scheme. For the 16-state TCM 16-QAM transmission we find, from Fig.4.13(b), that the performance of the KFE-MLSE receiver is nearly close to that of the combined MLSE structure. Although the KFE-MLSE structure is sub-optimum, it achieves a considerable coding gain over uncoded KFE reference system, with the advantage of reduced complexity.

Fig.4.14, similarly, gives the performance comparison of the 4-state, 8-state, 16-state TCM based KFE-MLSE receiver structures. Again, we can see the performance advantage of 8-state and 16-state TCM schemes over the 4-state TCM scheme. From Fig.4.14(b) we can note that the 16-state TCM based KFE-MLE achieves a good performance, which is close that attained with 128-state combined MLSE receiver. Thus, with the use of 8-state or 16-state TCM scheme, we can achieve a good performance with the KFE-MLSE receiver structure over an ISI channel, without any restriction on the ISI memory length  $L$  or the size of the signal constellation, unlike as in the case of combined MLSE receiver structure.

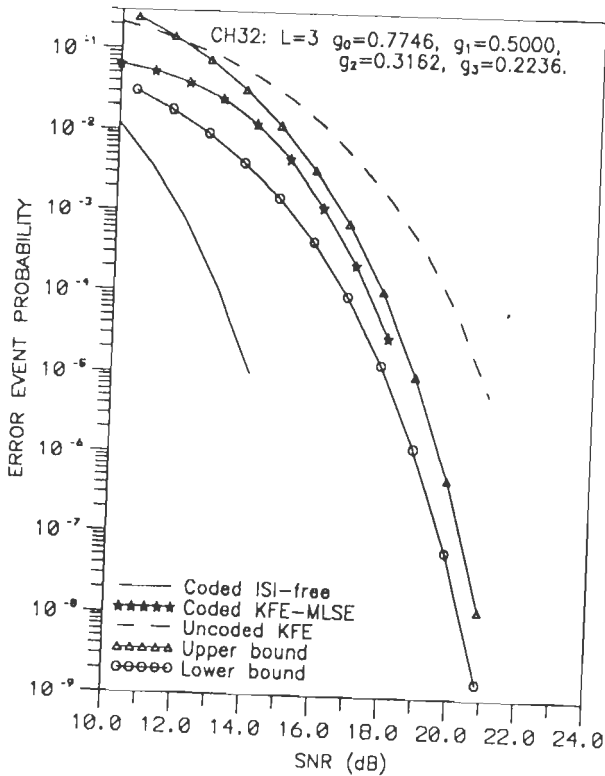
From the performance characteristics, we note that the coded KFE-MLSE receiver structures achieve a coding gain of about 2-2.5 dB over the uncoded KFE reference system for the same data rate, bandwidth and energy constraints.



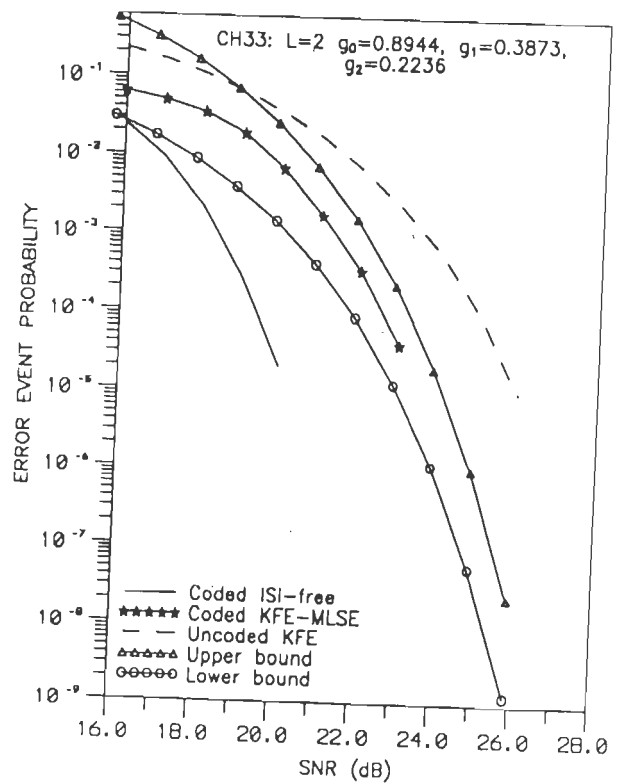
(a) 4-STATE 64-QAM TCM ON ISI CHANNEL CH13



(b) 4-STATE 64-QAM TCM ON ISI CHANNEL CH21

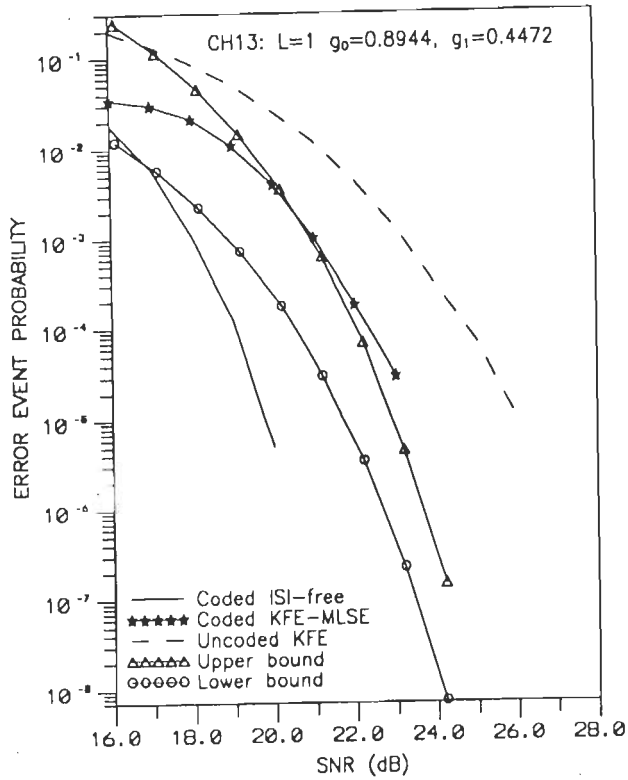


(c) 4-STATE 64-QAM TCM ON ISI CHANNEL CH32

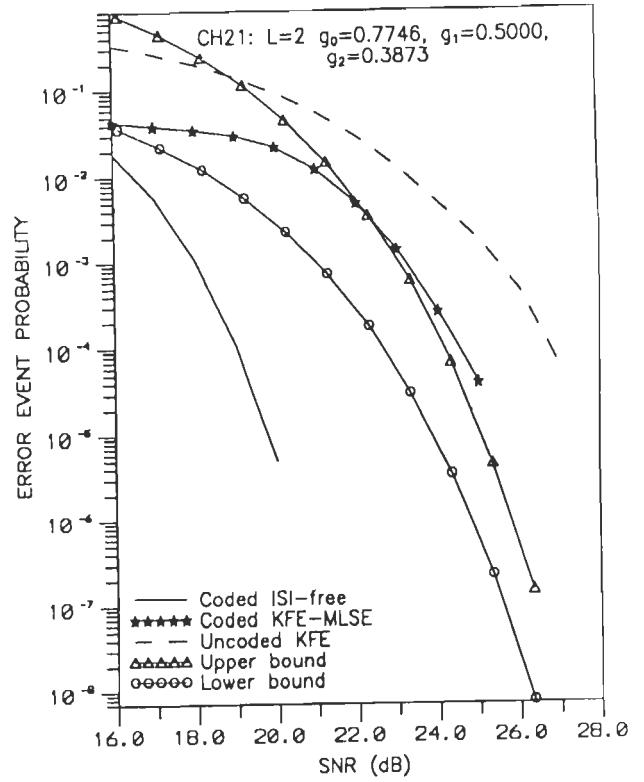


(d) 4-STATE 64-QAM TCM ON ISI CHANNEL CH33

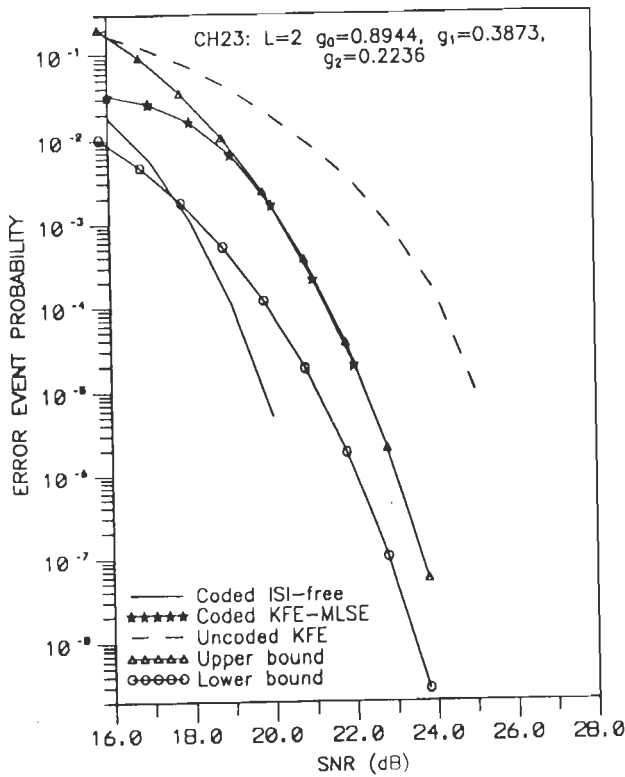
FIG.4.10 ERROR PERFORMANCE OF THE KFE-MLSE RECEIVER STRUCTURE FOR 4-STATE 64-QAM TCM TRANSMISSION ON DIFFERENT ISI CHANNELS.



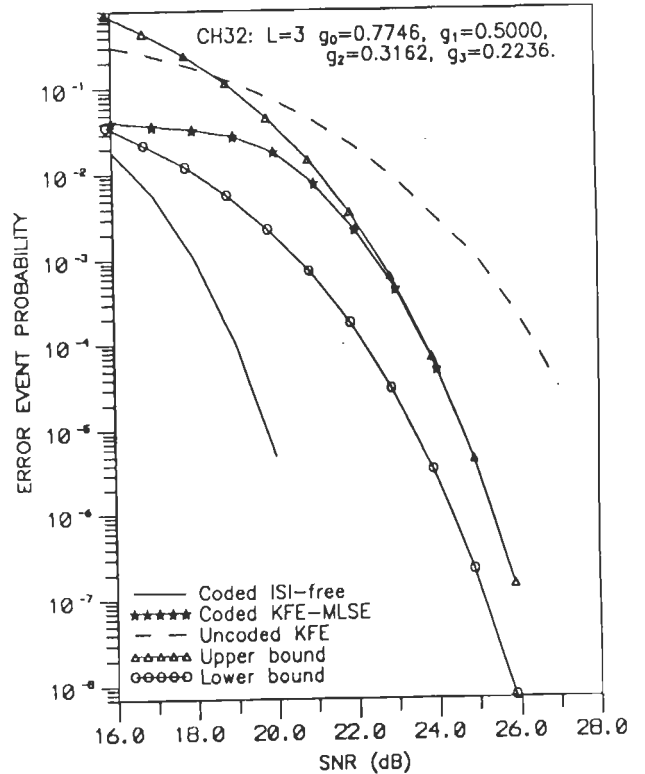
(a) 8-STATE 64-QAM TCM ON ISI CHANNEL CH13



(b) 8-STATE 64-QAM TCM ON ISI CHANNEL CH21

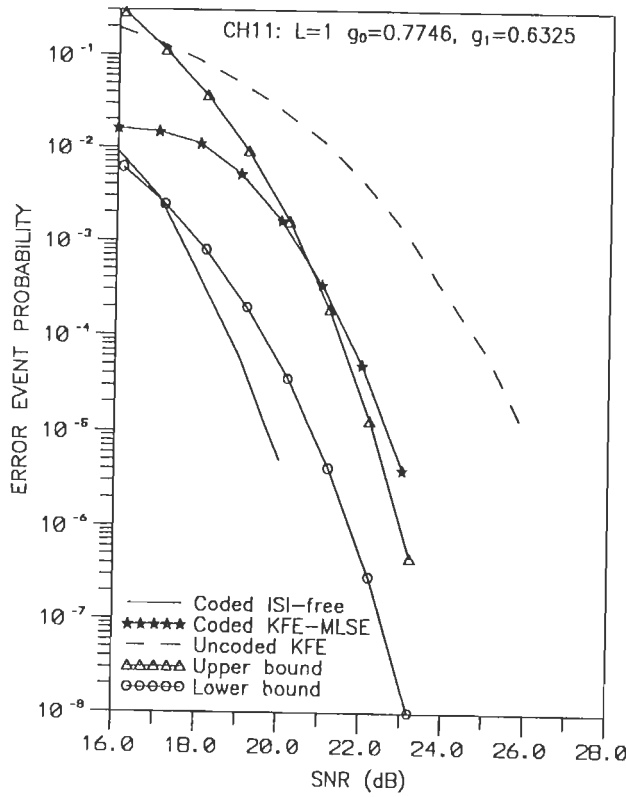


(c) 8-STATE 64-QAM TCM ON ISI CHANNEL CH23

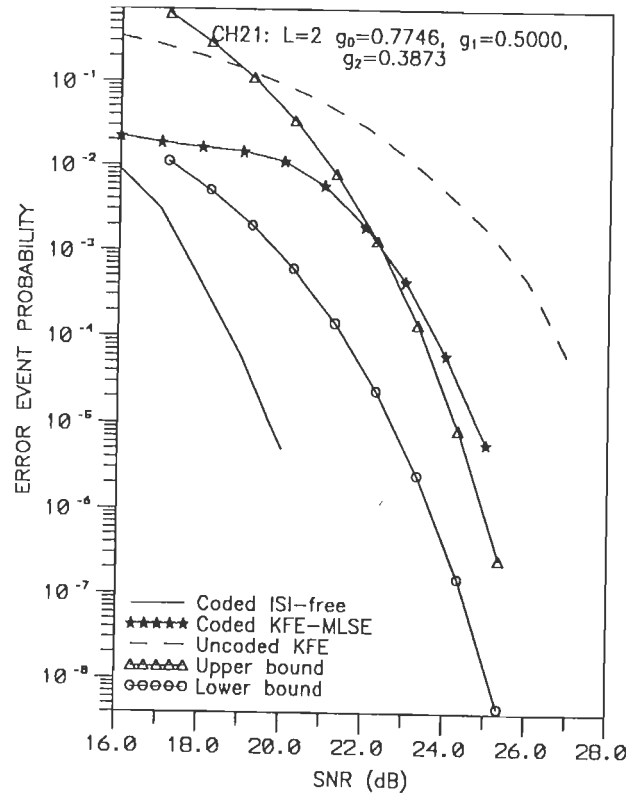


(d) 8-STATE 64-QAM TCM ON ISI CHANNEL CH32

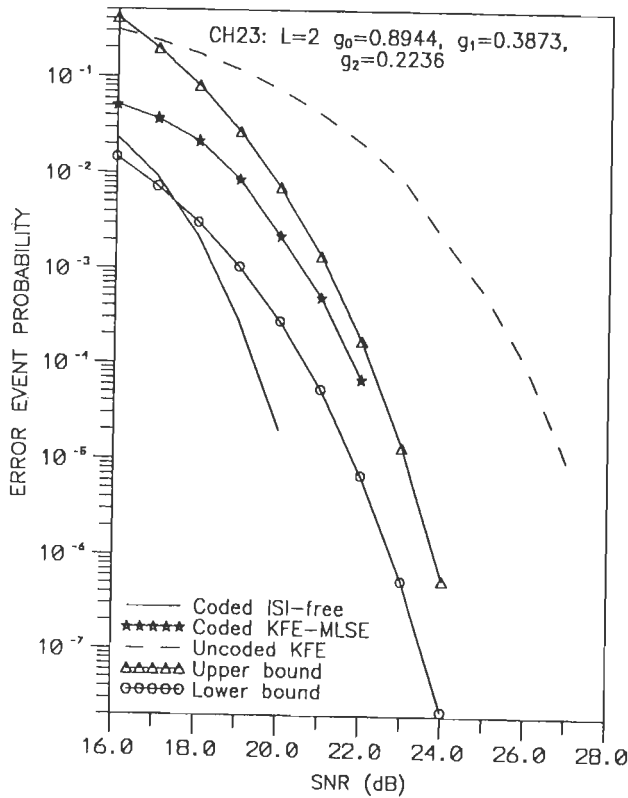
FIG.4.11 ERROR PERFORMANCE OF THE KFE-MLSE RECEIVER STRUCTURE FOR 8-STATE 64-QAM TCM TRANSMISSION ON DIFFERENT ISI CHANNELS.



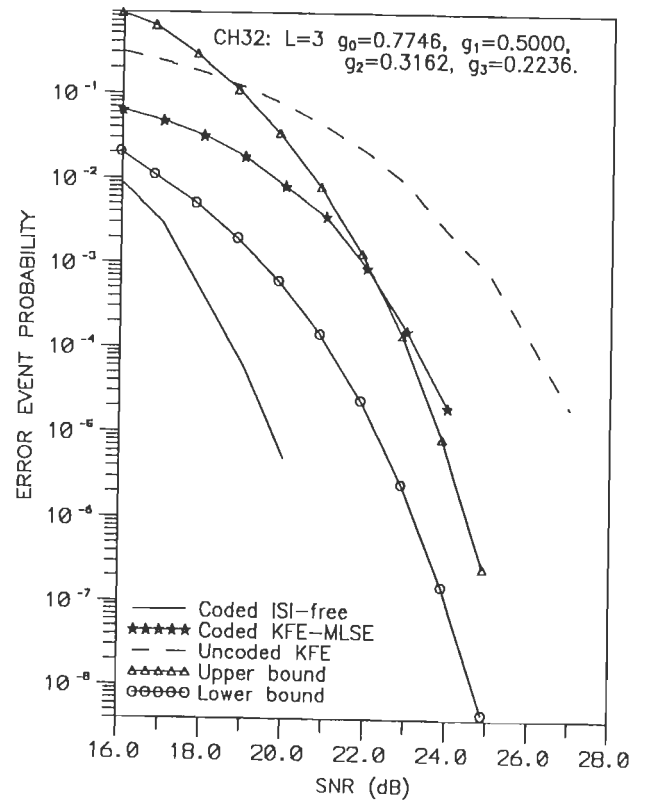
(a) 16-STATE 64-QAM TCM ON ISI CHANNEL CH11



(b) 16-STATE 64-QAM TCM ON ISI CHANNEL CH21

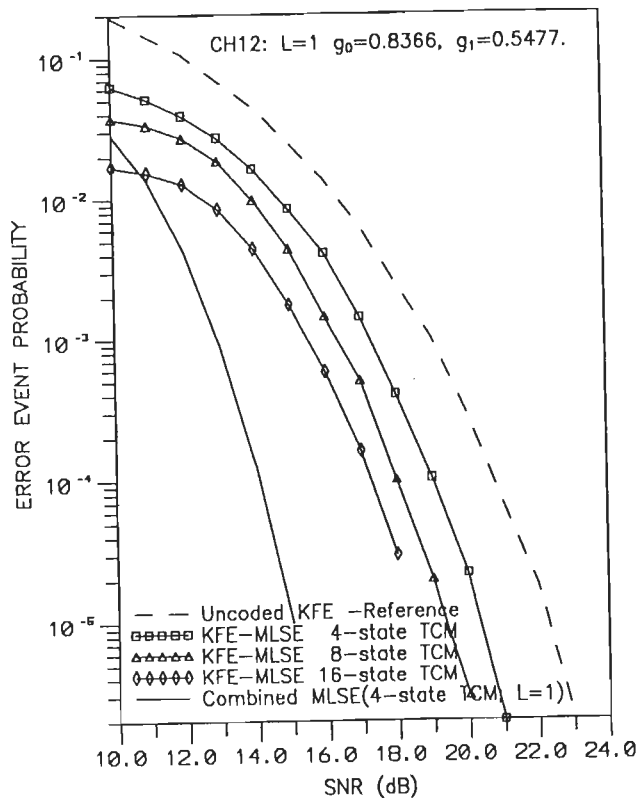


(c) 16-STATE 64-QAM TCM ON ISI CHANNEL CH23

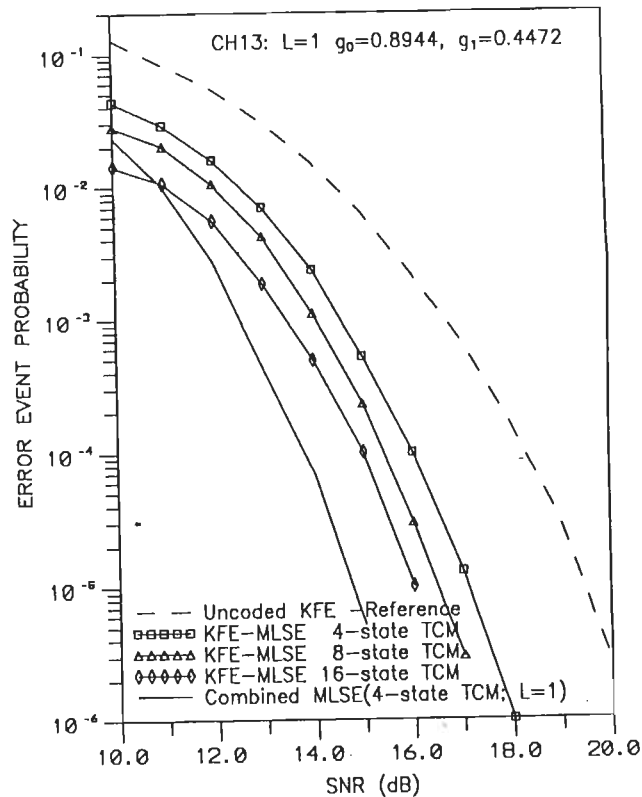


(d) 16-STATE 64-QAM TCM ON ISI CHANNEL CH32

FIG.4.12 ERROR PERFORMANCE OF THE KFE-MLSE RECEIVER STRUCTURE FOR 16-STATE 64-QAM TCM TRANSMISSION ON DIFFERENT ISI CHANNELS.

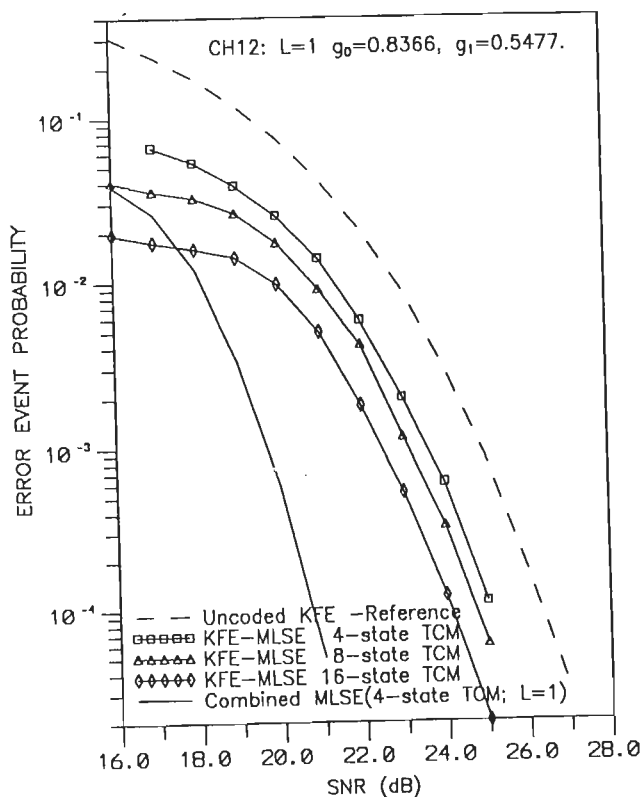


(a) ISI CHANNEL CH12:  $L=1$

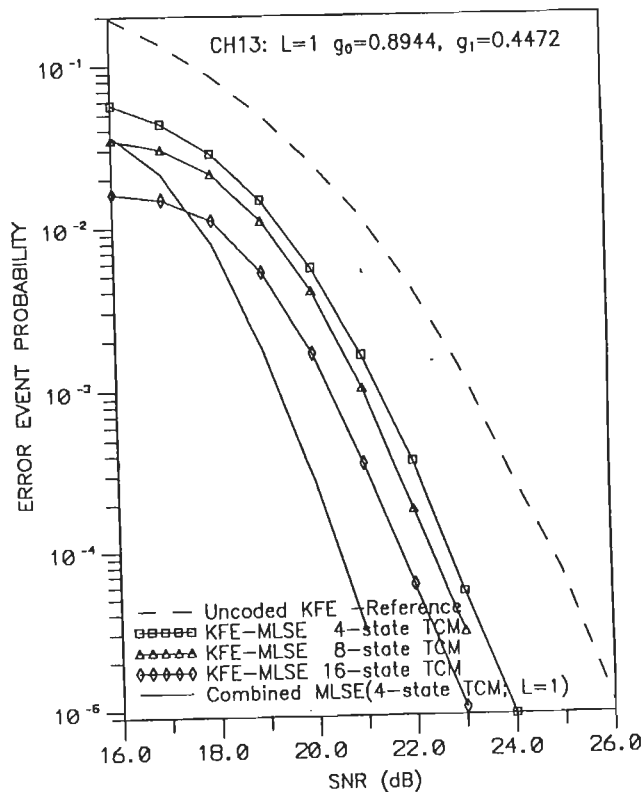


(b) ISI CHANNEL CH13:  $L=1$

FIG4.13 PERFORMANCE COMPARISON OF THE KFE-MLSE RECEIVER STRUCTURES USING DIFFERENT TCM SCHEMES FOR 16-QAM TRANSMISSION ON ISI CHANNEL.



(a) ISI CHANNEL CH12:  $L=1$



(b) ISI CHANNEL CH13:  $L=1$

FIG4.14 PERFORMANCE COMPARISON OF THE KFE-MLSE RECEIVER STRUCTURES USING DIFFERENT TCM SCHEMES FOR 64-QAM TRANSMISSION ON ISI CHANNEL.

Although the performance of the proposed KFE-MLSE structure is sub-optimum when compared to that of the coded combined MLSE receiver structure, the former has the advantage of practical implementation for the detection of TCM on ISI channels of large memory ( $L > 3$ ) whereas the latter structure is almost impractical to realize for such channels. Moreover, the error performance characteristics of the KFE-MLSE receiver structure can easily be evaluated through bounds using the procedure of section 3.5, that makes use of the steady-state characteristics such as the combined impulse response, overall noise variance, and the distance properties of the basic TCM scheme employed. Hence, we may conclude that the KFE-MLSE structure proposed, for the detection of the trellis-coded QAM signals in the presence of ISI and AWGN, is a practically viable (feasible) system which offers substantial coding gains over the uncoded reference system. However, it may be noted that the proposed KFE-MLSE structure is suboptimum compared to the (optimum) combined MLSE receiver structure.



## SUB-OPTIMUM REDUCED STATE ALGORITHMS FOR TCM DECODING ON ISI CHANNELS

---

### 5.1 INTRODUCTION

An alternative to the prefiltering technique is the use of reduced state algorithms which aim at reducing the states of the optimum combined ISI-Code trellis by channel truncation and/or by combining the states to form subset-states using the set-partitioning principle. These algorithms incorporate a built-in decision-feedback mechanism within the Viterbi decoder to cancel out the residual ISI terms during each path metric computation, based on the data symbol decisions associated with the path leading to that transition.

The complexity of the optimum decoder can be reduced by truncating the effective channel memory to  $J$  where  $0 \leq J \leq L$ , and the resulting structure is a sub-optimum truncated combined ISI-Code receiver. The  $(L-J)$  residual ISI terms which are not represented by the truncated combined ISI-Code trellis are estimated and subtracted from the branch metric computations using the path history decisions in the Viterbi algorithm. The state complexity of the truncated combined ISI-Code trellis is  $N_s(M/2)^J$ , where  $N_s$  is the number of encoder states and  $M$  is the size of the signal constellation employed in the TCM scheme [26].

With a TCM scheme employing large signal constellation, the reduction in state complexity may not be substantial even for a truncation length of  $J=1$ . A further reduction in state complexity is still desired. This can be achieved by incorporating the ideas of set-partitioning inherent in TCM to define the subset-



states for the truncated combined ISI-Code trellis. This approach leads to a reduced state decoder whose state complexity is independent of the constellation size  $M$ . Such decoder structures are referred to as reduced state sequence estimators (RSSE). The state complexity of the RSSE may range between that of the TCM encoder and that of the optimum receiver. As the state complexity of RSSE is increased, its performance approaches that of the optimum combined ISI-Code receiver [26, 42].

When the state complexity of RSSE reduces to that of the TCM encoder, the structure is referred to as the parallel decision-feedback decoder (PDFD). The PDFD is useful for a system with a large channel impulse response while the RSSE is more suitable for a system with large signal constellation [42].

The evaluation of error performance of these reduced state algorithms is, in general, difficult to perform analytically because of the decision-error propagation. The decisions, which are being used to cancel out the residual ISI, are derived from the path history and therefore are not the true estimates of the past symbols. Consequently, this leads to the possibility of error propagation in these algorithms and hence to the difficulty in evaluating the performance analytically. We have considered the performance evaluation of these algorithms through simulation.

Eyuboglu and Qureshi [41] had proposed the technique of RSSE decoding for uncoded transmission over time-dispersive channels, which they later applied to the coded-modulation schemes [42]. Chevillat and Eleftheriou [26] have independently proposed a similar approach for the decoding of TCM signals in the presence of ISI and AWGN. Simulation techniques have been used by both the investigators [26, 42] for the performance study of the RSSE structures using a 4-state 16-QAM TCM scheme, for a typical channel.

We, in the following, have presented the results of a detailed study of several RSSE structures, for the decoding of various Trellis-coded QAM signals (with different constellation sizes) transmitted over time-dispersive channels of

different orders of memory length, through simulation techniques.

Following the approach given in [26], we first consider the channel truncation technique to reduce the number of states in the combined ISI-Code trellis. We next consider the method of combining channel truncation with the ideas of set-partitioning principle to arrive at the RSSE structures. The simplest form of RSSE, namely the PDFD is considered next. We have constructed several reduced state trellis structures for the decoding of various TCM schemes employing different QAM signal constellations. The performance of these reduced state receiver structures for several TCM schemes have been studied, through simulation, on different ISI channels and the results are presented.

## 5.2 REDUCED STATE TRUNCATED COMBINED ISI-CODE RECEIVER

The state complexity of the optimum combined ISI-Code receiver can be reduced by truncating the effective channel memory to  $J$  and using a built-in DFE-like mechanism within the Viterbi decoder to cancel out the residual  $(L-J)$  ISI terms, that are not represented by the truncated combined state trellis. For a truncation memory length of  $J$ , the state complexity of such receivers is  $N_s(M/2)^J$ , where  $N_s$  is the number of TCM encoder states,  $M$  is alphabet size,  $M=2^{m+1}$ , and  $0 \leq J \leq L$ . The Viterbi decoder operates on this reduced state truncated combined ISI-Code trellis and the resulting receiver structure is sub-optimum.

Truncating the channel memory to  $J$  leads to a reduced state truncated combined ISI-Code trellis whose states are defined by [26],

$$\mu_n^J = (\alpha_n; a(n-1), a(n-2), \dots, a(n-J)) \quad \dots(5.1)$$

where  $0 \leq J \leq L$ , and  $\mu_n^0 = \alpha_n$

The performance degradation due to  $(L-J)$  ISI terms not represented by the truncated combined state  $\mu_n^J$  is compensated by incorporating an ISI-cancellation mechanism into the branch metric computation. The  $(L-J)$  residual ISI terms are estimated using the decisions derived from the path history associated with the

reduced states. Note that each truncated combined state  $\mu_n^J$  gives information on  $J$  past symbols  $\{a(n-i)\}$ ,  $1 \leq i \leq J$ , associated with that state.

Associated with each state  $\mu_n^J$ , there will be a unique survivor path with a history of path symbol estimates  $\{\dots, \hat{a}(n-L), \dots, \hat{a}(N-J-2), \hat{a}(n-J-1)\dots\}$  and a survivor path metric defined as  $\tilde{M}(n-1)(\mu_n^J)$ . The Viterbi algorithm computes recursively the survivor path metric as

$$\tilde{M}_n(\mu_{n+1}^J) = \min_{\{\mu_n^J\} \rightarrow \mu_{n+1}^J} \left\{ \tilde{M}_{n-1}(\mu_n^J) + \left| r(n) - \sum_{i=J+1}^L g_i \hat{a}(n-i) - \sum_{i=1}^J g_i a(n-i) - g_0 a(n) \right|^2 \right\} \quad \dots(5.2)$$

where the minimization is taken over all the branch transitions which originate from states  $\{\mu_n^J\}$  and merge into the successor state  $\mu_{n+1}^J$ . Also  $\{\hat{a}(n-i)\}$  for  $J+1 \leq i \leq L$  are the symbol decisions (estimates) derived from the path history, which correspond to  $(L-J)$  past symbols  $\{a(n-i)\}$  that are not represented by the truncated combined state  $\mu_n^J$ . Thus the second term of the branch metric computation corresponds to the cancellation of ISI due to  $(L-J)$  residual terms. It may be observed from (5.2) that the Viterbi receiver performs both equalization and TCM decoding jointly.

The form of (5.1) suggests a family of reduced state truncated combined ISI-Code receiver structures with state complexity ranging from  $N_s$  to  $N_s(M/2)^L$  for  $0 \leq J \leq L$ . In the present study, we have considered several truncated combined ISI-Code receiver structures for the decoding of Trellis-coded QAM signals over ISI channels with different orders of memory. In the following, we consider the design of some truncated combined ISI-Code trellis structures.

### 5.2.1 The 8-State Truncated Combined ISI-Code Trellis for 4-State 4-QAM

#### TCM Transmission for $L \geq 2$ and $J=1$

Consider the 4-state 4-QAM TCM transmission over a time-dispersive ISI

channel of memory length  $L=3$ . For the 4-state 4-QAM TCM, we have  $N_s=4$  and  $M=2^{m+1}=4$ . For optimum MLSE decoding, we could require a combined ISI-Code trellis with  $N_s(M/2)^L=4 \cdot 2^3=32$  states. Truncating the channel memory to  $J=1$ , we get a truncated combined ISI-Code trellis with  $N_s(M/2)^J=8$  states. Using the definition (5.1), the present state and the next state of the truncated combined ISI-Code trellis are given by

$$\mu_n^1 = (\alpha_n ; a(n-1)) \quad \dots(5.3)$$

and 
$$\mu_{n+1}^1 = (\alpha_{n+1} ; a(n)) \quad \dots(5.4)$$

where  $\alpha_n$  and  $\alpha_{n+1}$  are the states of the TCM encoder, and  $a(n)$  is the symbol allowed by the TCM coding rule along the state transition  $\mu_n \rightarrow \mu_{n+1}$ . Note that each state  $\mu_n^1$  gives information about the past symbol  $a(n-1)$ . The symbols  $a(n-1)$  and  $a(n)$  can be represented by the symbol labels  $Y_{n-1}$  and  $Y_n$  respectively, where  $Y_{n-1} = y_{n-1}^1 y_{n-1}^0$  and  $Y_n = y_n^1 y_n^0$ . For the 4-state TCM encoder of Fig.2.3(a), we have  $\alpha_n = (x_{n-2}^1, x_{n-1}^1)$ , and  $y_{n-1}^1 = x_{n-3}^1 \oplus x_{n-1}^1$  and  $y_{n-1}^0 = x_{n-2}^1$ . Substituting for  $\alpha_n$  and  $a(n-1)$  (in terms of  $Y_{n-1} = y_{n-1}^1 y_{n-1}^0$ ) in (5.3) and upon simplification we can write the present state  $\mu_n^1$  as

$$\mu_n^1 = (x_{n-3}^1, x_{n-2}^1, x_{n-1}^1) \quad \dots(5.5)$$

By similar procedure, we can write from (5.4), the next state  $\mu_{n+1}^1$  as

$$\mu_{n+1}^1 = (x_{n-2}^1, x_{n-1}^1, x_n^1) \quad \dots(5.6)$$

Realization of (5.5) and (5.6) results in an 8-state truncated combined ISI-Code trellis structure as shown in Fig.5.1. This trellis structure can be employed for the decoding of 4-state 4-QAM TCM signals transmitted over an ISI channel of memory length  $L \geq 2$ . Decoding is accomplished by the implementation of (5.2) through the Viterbi algorithm.

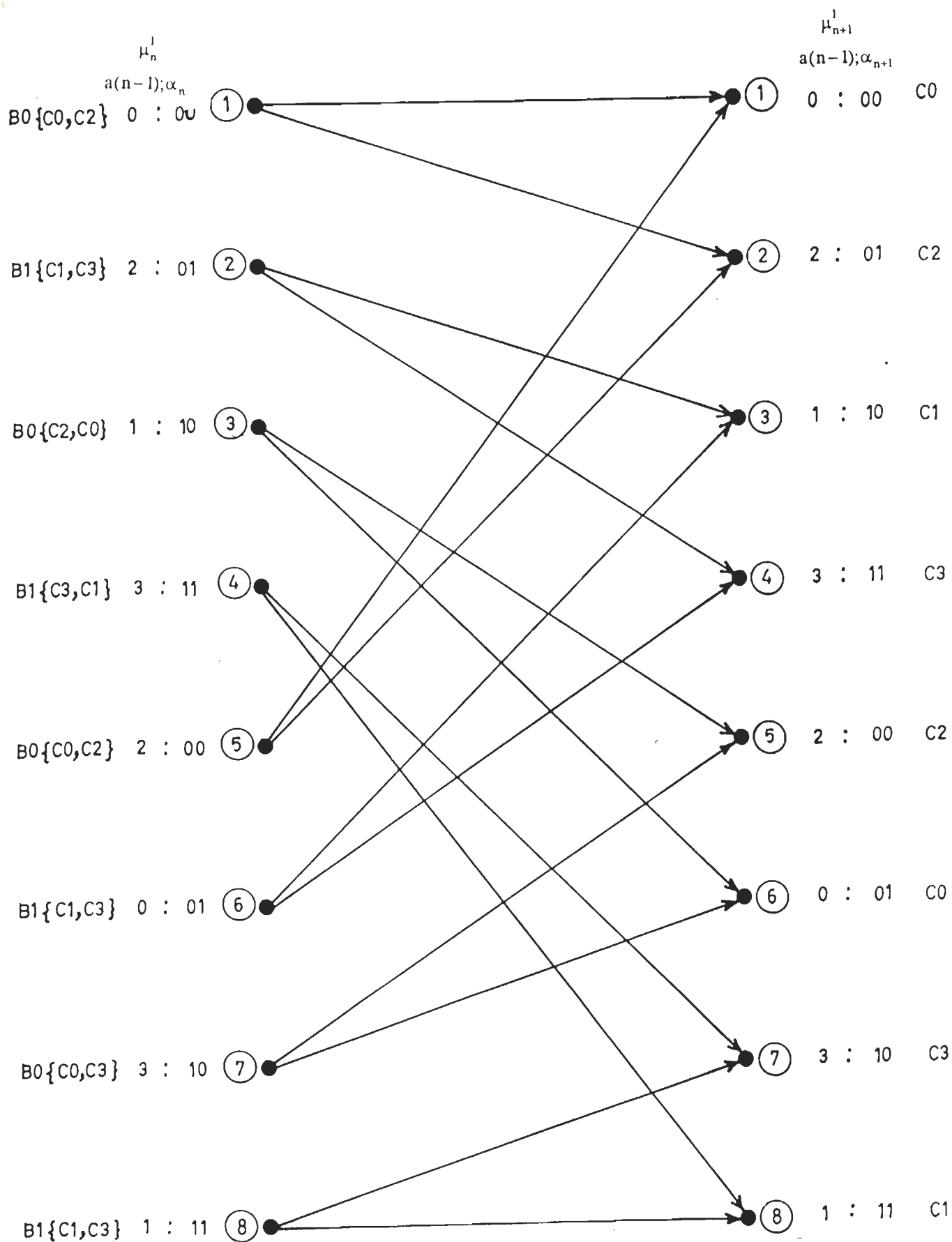


FIG.5.1 THE 8-STATE TRUNCATED COMBINED ISI-CODE TRELLIS STRUCTURE, FOR 4-STATE 4-QAM TCM TRANSMISSION OVER AN ISI CHANNEL OF MEMORY LENGTH  $L \geq 2$ , USING A TRUNCATION LENGTH  $J=1$ .

### 5.2.2 The 32-state Truncated Combined ISI-Code Trellis for 4-state 16-QAM

#### TCM Transmission for $L \geq 2$ and $J = 1$

Consider next the 4-state 16-QAM TCM transmission over a time-dispersive ISI channel of memory length  $L=3$ . For the 4-state TCM encoder of Fig.2.3(a), using a QAM signal constellation of size 16, we have  $N_s=4$  and  $M=2^{m+1}=16$ . For optimum MLSE decoding we need a combined ISI-Code trellis with  $N_s.(M/2)^L=4.8^3=2048$  states. By truncating the channel memory to  $J=1$ , we get a truncated combined ISI-Code trellis with only  $N_s.(M/2)^J=4.8=32$  states. The present state and the next state of this 32-state truncated combined ISI-Code trellis can be derived using (5.3) and (5.4) and noting that  $a(n)$  can be represented by its symbol label  $Y_n = y_n^3 y_n^2 y_n^1 y_n^0$  with  $y_n^3 = x_n^3$ ,  $y_n^2 = x_n^2$  and  $y_n^1, y_n^0$  are as defined earlier in sub-section 5.2.1. Following the procedure of the previous example, the present and next states of this truncated combined ISI-Code trellis are given as

$$\mu_n^1 = (x_{n-3}^1, x_{n-2}^1, x_{n-1}^1, x_{n-1}^2, x_{n-1}^3) \quad \dots(5.7)$$

and 
$$\mu_{n+1}^1 = (x_{n-2}^1, x_{n-1}^1, x_n^1, x_n^2, x_n^3) \quad \dots(5.8)$$

Note the similarity between (5.7), (5.8) and (3.18), (3.19). Therefore, the truncated combined ISI-Code trellis structure resulting from the realization of (5.7) and (5.8) will be same as the trellis structure shown in Fig.3.7, the only difference being in the implementation of the decoding algorithm. For the receiver using the truncated combined ISI-Code trellis, the decoding is accomplished by the implementation of (5.2) through the VA. This structure can be employed for the decoding of 4-state 16-QAM TCM signals transmitted over an ISI channel of memory length  $L \geq 2$ .

### 5.2.3 The 128-State Truncated Combined ISI-Code Trellis for 4-State 64-QAM

#### TCM Transmission for $L \geq 2$ and $J = 1$

We next consider the transmission of 4-state Trellis-Coded 64-QAM signals

over an ISI channel of length  $L=2$ . For optimum MLSE decoding, we would require a combined ISI-Code trellis with  $4.(64/2)^2=4098$  states. The state complexity can be reduced by truncating the channel memory to  $J=1$ , which results in a truncated combined ISI-Code trellis structure with  $4.(64/2)^1=128$  states. The present and next states of this truncated trellis can be defined using (5.3) and (5.4). Following the procedure used in the above example, it can be shown that the resulting trellis structure is same as that discussed in section 3.4.3, with the exception that the decoding is accomplished by the implementation of (5.2) through the VA. Note that this trellis structure may be employed for the decoding of 4-state 64-QAM TCM signals transmitted over an ISI channel of memory length  $L \geq 2$ .

#### **5.2.4 The 64-State Truncated Combined ISI-Code Trellis for 8-State 16-QAM TCM Transmission for $L \geq 2$ and $J=1$**

Consider the transmission of 8-state Trellis-Coded 16-QAM signals over an ISI channel of length  $L=2$ . For optimum MLSE decoding, we would require a combined ISI-Code trellis with  $8(16/2)^2=512$  states. The state complexity can be reduced by truncating the channel memory to  $J=1$ , that results in a truncated combined ISI-Code trellis structure with  $8(16/2)^1=64$  states. The present and next states of this truncated trellis can be defined using (5.3) and (5.4). Following the procedure used used in sections 5.2.1 and 5.2.2, it can be shown that the resulting trellis structure is same as that discussed in section 3.4.4, with the exception that the decoding is accomplished by the implementation of (5.2) through the VA. Again it may be noted that this 64-State truncated combined MLSE trellis structure may be employed for the decoding of 8-state 16-QAM TCM signals transmitted over an ISI channel of memory length  $L \geq 2$ .

### **5.3 REDUCED STATE SEQUENCE ESTIMATION**

From the discussions of the proceeding section, it may be observed that the state complexity of the sub-optimum truncated combined ISI-Code receiver

structures still remains substantially high with TCM schemes employing large signal constellations, although the channel memory length is truncated to  $J=1$ . In such cases, a further reduction in the state complexity is still desired.

We may recall that in the case of the optimum combined ISI-Code trellis or its truncated version, each state contains explicit information about the previous  $L$  or  $J$  data symbols associated with it, respectively. Instead, if some of the states can be grouped together so that they specify only the subsets to which the previous data symbols belong to, then a substantial reduction in the state complexity of the corresponding receiver is possible. This can be achieved by employing the ideas of signal set-partitioning inherent in the TCM design, and the resulting reduced state decoders are referred to as Reduced State Sequence Estimation (RSSE) structures, whose state complexity is independent of the size of the signal constellation  $M$ . In RSSE, the size  $M$  affects only the number of parallel transitions in the trellis structure [26].

Consider the transmission of  $m$  information bits per signaling interval using a rate  $\tilde{m}/(\tilde{m}+1)$  TCM encoder. During each signaling interval  $n$ , the  $(m+1)$  coded-bit label  $Y_n(m) = (y_n^m, y_n^{m-1}, \dots, y_n^1, y_n^0)$  selects a unique data symbol  $a(n)$  of the  $2^{m+1}$  signal constellation in accordance with TCM mapping rules. From the signal set-partitioning, we may recall that  $y_n^0$  determines the B-type subset of  $a(n)$ ,  $y_n^1$  the C-type subset and so on. Correspondingly, for each data symbol  $a(n-i)$  within the span of the truncated memory length  $J$ , the  $(m_i+1)$  bit label

$$Y_{n-i}(m_i) = (y_{n-i}^{m_i}, y_{n-i}^{m_i-1}, \dots, y_{n-i}^1, y_{n-i}^0) \quad \dots(5.5)$$

where  $m_i \leq m$  for  $1 \leq i \leq J$ , characterizes the depth of set-partitioning and determines the subset to which the symbol  $a_{n-i}$  belongs. Note that  $m_i = \tilde{m}$  corresponds to the depth of subset partitioning used by the TCM encoder.

Given the encoder state  $\alpha_n$  at time  $n$  and the label sequence  $\{Y_{n-1}(m_1), Y_{n-2}(m_2), \dots, Y_{n-J}(m_J)\}$ , the encoder state  $\alpha_{n-J}$  at time  $n-J$  can be uniquely determined if  $\tilde{m} \leq m_i \leq m$  for  $1 \leq i \leq J$ . Thus, the number of states in the truncated



combined ISI-Code trellis can be reduced by associating each code state  $\alpha_n$  with the label sequence  $\{Y_{n-1}(m_1), Y_{n-2}(m_2), \dots, Y_{n-J}(m_J)\}$  in place of the data symbol sequence  $\{a(n-1), a(n-2), \dots, a(n-J)\}$ . Using (5.1), the reduced state of the truncated ISI-Code trellis can be defined as [26],

$$\lambda_n^J = [\alpha_n; Y_{n-1}(m_1), Y_{n-2}(m_2), \dots, Y_{n-J}(m_J)] \quad \dots(5.6)$$

with  $0 \leq J \leq L$  and  $\lambda_n^0 = \alpha_n$ .

Equivalently, in terms of the corresponding information sequence  $\{X_{n-1}(m_1), X_{n-2}(m_2), \dots, X_{n-J}(m_J)\}$  where

$$X_{n-i}(m_i) = (x_{n-i}^1, x_{n-i}^2, \dots, x_{n-i}^{m_i}) \quad \dots(5.7)$$

the reduced state truncated combined trellis is given by

$$\lambda_n^J = [\alpha_{n-J}; X_{n-1}(m_1), X_{n-2}(m_2), \dots, X_{n-J}(m_J)] \quad \dots(5.8)$$

with  $0 \leq J \leq L$  and  $\lambda_n^0 = \alpha_n$

Under the condition,

$$m \geq m_1 \geq m_2 \geq \dots \geq m_J \geq \tilde{m} \quad \dots(5.9)$$

the reduced state defined by (5.6) or (5.8) leads to a family of valid reduced state trellis structures called Reduced State Sequence Estimation (RSSE) structures. Each code state is associated with  $2^{m_1+m_2+\dots+m_J}$  ISI states. Thus for an  $N_s$ -state TCM encoder, the number of states in the RSSE trellis is  $N_s \cdot 2^{m_1+m_2+\dots+m_J}$ . From each reduced state  $2^{m_1}$  transition groups originate with each group consisting of  $2^{m-m_1}$  parallel transitions. For  $m_1 < m$ , note that each state carries information about subsets rather than the individual data symbols.

The decoding is accomplished through VA by recursively computing the survivor path metric of the reduced states in accordance with

$$\tilde{M}_n(\lambda_{n+1}^J) = \min_{\{\lambda_n^J\} \rightarrow \lambda_{n+1}^J} \left\{ \tilde{M}_{n-1}(\lambda_n^J) + \left| r(n) - \sum_{i=J+1}^L g_i \hat{a}(n-i) - g_0 a(n) \right|^2 \right\} \quad \dots(5.10)$$

where the minimization is performed over the allowable branch transitions originating from states  $\{\lambda_n^J\}$  to the terminal successor state  $\lambda_{n+1}^J$ . From (5.10) it may be noted that the  $L$  ISI terms are cancelled out using the previous data symbol decisions  $\{\hat{a}(n-i)\}$  for  $1 \leq i \leq L$ , that are derived from the path history associated with the state  $\lambda_n^J$ .

For a given truncation length  $J$  and  $m_1 = m_2 = \dots = m_J = \tilde{m}$  we obtain the least complex RSSE structure with a state complexity of  $N_s \cdot 2^{\tilde{m}J}$ . The most complex RSSE structure with  $m_1 = m_2 = \dots = m_J = m$ , has a complexity of  $N_s \cdot 2^{mJ}$  states. Since  $0 \leq J \leq L$ , the state complexity of RSSE ranges between that of TCM encoder ( $N_s$ ) and that of the optimum combined ISI-Code receiver ( $N_s \cdot 2^{mL}$ ). Thus, (5.6) or (5.8) represents a family of RSSE structures with state complexity ranging between  $N_s$  and  $N_s \cdot 2^{mL}$ .

In the following, we consider the design of few RSSE structures for the decoding of Trellis-Coded QAM signals transmitted over time-dispersive ISI channels.

### 5.3.1 The 8-State RSSE Trellis for a 4-State Trellis-Coded QAM and $J=1$

Consider the transmission of 4-state 16-QAM TCM signals over an ISI channel of length  $L \geq 2$ . Assume that the channel memory is truncated to  $J=1$ . For the 4-state 16-QAM TCM of Fig. 2.3(a), we have  $N_s = 4$ ,  $M = 2^{m+1} = 16$ ,  $m=3$  and  $\tilde{m} = 1$ . Since  $J=1$ , and  $\tilde{m} \leq m_1 \leq m$ , let us choose  $m_1 = 1$ . Thus the number of states in the RSSE trellis is  $N_s \cdot 2^{m_1} = 8$ . From (5.6) the present state of the RSSE trellis is given by

$$\lambda_n^1 = (\alpha_n; Y_{n-1}(m_1)) \quad \dots(5.11)$$

where  $\alpha_n$  is the present state of the 4-state TCM encoder given by  $\alpha_n = x_{n-2}^1 x_{n-1}^1$  and  $Y_{n-1}(m_1=1) = (y_{n-1}^1, y_{n-1}^0)$

The next state is given by

$$\lambda_{n+1}^1 = (\alpha_{n+1}; Y_n(m_1)) \quad \dots(5.12)$$

where  $\alpha_{n+1}$  is the next state of the TCM encoder given by  $\alpha_{n+1} = x_{n-1}^1 x_n^1$  and  $Y_n(m_1) = (y_n^1, y_n^0)$

Note that for a 4-state TCM encoder of Fig.2.3(a), we have  $y_n^1 = x_n^1 \oplus x_{n-2}^1$ ,  $y_n^0 = x_{n-1}^1$  and therefore  $y_{n-1}^1 = x_{n-1}^1 \oplus x_{n-3}^1$ ,  $y_{n-1}^0 = x_{n-2}^1$ . Substituting for  $\alpha_n$ ,  $\alpha_{n+1}$ ,  $Y_{n-1}$  and  $Y_n$  in (5.11) and (5.12), we get

$$\lambda_n^1 = (x_{n-2}^1, x_{n-1}^1; x_{n-1}^1 \oplus x_{n-3}^1, x_{n-2}^1) \quad \dots(5.13)$$

and

$$\lambda_{n+1}^1 = (x_{n-2}^1, x_n^1; x_n^1 \oplus x_{n-2}^1, x_{n-1}^1) \quad \dots(5.14)$$

From (5.13), (5.14) it may be noted that  $\lambda_n^1$  is a function of  $(x_{n-3}^1, x_{n-2}^1, x_{n-1}^1)$  and  $\lambda_{n+1}^1$  is a function of  $x_{n-2}^1, x_{n-1}^1, x_n^1$ . Simple forms of  $\lambda_n^1$  and  $\lambda_{n+1}^1$  can be obtained directly by the use of (5.7) and (5.8). The present state can therefore be expressed as

$$\lambda_n^1 = (\alpha_{n-1}; X_{n-1}(m_1=1))$$

where  $\alpha_{n-1} = x_{n-3}^1, x_{n-2}^1$  and  $x_{n-1}(m_1=1) = x_{n-1}^1$ .

$$\text{Thus } \lambda_n^1 = (x_{n-3}^1, x_{n-2}^1, x_{n-1}^1) \quad \dots(5.15)$$

$$\text{and } \lambda_{n+1}^1 = (x_{n-2}^1, x_{n-1}^1, x_n^1) \quad \dots(5.16)$$

The transition  $\lambda_n^1 \rightarrow \lambda_{n+1}^1$  represent the C-type subset defined by

$$Y_n(1) = (y_n^1, y_n^0) = (x_n^1 \oplus x_{n-2}^1, x_{n-1}^1). \quad \dots(5.17)$$

The corresponding 8-state RSSE trellis structure can be derived using (5.13) and (5.14) or (5.15)-(5.17) and the resulting structure is shown in Fig.5.2. From each state  $2^{m_1}=2$  transition groups originate, each representing 4 parallel transitions (for 16-QAM). Since  $Y_n(1) = (y_n^1, y_n^0)$ , each transition group corresponds to C-type subset.

In general, this 8-state RSSE structure can be used for the decoding of 4-state M-QAM TCM signals ( $M=2^{m+1}$ ), since  $m$  influences only the number of parallel transitions and not the overall design. For 4-state 64 QAM TCM, there will be  $2^{m-m_1} = 2^{5-1} = 16$  parallel transitions per transition group.

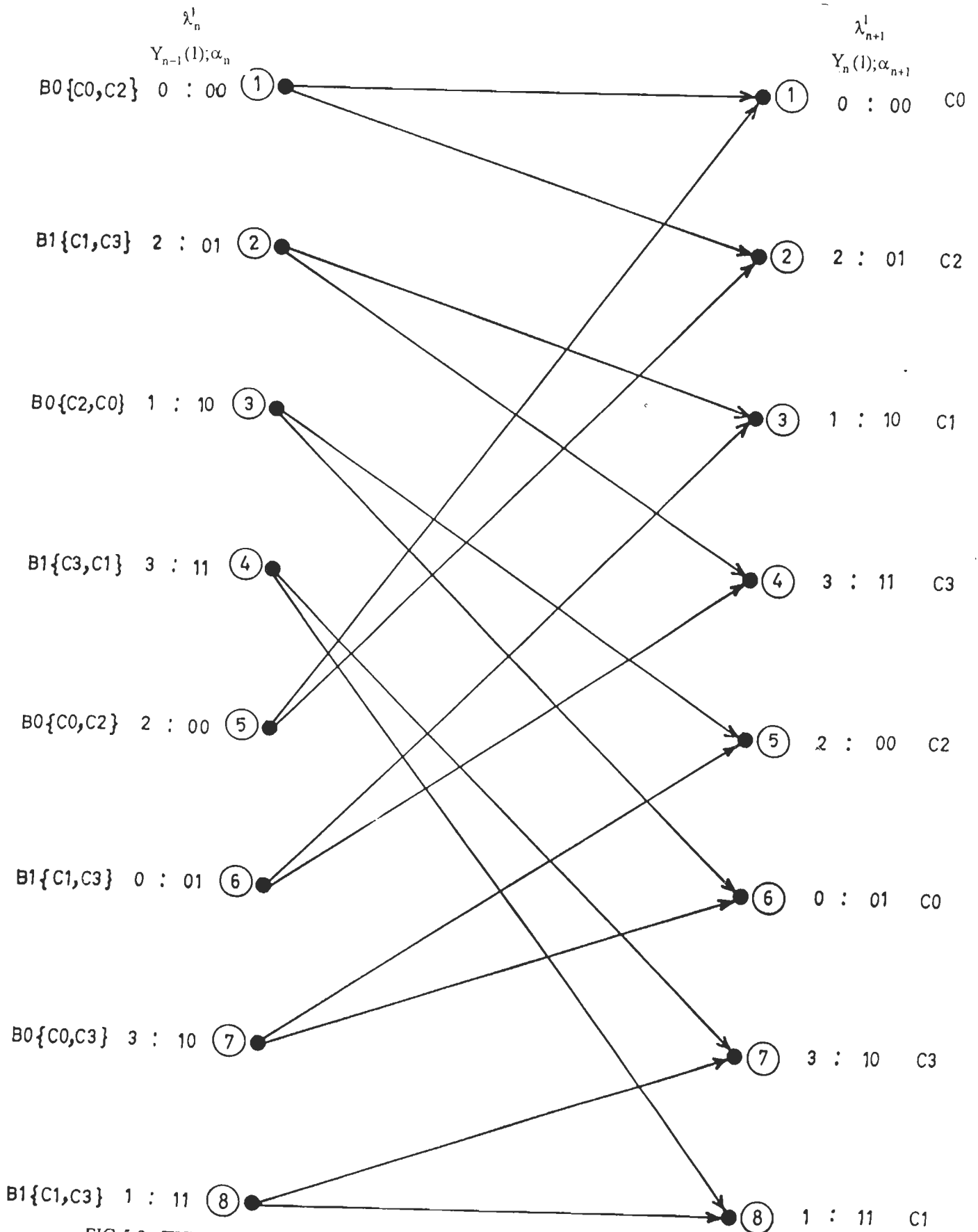


FIG.5.2 THE 8-STATE RSSE TRELLIS STRUCTURE, FOR 4-STATE M-QAM SIGNAL TRANSMISSION OVER AN ISI CHANNEL OF MEMORY LENGTH  $L \geq 2$ , USING TRUNCATION LENGTH  $J=1, m_1=1$ .

The decoding is accomplished through the implementation of (5.10) using the Viterbi algorithm.

### 5.3.2 The 16-State RSSE Trellis for 4-State Trellis-Coded QAM and J=1

Consider again the same example of 4-state 16-QAM TCM,  $L \geq 2$ ,  $J=1$ ,  $m=3$   $\tilde{m}=1$ , with only a change in the constraint  $m_1$ . By selecting  $m_1=2$ , the number of states in the RSSE structure is  $N_s \cdot 2^2=16$ , and from each state there will be  $2^{m_1}=4$  transition groups (D-type subset), each consisting of 2 parallel transitions. The use of (5.6) results in states

$$\lambda_n^1 = (x_{n-2}^1 \ x_{n-1}^1 ; y_{n-1}^2 \ y_{n-1}^1 \ y_{n-1}^0) \quad \dots(5.18)$$

and 
$$\lambda_{n+1}^1 = (x_{n-1}^1 \ x_n^1 ; y_n^2 \ y_n^1 \ y_n^0) \quad \dots(5.19)$$

The alternative definitions of  $\lambda_n^1$  and  $\lambda_{n+1}^1$  resulting from (5.8) are

$$\lambda_n^1 = (x_{n-3}^1 \ x_{n-2}^1 \ x_{n-1}^1 \ x_{n-1}^2) \quad \dots(5.20)$$

and 
$$\lambda_{n+1}^1 = (x_{n-2}^1 \ x_{n-1}^1 \ x_n^1 \ x_n^2) \quad \dots(5.21)$$

with the transition  $\lambda_n^1 \rightarrow \lambda_{n+1}^1$  being associated with a D-type subset given by

$$Y_n(2) = (y_n^2 \ y_n^1 \ y_n^0) \quad \dots(5.22)$$

The resulting 16-state RSSE structure is shown in Fig.5.3. For 4-state 64-QAM TCM, each transition group represents  $2^{5-2}=8$  parallel transitions. Decoding is accomplished through VA using (5.10).

### 5.3.3 The 32-State RSSE Trellis for 4-State Trellis-Coded QAM and J=2

Consider next a 4-state 64-QAM TCM,  $L \geq 3$  and  $J=2$ . Since  $\tilde{m} \leq m_i \leq m$  for  $1 \leq i \leq 2$ , select  $m_1=2$  and  $m_2=1$ . Then the number of states in the RSSE structure is  $N_s \cdot 2^{m_1+m_2}=32$ .

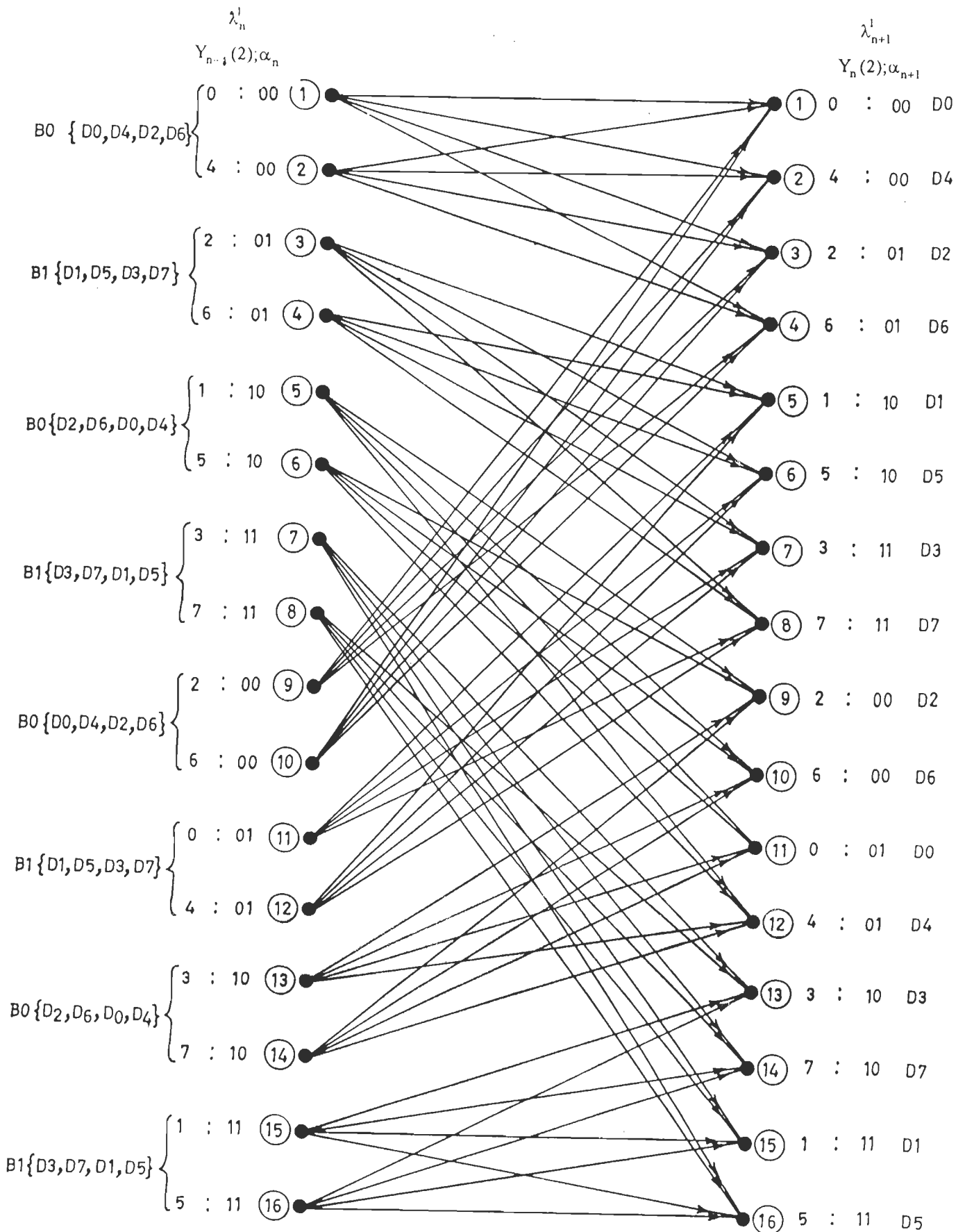


FIG.5.3 THE 16-STATE RSSE TRELLIS STRUCTURE, FOR 4-STATE M-QAM SIGNAL TRANSMISSION OVER AN ISI CHANNEL OF MEMORY LENGTH  $L \geq 2$ , USING TRUNCATION LENGTH  $J=1$ ,  $m_1=2$ .

Following (5.8), the states can be defined by

$$\lambda_n^2 = (\alpha_{n-2}; X_{n-1}(2) X_{n-2}(1))$$

or 
$$\lambda_n^2 = (x_{n-4}^1, x_{n-3}^1; x_{n-1}^1, x_{n-1}^2, x_{n-2}^1)$$

and 
$$\lambda_{n+1}^2 = (x_{n-3}^1, x_{n-2}^1, x_n^1, x_n^2, x_{n-1}^1)$$

Rearranging

$$\lambda_n^2 = (x_{n-4}^1, x_{n-3}^1, x_{n-2}^1, x_{n-1}^1, x_{n-1}^2) \quad \dots(5.23)$$

and 
$$\lambda_{n+1}^2 = (x_{n-3}^1, x_{n-2}^1, x_{n-1}^1, x_n^1, x_n^2) \quad \dots(5.24)$$

The transition  $\lambda_n^2 \rightarrow \lambda_{n+1}^2$  is associated with a D-type subset defined by

$$Y_n(2) = (y_n^2, y_n^1, y_n^0) \quad \dots(5.25)$$

Also 
$$Y_{n-1}(1) = (y_{n-1}^1, y_{n-1}^0) \quad \dots(5.26)$$

The resulting 32-state RSSE structure is shown in Fig.5.4. Note that each state is associated with  $2^{m_1}=4$  transition groups, each group representing 8 parallel transitions corresponding to 8-signal points of the D-type subset of 64-QAM constellation. This 32-state RSSE trellis structure can also be used for the decoding of 4-state 16-QAM TCM signals, wherein each transition group represents 2 parallel transitions corresponding to D-type subset of 16-QAM signal constellations. The decoding is accomplished by the implementation of (5.10) through the Viterbi algorithm.

#### 5.3.4 The 32-State RSSE Receiver for 8-State Trellis-Coded QAM and J=1

We next consider the transmission of 8-state 16-QAM TCM over an ISI channel of length  $L \geq 2$ . Truncating the channel to  $J=1$ , we have  $m_j = m_1$ . For 8-state 16-QAM TCM encoder of Fig.2.3(b), we have  $N_s = 8$ ,  $M = 2^{m+1} = 16$ ,  $\tilde{m} = 2$  and  $\alpha_n = x_{n-2}^1 x_{n-1}^2 x_{n-1}^1$ ,  $y_n^3 = x_n^3$ ,  $y_n^2 = x_{n-1}^2 \otimes x_n^1$ ,  $y_n^1 = x_n^2 \otimes x_{n-2}^1$ ,  $y_n^0 = x_{n-1}^1$ . The condition  $\tilde{m} \leq m_1 \leq m$  suggests  $2 \leq m_1 \leq 3$ , and let us consider  $m_1 = 2$ . Thus, the number of states in the RSSE structure is

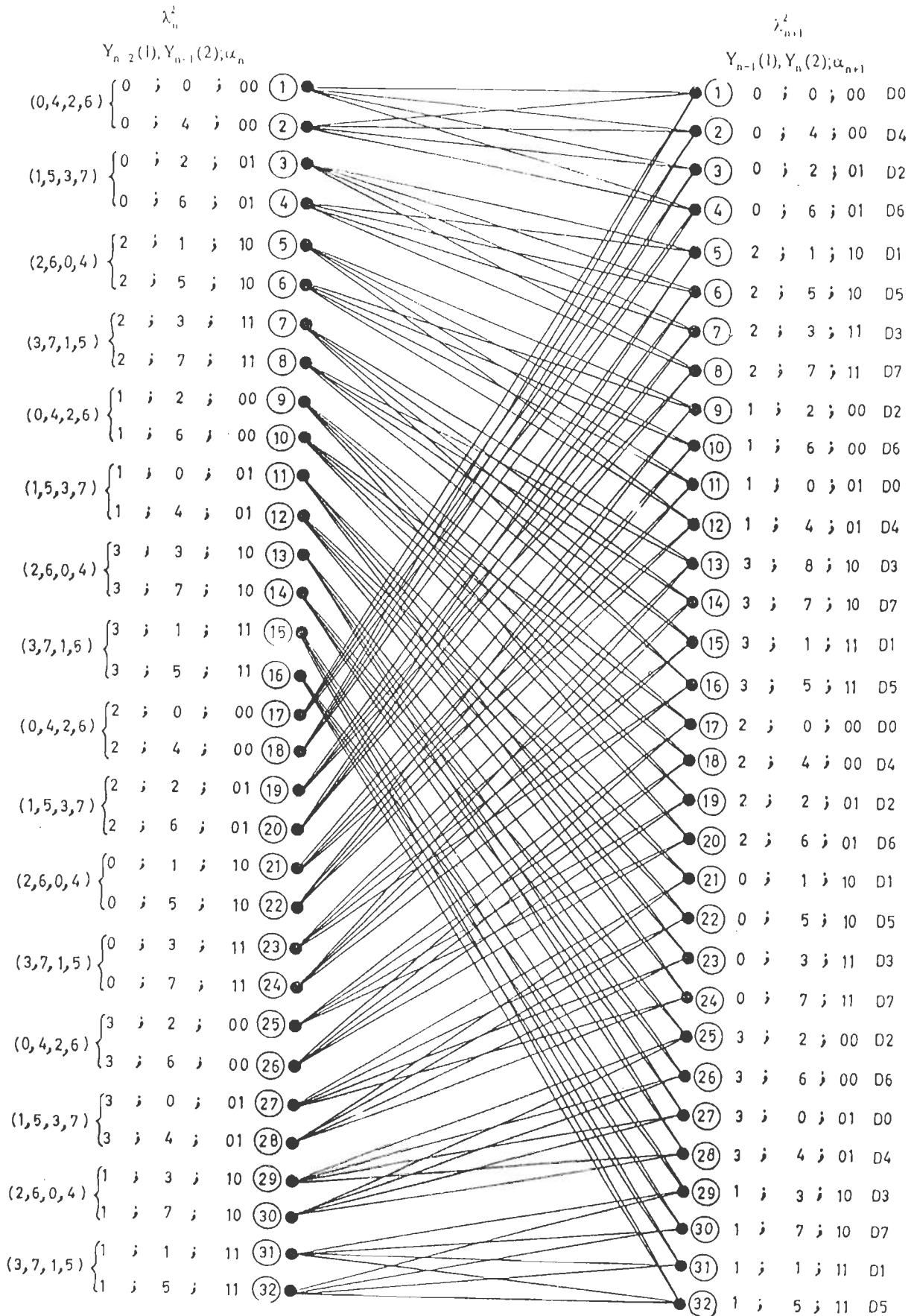


FIG. 5.4 THE 32-STATE RSSE TRELLIS STRUCTURE, FOR 4-STATE M-QAM SIGNAL TRANSMISSION OVER AN ISI CHANNEL OF MEMORY LENGTH  $L \geq 2$ , USING TRUNCATION LENGTH  $J=2, m_1=2, m_2=1$ .



$N_s 2^{m_1} = 32$ . Following (5.8), the present state and the next state are given by

$$\lambda_n^1 = (\alpha_{n-1}; X_{n-1}(2))$$

and  $\lambda_{n+1}^1 = (\alpha_n; X_n(2))$

where  $X_{n-1}(2) = x_{n-1}^1 x_{n-1}^2$  and  $X_n(2) = x_n^1 x_n^2$ .

Substituting for  $\alpha_{n-1}$ ,  $\alpha_n$ ,  $X_{n-1}(2)$  and  $X_n(2)$  we get,

$$\lambda_n^1 = (x_{n-3}^1, x_{n-2}^2, x_{n-2}^1, x_{n-1}^2, x_{n-1}^1) \quad \dots(5.27)$$

and  $\lambda_{n+1}^1 = (x_{n-2}^1, x_{n-1}^2, x_{n-1}^1, x_n^2, x_n^1) \quad \dots(5.28)$

Also, the transition  $\lambda_n^1 \rightarrow \lambda_{n+1}^1$  represents a D-type subset of the signal constellation given by,

$$Y_n(2) = (y_n^2 y_n^1 y_n^0) \quad \dots(5.29)$$

Correspondingly,  $Y_{n-1}(2) = (y_{n-1}^2 y_{n-1}^1 y_{n-1}^0) \quad \dots(5.30)$

The resulting RSSE structure corresponding to (5.27)-(5.30) is shown in Fig.5.5. Note that each state is associated with  $2^{m_1} = 4$  transition groups, each representing D-type subset consisting of 2 parallel transitions. The same structure can be used for 8-state 64-QAM TCM decoding, in which case each transition group represents 8 parallel transitions corresponding 8 signals points of the D-type subset of 64-QAM.

The decoding of the 32-state RSSE trellis is accomplished by implementing (5.10) in the Viterbi algorithm.

#### 5.4 PARALLEL DECISION FEEDBACK DECODING

From the preceding section, we have observed that substantial reduction in the state complexity of the combined ISI-Code structure is achieved by

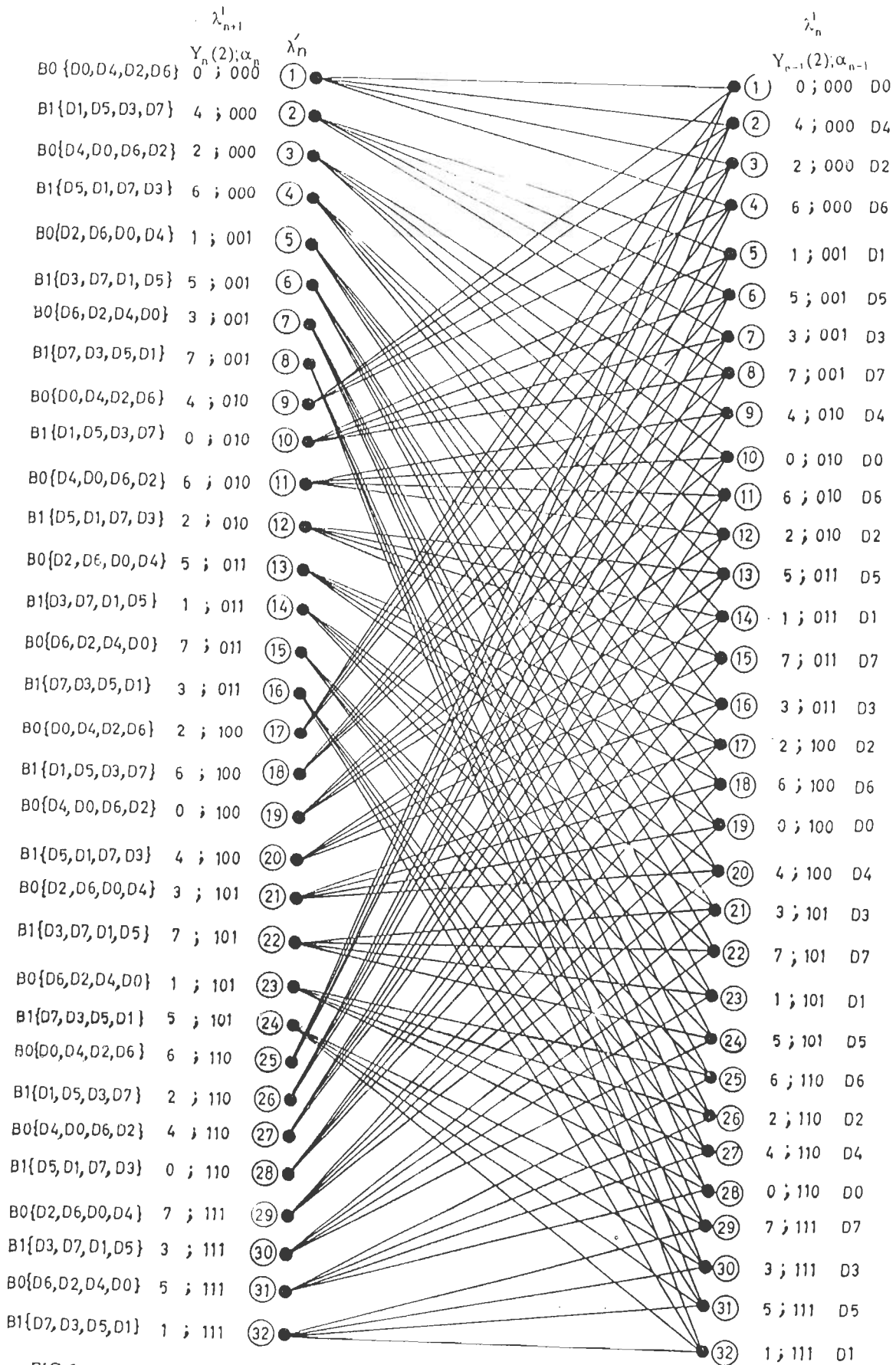


FIG.5.5 THE 32-STATE RSSE TRELLIS STRUCTURE, FOR 8-STATE M-QAM SIGNAL TRANSMISSION OVER AN ISI CHANNEL OF MEMORY LENGTH  $L \geq 2$ , USING TRUNCATION LENGTH  $J=1$ ,  $m_1=2$ .

incorporating channel truncation and also the set-partitioning ideas inherent in TCM code construction. The RSSE structures have state complexities ranging from TCM encoder states  $N_s$  to the optimum combined ISI-Code receiver states  $N_s \cdot 2^{ml}$ .

When the state complexity of the RSSE structure reduces to that of encoder states  $N_s$  (for  $J=0$ ), the reduced structure is referred to as parallel decision feedback decoding (PDFD). The Viterbi decoder operates directly on the TCM code trellis. The decoding is accomplished by recursively computing the survivor path metric corresponding to the state  $\alpha_{n+1}$  according to [26]

$$\tilde{M}_n(\alpha_{n+1}) = \min_{\{\alpha_n\} \rightarrow \alpha_{n+1}} \left\{ \tilde{M}_{n-1}(\alpha_n) + \left| r(n) - \sum_{i=1}^L g_i \hat{a}(n-i) - g_0 a(n) \right|^2 \right\} \quad \dots(5.31)$$

where the minimization is performed over all the trellis branches originating from code states  $\{\alpha_n\}$  and leading into the successor state  $\alpha_{n+1}$ . It can be noted that the  $L$  ISI terms are cancelled out in a way reminiscent of a DFE in cascade with a TCM Viterbi decoder. The distinctive feature of PDFD is that instead of using only one sequence of decisions, as in the feedback path of DFE, the equalization is accomplished by using a unique sequence of decision for *each* state in the trellis. These feedback sequences are based on the history of the surviving path of each state. As a result, instead of calculating the metrics with one received sample per trellis stage, there will be a unique decision-feedback equalized sample for each state per stage. This will result in an increase in computational complexity which is well justified by the improved performance [42, 138].

In the following, we consider the performance of these reduced state decoders on different ISI channels, through simulation.

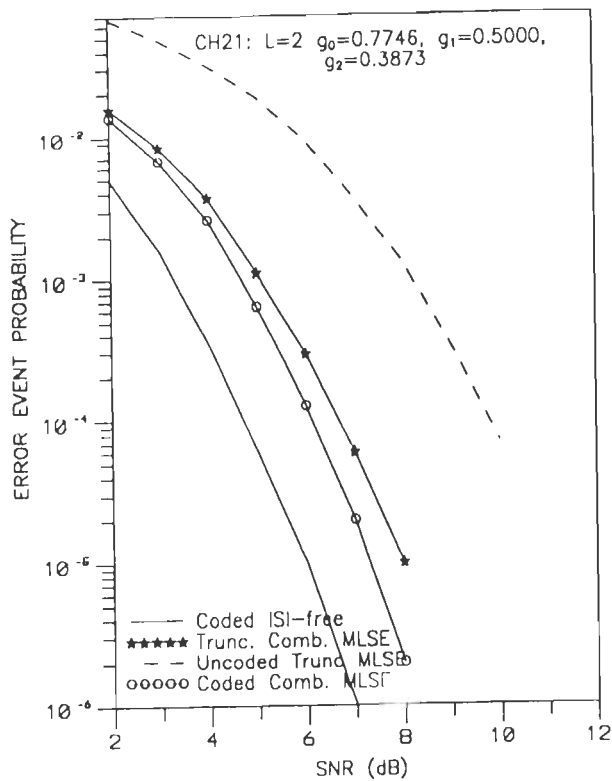
## 5.5 RESULTS AND DISCUSSION

In this section, we present the error performance of the reduced complexity sequence estimation techniques which are employed for the sub-optimum detection of trellis-coded QAM signals transmitted over the time-dispersive ISI channels. The

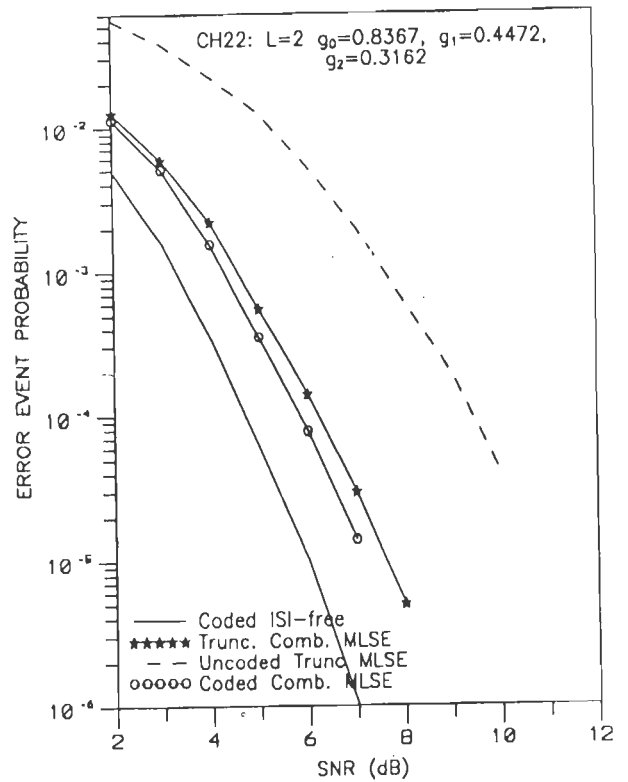
performance characteristics of the various structures, as discussed earlier in sections 5.2–5.4, have been derived through simulation. In order to estimate the coding gain achievable with the use of the coded truncated combined MLSE receiver structures, we consider an uncoded truncated MLSE receiver structure as the reference system. Similarly for the coded RSSE/PDFD structure, the reference employed correspondingly is an uncoded RSSE/PDFD structure. The ISI channels, used in the study, are assumed to be time-invariant and known, and correspond to those listed in Table 3.1.

The baseband TCM data transmission system considered for the study is the same as shown in Fig.3.4, the implementation of which has been discussed earlier in section 3.6. The receiver is a reduced complexity structure based on the techniques of channel truncation and reduced state sequence estimation as discussed in sections 5.2–5.4.

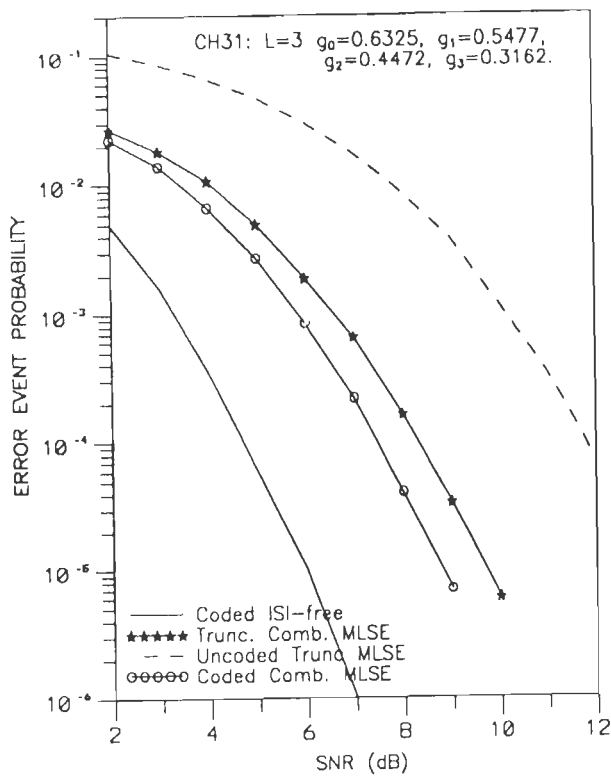
The error performance characteristics of the various coded truncated combined MLSE structures (of section 5.2) have been shown in Fig.5.6–5.10. The error performance of the 8-state truncated combined ISI-code trellis structure of section 5.2.1 (channel truncation length  $J=1$ ), which is used for the decoding of the 4-state 4-QAM TCM signals transmitted over an ISI channel of memory length  $L \geq 2$ , is shown in Fig.5.6. The reference system is a 2-state truncated uncoded MLSE structure ( $J=1$ ). It may be noted that the coded truncated MLSE structure achieves a gain of 2.5–3.0 dB relative to the uncoded reference system, while it suffers a degradation in the range of 0.5–1.0 dB over the optimum combined MLSE structure. Fig.5.7 depicts the error performance of the 16-state truncated combined MLSE structure (channel truncation length  $J=2$ ), which is employed for the detection of 4-state 4-QAM TCM signals transmitted over an ISI channel of  $L \geq 3$ . The truncated combined MLSE structure achieves a coding gain in the range of 2.0–2.5 dB over the uncoded truncated MLSE structure ( $J=2$ ), while exhibiting a performance loss of only 0.3–0.5 dB over the optimum combined MLSE structure. From Fig.5.7(a), we observe that the performance of the truncated MLSE approaches that of the optimum



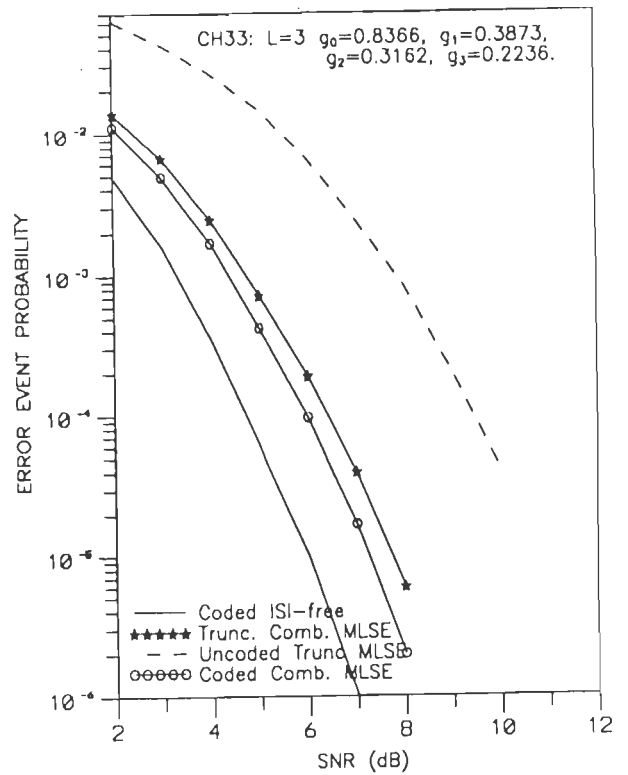
(a) ISI CHANNEL CH21:  $L=2$ ,  $J=1$ .



(b) ISI CHANNEL CH22:  $L=2$ ,  $J=1$ .

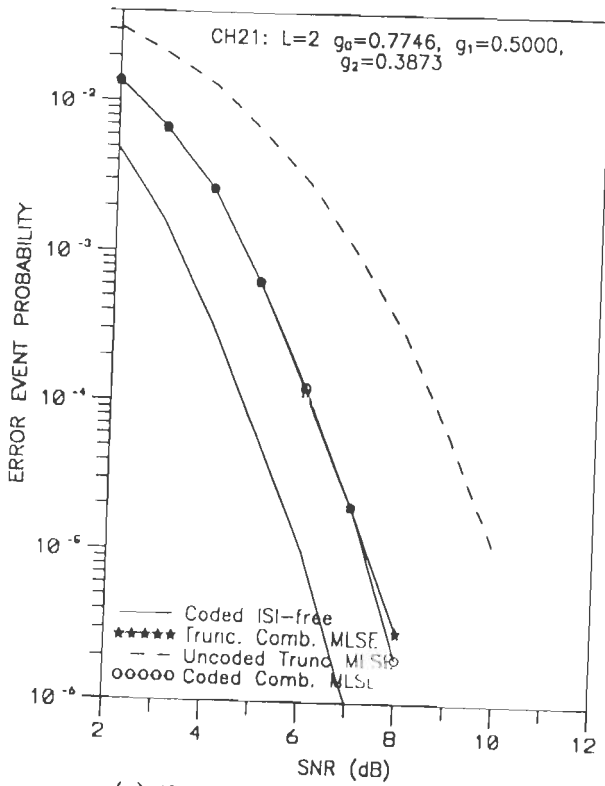


(c) ISI CHANNEL CH31:  $L=3$ ,  $J=1$ .

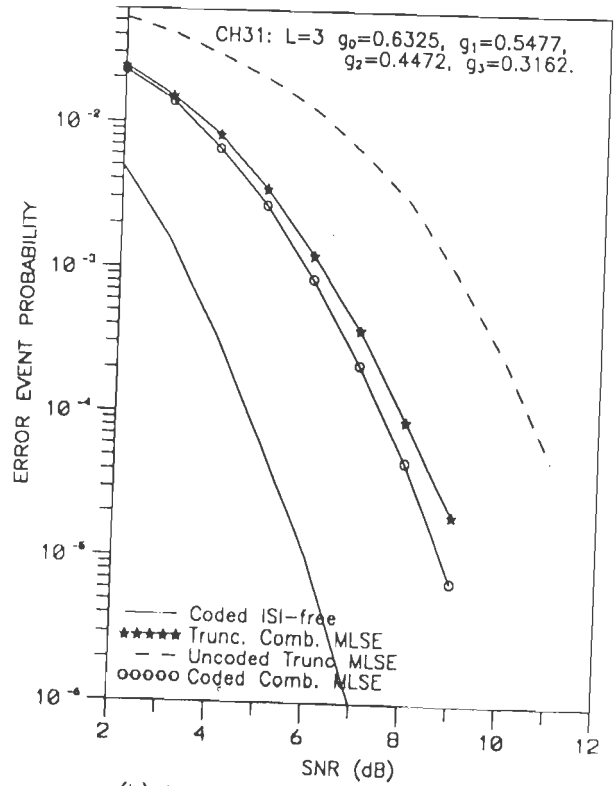


(d) ISI CHANNEL CH33:  $L=3$ ,  $J=1$ .

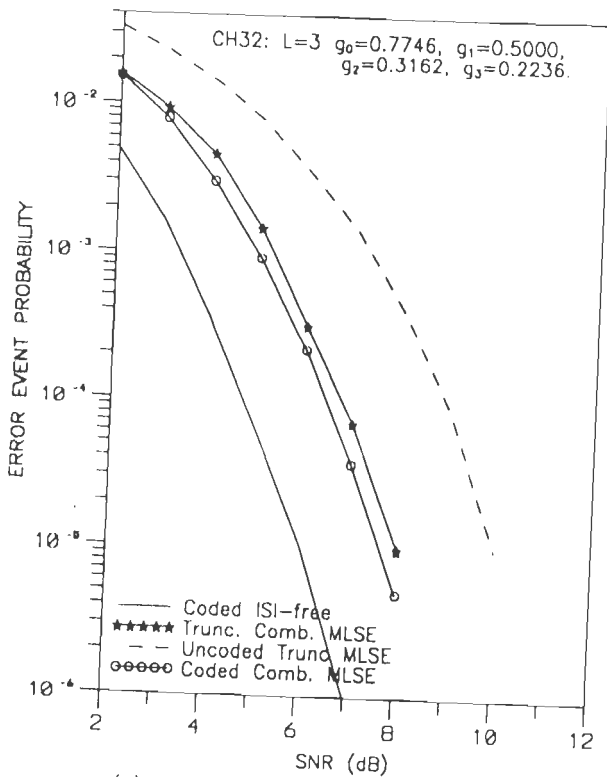
FIG.5.6 ERROR PERFORMANCE OF THE TRUNCATED COMBINED MLSE RECEIVER WHICH EMPLOYS AN 8-STATE TRUNCATED COMBINED ISI-CODE TRELLIS STRUCTURE FOR THE DETECTION OF 4-STATE 4-QAM TCM SIGNALS OVER AN ISI CHANNEL OF MEMORY  $L \geq 1$ .



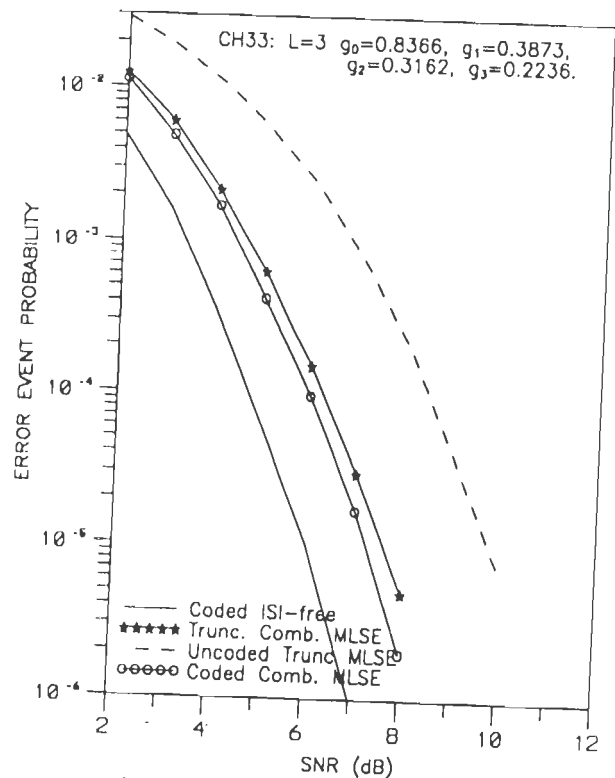
(a) ISI CHANNEL CH21:  $L=2$ ,  $J=2$ .



(b) ISI CHANNEL CH31:  $L=3$ ,  $J=2$ .



(c) ISI CHANNEL CH32:  $L=3$ ,  $J=2$ .



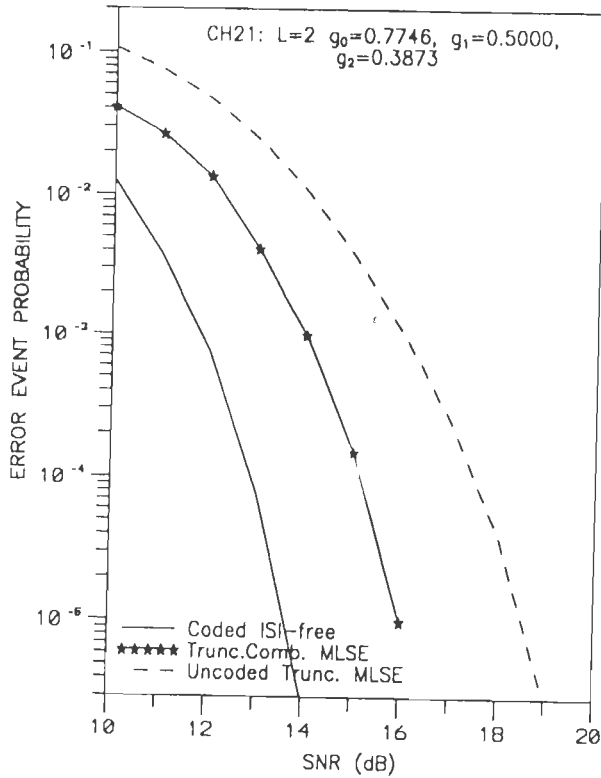
(d) ISI CHANNEL CH33:  $L=3$ ,  $J=2$ .

FIG.5.7 ERROR PERFORMANCE OF THE TRUNCATED COMBINED MLSE RECEIVER WHICH EMPLOYS A 16-STATE TRUNCATED COMBINED ISI-CODE TRELLIS STRUCTURE FOR THE DETECTION OF 4-STATE 4-QAM TCM SIGNALS OVER AN ISI CHANNEL OF MEMORY  $L/2$ .

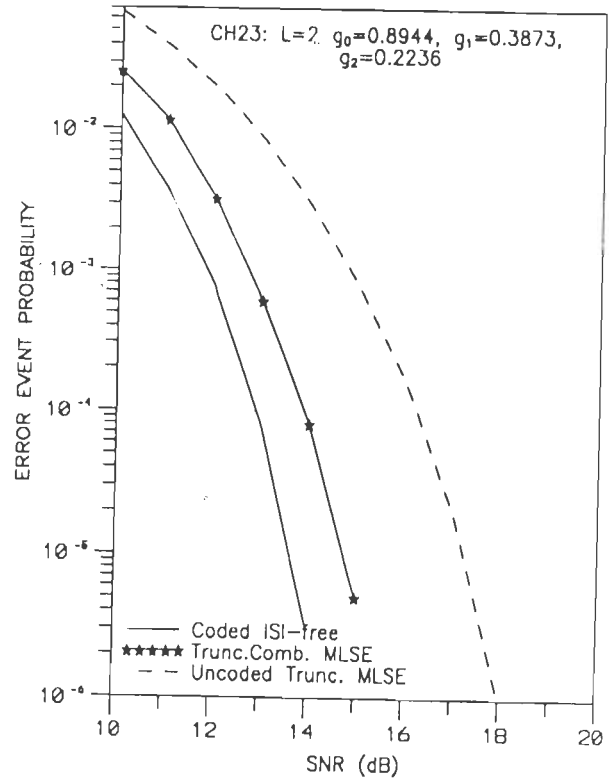
MLSE structure as  $J \rightarrow L$ , which is to be expected.

The performance characteristics of the truncated combined MLSE receiver structures of section 5.2.2–5.2.4, have been shown respectively in Fig.5.8–5.10. Fig.5.8 shows the error performance of the 32-state truncated combined ISI-code trellis structure employed for the detection of 4-state 16-QAM TCM signals over an ISI channel of memory length  $L \geq 2$ . Similarly, Fig.5.9 and Fig.5.10 show correspondingly the performance characteristics of the 128-state and 64-state truncated combined ISI-code trellis structures (of section 5.2.3–5.2.4) used for the decoding 4-state 64-QAM and 8-state 16-QAM TCM signals, respectively. It may be noted that the performance of the coded truncated MLSE structure is compared only with the uncoded truncated MLSE reference system, as the combined MLSE structures have not been realized for 16-QAM/64-QAM TCM transmission on ISI channels of memory length  $L \geq 2$ , due to the reasons of complexity in practical implementation as discussed earlier in section 3.4. From the performance characteristics of Fig.5.8–5.10, we observe that the coding gain achieved is 2.0–2.5 dB with the use of truncated receiver structures of sections 5.2.1–5.2.3 which are based on 4-state TCM schemes, while it is 3.0–3.75 dB for the receiver structure of section 5.2.4 which is based on an 8-state TCM scheme. The use of 8-state or 16-state TCM scheme improves the performance of the combined MLSE/truncated MLSE structures by 0.5–1.0 dB relative to that attainable with the use of 4-state TCM scheme, but at the cost of increased state complexity and increased computational burden.

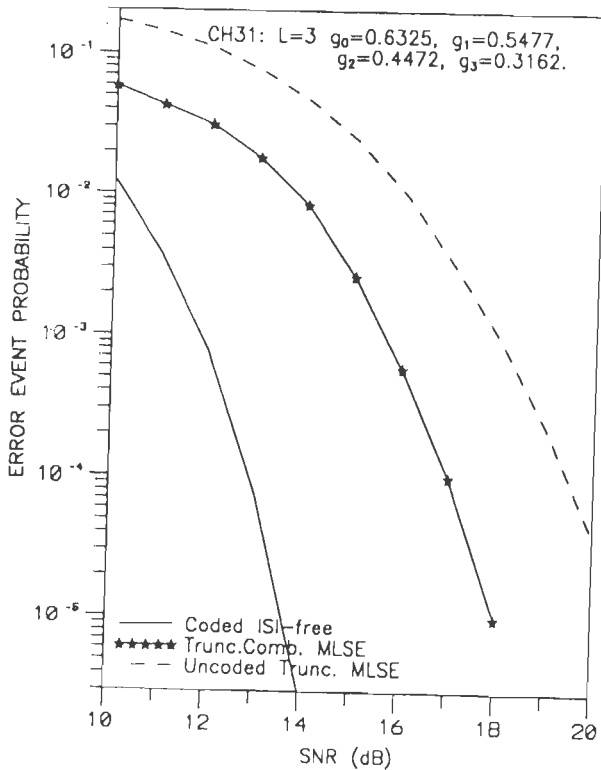
The reduction in state complexity and hence a saving in computations can be achieved by combining channel truncation technique with the ideas of set-partitioning as discussed in section 5.3. The performance characteristics of the reduced state sequence estimators (RSSE) have been shown in Fig.5.11–5.13, for different orders of state reduction as discussed in section 5.3.1–5.3.4. It may be recalled that, the 8-state, 16-state and 32-state RSSE structures of section 5.3.1–5.3.4 can be employed for the detection of M-QAM TCM signals ( $M=16$  or  $64$ )



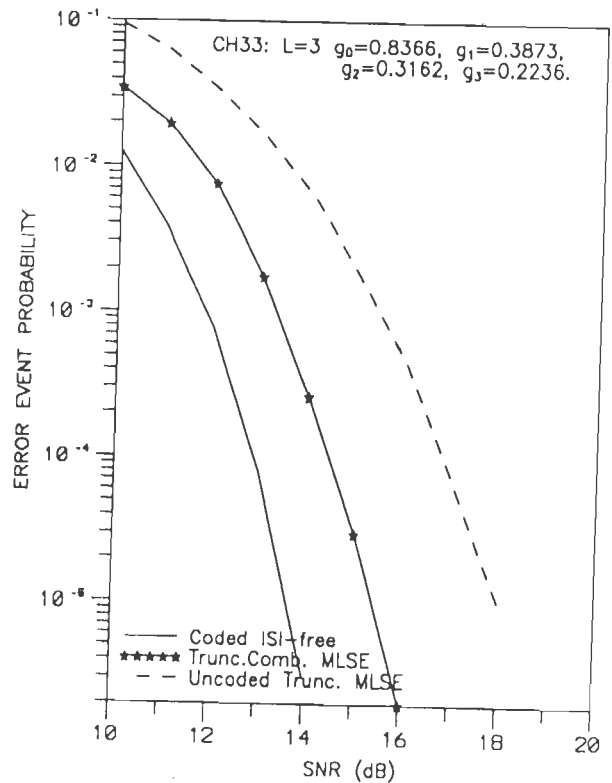
(a) ISI CHANNEL CH21:  $L=2$ ,  $J=1$ .



(b) ISI CHANNEL CH23:  $L=2$ ,  $J=1$ .



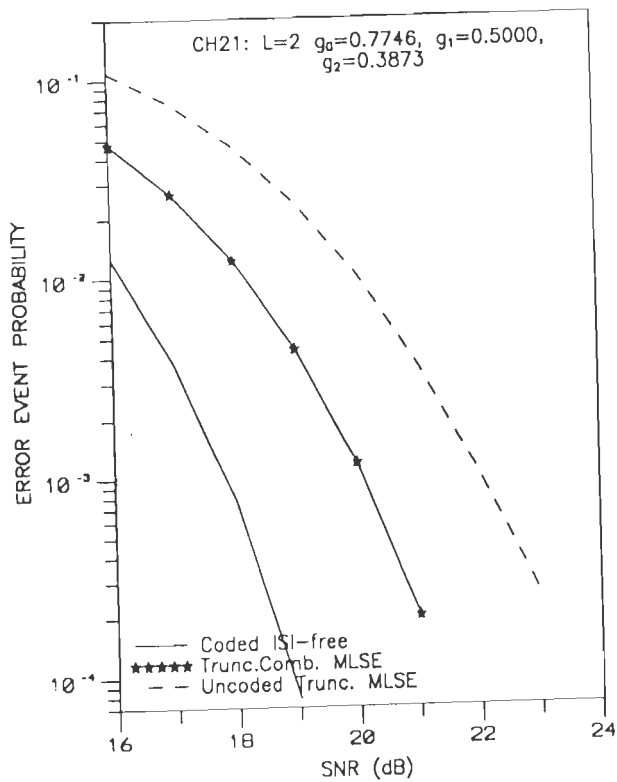
(c) ISI CHANNEL CH31:  $L=3$ ,  $J=1$ .



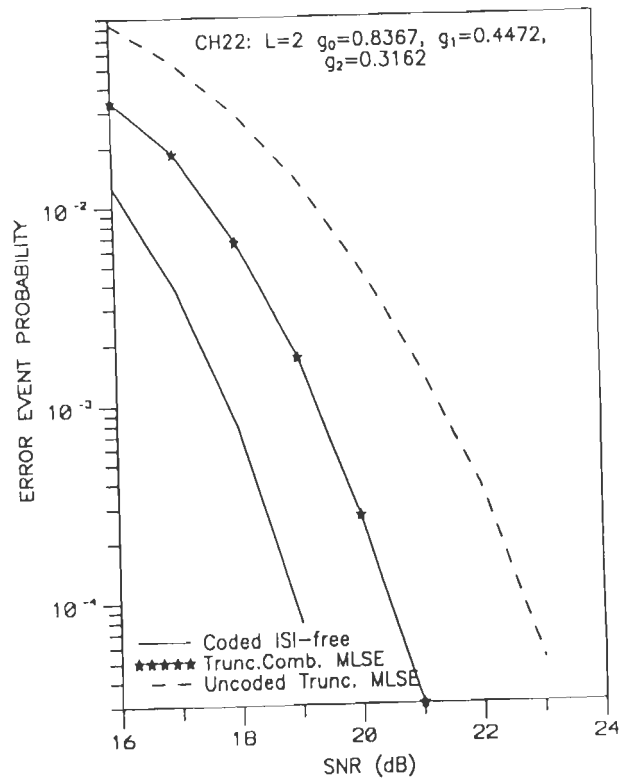
(d) ISI CHANNEL CH33:  $L=3$ ,  $J=1$ .

FIG.5.8 ERROR PERFORMANCE OF THE TRUNCATED COMBINED MLSE RECEIVER WHICH EMPLOYS A 32-STATE TRUNCATED COMBINED ISI-CODE TRELLIS STRUCTURE FOR THE DETECTION OF 4-STATE 16-QAM TCM SIGNALS OVER AN ISI CHANNEL OF MEMORY  $L$ .)1.

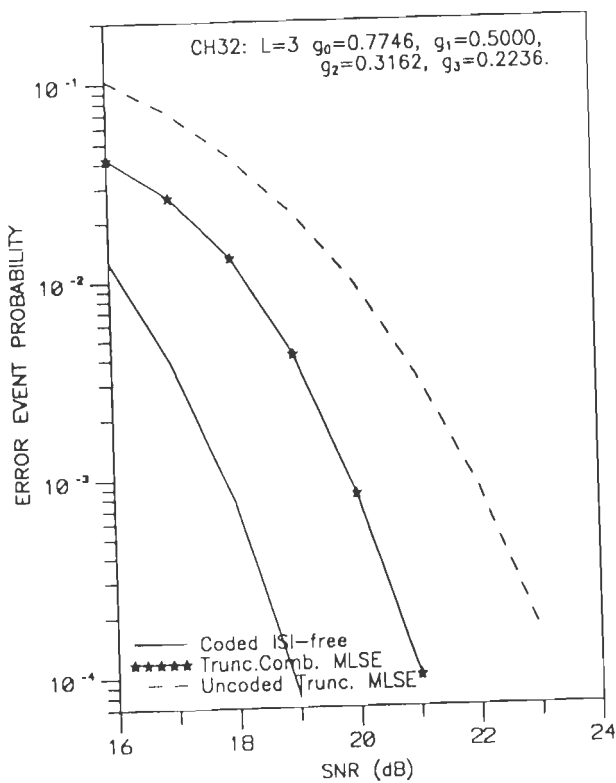




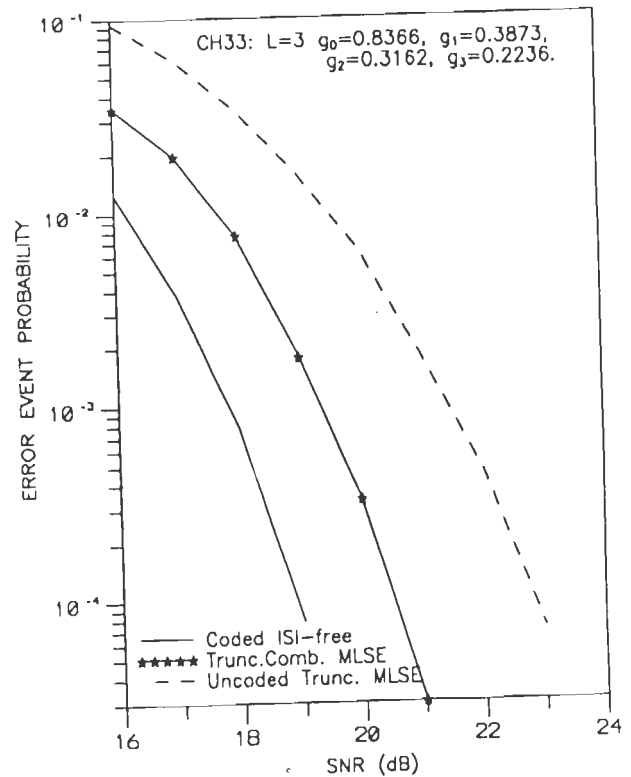
(a) ISI CHANNEL CH21:  $L=2$ ,  $J=1$ .



(b) ISI CHANNEL CH22:  $L=2$ ,  $J=1$ .

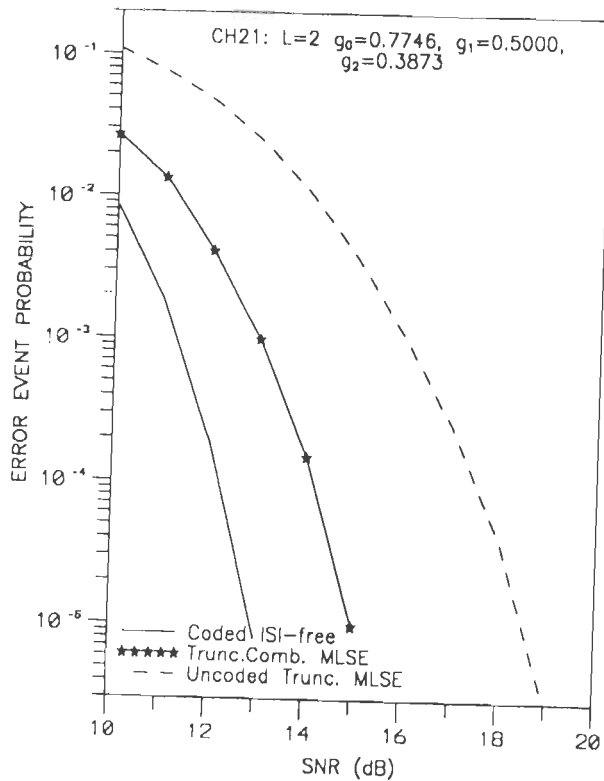


(c) ISI CHANNEL CH32:  $L=3$ ,  $J=1$ .

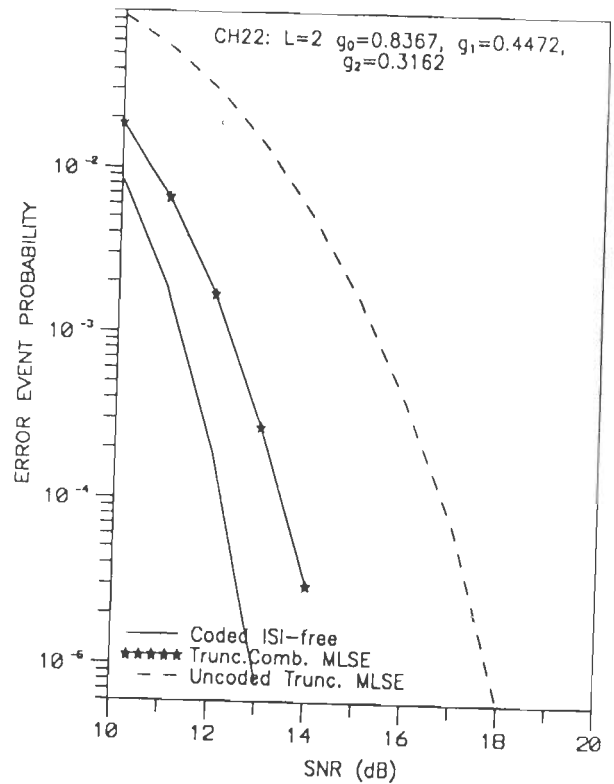


(a) ISI CHANNEL CH33:  $L=3$ ,  $J=1$ .

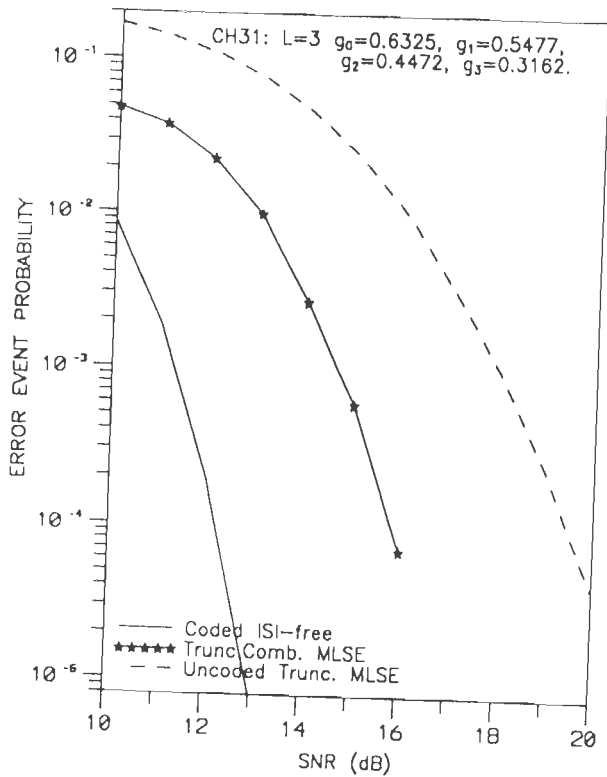
FIG.5.9 ERROR PERFORMANCE OF THE 128-STATE TRUNCATED COMBINED ISI-CODE TRELLIS STRUCTURE USED FOR THE DETECTION OF 4-STATE 64-QAM TCM SIGNALS OVER AN ISI CHANNEL OF MEMORY  $L > 1$ .



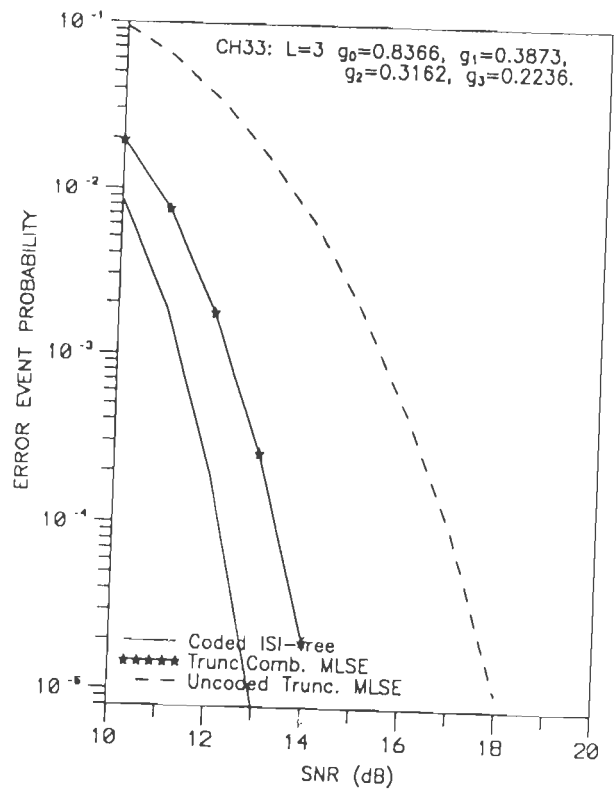
(a) ISI CHANNEL CH21:  $L=2$ ,  $J=1$ .



(b) ISI CHANNEL CH22:  $L=2$ ,  $J=1$ .



(c) ISI CHANNEL CH31:  $L=3$ ,  $J=1$ .



(d) ISI CHANNEL CH33:  $L=3$ ,  $J=1$ .

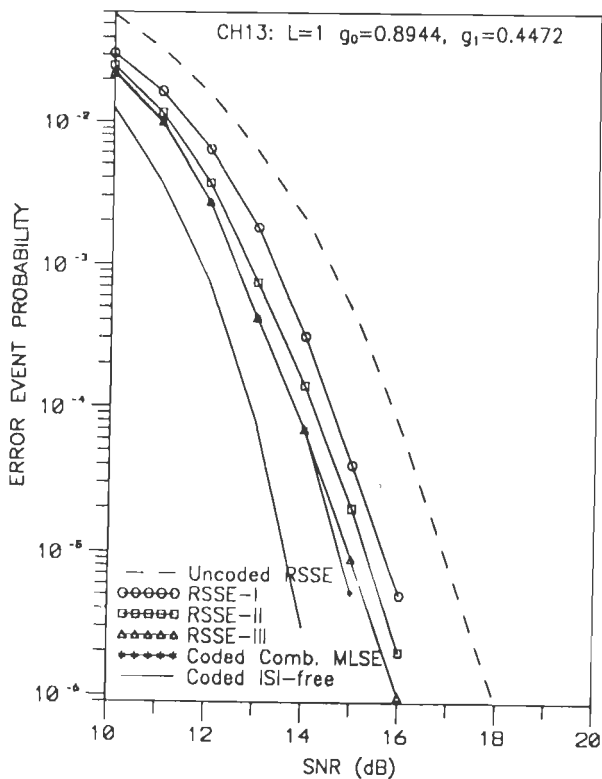
FIG.5.10 ERROR PERFORMANCE OF THE 64-STATE TRUNCATED COMBINED ISI-CODE TRELLIS STRUCTURE USED FOR THE DETECTION OF 8-STATE 16-QAM TCM SIGNALS OVER AN ISI CHANNEL OF MEMORY  $L = 1$ .

transmitted over an ISI channel of memory length  $L > 1$ . The size of the signal constellation  $M$  affects only the number of parallel transitions.

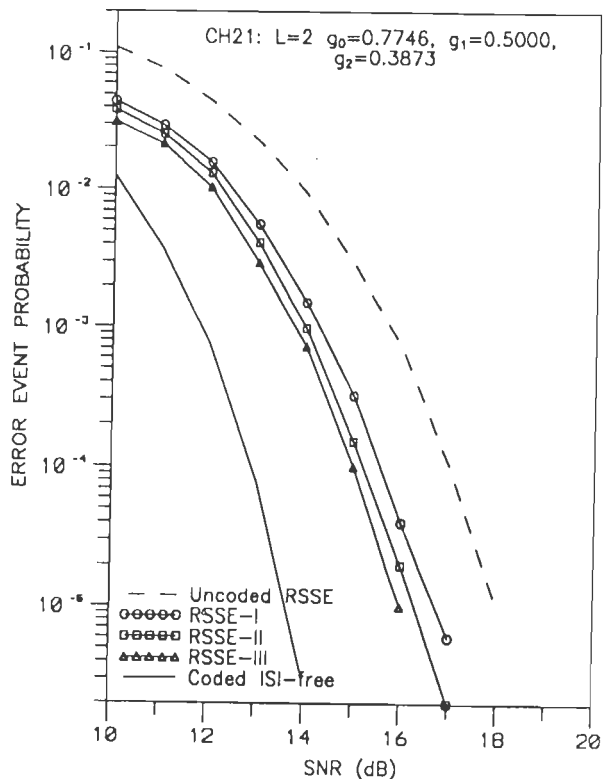
Fig.5.11 shows the performance of the different RSSE structures used for the detection of 4-state trellis coded 16-QAM signals in the presence of ISI and AWGN. The reference is an uncoded RSSE structure having the same data rate, bandwidth and signal energy as that of the coded system. In the figure RSSE-I, RSSE-II and RSSE-III correspond respectively to the 8-state, 16-state and 32-state RSSE structures of section 5.3.1–5.3.3. From the performance characteristics of Fig.5.11, we observe that the 8-state RSSE structure RSSE-I achieves a gain of 1.25–2.0 dB over the uncoded RSSE reference structure, while it suffers a degradation of about 1 dB relative to the optimum combined MLSE performance. The corresponding gains of RSSE-II and RSSE-III are 1.5–2.25 dB and 2.0–2.75 dB respectively. The structure RSSE-II suffers a loss of about 0.5 dB relative to the combined MLSE performance. We may note, from Fig.5.11(a), that the performance of the 32-state RSSE structure RSSE-III is almost same as that of the 32-state combined MLSE structure (of section 3.4.2).

Similarly, Fig.5.12 shows the performance of the three RSSE structures RSSE-I, RSSE-II and RSSE-III for the 4-state 64-QAM TCM transmission over an ISI channel of memory length  $L \geq 1$ . From Fig.5.12, we may note that the 8-state RSSE structure RSSE-I (of section 5.3.1) achieves a gain of about 1.5–1.75 dB over uncoded RSSE reference system, while the 16-state and 32-state RSSE structures RSSE-II and RSSE-III achieve correspondingly a gain of about 2.00–2.25 dB and 2.5–2.75 dB. We observe that the performance of the RSSE structure improves with an increase in the state complexity and in the limit its performance approaches that of the combined MLSE structure.

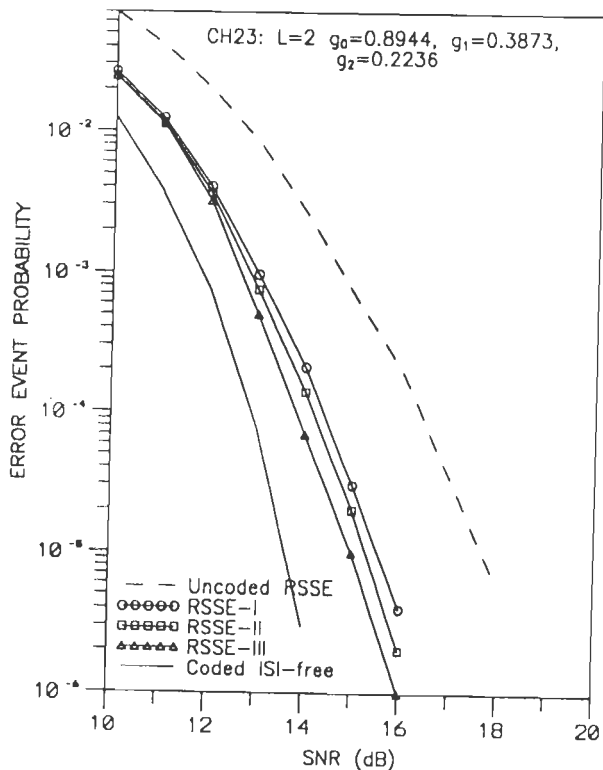
Fig.5.13 shows the performance characteristics of the 32-state RSSE structure RSSE-IV (of section 5.3.4), which is employed for the decoding of 8-state 16-QAM TCM signals in the presence of ISI and AWGN. The structure RSSE-IV achieves a gain of about 2.25–3.0 dB relative to the uncoded RSSE reference system. In Fig.5.13(a)



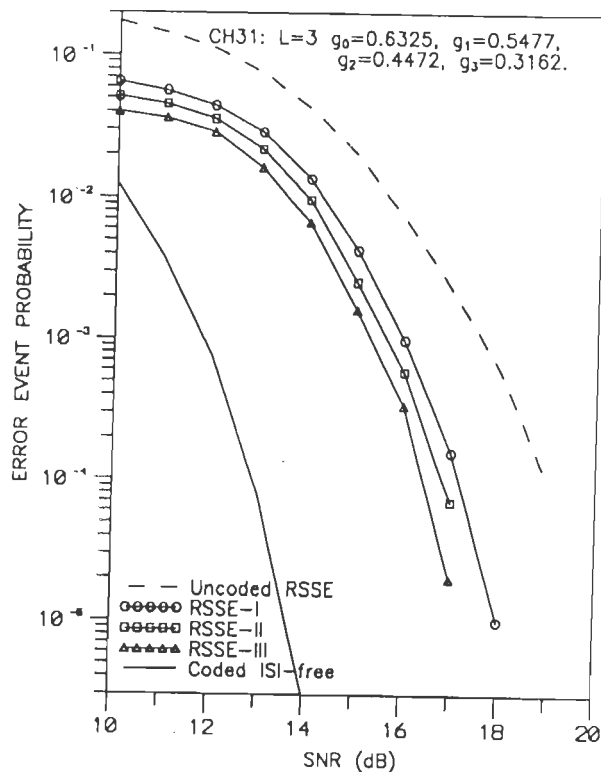
(a) 4-state 16-QAM TCM on CH13:  $L=1$



(b) 4-state 16-QAM TCM on CH21:  $L=2$

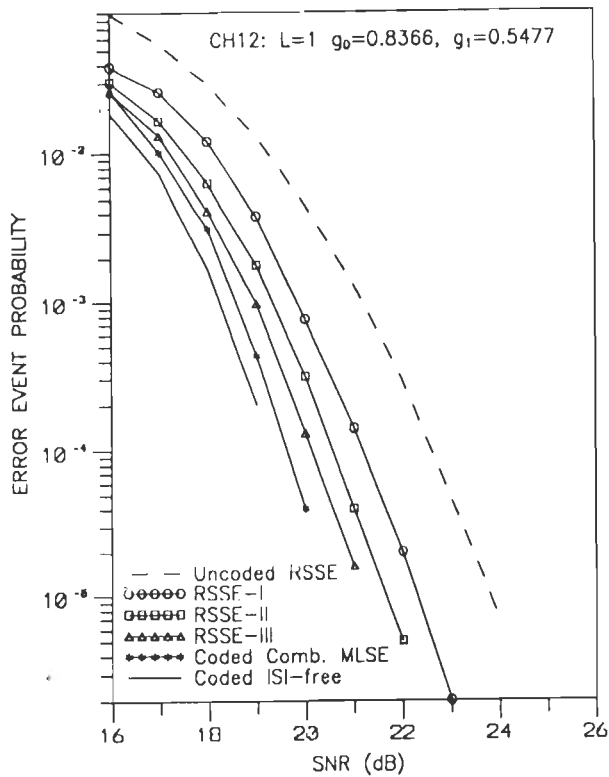


(c) 4-state 16-QAM TCM on CH23:  $L=2$

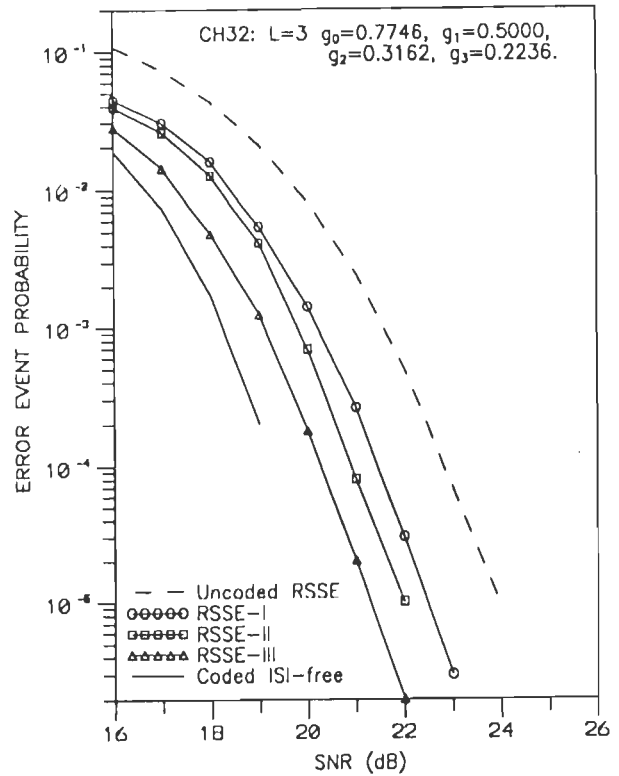


(d) 4-state 16-QAM TCM on CH31:  $L=3$

FIG.5.11 ERROR PERFORMANCE OF THE DIFFERENT RSSE RECEIVER STRUCTURES USED FOR THE DETECTION OF THE 4-STATE 16-QAM TCM SIGNALS OVER AN ISI CHANNEL OF MEMORY  $L$ .

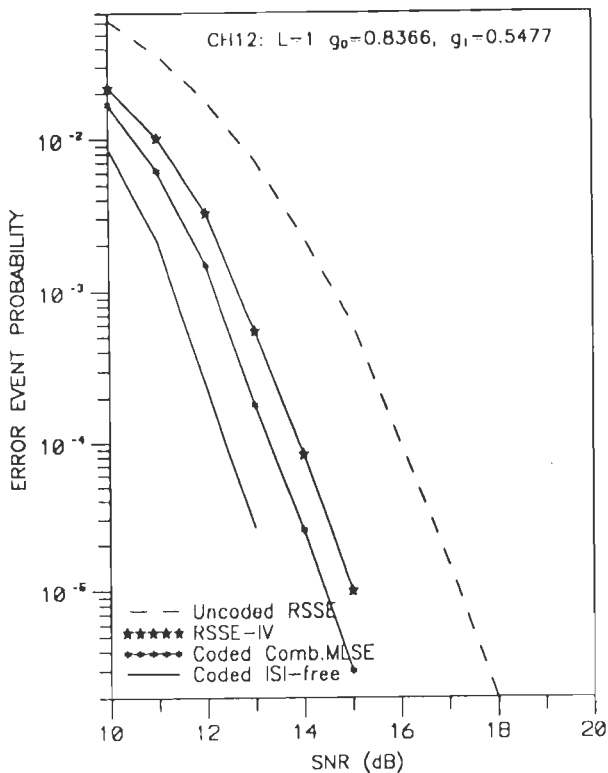


(a) 4-state 64-QAM TCM on CH12:  $L=1$

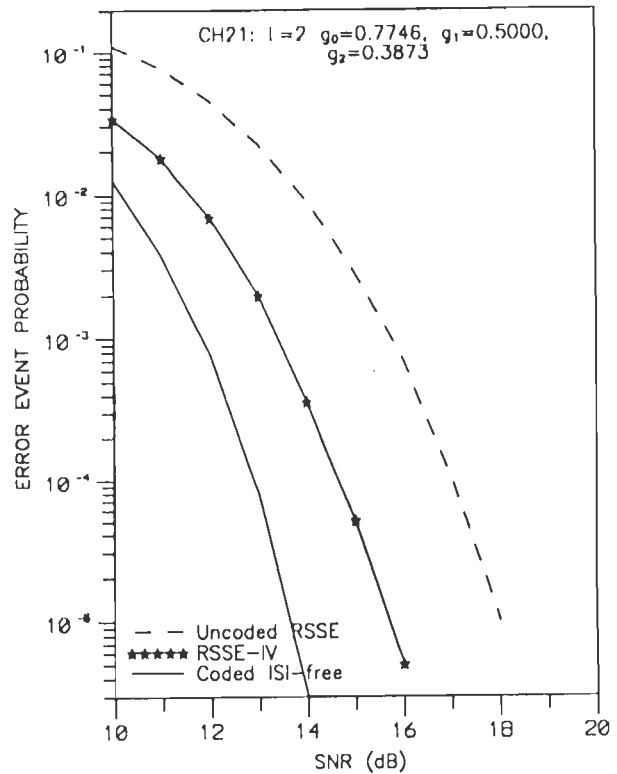


(b) 4-state 64-QAM TCM on CH32:  $L=3$

FIG.5.12 ERROR PERFORMANCE OF THE DIFFERENT RSSE RECEIVER STRUCTURES USED FOR THE DETECTION OF THE 4-STATE 64-QAM TCM SIGNALS OVER AN ISI CHANNEL OF MEMORY  $L$ .

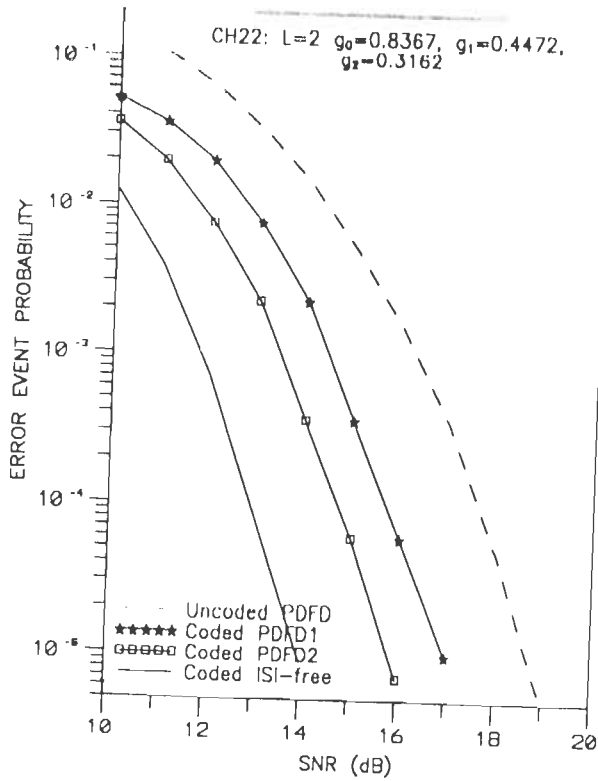


(a) 8-state 16-QAM TCM on CH12:  $L=1$

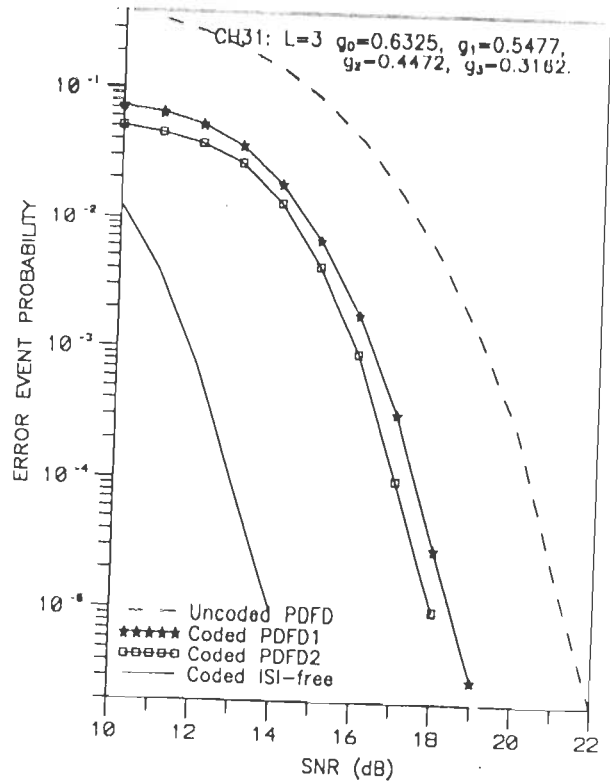


(b) 8-state 16-QAM TCM on CH21:  $L=2$

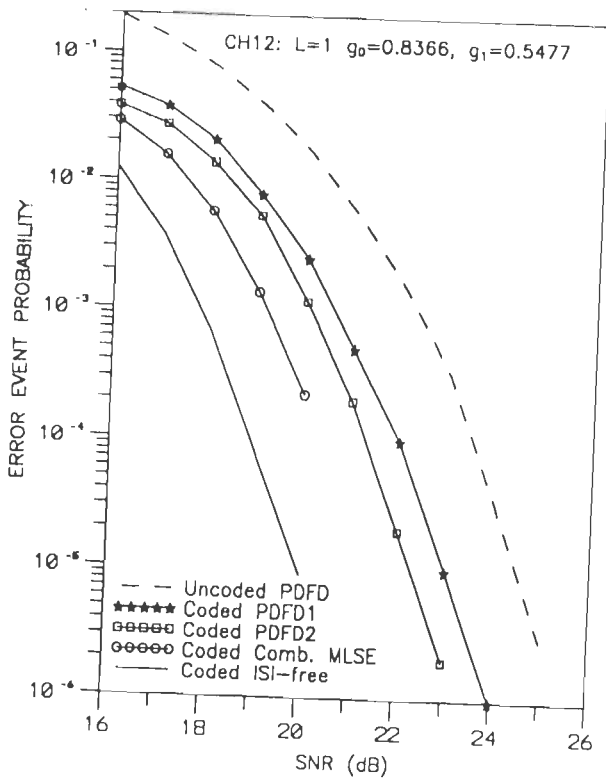
FIG.5.13 ERROR PERFORMANCE OF THE RSSE RECEIVER STRUCTURE (RSSE-IV) USED FOR THE DETECTION OF THE 8-STATE 16-QAM TCM SIGNALS OVER AN ISI CHANNEL OF MEMORY  $L$ .



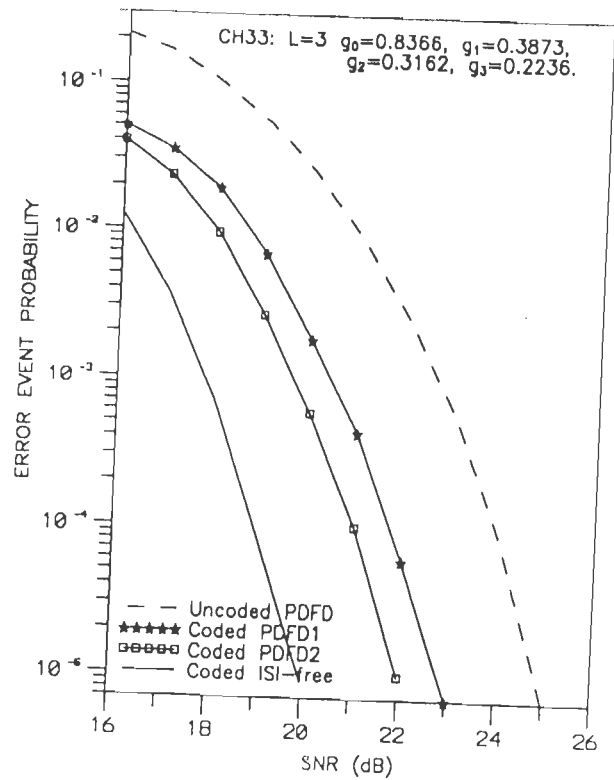
(a) 16-QAM TCM ON CH22:  $L=2$ ,  $J=0$



(b) 16-QAM TCM ON CH31:  $L=3$ ,  $J=0$



(c) 64-QAM TCM on CH12:  $L=1$ ,  $J=0$



(d) 64-QAM TCM ON CH33:  $L=3$ ,  $J=0$

FIG.5.14 ERROR PERFORMANCE OF THE DIFFERENT PDFD RECEIVER STRUCTURES EMPLOYED FOR THE DETECTION OF M-QAM TCM SIGNALS OVER AN ISI CHANNEL.

the performance of the 32-state RSSE structure RSSE-IV is compared with that of the 64-state combined MLSE structure (of section 3.4.4). The RSSE structure RSSE-IV suffers a performance degradation of about 0.75–1.0 dB over the optimum combined MLSE structure.

The PDFD receiver structure is a special case of RSSE structure for  $J=0$ . The state complexity of the PDFD structure equals that of the basic TCM encoder employed for the data transmission. The performance of the PDFD structure is compared with that of an uncoded PDFD reference structure. Fig.5.14 shows the error performance of the two reduced state structures PDFD1 and PDFD2, which correspond respectively to the 4-state and 8-state PDFD receiver structures. While Fig.5.14(a)–(b) give the error performance of the PDFD structures for 16-QAM TCM transmission, Fig.5.14(c)–(d) corresponds to that of 64-QAM TCM transmission. We observe from the performance characteristics that the 4-state PDFD structure (PDFD1) achieves a gain of 1.5–2.0 dB over the uncoded reference system, while the 8-state PDFD structure (PDFD2) shows a coding gain of 2.25–3.0 dB over the uncoded reference. The PDFD1 and PDFD2 structures suffer a performance degradation of about 1.75 dB and 1.25 dB respectively relative to the optimum combined MLSE structure on ISI channels of memory length  $L=1$ .

From the study presented above, we observe that the truncated MLSE structures give performance close to that of the combined MLSE structure, with a small degradation in the range of 0.5–1.0 dB. A further reduction in state complexity can be achieved by the use of the RSSE structures that incorporate the ideas of set-partitioning inherent in the TCM design. The performance of the RSSE structures approaches that of the combined MLSE structure as the state complexity increases. As the state complexity of the RSSE is reduced to that of the TCM encoder, we get the PDFD structure whose performance is quite significant over the uncoded reference, although there is significant performance degradation relative to the optimum combined MLSE structure.

# ADAPTIVE RECEIVER STRUCTURES FOR TCM TRANSMISSION OVER TIME-DISPERSIVE FADING CHANNELS

---

## 6.1 INTRODUCTION

The continuing growth of mobile telephone traffic and the need for its integration with digital communication facilities has spurred an active research and subsequent development of high-capacity digital mobile radio systems in recent years. The digital mobile-radio channels are characterized as rapidly time-varying channels which are highly susceptible to multipath-induced ISI and sometimes exhibit deep fades. The fact that the coded-modulation schemes can provide significantly improved performance over bandlimited channels, has made TCM schemes attractive for applications over fading channels also. To combat the effect of ISI on such (rapidly) time-varying fading channels relatively complex adaptive equalization procedures and, to overcome the effects of severe fades on such channels, the more effective diversity combining techniques have to be employed [2, 4, 101].

Since the publication of spectrally efficient TCM schemes by Ungerboeck [126], there has been an active research and applications of TCM schemes, particularly M-PSK TCM, for satellite channels [8, 13, 30]. However, in recent years there is an increased interest in the use of M-QAM TCM schemes for fading channels due to their excellent spectral-efficiency and power-efficiency over M-PSK schemes. It has been reported that [35, 55], the M-QAM TCM schemes outperform M-PSK TCM schemes when the receiver can be provided with channel state



information, and hence it is argued that the high data rate requirements of future digital satellite communications and digital mobile communications can be met only with the use of M-QAM TCM schemes [131].

In addition to the use of coded-modulation schemes, the most effective technique to reduce the effect of severe fading present on such time-varying channels is through the use of diversity reception. The diversity technique is based on the notion that the probability of the signals received on  $D$ -different independent paths will fade simultaneously is extremely small [97]. In diversity reception, the receiver is provided with several replicas of the same information transmitted over  $D$ -independent fading channels.

The optimum combined MLSE receiver structure or its sub-optimum variants, requires an exact knowledge of the channel characteristics for the equalization and decoding of TCM signals. So far our study has been constrained under the assumption that the channel is time-invariant and known. But in reality, the channel is usually non-stationary (time-variant) and is unknown. Therefore for proper detection, the receiver needs to be equipped with an adaptive channel estimator for the identification of time-varying channel parameters.

A wide range of adaptive algorithms for channel estimation have been reported in the literature [101, 104], the most common being the least-mean squares (LMS) algorithm and the recursive least-squares (RLS) algorithm. The LMS is simple to implement and hence finds wide applications. The RLS algorithm exhibit faster convergence and better tracking capability than LMS algorithm, and is well suited for applications on time-varying ISI channels [37, 101]. The inherent decision delay of the Viterbi algorithm employed in the optimum MLSE decoder or its suboptimum variants, will result in delayed channel estimation and hence poor tracking especially when the channel characteristics are rapidly time-varying. To circumvent this problem, a new channel estimation procedure has been reported in recent years [65, 112]. This scheme maintains a separate channel estimator for each state of the Viterbi decoder and uses the delay-free decisions, associated

with the survivor path leading into that state, for the updating of channel coefficients through the LMS or RLS adaptive algorithm. This new channel estimation procedure, called as respective-state channel estimation (RCE) or per-state processing (PSP) channel estimation, has been shown [66, 105] to exhibit excellent tracking performance on rapidly time-varying ISI channels.

In this chapter, we first consider the discrete-time model of the fading channel. We next consider the channel estimators based on LMS/RLS adaptation algorithms which employ delayed-decision updating for estimating the channel coefficients, for applications on slow fading channels. For applications on rapidly time-varying channels, we consider the channel estimation employing a more complex respective-state channel estimation procedure that uses delay-free decisions to update the channel coefficients through LMS/RLS adaptation. The error performance and tracking characteristics of these channel estimators have been studied through simulation. Also, a study has been performed to determine the error rate performance of several adaptive TCM receiver structures on fading channels, through simulation. We then consider the use of D-diversity reception for the decoding of Trellis-Coded QAM signals transmitted over a severe fading channel. Finally, we present the results of the study on the error rate performance of different adaptive receivers through simulation.

## **6.2 FADING CHANNEL MODEL FOR TCM TRANSMISSION**

Many of the physical digital communication channels such as HF shortwave ionospheric propagation channels, troposcatter radio, digital mobile radio, and digital satellite channels are often modeled as time-variant multipath fading channels. Three phenomena namely time-spread, Doppler spread, and multipath fading have been recognized as the main impairments to reliable communication over these channels. The time-spread causes ISI, the Doppler spread necessitates a fast convergent algorithm for adaptive equalization, and the multipath fading also results in a very low received signal when the channel exhibits a deep fade and

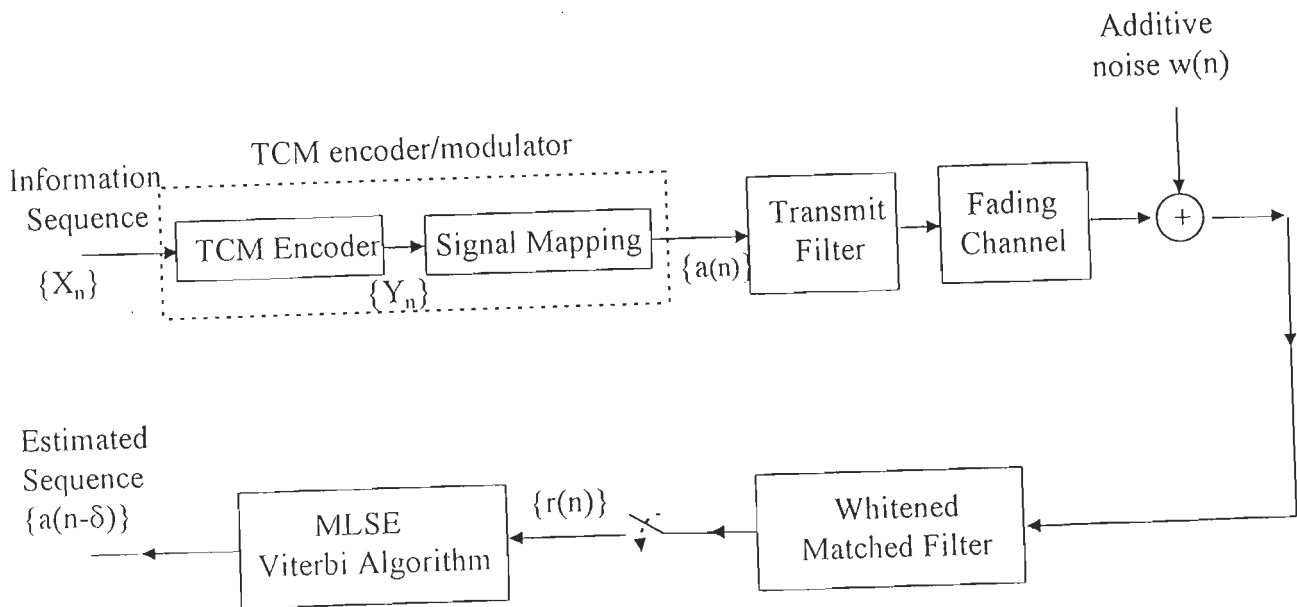


FIG. 6.1 TCM DATA TRANSMISSION OVER A FADING CHANNEL.

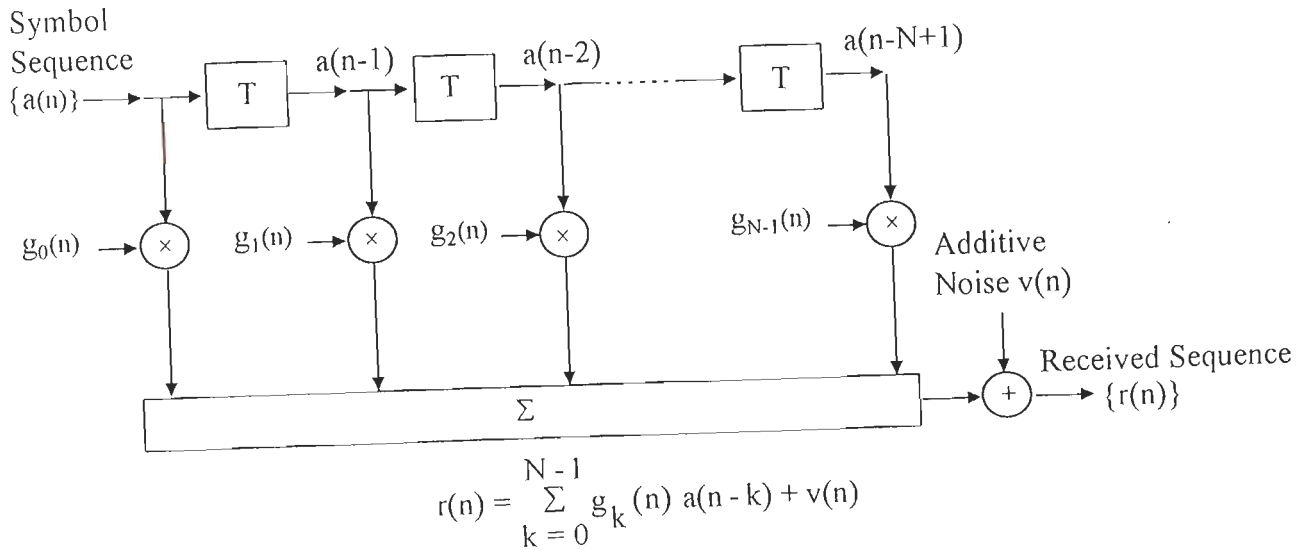


FIG. 6.2 TAPPED DELAY LINE MODEL OF A FADING DISPERSIVE CHANNEL.

necessitates the use of diversity techniques [117].

The fading dispersive channel can be modeled as a randomly time-variant linear filter [5, 62], which can be completely specified in terms of the time-varying channel impulse response, as detailed in Appendix C.

Consider the equivalent baseband transmission system for the transmission of TCM signals over a time-dispersive fading channel as shown in Fig.6.1. The system transmits  $m$  information bits  $X_n$  per signaling interval. The TCM encoder produces  $m+1$  coded bits  $Y_n$  which are mapped into a channel signal  $a(n)$  of the  $2^{m+1}$ -QAM signal constellation, in accordance with the mapping rules of TCM [126]. For optimum detection, the received signal is passed through a linear filter matched to the channel characteristics and the output of the whitened-matched filter is sampled periodically at the symbol rate. Thus, at the sampling instant  $n$ , the sampled complex value of the received signal is given by

$$r(n) = \sum_{k=0}^{N-1} g_k(n) \cdot a(n-k) + v(n) \quad \dots(6.1)$$

where  $g_k(n)$  represents randomly time-varying coefficients of the finite duration channel impulse response, and takes into account the effects of the transmit filter, the actual channel and the receiver filter.  $v(n)$  represents the sampled value of the complex AWGN process with zero-mean and variance  $\sigma_v^2$  in each dimension and  $a(n)$ 's are the transmitted TCM QAM symbols.

Thus, TCM transmission over a time-dispersive fading channel can be modeled as a finite duration tapped-delay-time (TDL) filter with randomly time-varying coefficients  $g_k(n)$  at tap spacings of  $T$  as shown in Fig.6.2, where  $T$  represents the sampling (baud) interval. The time-variant tap weights  $\{g_k(n)\}$  are assumed to be statistically independent complex-valued Gaussian random variables having zero mean and variance  $P_k$  in each dimension given by

$$P_k = (1/2) E[|g_k(n)|^2], \quad \text{for } k = 0, 1, \dots, N-1. \quad \dots(6.2)$$

Note that  $P_k$ 's define the delay power spectrum or the power impulse response of the channel.

The time-variations in the channel characteristics are taken into account by filtering the random tap coefficients through a first-order low-pass filter whose 3dB bandwidth  $B$  is of the order of fade rate in Hz, as detailed in Appendix C. This leads to the following model for the tap gains of the fading dispersive channel [88],

$$g_k(n+1) = g_k(n) \exp(-\alpha T) + \sqrt{P_k(1-\exp(-2\alpha T))} u_k(n) \quad \dots(6.3)$$

where  $u_k(n)$  denotes the samples of zero-mean, unit-variance complex Gaussian noise process. In (6.3),  $\alpha=2\pi B$  where  $B$  is fade rate in Hz, and  $T$  is the sampling interval (baud interval).

### 6.3 CHANNEL ESTIMATION

Given the received sequence  $\{r(n)\}$ , the problem is to recover the symbol sequence  $\{a(n)\}$ , as reliably as possible, within the constraints imposed by the receiver structure. Several adaptive receiver structures have been reported in the literature [77, 104] for the recovery of the data in the presence of the unknown channel interference and noise.

The estimation of random time-varying channel coefficients  $\{g_k(n)\}$ , given the measurements of the related process  $\{r(n)\}$  will constitute the channel estimation problem. The general configuration of an adaptive channel estimator used in connection with an optimum MLSE detector or its suboptimum variants is as shown in Fig.6.3. The channel estimator approximates the actual channel with a discrete finite-state machine (linear time-variant filter) in exactly the same manner as that of Fig.6.2. A recursive adaptive algorithm is employed to estimate the channel coefficients by minimizing the error between the actual received sequence and the estimated received sequence available from the output of the linear filter [101].

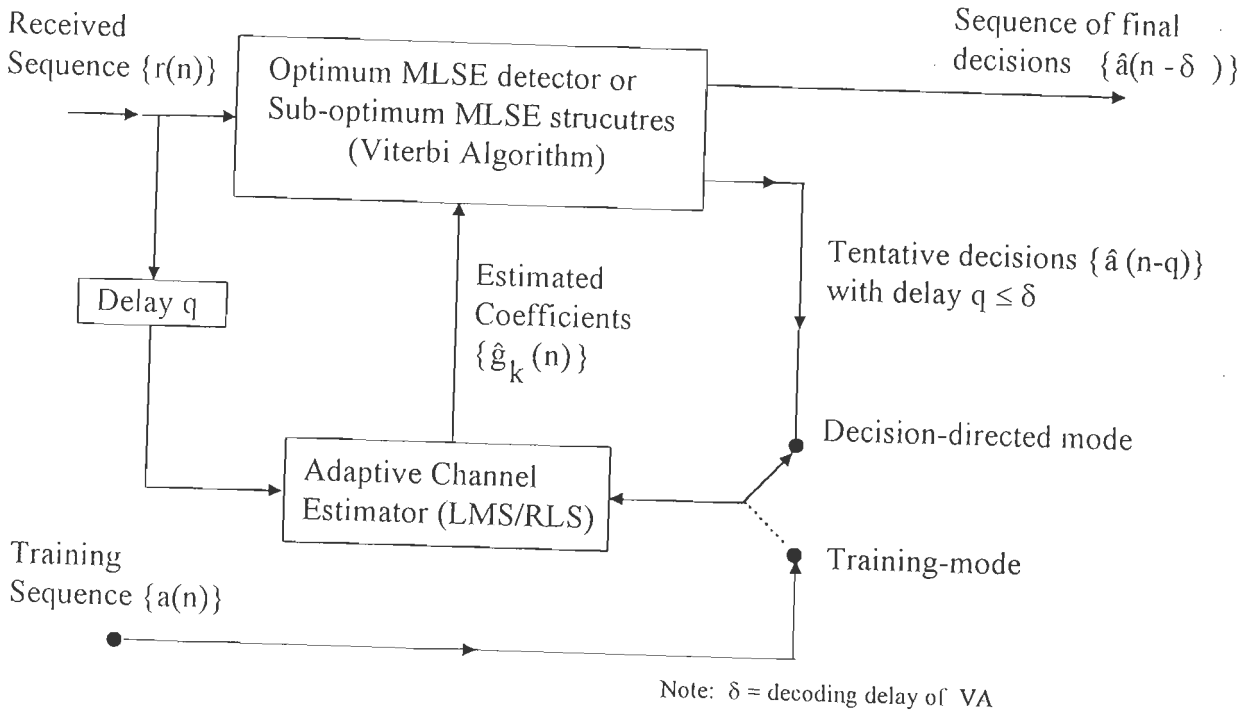


FIG. 6.3 GENERAL STRUCTURE OF AN ADAPTIVE MLSE RECEIVER.

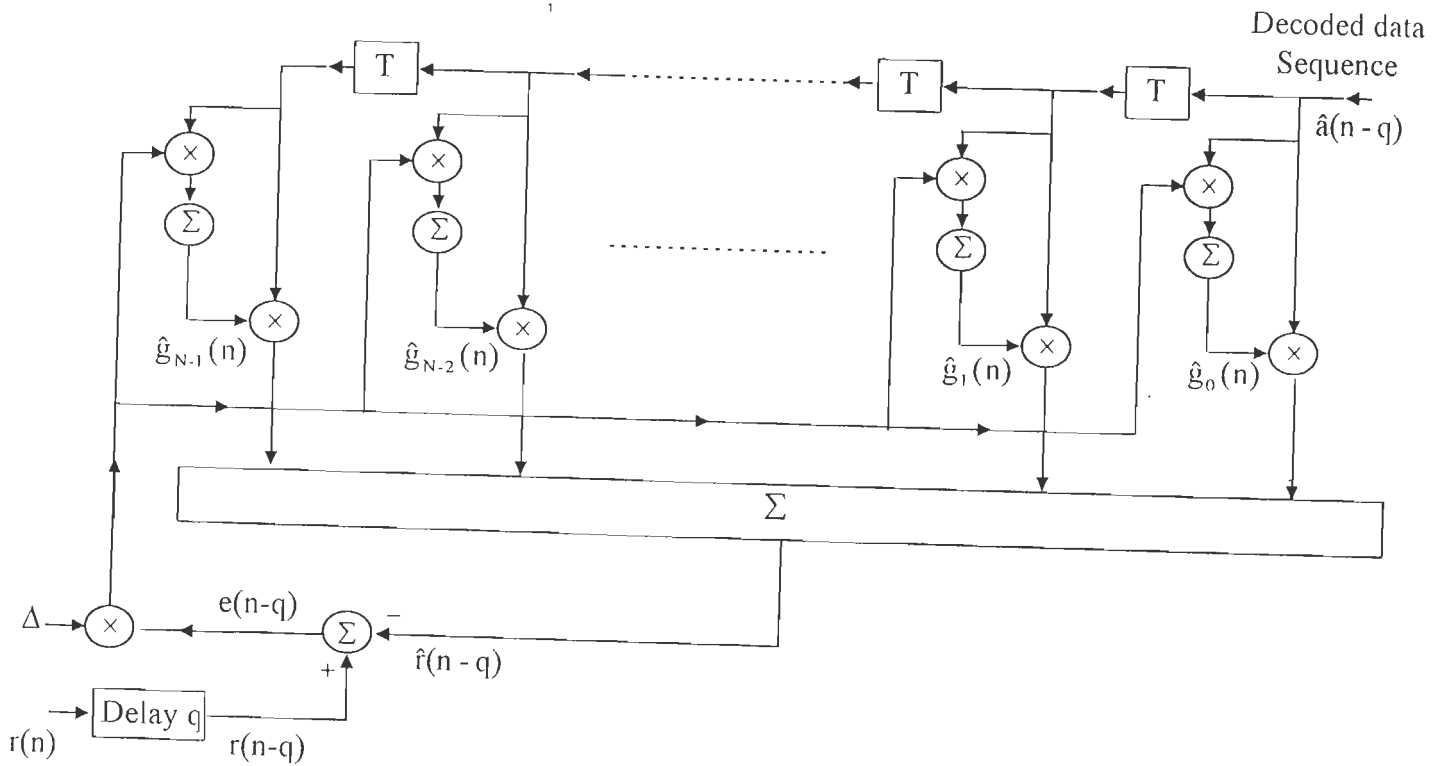


FIG. 6.4 STEPEST-DESCENT LMS CHANNEL ESTIMATOR.

The channel estimator is initially operated in the training mode (start-up mode) to estimate the tap coefficients, during which a known data sequence  $\{a(n)\}$  is used to form the filter output  $\{\hat{r}(n)\}$ . Followed by this, it is operated in the decision-directed mode (adaptive-mode) for tracking the channel estimates, during which the detected data sequence  $\{\hat{a}(n)\}$  is used to form the filter output  $\{\hat{r}(n)\}$ . It has been shown that [78] by forming an error sequence  $\{\epsilon(n)=r(n)-\hat{r}(n)\}$  and applying a suitable minimization criterion, one obtains as the optimum filter coefficients the actual channel parameters  $\{g_k(n)\}$ .

The adaptation algorithm employed in channel estimation should exhibit fast convergence during the training phase, better tracking capability during the adaptive phase, and a low computational complexity. The stochastic gradient-type algorithms, such as LMS algorithms are the simplest and the most widely used adaptation algorithms when the channel characteristics are slowly time-varying. The recursive least-squares (RLS) adaptation algorithms exhibit faster convergence and better tracking capabilities than LMS algorithms and are considered to be suitable for time-varying channels [44, 74, 100]. Unlike LMS, the convergence rate of RLS is insensitive to the eigenvalue spread of the signal autocorrelation matrix.

The channel estimator, in the adaptive mode, uses the decoded data decisions to update the estimates of the tap gain coefficients. It is well known that reliable data decisions from the Viterbi decoder will be available only after a fixed decision delay  $\delta$  [47]. Therefore for channels with large memory and in particular for the combined ISI and TCM decoding, this  $\delta$  can be very large. Consequently, this leads to a delay in the channel estimation and hence results in poor tracking of the channel response in a time-varying environment. Thus, the conventional channel estimation techniques employed in adaptive MLSE structures suffer from poor tracking on a rapidly time varying ISI channel. Kubo et al. [65] and Seshadri [112] have, independently, proposed a new channel estimation technique that facilitates delay-free channel estimation by maintaining a separate

channel estimator for each state of the Viterbi algorithm. The respective-state channel estimates are updated through LMS/RLS algorithm by making use of the zero-delay decisions associated with the survivor path leading into that state. As the procedure involves the estimation of channel coefficients for each state per baud interval, the method is often referred to as per-state processing (PSP) or Respective-state Channel Estimation (RCE) [24, 66, 105]. Since the estimates of the channel impulse response are not influenced by the decoding delay  $\delta$  of the VA, the performance of this estimation procedure is shown to be much superior to that of conventional channel estimators for rapidly time-varying ISI channels. However, the price paid for this improved performance is the increased complexity in implementation, which depends on the number of states in the trellis on which the VA operates.

Kubo et al. [65, 66] have considered the study of the respective-state channel estimators for uncoded transmission, as well as trellis-coded QPSK transmission using the LMS adaptation criterion. In this work, we have considered a study of these respective-state channel estimators based on both LMS and RLS algorithms and their applications to the detection of Trellis-Coded QAM signals over time-varying ISI channels using various trellis structures discussed earlier.

### 6.3.1 Channel Estimation Using LMS Algorithm

The channel estimator based on LMS adaptation as shown in Fig.6.4, has a structure identical to that of a linear transversal filter. In fact, the channel estimator is a replica of the equivalent discrete-time channel filter that models the ISI. The estimated channel tap gains  $\{\hat{g}_k(n)\}$  are adjusted recursively by the steepest-descent LMS algorithm to minimize the mean-square error between the actual received sequence  $\{r(n)\}$ , and the estimated received sequence  $\{\hat{r}(n)\}$  available at the output of the estimation filter. The speed of the convergence and the adaptation rate are controlled by the value of the adjustment parameter  $\Delta$ . It may be noted that a delay  $q$ , equal to the decision delay  $\delta$  of the VA, is



introduced to properly time the comparison between the received sequence  $\{\hat{r}(n)\}$  and the estimated received sequence  $\{\hat{r}(n-q)\}$ .

For decision-directed mode of operation, the adaptive LMS algorithm for complex signals is then described by the following equations [75, 78, 140].

Filter output:

$$\hat{r}(n) = \hat{A}^T(n) \cdot \hat{G}(n) \quad \dots(6.5)$$

Error :

$$e(n) = r(n) - \hat{r}(n) \quad \dots(6.6)$$

Coefficient update :

$$\hat{G}(n) = \hat{G}(n-1) + \Delta \cdot e(n) \cdot \hat{A}^*(n) \quad \dots(6.7)$$

where  $\hat{A}(n)$  is an N-component input vector to the filter at the time instant n, defined as

$$\hat{A}(n) = [\hat{a}(n), \hat{a}(n-1), \dots, \hat{a}(n-N+1)]^T \quad \dots(6.8)$$

$\hat{G}(N)$  is an N-component vector of tap gain estimates, defined by

$$\hat{G}(N) = [\hat{g}_0(n), \hat{g}_1(n), \dots, \hat{g}_{N-1}(n)]^T \quad \dots(6.9)$$

$r(n)$  is the desired reference signal and  $\hat{r}(n)$  is the estimated filter output,  $\Delta$  is the step size for coefficient adaptation, and  $\tau$ ,  $*$  represent the transpose and complex conjugate operations, respectively.

For mathematical tractability, it is assumed that the detected data sequence  $\{\hat{a}(n)\}$  is correct, that is  $\hat{a}(j)=a(j)$  for all j. Then the mean-square error between the received signal  $r(n)$  and its estimate  $\hat{r}(n)$  is given by

$$\varepsilon(n) = E \{|r(n) - \hat{r}(n)|^2\} \quad \dots(6.10)$$

It has been shown that [78, 139], as long as the data sequence  $\{a(n)\}$  is uncorrelated, the optimum tap gain coefficients  $\{\hat{g}_k(n)\}$  are exactly equal to the

respective values of the equivalent discrete-time channel response  $\{g_k(n)\}$ . Then, the minimum mean-square error is simply equal to the noise variance  $N_0 = 2\sigma_v^2$ , where  $\sigma_v^2$  is the noise variance in each dimension.

### 6.3.2 Channel Estimation Using RLS Algorithm

We next consider the channel estimator based on RLS adaptation algorithm. Structure-wise the estimator is identical to that of Fig.6.4 and approximates the discrete-time channel of Fig.6.2. The estimated tap-gain coefficients  $\{\hat{g}_k(n)\}$  are adjusted recursively using a least-squares cost criterion.

Let  $\hat{G}_N(n)$  represent an N-dimensional vector of the estimated channel coefficients defined at time instant n as

$$\hat{G}_N(n) = [\hat{g}_0(n), \hat{g}_1(n), \dots, \hat{g}_{N-1}(n)]^T \quad \dots(6.11)$$

Also, let  $\hat{A}_N(n)$  represent an N-dimensional vector of decoded data symbols defined at time instant n as

$$\hat{A}_N(n) = [\hat{a}(n), \hat{a}(n-1), \dots, \hat{a}(n-N+1)]^T \quad \dots(6.12)$$

Suppose we have  $\hat{G}_N(n-1)$  and the inverse covariance matrix  $P_{NN}(n-1)$  of the decoded data symbols. When the decoded signal component  $\hat{a}(n)$  is received, we have  $\hat{A}_N(n)$ . Then the recursive least-squares (RLS) computation, in complex form, for the time update of  $\hat{G}_N(n)$  and  $P_{NN}(n)$  proceeds as follows [1]:

Compute the filter output:

$$\hat{r}(n) = A_N^T(n) \cdot \hat{G}_N(n-1) \quad \dots(6.13)$$

Compute the error:

$$e(n/n-1) = r(n) - \hat{r}(n) \quad \dots(6.14)$$

Compute the Kalman gain vector:

$$\mathbf{K}_N(n) = \frac{\mathbf{P}_N(n-1) \hat{\mathbf{A}}_N^*(n)}{\lambda + \hat{\mathbf{A}}_N^\tau(n) \mathbf{P}_{NN}(n-1) \hat{\mathbf{A}}_N^*(n)} \quad \dots(6.15)$$

Update the inverse correlation matrix:

$$\mathbf{P}_{NN}(n) = \frac{1}{\lambda} [\mathbf{P}_{NN}(n-1) - \mathbf{K}_N \hat{\mathbf{A}}_N^\tau(n) \mathbf{P}_{NN}(n-1)] \quad \dots(6.16)$$

Update the channel coefficients vector:

$$\hat{\mathbf{G}}_N(n) = \hat{\mathbf{G}}_N(n-1) + \mathbf{K}_N(n) \cdot e(n/n-1) \quad \dots(6.17)$$

or

$$\hat{\mathbf{G}}_N(n) = \hat{\mathbf{G}}_N(n-1) + \mathbf{P}_{NN}(n) \cdot \hat{\mathbf{A}}_N^*(n) \cdot e(n/n-1) \quad \dots(6.18)$$

Initialization:

$$\hat{\mathbf{G}}_N(0) = \hat{\mathbf{A}}_N(0) = \mathbf{0} \quad \dots(6.19)$$

and

$$\mathbf{P}_{NN}(0) = \delta^{-1} \mathbf{I}$$

where  $\delta$  is a small positive constant, and  $\mathbf{I}$  is  $N \times N$  identity matrix. Note that in (6.11)-(6.18),  $n$  stands for the discrete time index,  $\tau$  for transpose, and  $*$  for complex conjugate operation. The parameter  $\lambda$  is some positive constant close to but less than unity, used for the exponential weighing of the past signal. The factor  $1/(1-\lambda)$  represents the memory of the algorithm.

The objective of the least-squares algorithm is to generate an optimum tap coefficient vector  $\hat{\mathbf{G}}_N(n)$  at time  $n$ , which minimizes the weighted squared-error [1, 37],

$$\begin{aligned} \epsilon(n) &= \sum_{i=0}^n \lambda^{n-i} e(i/n) \cdot e^*(i/n) \\ &= \sum_{i=0}^n \lambda^{n-i} |r(i) - \hat{\mathbf{G}}_N^\tau(n) \hat{\mathbf{A}}_N(i)|^2 \quad \dots(6.20) \end{aligned}$$

In the sense of this error minimization criterion, the RLS estimation algorithm makes the best possible use of all the available data  $\{\hat{\mathbf{A}}_N(i), r(i)\}$  upto the time

n. Therefore, in this sense it converges and tracks as fast as possible. Although, the RLS algorithms are well suited for applications in a time-varying environment because of fast convergence and better tracking capability, they are too complex to implement compared to the LMS algorithms.

In the conventional channel estimation procedure using either LMS or RLS algorithm, a decision delay of  $q \leq \delta$  needs to be incorporated to properly time the comparison between the reference and the input to the estimation filter. This causes a delay in the channel estimation and hence results in poor tracking which may not be tolerable in a rapidly time-varying environment.

### 6.3.3 Delay-free Channel Estimation Using Per-Survivor Processing

The conventional channel estimation techniques, as discussed in the proceeding subsections, which are normally employed in the adaptive MLSE structures suffer from poor tracking capability in a time-varying environment due to the decision delay  $\delta$  inherent in the Viterbi algorithm. A large delay in the channel estimation may not be tolerable in applications, such as digital mobile radio and mobile satellite communications, where the channel characteristics are rapidly time-varying [65]. Some researchers have employed tentative decisions with delay  $q \leq \delta$  for channel updating [112]. A decrease in  $q$  results in erroneous channel estimation since premature decisions from VA (for  $q \ll \delta$ ) are subject to higher error rate. An increase in  $q$  causes degradation in tracking due to the delay in channel estimation. Many of the adaptive algorithms desire zero-delay tentative decisions (with  $q=0$ ). Since these zero-delay decisions are subject to a higher error compared to the global decisions with  $q=\delta$ , the step-size of the adaptation algorithm should be made smaller. This is in contrast to the need for large step-size for tracking fast varying channels. Therefore, the conventional channel estimation techniques for adaptive MLSE fail to provide delay-free channel estimation and better tracking of rapidly time-varying channels.

In order to achieve better tracking with large step-size adaptation as well

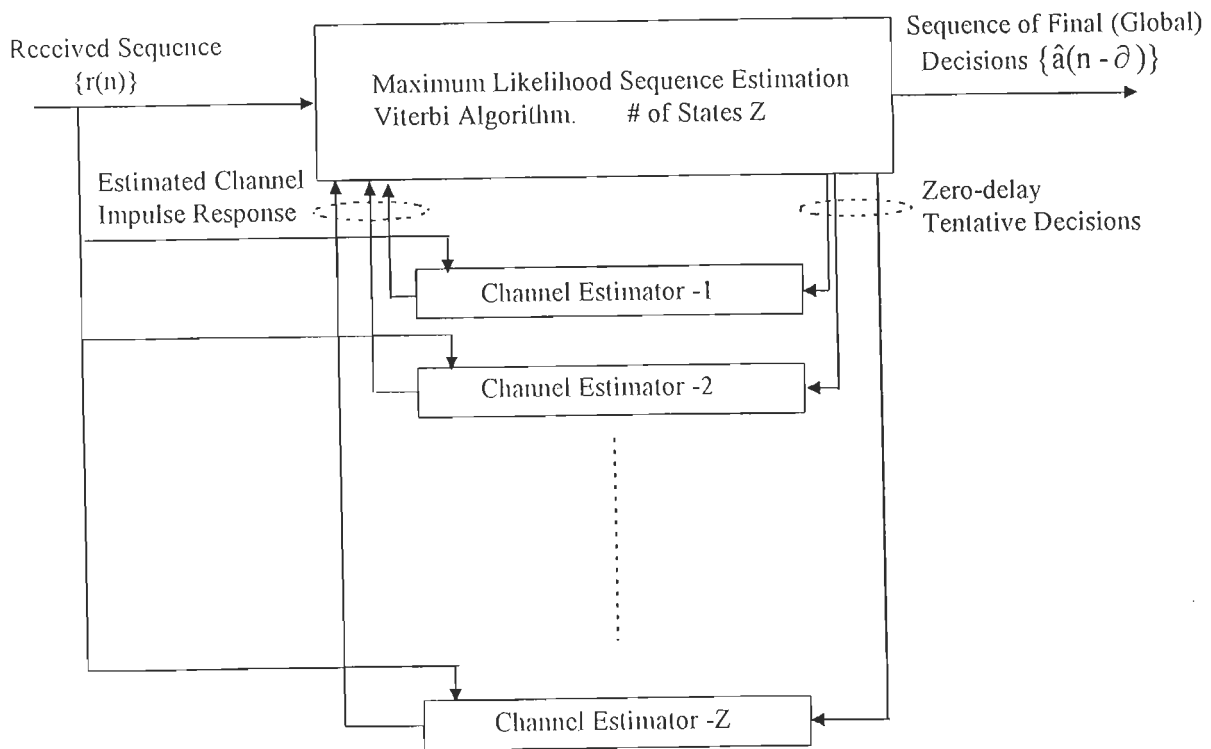


FIG. 6.5 ADAPTIVE MLSE STRUCTURE USING PSP CHANNEL ESTIMATION.

as delay-free channel estimation with zero-delay tentative decisions, Kubo et al. [65] and Seshadri [112] have independently proposed a new channel estimation procedure known as the Respective-state Channel estimation (RCE) [66] or the per-survivor-processing (PSP) channel estimation. This procedure maintains a separate channel estimator for each state of the Viterbi algorithm, as shown in Fig.6.5. The data symbol decision of zero-delay associated with the survivor path leading into the trellis state is used to form the estimator filter output and hence a delay-free updating of the tap-gain coefficients of the corresponding channel estimator of that state. Thus, a set of estimated channel coefficients are maintained per state, per trellis depth. The updating of the per-state channel estimates is accomplished through LMS or RLS adaptation algorithm. The set of channel coefficients so derived for each state, are used in the branch-metric calculation of that state during the next iteration.

This procedure of respective-state channel estimation improves the performance on fast varying ISI channels, due to the delay-free channel estimation. Moreover, it can start-up without the knowledge of a training sequence, meaning that the procedure is well suited for blind equalization [112].

#### **6.4 DECODING OF TCM SIGNALS TRANSMITTED OVER TIME-DISPERSIVE MULTI-PATH FADING CHANNEL USING D-DIVERSITY RECEPTION**

In addition to the use of coded-modulation, the multipath fading can be effectively mitigated through the use of diversity techniques where the receiver is provided with multiple independently faded replicas of the transmitted information symbol. The diversity is effective since the probability of receiving simultaneously two or more independently faded channels with deep fade is very small.

Consider the transmission of TCM signals over D-independently fading channels as shown in Fig.6.6. The system transmits  $m$  information bits  $X_n$  per signaling interval. The TCM encoder produces  $m+1$  coded bits  $Y_n$  which are mapped into a

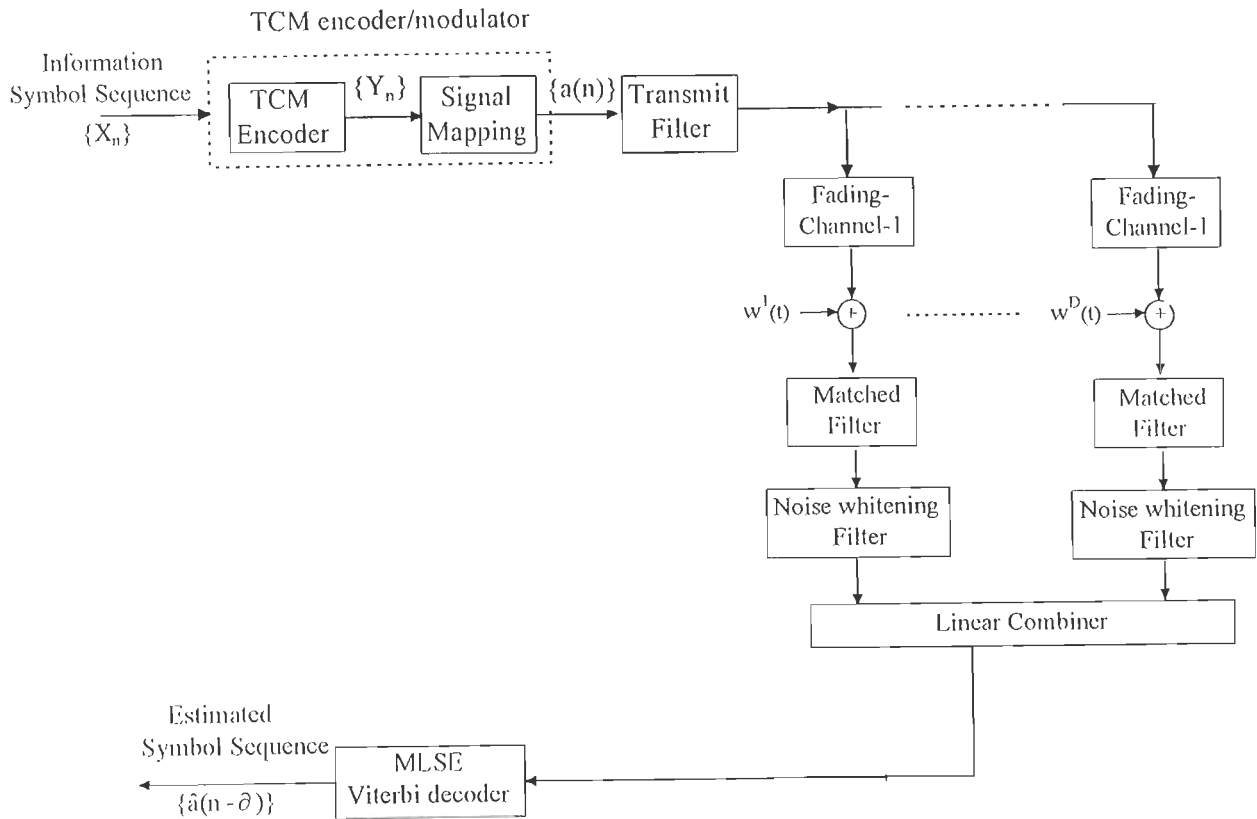


FIG.6.6 TCM DATA TRANSMISSION SYSTEM OVER D-DIVERSITY FADING CHANNEL.

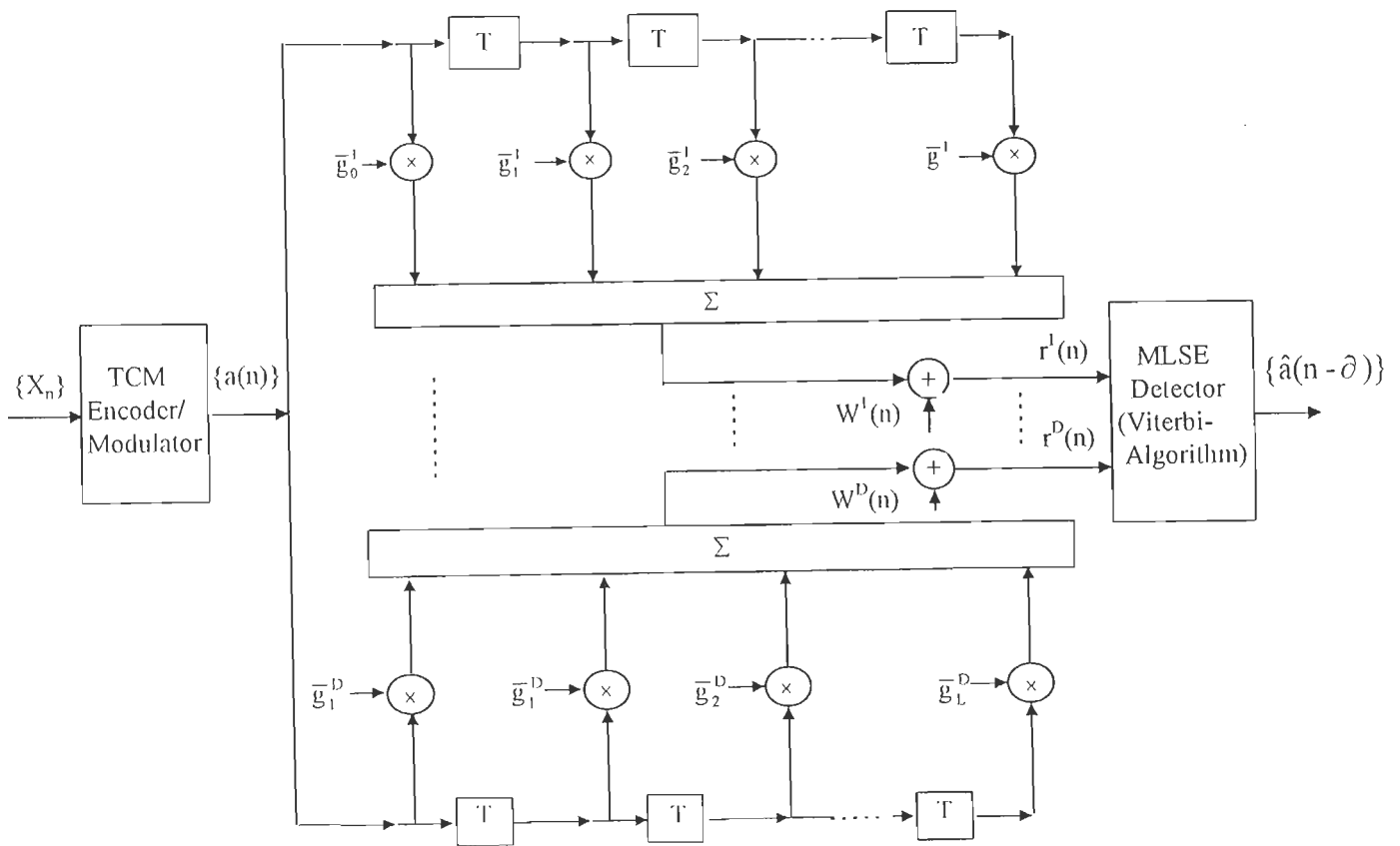


FIG.6.7 DISCRETE-TIME WHITE NOISE CHANNEL MODEL FOR BASEBAND TCM TRANSMISSION OVER D-DIVERSITY FADING CHANNEL.

channel signal  $a(n)$  of the  $2^{m+1}$ -QAM signal constellation, in accordance with the mapping rules of TCM [126].

The receiver observes a combined waveform emerging from  $D$ -independent time-dispersive fading channels, each corrupted with an independent AWGN process  $w_i(t)$ . A matched filter is used to maximize the SNR at the sampling instant and a noise whitening filter may be used to whiten the colored noise at the output of the matched filter for a convenient system modeling.

The equivalent discrete-time white-noise model corresponding to the  $D$ -diversity fading channel is as shown in Fig.6.7 [99, 117, 119]. The tap-gain coefficients  $\{g_i^d(n)\}$  are modeled as independent zero-mean complex-valued Gaussian random processes with variances  $P_i^d = (1/2) \cdot E[|g_i^d(n)|^2]$  in each dimension. The sampled value of the complex signal received on the  $d^{\text{th}}$  diversity branch at time instant  $n$  is then given by

$$r^d(n) = \sum_{i=0}^L g_i^d(n) \cdot a(n-i) + v^d(n) \quad \dots(6.21)$$

where  $L$  is the memory length of the time-dispersive fading channel and  $v^d(n)$  is the sampled value of the i.i.d zero mean complex AWGN process on the  $d^{\text{th}}$  diversity branch.

Following the analysis as given in section 3.3, we can represent the discrete-time model of Fig.6.7 by a combined finite-state machine or equivalently by a combined ISI-code trellis whose states are given by

$$\mu_n = (\alpha_n; a(n-1), a(n-2), \dots, a(n-L)) \quad \dots(6.22)$$

with  $\alpha_n$  and  $\{a(n-i)\}$  as have been defined earlier in section 3.3. It may be recalled that for a TCM encoder with  $N_s$ -states and a signal constellation of  $M=2^{m+1}$  points, the number of states in the combined ISI-code trellis is  $N_s \cdot (M/2)^L$  states with  $L$  representing the memory length of the time-dispersive fading channel.



Let  $R(i) \equiv (r^1(i), r^2(i), \dots, r^D(i))$  represent the linearly combined waveform of the sampled received signals over  $D$ -diversity branches at the sampling instant  $i$ . After the reception of the sequence  $\{R(i)\}_{i=1}^n$ , the combined MLSE receiver makes a decision in favour of the sequence  $\{a(i)\}_{i=1}^n$ , which maximizes the joint conditional probability density [117],

$$P\{R(n), R(n-1), \dots, R(1) / a(n), a(n-1), \dots, a(1)\} \quad \dots(6.23)$$

or equivalently, the logarithm of this function,

$$\ln[P\{R(n), R(n-1), \dots, R(1) / a(n), a(n-1), \dots, a(1)\}] \quad \dots(6.24)$$

Since the noise samples  $\{v^d(i)\}$  are independent and  $R(i)$  depends upon the most recent  $L$  transmitted symbols, we can write

$$\begin{aligned} & \ln[P\{R(n), R(n-1), \dots, R(1) / a(n), a(n-1), \dots, a(1)\}] \\ &= \ln[P\{R(n-1), R(n-2), \dots, R(1) / a(n-1), a(n-2), \dots, a(1)\}] \\ & \quad + \ln[P\{R(n) / a(n), a(n-1), \dots, a(n-L)\}] \quad \dots(6.25) \end{aligned}$$

where  $a(j) = 0$  for  $j \leq 0$ . Assuming that the first term has been computed earlier, the second term called the branch metric needs to be computed for each incoming signal waveform  $R(n)$ . Using the discrete-time white-noise model,

$$\ln[P\{R(n) / a(n), a(n-1), \dots, a(n-L)\}]$$

is equivalent to

$$- \sum_{d=1}^D \left| r^d(n) - \sum_{i=0}^L g_i^d(n) \cdot a(n-i) \right|^2$$

Thus, the branch metric which minimizes the path metric is given by

$$\text{Branch metric} = \sum_{d=1}^D \left| r^d(n) - \sum_{i=0}^L g_i^d(n) \cdot a(n-1) \right|^2 \quad \dots(6.26)$$

Hence, the decoding is accomplished by the Viterbi algorithm operating over the combined ISI-Code trellis which computes recursively the survivor path metric as given by

$$\tilde{M}_n(\mu_{n+1}) = \min_{\{\mu_n\}} \rightarrow \mu_{n+1} \left\{ \tilde{M}_{n-1}(\mu_n) + \sum_{d=1}^D |r^d(n) - \sum_{i=0}^L g_i^d(n) \cdot a(n-i)|^2 \right\} \dots(6.27)$$

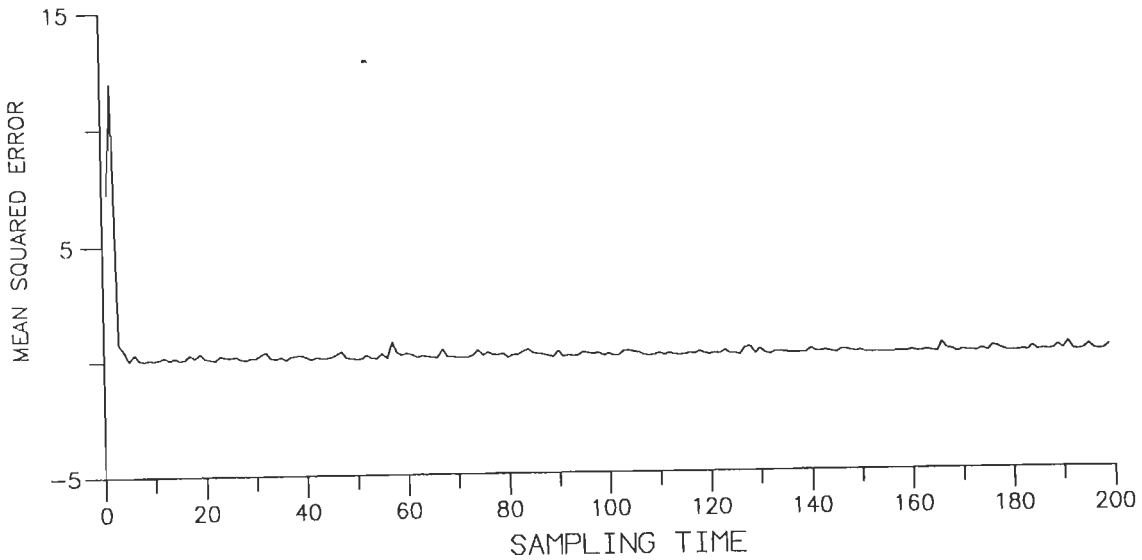
where the minimization is performed over all the trellis branch transitions originating from states  $\{\mu_n\}$  and merging into the successor state  $\mu_{n+1}$ . The terms  $\{a(n-i)\}$  for  $i=1,2,\dots,L$  take into account the ISI due to the previous  $L$  symbols.

Since the state complexity of the combined ISI-Code trellis makes its practical implementation almost prohibitive even for moderate ISI, several reduced complexity sub-optimum receiver structures, as discussed earlier, have been considered for the study of D-diversity reception. The error performance of the various D-diversity receiver structures for TCM decoding under multi-path fading environment have been studied for different orders of diversity  $D$ , through simulation.

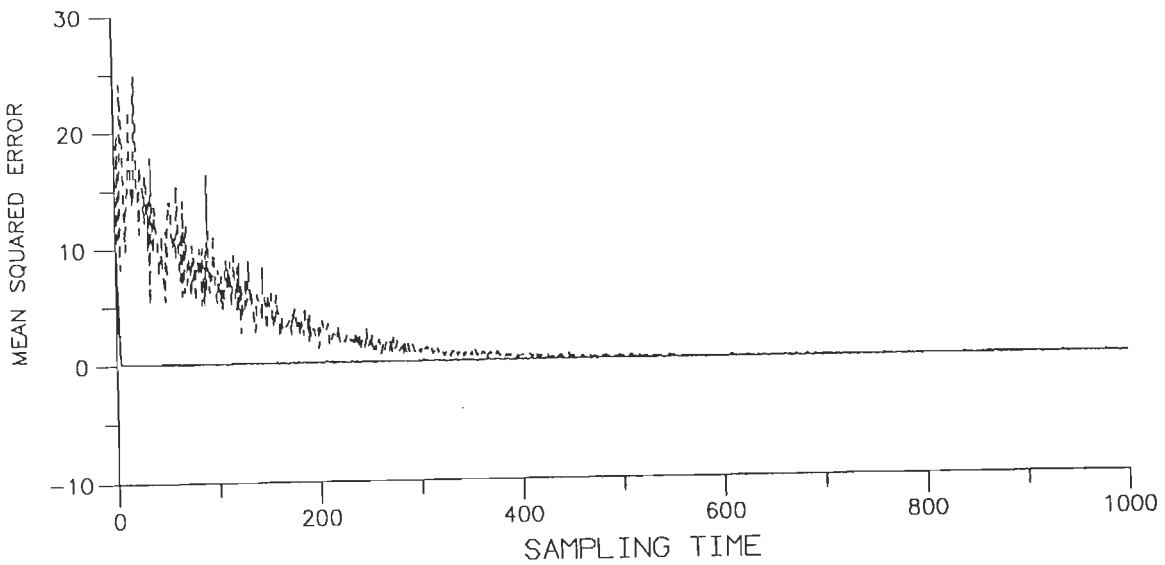
## 6.5 RESULTS AND DISCUSSION

In this section, we present the performance characteristics of the various adaptive receiver structures, which are employed for the decoding of trellis-coded QAM signals transmitted over the time-dispersive fading channels. In the study, we consider the use of channel estimators which employ delayed-decision updating as well as delay-free updating, of the channel coefficients. We also consider the use of D-diversity reception in order to overcome the effect of severe fading present on the multi-path fading channels.

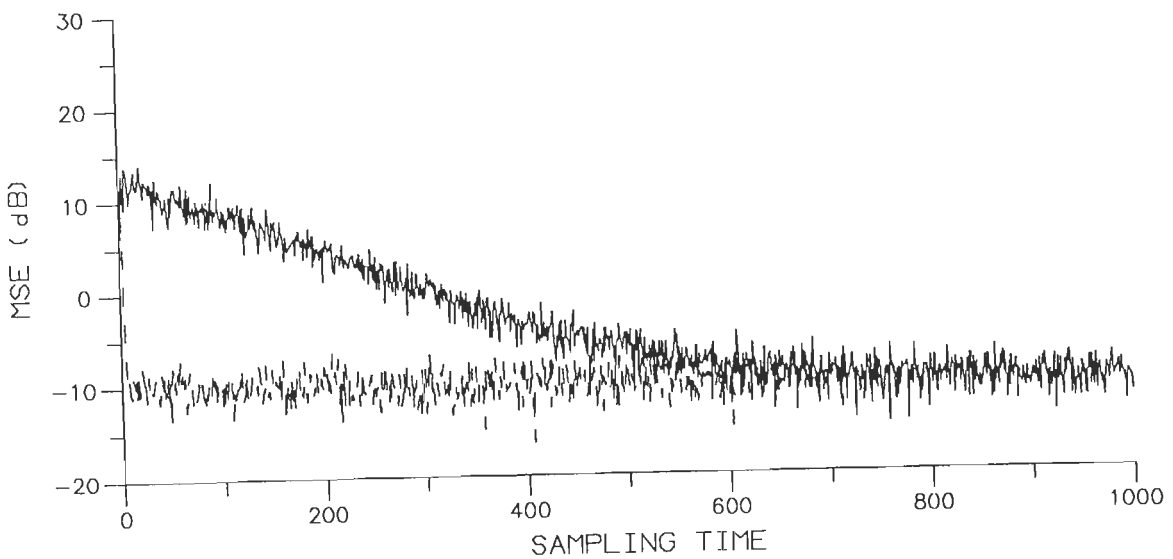
For the study, we consider the baseband TCM data transmission system as shown earlier in Fig.6.1. The system is implemented in the same manners as in the case of the time-invariant system, discussed earlier in sections 3.6 and 5.5, with the exception that the channel is modeled as a finite duration tapped-delay line



(a) CONVERGENCE CHARACTERISTICS THE RLS CHANNEL ESTIMATOR.



(b) CONVERGENCE CHARACTERISTICS OF LMS AND RLS ESTIMATORS



(c) CONVERGENCE CHARACTERISTICS OF LMS AND RLS ESTIMATORS

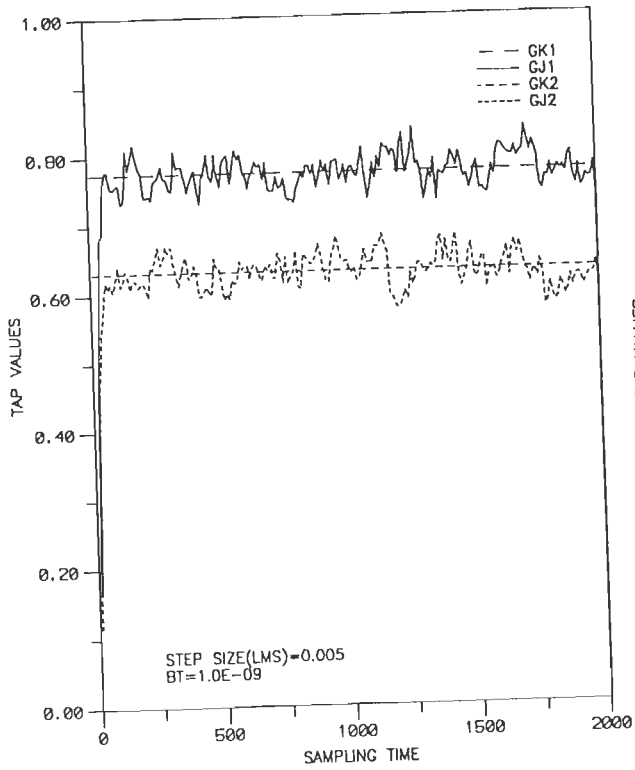
FIG.6.8 CONVERGENCE CHARACTERISTICS OF THE LMS AND RLS CHANNEL ESTIMATORS ON A TIME-DISPERSIVE FADING CHANNEL AT  $BT=10^{-6}$ .

filter with randomly time-varying tap coefficients  $g_k(n)$ , as shown in Fig.6.2. As discussed earlier, the tap gain coefficient  $g_k(n)$  are generated as complex-valued Gaussian random variables having zero-mean and variance  $P_k$  in each dimension as defined by (6.2). For the simulation of time variant tap coefficients  $g_k(n)$ , we make use of the relation (6.3). The power impulse response of the two-tap fading dispersive channel considered in the simulation is assumed to be  $P_1=0.6$  and  $P_2=0.4$ . In order to compute the mean square error of the channel estimators and the error performance of the adaptive receiver structures, we have considered the averaging over 10 independent simulation runs where each run is of size 10,000 data symbols.

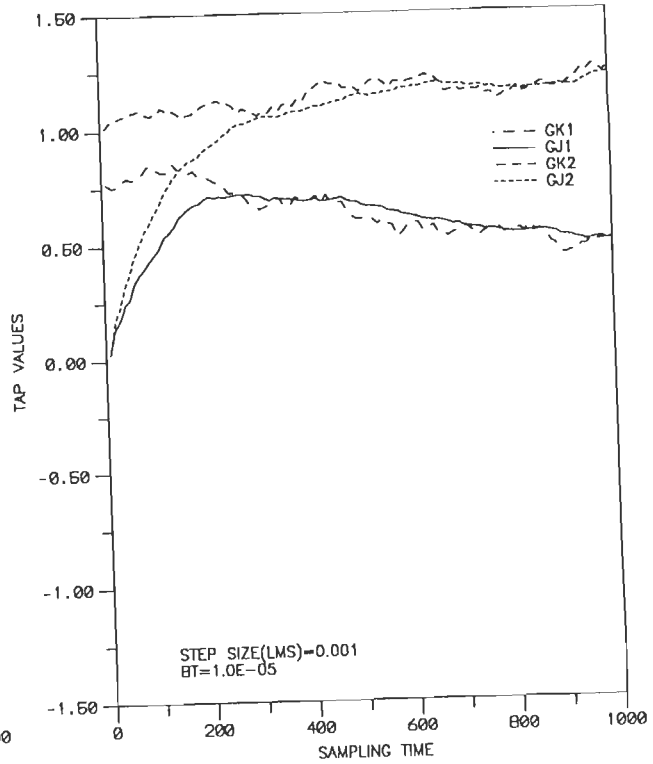
The performance characteristics of the LMS and RLS channel estimator for fading channel have been studied through simulation. In Fig.6.8(a)–(b), we have shown the typical convergence characteristics of the RLS channel estimator at a fade rate of  $BT=10^{-6}$  by considering the absolute value of the mean squared error, while in Fig.6.8(b) we have shown the convergence characteristics of both RLS and LMS channel estimators for the same situation. Fig.6.8(c) shows the convergence characteristics of both LMS and RLS channel estimators, where the mean squared error is expressed in decibels. From Fig.6.8, we may note that the RLS algorithm exhibits much faster convergence than the LMS algorithm.

Fig.6.9 shows the tracking characteristics of both the LMS and RLS channel estimators. In the figure GK1, GK2 represent the random complex-valued channel coefficients, while GJ1 and GJ2 represent respectively the estimated channel coefficients. LMS and RLS exhibit almost the similar tracking performance for the fading rates considered.

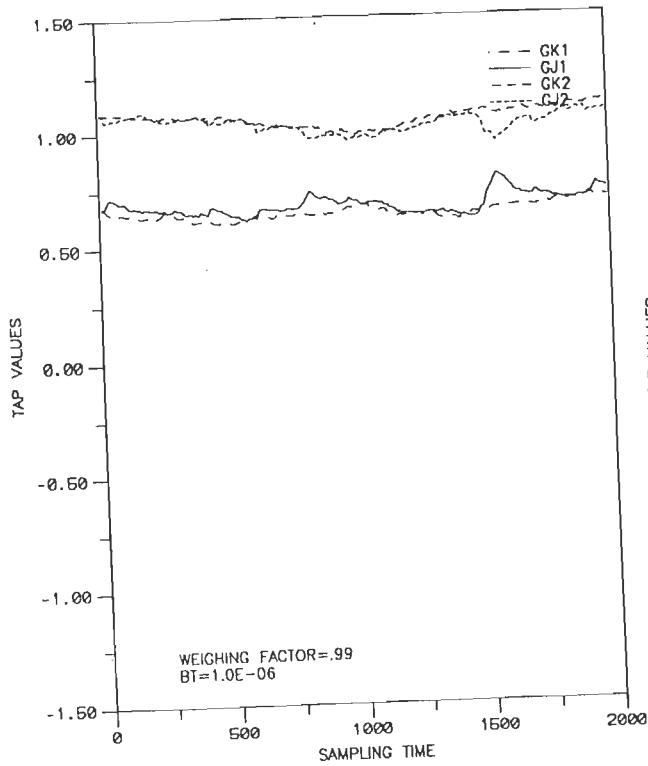
We have considered the use of the conventional LMS channel estimator, that makes use of the delayed decision data estimates from the Viterbi decoder, as well as the LMS channel estimator based on the per-survivor processing (PSP). The two channel estimators are correspondingly referred to as 'Con.LMS' and 'PSP LMS' in the legend of the Fig.6.10. The Fig.6.10 shows the error performance comparison of



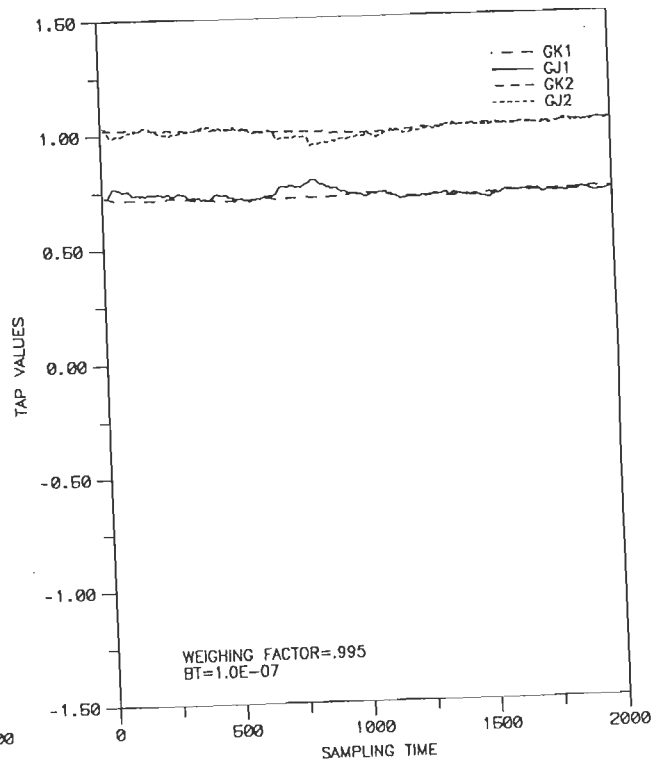
(a) TRACKING CHARACTERISTICS OF LMS CHANNEL ESTIMATOR



(b) TRACKING CHARACTERISTICS OF LMS CHANNEL ESTIMATOR



(c) TRACKING CHARACTERISTICS OF RLS CHANNEL ESTIMATOR



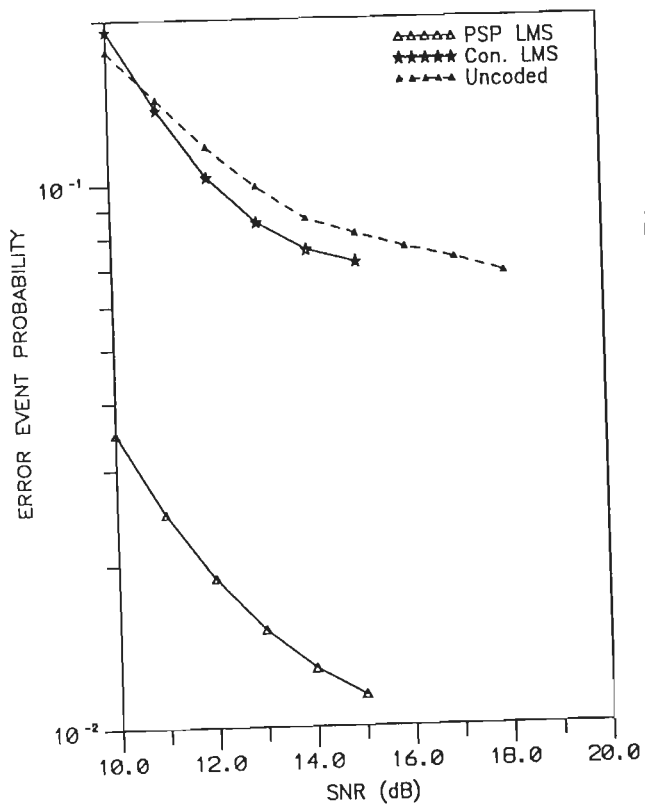
(d) TRACKING CHARACTERISTICS OF RLS CHANNEL ESTIMATOR

FIG.8.9 TRACKING CHARACTERISTICS OF RLS AND LMS CHANNEL ESTIMATORS.

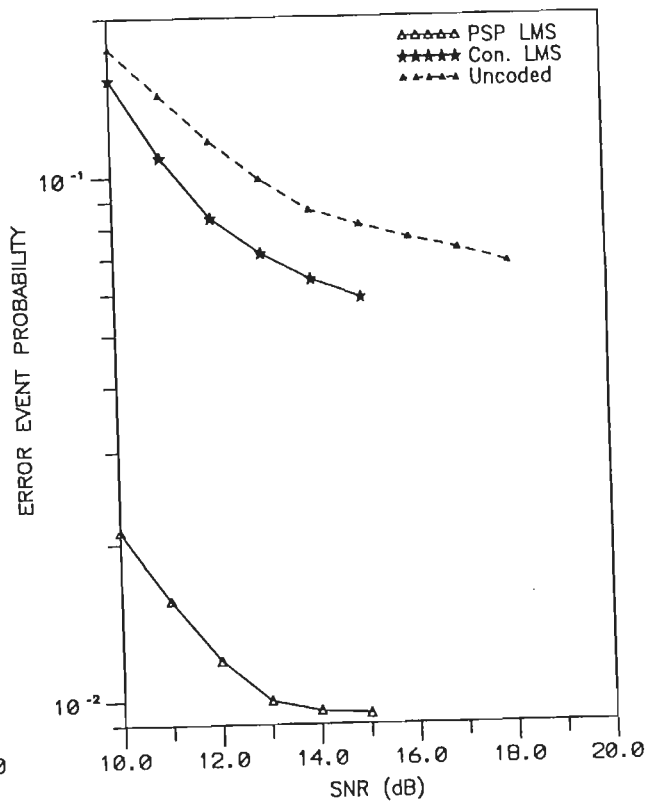
the various adaptive receiver structures using 'Con.LMS' and 'PSP LMS'. For all cases considered the fade rate is assumed to  $BT=10^{-6}$ . As can be noted from the figure, there is an improvement in the probability of error event by a factor of 10 with the use of the PSP channel estimators (at lower SNR) relative to the use of conventional LMS channel estimator. From Fig.6.10(c), we observe that there is an improvement in the error performance of the RSSE-II structure using the PSP estimator by about 1 dB at  $P_e \geq 10^{-3}$ , relative to the use of the conventional LMS channel estimator. The difference in the error performance of the coded adaptive receiver structure is large at lower SNR, while it decreases at higher SNR, as is to be expected. Henceforth in our further work, we consider only the use of the LMS channel estimator based on the PSP technique.

We next consider the error performance characteristics of a 4-state 16-QAM TCM signal transmitted over a time dispersive multipath fading channel for three different fade rates and different orders of diversity  $D$ . The fade rate employed in the study, are  $BT=10^{-5}$ ,  $10^{-6}$  and  $10^{-7}$ . Fig.6.11(a)-(c) show the performance of the adaptive PDFD structure for different fade rates at a given diversity  $D$ , for the transmission of 4-state 16-QAM TCM signals over fading dispersive channel. From Fig.6.11(a)-(c), we note that the effects of fading rate has less influence on the error performance for  $D=2$  and  $D=3$ . Fig.6.11(a)-(e) show the error performance of the PDFD structure at a given fade rate for different orders of diversity  $D$ . We may note that at a given fade rate, the performance improves significantly with the use of diversity  $D=2$  and  $D=3$ . For diversity-order  $D=2$ , the gain in performance for the PDFD structure is nearly 3 dB at  $P_e=10^{-3}$  relative to the uncoded reference system. With the use of diversity  $D=3$ , we observe that the corresponding gain is about 3.5 dB at  $P_e \geq 10^{-4}$  relative to the uncoded reference system.

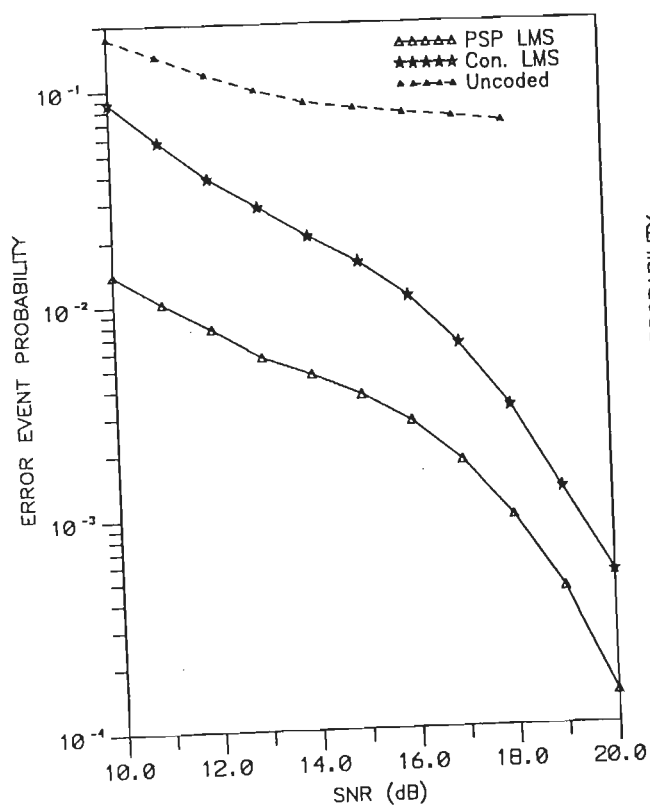
The error performance of the 8-state adaptive RSSE structure RSSE-I, as discussed in section 5.3.1, which is employed for the decoding of 4-state 16-QAM TCM signals transmitted over the time dispersive channel is shown in Fig.6.12. The



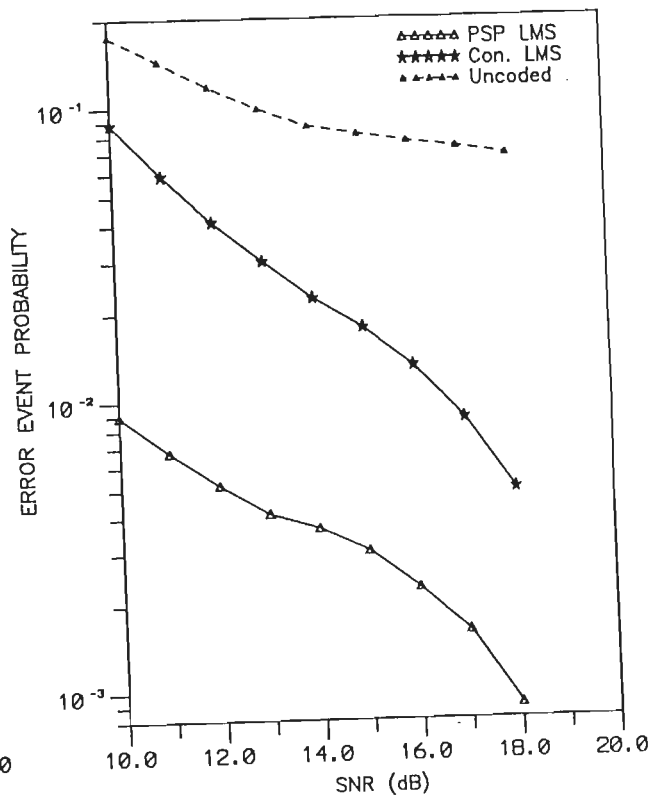
(a) PDFD STRUCTURE ; FADE RATE  $BT=10^{-6}$ .



(b) KFE-MLSE STRUCTURE; FADE RATE  $BT=10^{-6}$ .

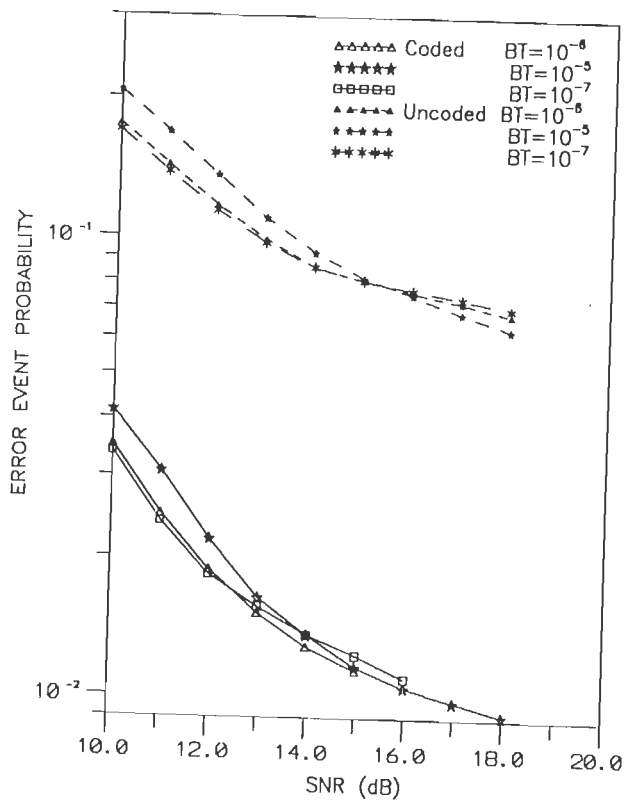


(c) RSSE-II STRUCTURE ; FADE RATE  $BT=10^{-6}$ .

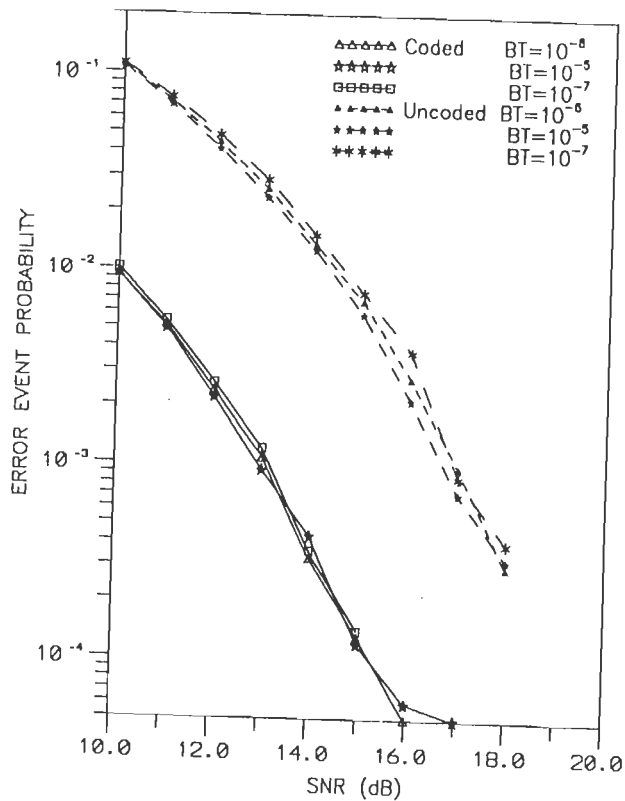


(d) RSSE-IV STRUCTURE ; FADE RATE  $BT=10^{-6}$ .

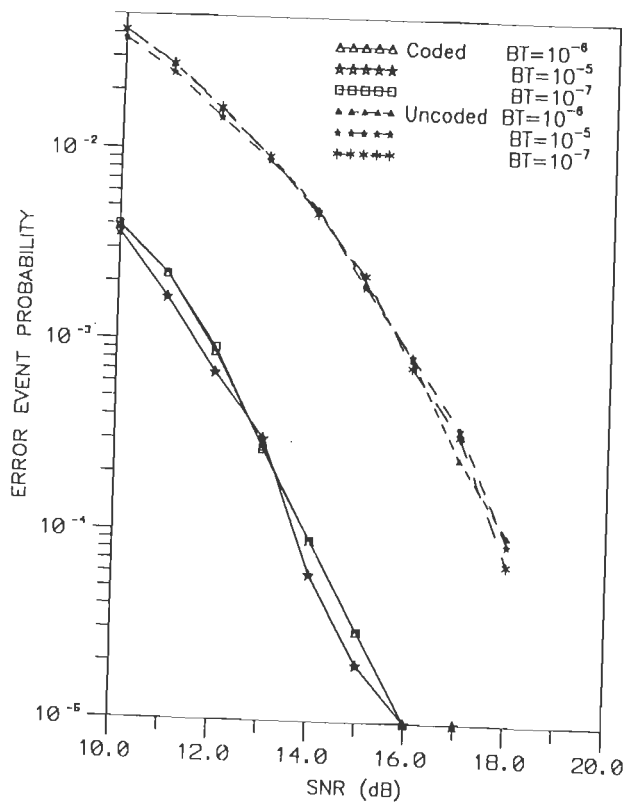
FIG.6.10 ERROR PERFORMANCE COMPARISON OF THE VARIOUS RECEIVER STRUCTURES USING CONVENTIONAL LMS CHANNEL ESTIMATOR AND THE PSP CHANNEL ESTIMATOR



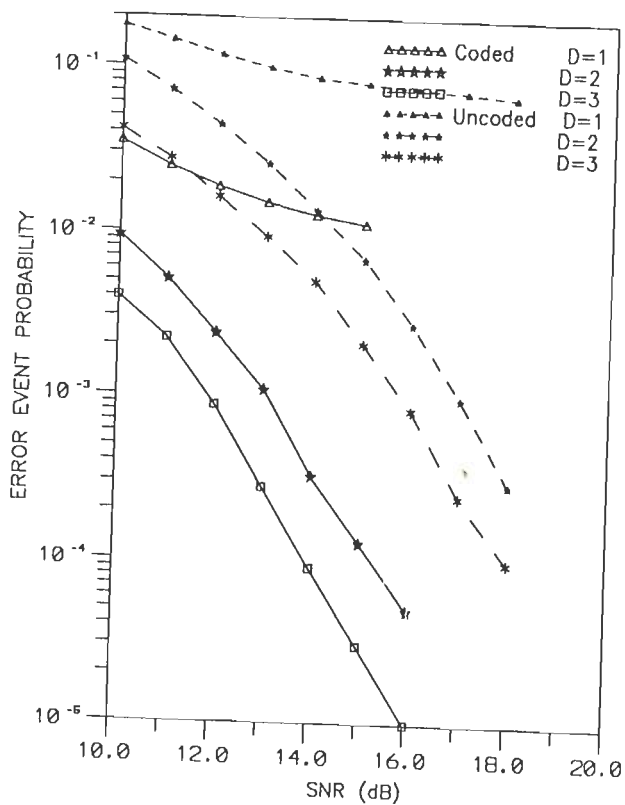
(a) PDFD STRUCTURE ; DIVERSITY  $D=1$ .



(b) PDFD STRUCTURE ; DIVERSITY  $D=2$ .



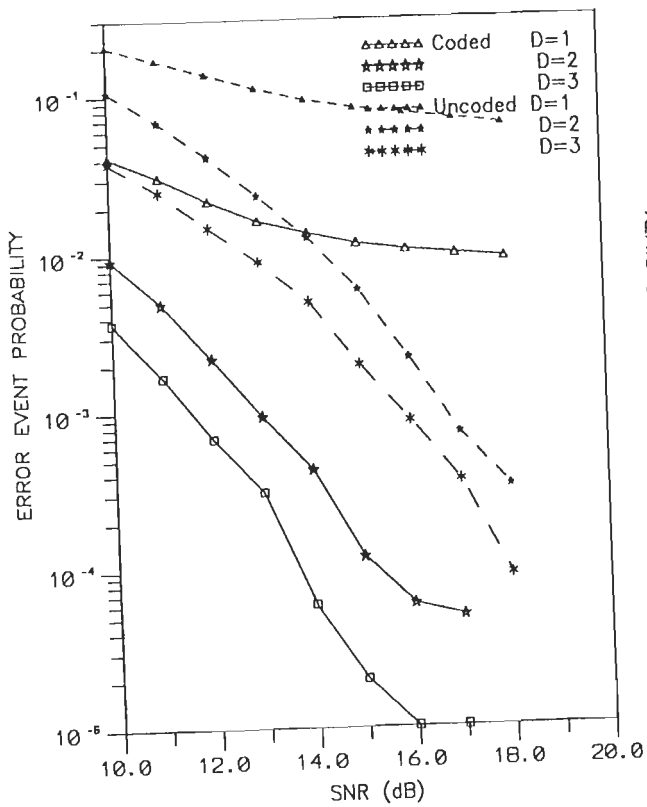
(c) PDFD STRUCTURE ; DIVERSITY  $D=3$ .



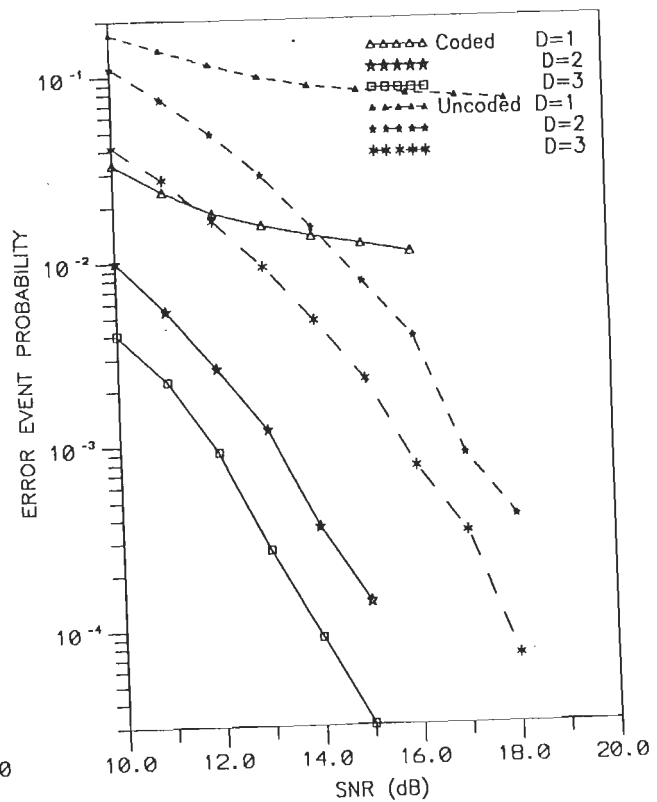
(d) PDFD STRUCTURE ; FADE RATE  $BT=10^{-6}$ .

FIG. 6.11 (CONTINUED)



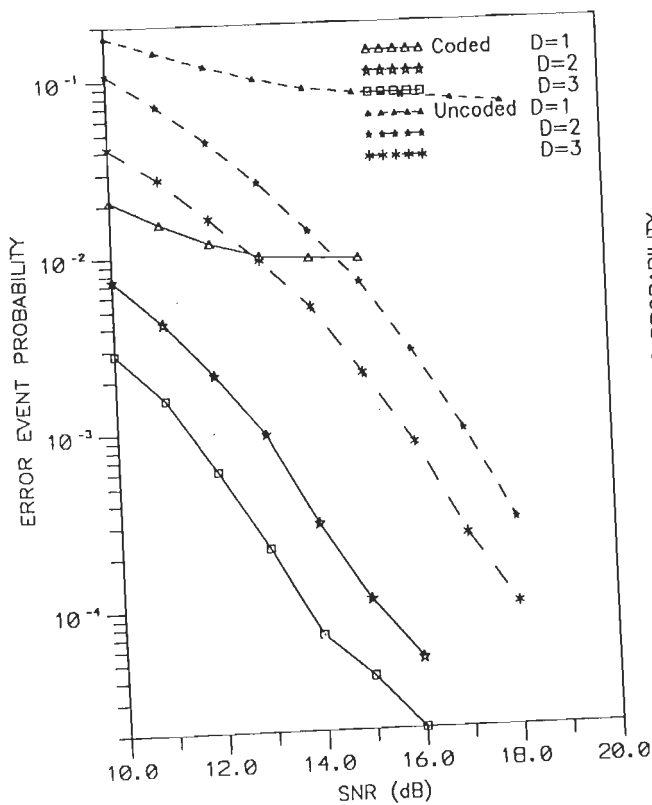


(e) PDFD STRUCTURE ; FADE RATE  $BT=10^{-5}$ .

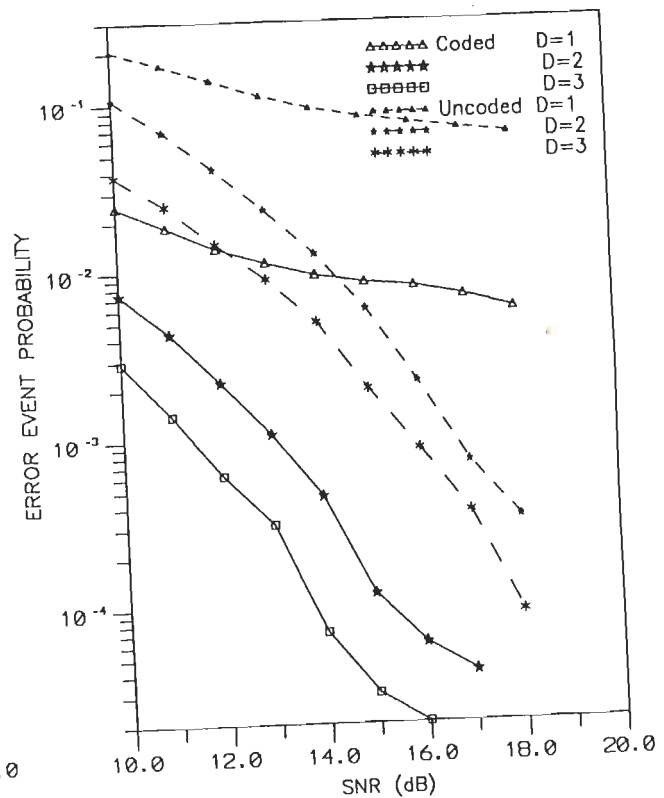


(f) PDFD STRUCTURE ; FADE RATE  $BT=10^{-7}$ .

FIG.6.11 ERROR PERFORMANCE OF THE PDFD RECEIVER STRUCTURES EMPLOYING D-DIVERSITY RECEPTION FOR THE DECODING OF 4-STATE 16-QAM TCM SIGNALS TRANSMITTED OVER MULTI-PATH(TIME-DISPERSIVE) FADING CHANNEL.



(a) RSSE-I STRUCTURE ; FADE RATE  $BT=10^{-6}$ .



(b) RSSE-I STRUCTURE ; FADE RATE  $BT=10^{-5}$ .

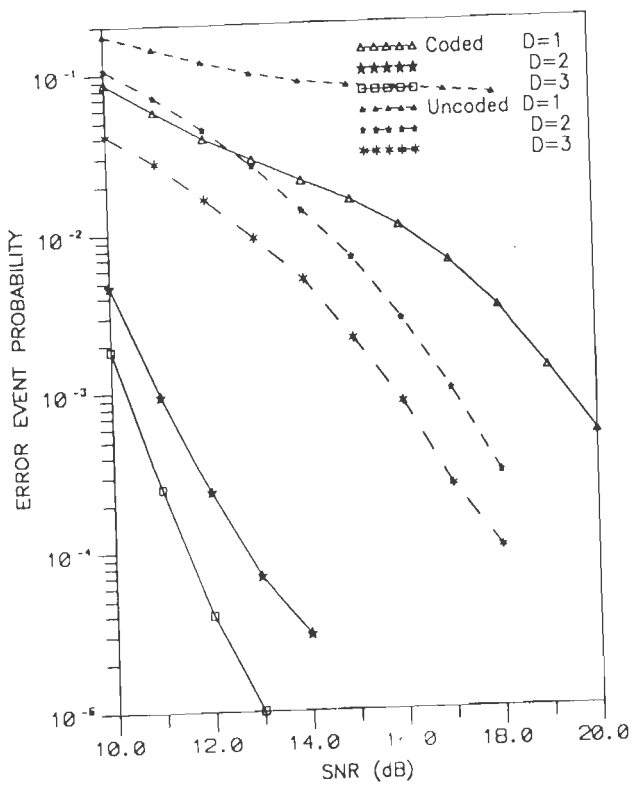
FIG.6.12 ERROR PERFORMANCE OF THE RSSE-I RECEIVER STRUCTURE EMPLOYING D-DIVERSITY RECEPTION FOR THE DECODING OF 4-STATE 16-QAM TCM SIGNALS TRANSMITTED OVER MULTI-PATH(TIME-DISPERSIVE) FADING CHANNEL.

figure shows the performance of the adaptive RSSE-I structure for different orders of diversity  $D$ , at a given fade rate. For the adaptive RSSE-I structure considered, it shows an improvement in performance which is about 3.5 dB and 4.0 dB relative to the corresponding uncoded reference systems, at  $D=2$  and  $D=3$  respectively. We note that as the fade rate increases (i.e. with  $10^{-5}$ ), the gain in performance decreases by about 0.5–0.75 dB.

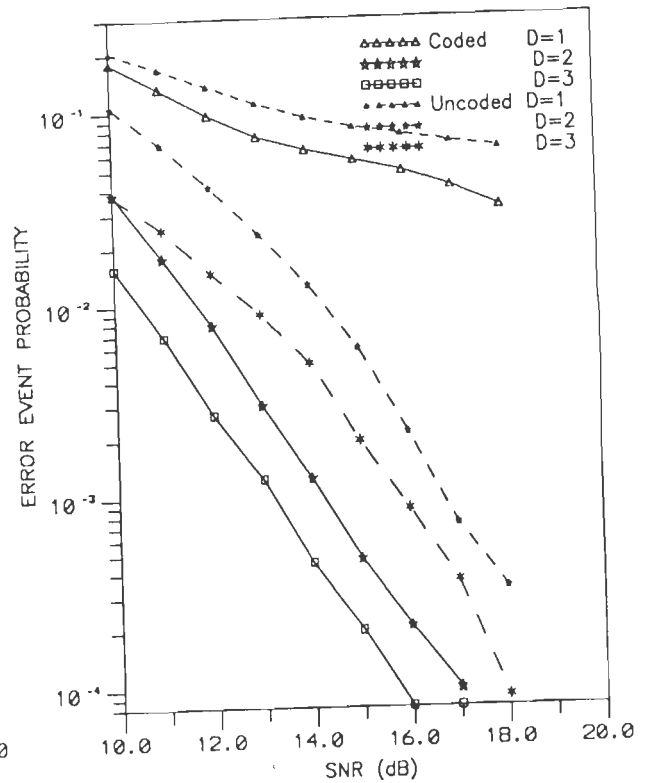
Similarly Fig.6.13(a) shows the error performance characteristics of the adaptive KFE-MLSE structure employing the PSP LMS channel estimator for different values of  $D$  at a fade rate of  $BT=10^{-6}$ , while Fig.6.13(b) shows the results corresponding to fade rate  $BT=10^{-5}$ . From Fig.6.13(a) we may note that, there is an improvement in the performance by about 5.0 dB relative to the uncoded reference with the use of  $D=2$  at  $BT=10^{-6}$  and  $P_e=10^{-3}$ , while the improvement is about 6 dB with  $D=3$  at  $P_e=10^{-4}$  for the same fade rate. As the fade rate is increased to  $BT=10^{-5}$ , the gain in performance decreases as is evident from Fig.6.13(b). We note from Fig.6.13(b) that the improvement in the error performance is about 2.5 dB relative to the uncoded reference, with the use of  $D=2$  and  $D=3$  at  $P_e=10^{-3}$ .

Fig.6.14 gives correspondingly the error performance characteristics of the 16-State and 32-State RSSE structures, RSSE-II and RSSE-IV of section 5.3.2 and 5.3.4. With the RSSE-II structure the performance improvement is of the order of about 6.5 dB at  $D=2$  at  $P_e=10^{-3}$ , while it is about 7.0 dB with  $D=3$  at  $P_e=10^{-4}$ . It can be noted that the performance characteristics of the 32-State RSSE structure RSSE-IV is shown only for  $D=1$  and  $D=2$ . The characteristics show an improvement of the order of about 7.0 dB at  $D=2$  relative to the uncoded reference structure.

In the simulation study presented we have considered the use of the TCM codes designed for AWGN channels, for transmission over fading dispersive channels. From the study we observe that the PSP channel estimators give a better performance over the conventional channel estimators. The improvement in performance of the PSP channel estimators is significantly high at lower SNR relative to the use of conventional channel estimators. From the study we observe that the use of the 16-

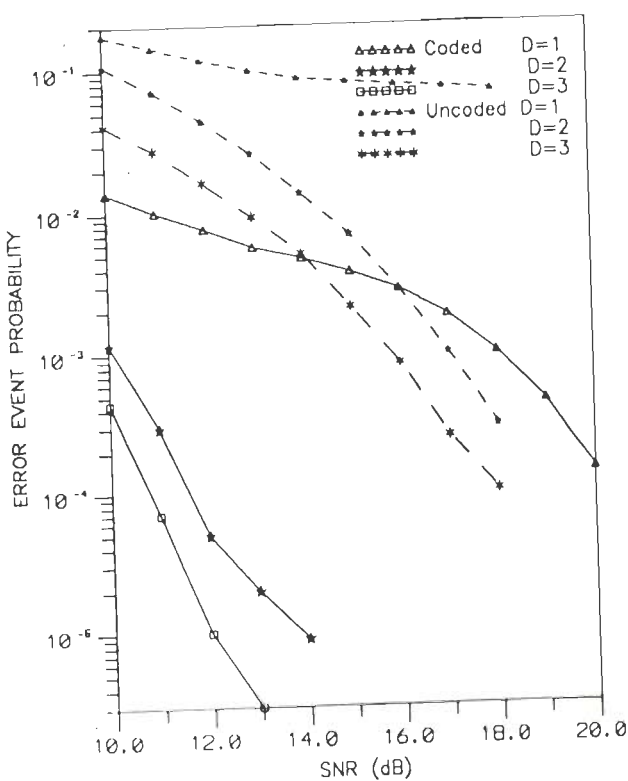


(a) KFE-MLSE STRUCTURE ; FADE RATE  $BT=10^{-6}$ .

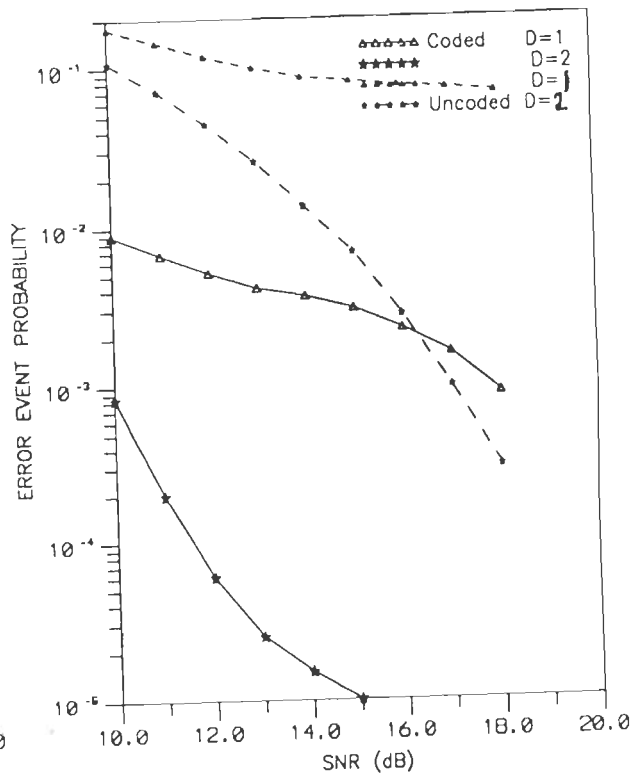


(b) KFE-MLSE STRUCTURE ; FADE RATE  $BT=10^{-5}$ .

FIG.6.13 ERROR PERFORMANCE OF THE KFE-MLSE RECEIVER STRUCTURES USING D-DIVERSITY RECEPTION FOR THE DECODING OF 4-STATE 16-QAM TCM SIGNALS TRANSMITTED OVER MULTI-PATH(TIME-DISPERSIVE) FADING CHANNEL.



(a) RSSE-II STRUCTURE ; FADE RATE  $BT=10^{-6}$ .



(b) RSSE-IV STRUCTURE ; FADE RATE  $BT=10^{-6}$ .

FIG.6.14 ERROR PERFORMANCE OF THE VARIOUS RECEIVER STRUCTURES USING D-DIVERSITY RECEPTION FOR THE DECODING 16-QAM TCM SIGNALS TRANSMITTED OVER MULTI-PATH(TIME-DISPERSIVE) FADING CHANNEL.

state and 32-state adaptive RSSE structures RSSE-I and RSSE-II yields significant improvement as compared to the other sub-optimum structures over fading dispersive channels. In particular RSSE-IV yields the best performance, but at the cost of moderate increase in computational complexity as compared to the other structures considered in the study. Further, we observe that there is a significant improvement in the performance with the use of diversity.

## CONCLUSIONS

---

In this chapter, we conclude the thesis by summarizing some of the important results of the present work and also suggest some problems for further investigation.

We have first presented a study of the TCM schemes for applications on AWGN channel. The design of several trellis-coded QAM schemes have been presented. The performance evaluation of the TCM schemes on AWGN channel has been discussed and a new method for computing the distance spectrum of the TCM codes has been presented. Using this method, the upper and lower bounds on the error event probability have been evaluated. The performance bounds so derived have been compared with the simulation results.

From the error performance characteristics of the various TCM schemes, we observe that the 4-state TCM schemes achieve a gain of nearly 3 dB relative to an uncoded reference system, without compromising the spectral efficiency or power efficiency. With 8-state and 16-state TCM schemes the respective gains are approximately 4 dB and 5 dB at  $P_e \geq 10^{-5}$ . Also, we find that the upper and lower bounds on the error event probability, obtained through the use of the distance spectrum computing algorithm, are quite tight in the sense that the simulation results lie well within the computed bounds. Therefore, the proposed distance spectrum computing algorithm is quite effective in the evaluation of the performance bounds of all Ungerboeck TCM codes on AWGN channels.

We have next considered the application of TCM schemes for data transmission over time-dispersive ISI channels. The TCM scheme in combination with the MLSE equalizer promises to provide the optimum performance, which is very close to ISI-free performance. The resulting combined MLSE receiver structure, although optimum, has a computational complexity that grows exponentially with the ISI memory length. In the present work, we have considered the design of several combined ISI-code trellis structures for the optimum detection of the trellis-coded QAM signals in the presence of ISI and AWGN. The error performance of the above receiver structures has been obtained for a wide variety of ISI channels, through evaluation of bounds and simulation. From the simulation results, we find that the coded combined MLSE structures does achieve a gain of about 2-3 dB relative to the uncoded MLSE structure over ISI channels, for the same data rate, bandwidth and signal energy. We also observe that the upper and lower bounds, which are computed by the new procedure that makes use of the error sequence of the basic TCM encoder and the discrete channel impulse response, do agree with the simulation results. Hence, the proposed method is quite effective in evaluating the performance bounds of the combined ISI-code receiver structures.

The fact that inspite of its optimum performance the combined MLSE structure becomes too impractical, keeps open the problem of search for a reduced complexity structure which can be used for the detection of trellis-coded QAM signals transmitted over ISI channels. We have presented a reduced complexity KFE-MLSE structure for the sub-optimum detection of trellis-coded QAM signals over ISI channels. From the error performance characteristics, the KFE-MLSE structures based on 4-state TCM scheme, achieve a significant coding gain of the order of 2-2.5 dB relative to the uncoded KFE reference system. Higher coding gains in the range of 3-4 dB are possible with the use of KFE-MLSE structures which employ 8-state or 16-state TCM schemes. We have also presented a method for the computation of the performance bounds for the KFE-MLSE structures, (through the use of spectral factorization technique and innovation representation) by finding the

combined impulse response and the overall noise variance. Using this approach estimates of the upper and lower bounds on the error event probability have been computed. For a wide variety of ISI channels considered, we find that the simulation result is confined within the computed upper and lower bounds. The proposed KFE-MLSE structure therefore is analyzable and is a practically feasible system for the detection of trellis-coded QAM signals over ISI channels of large memory length, although its performance is sub-optimum when compared with that of the combined MLSE receiver structure.

We have next considered a study of the reduced complexity receiver structures which incorporate the technique of channel truncation and the set-partitioning ideas inherent in the TCM design. The performance of these truncated combined MLSE structures and reduced state estimates (RSSE and PDFD) have been determined for a wide variety of ISI channels through simulation. The results indicate that the truncated combined MSLE structure achieves performance which is close to that of the combined MLSE structure (for truncation length  $J \rightarrow L$ ). With RSSE and PDFD receiver structures, we find a drop in the performance gain relative to the truncated MLSE version. Relative to the KFE-MLSE structure, these reduced state techniques show an improved performance (with a gain in the range of 1.0–1.5 dB), but at the cost of increased complexity.

We have finally presented a study of trellis-coded QAM on fading channels. A tapped delay line model is used for the simulation of random time-varying channel coefficients. The performance of the receiver structures, considered earlier, have been obtained through simulation for different fade rates. Since the channel is unknown and time-varying, the channel estimators have been implemented to estimate the tap-gain coefficients. The channel tracking characteristics have been studied through the use of the LMS and the RLS algorithms. To circumvent the problem of decision delay (inherent of the Viterbi algorithm) for the tracking of rapidly time-varying fading channel, a recently proposed PSP channel estimator has been employed. This new procedure of channel estimation shows improved performance over

the conventional channel estimators, especially when the number of trellis states is large.

To overcome the effects of severe fading, a consequence of multipath fading channels, the D-diversity receiver structures have been employed. Although there is an increase in the complexity of the receiver structure we find a significant improvement in the performance for orders of diversity,  $D \geq 2$ .

### SUGGESTIONS FOR FURTHER WORK

In the present work, we have proposed the KFE-MLSE structure, a prefilling technique making use of the Kalman filter, as a physically viable reduced complexity receiver for the decoding of trellis coded QAM signals in the presence of ISI and AWGN. In the present scheme the Kalman filter is used for the channel equalization. The Kalman filter can be used for both channel estimation and channel equalization [68, 69]. By incorporating the per-survivor processing (PSP) technique into the Kalman filter, it would be interesting to realize efficient Kalman-based PSP channel estimators that are highly suitable for rapidly time-varying multipath radio channels.

In the present work, we have considered a new method following the approach adopted by Magee and Proakis [79], in order to evaluate the upper and lower bound estimates of the error event probability for the coded combined MLSE receiver structure. This method, which makes use of the error sequence of the basic TCM encoder and the discrete impulse response of the channel, yields reasonably good performance bounds. It would be interesting to extend this approach for the performance evaluation of the trellis-coded RSSE structures. However, it may be noted that the MLSE and RSSE have different error structures, and in RSSE there is error propagation introduced by the algorithm [118]. These factors have to be properly accounted for, in the application of this method.

In recent years, several generalizations of the Viterbi algorithm have appeared in the literature [39, 58, 114, 120], amongst which the List-type Viterbi



decoding is getting much attention. Seshadri and Sundberg have reported in [114] an improvement of the order of 3 dB with the use of List-type Viterbi algorithm over the use of conventional VA. The application of List-type VA to the reduced complexity receiver structures considered in the present work, could be worthwhile and may also result in a further reduction in the computational burden. A further investigation into the various generalizations of the VA for their application to coded modulation schemes is also desirable.

Our work is constrained to the study of two dimensional trellis-coded QAM schemes. In recent years, there is an increased interest in the use of 4-dimensional TCM schemes, particularly in the design of 19.2 Kb/s modems which are employed for the transmission of compressed digital audio/video signals [136]. The present work can be extended to the study of 4-D TCM schemes. As pointed out in [136, 144], the performance on fading channels can be improved with the use of multilevel coding, wherein the block-coded modulation and TCM schemes are used in combination, to achieve higher gain than is possible with the use of a single coded scheme alone. Construction of multidimensional M-ary QAM TCM codes for AWGN and fading channels based on the multilevel approach is another topic for further investigation. A further work in the direction of reduced complexity decoding techniques for multilevel multidimensional TCM schemes for their applications on fading channels could be worth investigating.

# APPENDIX A

## SPECTRAL FACTORIZATION

Consider the problem of obtaining the polynomial  $D(z)$  given  $\gamma(z)$  as

$$\gamma(z) = \sum_{i=-J}^J \gamma_i z^i \quad \dots(A.1)$$

such that

$$\gamma(z) = D(z).D^*(z^{-1}) \quad \dots(A.2)$$

and  $D(z)$  has all its roots outside the unit circle. This is the so called spectral factorization problem [106]. To solve this problem, consider the application of Cholesky factorization algorithm [107, 141] to (A.1), by defining a positive definite Toeplitz matrix  $P_n$  of order  $(n+1)$  by  $(n+1)$  as [83]

$$P_n = \begin{bmatrix} \gamma_0 & \gamma_1 & \dots & \gamma_n \\ \gamma_{-1} & \gamma_0 & \dots & \gamma_{n-1} \\ \vdots & \vdots & \ddots & \vdots \\ \gamma_n & \gamma_{n+1} & \dots & \gamma_0 \end{bmatrix} \quad \dots(A.3)$$

where  $\gamma_n = 0$  for  $|n| \geq J+1$

At any stage  $n$ , the matrix  $P_n$  by a congruent transformation may be written as

$$P_n = F_n B_n F_n^{*T} \quad \dots(A.4)$$

where  $F_n$  is a complex lower triangular matrix defined by

$$F_n = \begin{bmatrix} 1 & & & 0 \\ f_{10} & 1 & & \\ f_{20} & f_{21} & 1 & \\ \vdots & \vdots & \vdots & \vdots \\ f_{n0} & f_{n1} & \dots & 1 \end{bmatrix} \quad \dots(A.5)$$

and  $B_n$  is a positive definite diagonal matrix defined by

$$B_n = \begin{bmatrix} b_{00} & & 0 \\ & b_{11} & \\ 0 & & b_{nn} \end{bmatrix} \quad \dots(A.6)$$

To find the matrices  $F_n$  and  $B_n$  at stage  $n$ , it suffices to find the  $n$ -th row of  $F_n$  and  $n$ -th diagonal element of  $B_n$ . The algorithm to compute these elements at stage  $n$  is given by

$$\sum_{i=0}^j f_{ni} b_{ii} f_{ji}^* = \gamma_{j-n} \quad \text{for } j = 0, 1, \dots, n \quad \dots(A.7)$$

It has been observed that at sufficiently large  $n$ , the elements of the last row of  $F_n$  as well as  $b_{nn}$  converge. The computation experience reveals that convergence occurs within about  $(15+J)$  stages. Their polynomial  $D(z)$  is given by [83],

$$\begin{aligned} D(z) &= \lim_{n \rightarrow \infty} \sqrt{b_{nn}} [1 + f_{n,n-1}^* z + \dots + f_{n,n-J}^* z^J] \\ &= d_0 (1 + d_1 z + d_2 z^2 + \dots + d_J z^J) \quad \dots(A.8) \end{aligned}$$

To illustrate the Cholesky factorization procedure, we consider, the factorization of the polynomial

$$\gamma(z) = \sum_{i=-1}^1 \gamma_i z^i$$

where  $\gamma_{-1} = -(0.85+j0.18)$   $\gamma_0 = 1.7549$   $\gamma_1 = -(0.85-j0.18)$ .

The corresponding matrices  $P_n$ ,  $F_n$ ,  $B_n$  at various stages of  $n$  are given as

$$P_0 = [1.7549] \quad F_0 = [1] \quad B_0 = [1.7549]$$

$$P_1 = \begin{bmatrix} 1.7549 & -(0.85-j0.18) \\ -(0.85+j0.18) & 1.7549 \end{bmatrix} \quad F_1 = \begin{bmatrix} 1 & 0 \\ \frac{-(0.85+j0.18)}{1.7549} & 1 \end{bmatrix}$$

$$B_1 = \begin{bmatrix} 1.7549 & 0 \\ 0 & 1.7549 \end{bmatrix}$$

Continuing the procedure upto  $n=10$ , we get

$$P_{10} = \begin{bmatrix} 1.7549 & -(0.85-j0.18) & 0 & 0 & \dots & 0 \\ -(0.85+j0.18) & 1.7549 & (-0.85-j0.18) & 0 & \dots & 0 \\ 0 & -(0.85+j0.18) & 1.7549 & -(0.85-j0.18) & \dots & 0 \\ 0 & 0 & \dots & 1.7549 & \dots & 0 \\ \vdots & \vdots & \vdots & \vdots & \ddots & \vdots \\ 0 & 0 & \dots & \dots & \dots & 1.7549 \end{bmatrix}$$

Performance the factorization, the matrices  $F_{15}$ ,  $B_{15}$  can be written as

$$F_{10} = \begin{bmatrix} 1 & & & 0 \\ \frac{-(0.85+j0.18)}{1.7549} & 1 & & \\ 0 & \frac{-(0.85+j0.18)}{1.3247} & & \\ \vdots & & \frac{-(0.85+j0.18)}{1.0157} & 1 \\ 0 & & \dots & \dots & 1 \end{bmatrix}$$

and  $B_{10} = \begin{bmatrix} 1.7549 & & & 0 \\ & 1.3247 & & \\ & & & \\ 0 & & 1.0157 & 1.0117 \end{bmatrix}$

Thus the polynomial  $\gamma(z)$  can be factored as

$$\gamma(z) = D(z) D^*(z^{-1})$$

$$\text{where } D(z) = \sqrt{b_{10,10}} [1 + f_{10,9}^* z]$$

$$\text{or } D(z) = 1.0058 [1 - (0.84 - j0.1779)z].$$

## APPENDIX B

### VARIANCE OF ARMA(P,Q) PROCESS

Consider the general form of an autoregressive moving average process ARMA (p,q) for  $q \geq p$  defined by

$$\begin{aligned} W(n) + \phi_1 W(n-1) + \phi_2 W(n-1) + \dots + \phi_p W(n-p) \\ = Q_0 V(n) + Q_1 V(n-1) + Q_2 V(n-2) + \dots + Q_q V(n-q) \end{aligned} \quad \dots(B.1)$$

where  $V(n)$  is a white noise input process that results in a colored output process  $W(n)$

Multiplying (B.1) by  $W(n-k)$  and taking the expectation, we get,

$$\begin{aligned} E[W(n) W(n-k)] + \phi_1 E[W(n-1) W(n-k)] + \dots + \phi_p E[W(n-p) W(n-k)] \\ = Q_0 E[W(n-k) V(n)] + Q_1 E[W(n-k) V(n-1)] + \dots + Q_q E[W(n-k) V(n-q)] \end{aligned}$$

$$\begin{aligned} \text{or } \xi(k) + \phi_1 \xi(k-1) + \phi_2 \xi(k-2) + \dots + \phi_p \xi(k-p) \\ = Q_0 \xi_{wv}(k) + Q_1 \xi_{wv}(k-1) + \dots + Q_q \xi_{wv}(k-q) \end{aligned} \quad \dots(B.2)$$

where  $\xi(j)$  represents the variance function defined by  $\xi(j) = E[W(n) W(n-j)]$  and  $\xi_{wv}(j)$  represents the cross covariance function between  $W$  and  $V$  defined by  $\xi_{wv}(j) = E[W(n-j) V(n)]$ . Since  $W(n-j)$  depends only on  $V(i)$  which have occurred upto time  $(n-j)$ , it follows that  $E[W(n-j)V(n)] = 0$  for  $j > 0$  because  $W(n-j)$  and  $v(n)$  are uncorrelated for  $j > 0$ .

$$\begin{aligned} \text{Thus } \xi_{wv}(j) = 0 \quad \left. \begin{array}{l} j > 0 \\ \text{and } \xi_{wv}(j) \neq 0 \quad j \leq 0 \end{array} \right\} \quad \dots(B.3) \end{aligned}$$

Applying (B.3) in (B.2) we get

$$\xi(k) + \phi_1 \xi(k-1) + \dots + \phi_p \xi(k-p) = 0 \quad \dots(B.4)$$

for  $(k-q) \geq 1$  or  $k \geq q+1$

The variance of the process W is given by  $\xi(0) = E[W(i)W(i)]$ . From (B.2) we can write for

$$\begin{aligned} k=0 ; \xi(0) + \phi_1 \xi(1) + \phi_2 \xi(2) + \dots + \phi_p \xi(p) &= Q_0 \xi_{wv}(0) + Q_1 \xi_{wv}(-1) \\ &+ \dots + Q_q \xi_{wv}(-q) \end{aligned}$$

$$\begin{aligned} k=1 ; \xi(1) + \phi_1 \xi(0) + \phi_2 \xi(1) + \dots + \phi_p \xi(p-1) &= Q_1 \xi_{wv}(0) + Q_2 \xi_{wv}(-1) \\ &+ \dots + Q_q \xi_{wv}(-q+1) \end{aligned}$$

.

.

.

$$\begin{aligned} k=p ; \xi(p) + \phi_1 \xi(p-1) + \dots + \phi_p \xi(0) &= Q_p \xi_{wv}(0) + Q_{p+1} \xi_{wv}(-1) \\ &+ \dots + Q_q \xi_{wv}(-q+p) \quad \dots(B.5) \end{aligned}$$

These  $(p+1)$  equations of (B.5) are required to be solved for  $\xi(0), \xi(1), \dots, \xi(p)$ . This can be done by finding the  $(q+1)$  cross covariance functions  $\xi_{wv}(0), \xi_{wv}(-1), \dots, \xi_{wv}(-q)$ . To obtain  $\xi_{wv}(0)$ , multiply (B.1) by  $V(n)$  and take expectation on both sides to get

$$\begin{aligned} E[W(n) V(n)] + \phi_1 E[W(n-1)V(n)] + \dots + \phi_p E[W(n-p)V(n)] &= \\ Q_0 E[V(n) V(n)] + Q_1 E[V(n-1) V(n)] + \dots + Q_q E[V(n-q)V(n)] &\dots(B.6) \end{aligned}$$

Note that  $E[W(i)V(j)] = \xi_{wv}(j-i)$

$$\begin{aligned} \text{where } \xi_{wv}(j-i) &= 0 \quad \text{for } (j-i) > 0 \\ &\neq 0 \quad \text{for } (j-i) \leq 0 \quad \dots(B.7) \end{aligned}$$

$$\begin{aligned} \text{Also } E[V(i) V(j)] &= \sigma_v^2 & \text{if } i = j \\ &= 0 & \text{elsewhere} \end{aligned} \quad \dots(\text{B.8})$$

since  $V(n)$  represents iid white noise sequence (process). Substituting of (B.7) and (B.8) in (B.6) yields,

$$\xi_{wv}(0) = Q_0 \sigma_v^2 \quad \dots(\text{B.9})$$

Similarly to obtain  $\xi_{wv}(-j)$ , multiply (B.1) by  $V(n-j)$  and taking expectation we can find all  $\xi_{wv}(-j)$  for  $j=1, 2, \dots, q$ .

Thus, we get  $(q+1)$  equations as

$$\begin{aligned} \xi_{wv}(0) &= Q_0 \sigma_v^2 \\ \xi_{wv}(-1) &= Q_1 \sigma_v^2 - \phi_1 \xi_{wv}(0) \\ \xi_{wv}(-2) &= Q_2 \sigma_v^2 - \phi_1 \xi_{wv}(-1) - \phi_2 \xi_{wv}(0) \\ &\vdots \\ &\vdots \\ &\vdots \\ \xi_{wv}(-q) &= Q_q \sigma_v^2 - \phi_1 \xi_{wv}(-q+1) - \dots - \phi_p \xi_{wv}(-q+p) \end{aligned} \quad \dots(\text{B.10})$$

Thus, given  $\sigma_v^2$  of the process  $V(t)$  and the coefficients  $\{\phi_i\}$ ,  $\{Q_i\}$ , (B.5) can be solved using (B.10) and hence the variance  $\xi(0)$ .



## APPENDIX C

### FADING DISPERSIVE CHANNEL

The fading dispersive channel can be modeled as a randomly time-variant linear filter [5, 62], which can completely be specified at time instant  $t$  by an impulse response  $\tilde{g}(\tau;t)$  due to an impulse excitation applied  $\tau$  seconds earlier.

Let  $a(t)$  be the equivalent baseband signal transmitted over the channel. Then the received signal, in the absence of noise, may be expressed as [100],

$$r(t) = \int_{-\infty}^{\infty} \tilde{g}(\tau;t) a(t-\tau) d\tau \quad \dots(C.1)$$

where  $g(\tau;t)$  is the time-variant impulse response of the baseband channel. If  $A(f)$  is the frequency domain representation of  $a(t)$ , then (C.1) may be expressed in terms of the transfer function  $\tilde{G}(f;t)$  as

$$r(t) = \int_{-\infty}^{\infty} \tilde{G}(f;t) A(f) e^{jw\pi ft} df \quad \dots(C.2)$$

It may be observed from (C.2) that the channel distorts the signal  $A(f)$ . The changes in the received signal strength due to time-variations in  $G(f;t)$  is termed as 'fading'. In (C.1),  $\tilde{g}(\tau;t)$  may be viewed as the complex gains of a densely tapped delay line (TDL).

If the channel is bandlimited to  $|f| \leq W/2$ , then it can be shown that [100]

$$r(t) = \frac{1}{W} \sum_{K=-\infty}^{\infty} a(t-k/W) g(k/W;t) \quad \dots(C.3)$$

Defining the set of time-variable channel coefficients as

$$g_k(t) = \frac{1}{W} g(k/W;t) \quad \dots(C.4)$$

we can express (C.3) as

$$r(t) = \sum_{K=-\infty}^{\infty} g_k(t) a(t-k/W) \quad \dots(C.5)$$

Thus, the time-variant multipath fading channel can be modeled as a TDL filter with a tap spacing of  $T=1/W$  and tap coefficients  $\{g_k(n)\}$ . For a practical channel the propagation delay will be of finite spread and therefore, the TDL model as represented by (C.5) can be terminated with  $N=T_m W+1=L+1$  taps where  $T_m$  is the total multipath spread and  $L$  corresponds to the memory length of the channel. Thus we can write (C.5) as

$$r(t) = \sum_{k=0}^{N-1} g_k(t) a(t-kT) \quad \dots(C.6)$$

where  $T=1/W$ . Therefore, the noise corrupted received signal at the sampling instant  $t=nT$  can be expressed as

$$r(n) = \sum_{K=0}^{N-1} g_k(n) a(n-k) + v(n) \quad \dots(C.7)$$

where  $v(n)$  is the sampled value of the complex AWGN with zero mean and variance  $\sigma_v^2$  in each dimension. The TDL model of the fading channel corresponding to (C.7) has been shown earlier in Fig.6.2.

In the TDL model, the time-variant tap weights  $\{g_k(n)\}$  are assumed to be statistically independent complex-valued Gaussian random variables having zero-mean and the variance  $P_k$  in each dimension given by

$$P_k = \frac{1}{2} E [ |g_k(n)|^2 ], \quad \text{for } k = 0, 1, \dots, N-1 \quad \dots(C.8)$$

Note that  $P_k$ 's define the delay power spectrum or the power impulse response of the channel.

In practice, the channel exhibits variations that are smaller than the rate of data transmission. The slow fading is appropriate for a number of channels such as troposcatter and HF radio communication channels.

For simulation, the tap-gain coefficients  $g_k(0)$ ,  $k=1,2,\dots, N-1$ , are generated as complex-valued Gaussian random variables with zero mean and variance  $P_k$  in each dimension. The slow variations in the channel are taken into account by filtering the random tap coefficients through a first order low-pass RC filter whose 3-dB bandwidth  $B$  is of the order fade rate in Hertz. Thus, the tap coefficients will have a power spectrum  $S_k(\omega)$  of the form [88],

$$S_k(\omega) = P_k \frac{2\alpha}{\alpha^2 + \omega^2}; \quad k = 0,1,\dots, N-1 \quad \dots(C.9)$$

where  $\alpha = 2\pi B$  radians/sec and  $B =$  fade rate in Hz

This leads to the following model for the tap gains of the fading dispersive channel.

$$g_k(n+1) = g_k(n) \exp(-\alpha T) + \sqrt{P_k(1-\exp(-2\alpha T))} u_k(n) \quad \dots(C.10)$$

where  $u_k(n)$  is the sampled value of zero-mean, unit-variance complex white Gaussian noise process and  $T$  is the sampling interval, which is assumed to be the baud interval.

## REFERENCES

1. Alexander, S.T., "A derivation of the complex fast Kalman algorithm", *IEEE Trans. Acoust., Speech, Signal processing*, Vol. ASSP-32, pp 1230-1232, Dec. 1984.
2. Aria, G.D., Piermarini, Roberto and Zingarelli, V., "Fast adaptive equalizers for narrow-band TDMA mobile radio", *IEEE Trans. Veh. Tech.*, Vol. 40, pp. 392-404, May 1991.
3. Bahl, L.R., Cullum, C.D., Frazer, W.D. and Jelinek, F., "An efficient algorithm for computing free distance", *IEEE Trans. Inform. Theory*, Vol. IT-18, pp. 437-439, May 1972.
4. Balaban, P. and Salz, J., "Optimum diversity combining and equalization in digital data transmission with applications to cellular mobile radio-Part I:Theoretical considerations, and Part II : Numerical results", *IEEE Trans. Commun.*, Vol. 40, pp. 855-907, May 1992.
5. Bello, P.A., "Characterization of randomly time-variant linear channels", *IEEE Trans. Commun. Sys.*, Vol. CS-11, pp. 360-393, Dec. 1963.
6. Benedetto, S. and Biglieri, E., "On linear receivers for digital transmission systems", *IEEE Trans. on Commun. Tech.*, Vol. COM-22, pp. 1205-1215, Sept. 1974.
7. Benedetto, S., Marson, M. A., Albertengo, G. and Giachin, E., "Combined coding and modulation : Theory and applications", *IEEE Trans. Inform. Theory*, Vol. 34, pp. 223-236, Mar. 1988.
8. Benedetto, S., Marsan, M.A., Masera, G., Olmo, G. and Zhang, Z., "Encoded 16-PSK : A study for the receiver design", *IEEE J. Select. Areas Commun.*, Vol. 7, pp. 1381-1390., Dec. 1989.
9. Benedetto, S., Mondin, M. and Montorsi, G., "Performance evaluation of trellis-coded modulation schemes", *IEEE Proc.*, Vol. 82, pp.833-855, June 1994.
10. Benedetto, S., Mondin, M., Montorsi, G. and Mallard, L., "Geometrically uniform multidimensional PSK trellis codes", *Electron. lettrs.*, Vol. 28, no. 4, pp. 1286-1288, July 1992.
11. Belfiore, C.A. and Park, J.H., Jr., "Decision feedback equalization", *Proc. IEEE*, Vol. 67, pp. 1143-1156, Aug. 1979.

12. Berlekamp, E.R., Peile, R.E., and Pope, S.P., "The application of error control to communications", *IEEE Commun. Mag.*, Vol. 25, no. 4, pp. 44-57, April 1987.
13. Biglieri, E., "High-level modulation and coding for nonlinear satellite channels", *IEEE Trans. Commun.*, Vol. COM-32, pp. 616-626, May 1984.
14. Biglieri, E., Divsalar, D., McLane, P.J. and Simon, M.K., *Introduction to Trellis-Coded Modulation with Applications*, New York : MacMillan, 1991.
15. Biglieri, E. and Elia, M., "Multidimensional modulation and coding for band-limited digital channels", *IEEE Trans. Inform. Theory*, Vol. 34, pp. 803-809, July 1988.
16. Biglieri, E. and McLane, P.J., "Uniform distance and error probability properties of TCM schemes", *IEEE Trans. Commun.*, Vol. 39, pp. 41-52, Jan. 1991.
17. Box, G.E.P. and Jenkins, G.M., *Time Series Analysis : Forecasting and Control*, San Francisco, Holdenday, 1970.
18. Calderbank, A.R., "Multilevel codes and multistage decoding", *IEEE Trans. Commun.*, Vol. 37, pp. 222-229, Mar. 1989.
19. Calderbank, R. and Mazo, J.E., "A new description of trellis codes", *IEEE Trans. Inform. Theory*, Vol. IT-30, pp. 784-791, Nov. 1984.
20. Calderbank, R. and Sloane, N.J.A., "Four-dimensional modulation with an eight-state trellis code", *AT & T Tech. J.*, Vol. 64, pp. 1005-1018, 1985.
21. Calderbank, R. and Sloane, N.J.A., "An eight-dimensional trellis code", *IEEE Proc.*, Vol. 74, pp. 757-759, May 1986.
22. Calderbank, A.R. and Sloane, N.J.A., "New trellis codes based on lattices and cosets", *IEEE Trans. Inform. Theory*, Vol. IT-33, pp. 177-195, Mar. 1987.
23. Carlisle, C.J., Shafi, M. and Kennedy, W.K., "Trellis-coded modulation on digital microwave radio systems - Simulations for multipath fading channels", *IEEE Trans. Commun.*, Vol. 39, pp. 488-495, April 1991.
24. Castellini, G., Conti, F., Re, E.D. and Pierucci, L., "A continuously adaptive MLSE receiver for mobile communications : Algorithm and performance", *IEEE Trans. Commun.*, Vol. 45, pp. 80-88, Jan. 1997.
25. Cavers, J.K. and Ho, P., "Analysis of the error performance of trellis-coded modulations in Rayleigh-fading channels", *IEEE Trans. Commun.*, Vol. 40, pp. 74-83, Jan. 1992.
26. Chevillat, P.R. and Eleftheriou, E., "Decoding of trellis-encoded signals in the presence of intersymbol interference and noise", *IEEE Trans. Commun.*, Vol. COM-37, no. 7, pp. 669-676, July 1989.

27. Chiu, M., and Chao, C., "Performance of joint equalization and trellis-coded modulation on multipath fading channels", *IEEE Trans. Commun.*, Vol. 43, no. 2/3/4, pp. 1230-1234, Feb./March/April 1995.
28. Cusack, E.L., "Error control codes for QAM signalling", *Electr. Lett.*, Vol. 20, pp. 62-63, Jan. 1984.
29. Divsalar, D. and Simon, M.K., "Trellis coding with asymmetric modulations", *IEEE Trans. Commun.*, Vol. COM-35, pp. 130-141, Feb. 1987.
30. Divsalar, D. and Simon, M.K., "Trellis-coded modulation for 4800-9600 bits/s transmission over a fading mobile satellite channel", *IEEE, J. Select., Areas Commun.*, Vol. SAC-5, pp. 162-175, Feb. 1987.
31. Divsalar, D. and Simon, M.K., "Multiple trellis coded modulation (MTCM)", *IEEE Trans. Commun.*, Vol. 36, pp. 410-418, April 1988.
32. Divsalar, D. and Simon, M.K., "The design of trellis coded MPSK for fading channels - Part I : Performance criteria, and Part II : Set partitioning for optimum code design", *IEEE Trans. Commun.*, Vol. 36, pp. 1004-1021, Sept. 1988.
33. Divsalar, D. and Simon, M.K., "Maximum-likelihood differential detection of uncoded and trellis coded amplitude phase modulation over AWGN and fading channels-Metrics and performance", *IEEE Trans. Commun.*, Vol. 42, pp. 76-89, Jan. 1994.
34. Dreyfus, S.E., "An appraisal of some shortest-path algorithms", *Oper. Res.*, Vol. 17, pp. 395-412, May 1969.
35. Du, J. and Vucetic, B., "New 16-QAM trellis codes for fading channels", *Electron. Lett.*, Vol. 27, no. 12, pp. 1009-1010, June 1991.
36. Edbauer, F., "Performance of interleaved trellis-coded differential 8-PSK modulation over fading channels", *J. Select. Areas Commun.*, Vol. 7, pp. 1340-1346, Dec. 1989.
37. Eleftheriou, E. and Falconer, D.D., "Tracking properties and steady-state performance of RLS adaptive filter algorithms", *IEEE Trans. Acoust., Speech, Signal processing*, Vol. ASSP-34, pp. 1097-1110, Oct. 1986.
38. Eleftheriou, E. and Falconer, D.D., "Adaptive equalization techniques for HF channels", *IEEE J. Select. Areas Commun.*, Vol. SAC-5, pp. 238-247, Feb. 1987.
39. Erfanian, J., Pasupathy, S., and Gulak, G., "Reduced complexity symbol detectors with parallel structures for ISI channels", *IEEE Trans. Commun.*, Vol. 42, no. 2/3/4, pp. 1661-1671, Feb./March/April, 1994.
40. Eyuboglu, M.V., "Detection of coded modulation signals on linear, severely distorted channels using decision-feedback noise prediction with interleaving", *IEEE Trans. Commun.*, Vol. 36, pp. 401-409, April. 1988.

41. Eyuboglu, M.V. and Qureshi, S.U.H., "Reduced-state sequences estimation with set partitioning and decision feedback", *IEEE Trans. Commun.*, Vol. 36, pp. 13-20, Jan. 1988.
42. Eyuboglu, M.V. and Qureshi, S.U.H., "Reduced-state sequence estimation for coded modulation on intersymbol interference channels", *IEEE J. Select Areas Commun.*, Vol. 7, p. 989-995, Aug. 1989.
43. Falconer, D.D. and Magee, F.R., "Adaptive channel memory truncation for maximum likelihood sequence estimation", *B.S.T.J.*, Vol. 52, pp. 1541-1562, Nov. 1973.
44. Falconer, D.D. and Ljung, L., "Application of fast Kalman estimation to adaptive equalization", *IEEE Trans. Commun.*, Vol. COM-26, pp. 1439-1446, Oct. 1978.
45. Feher, K., "Modems for emerging digital cellular-mobile radio system", *IEEE Trans. Veh. Tech.*, Vol. 40, pp. 355-365, May 1991.
46. Forney, G.D., Jr., "Maximum-likelihood sequence estimation of digital sequences in the presence of intersymbol interference", *IEEE Trans. Inform. Theory*, Vol. IT-18, pp. 363-378, May 1972.
47. Forney, G.D., Jr., "The Viterbi Algorithm", *Proc. IEEE*, Vol. 61, pp 268-279, May 1973.
48. Forney, G.D., Jr., "Coset codes-Part I :Introduction and geometrical classification", *IEEE Trans. Inform. Theory*, Vol. 34, pp. 1123-1151., Sept. 1988.
49. Forney, G.D., Jr., "Geometrically uniform codes", *IEEE Trans. Inform. Theory*, Vol. 37, pp. 1241-1260, Sept. 1991.
50. Forney, G.D., Jr. and Eyuboglu, M.V., "Combined equalization and coding using precoding", *IEEE Commun. Mag.*, Vol. 29, no. 12, pp. 25-34, Dec. 1991.
51. Forney, G.D., Jr., Gallager, R.G., Lang, G.R., Longstaff, F.M. and Qureshi, S.U.H., "Efficient modulation for band-limited channels", *IEEE J. Select. Areas Commun.*, Vol. SAC-2, pp. 632-647, Sept. 1984.
52. Forney, G.D., Jr., and Wei, L.F., "Multidimensional constellations - Part I: Introduction, figures of merit, and generalized cross constellations", *IEEE J. Select. Areas Commun.*, Vol. 7, pp. 877-892, Aug. 1989.
53. Foschini, G.J., Gitlin, R.D. and Weinstein, S.B., "Optimization of two-dimensional signal constellations in the presence of Gaussian noise", *IEEE Trans. Commun.*, Vol. COM-22, pp. 28-37, Jan. 1974.
54. Fossorier, M.P.C., and Lin, S., "Effects of the catastrophic behaviour of TCM schemes with partially overlapped signal constellations", *IEEE Trans. Commun.*, Vol. 43, no. 2/3/4, pp. 687-690, Feb./March/April 1995.

55. Gagnon, F. and Haccoun, D., "Coding and modulation schemes for slow fading channels", *IEEE Trans. Commun.*, Vol. 43, no. 2/3/4, pp. 858-868, Feb./March/April 1995.
56. Godard, D.N., "Channel equalization using a Kalman filter for fast data transmission", *IBM J. Res. Dev.*, Vol. 18, pp. 267-273, May 1974.
57. Hallen, A.D. and Heegard, C., "Delayed decision-feedback sequence estimation", *IEEE Trans. Commun.*, Vol. 37, pp. 428-436, May 1989.
58. Hashimoto, T., "A list-type reduced-constraint generalization of the Viterbi algorithm", *IEEE Trans. Inform. Theory*, Vol. IT-33, pp. 865-876, Nov. 1987.
59. Heller, J.A. and Jacobs, I.M., "Viterbi decoding for satellite and space communication", *IEEE Trans. Commun. Tech.*, Vol. COM-19, pp. 835-848, Oct. 1971.
60. Ho, P. and Fung, D.K.P., "Error performance of interleaved trellis-coded PSK modulations in correlated Rayleigh fading channels", *IEEE Trans. Commun.*, Vol. 40, pp. 1800-1809, Dec. 1992.
61. Imai, H. and Hirakawa, S., "A new multilevel coding method using error-correcting codes", *IEEE Trans. Inform. Theory*, Vol. IT-23, pp. 371-377, May 1977.
62. Kailath, T., "Channel characterization : Time-variant dispersive channels", Ch. 6 in *Lectures on Communications Systems Theory*, E.J. Baghdady, Ed., New York : McGraw-Hill, 1961.
63. Kailath, T., "An innovation approach to least-sequence estimation, Part I : Linear filtering in additive white noise", *IEEE Trans. Auto. Control*, Vol. AC-13, pp. 646-655, Dec. 1968.
64. Kofman, Y., Zehavi, E. and Shamai, S., "Performance analysis of a multilevel coded modulation system", *IEEE Trans. on Commun.*, Vol. 42, no. 2/3/4, pp. 299-312, Feb./March/April 1994.
65. Kubo, H., Murakami, K. and Jujino, T., "An adaptive maximum-likelihood sequence estimator for fast time-varying intersymbol interference channels", *IEEE Trans. Commun.*, Vol. 42, no. 2/3/4, pp. 1872-1880, Feb./March/April, 1994.
66. Kubo, H., Murakami, K. and Jujino, T., "Adaptive maximum-likelihood sequence estimation by means of combined equalization and decoding in fading environments", *IEEE J. Select. Areas Commun.*, Vol. 13, pp. 102-109, Jan. 1995.
67. Larsen, K.J., "Comments on 'An efficient algorithm for computing free distance'", *IEEE Trans. Inform. Theory*, Vol. IT-19, pp. 577-579, July 1973.



68. Lawrence, R.E. and Kaufman, H., "The Kalman filter for the equalization of a digital communication channel", *IEEE Trans. Commun. Tech.*, Vol. COM-19, pp 1137-1141, Dec. 1971.
69. Lee, T.S. and Cunningham, D.R., "Kalman filter equalization for QPSK communication", *IEEE Trans Commun.*, Vol. COM-24, pp. 361-364, March 1976.
70. Lee, W.U. and Hill, F.S., "A maximum-likelihood sequence estimator with decision feedback equalization", *IEEE Trans. Commun. Tech.*, Vol. COM-25, pp. 971-979, Sept. 1977.
71. Lee, A.C.M. and McLane, P.J., "Convolutionally interleaved PSK and DPSK trellis codes for shadowed, fast fading mobile satellite communication channels", *IEEE Trans. Veh. Technol.*, Vol. 39, pp. 37-47, Feb. 1990.
72. Levy, L.S., *Discrete Structures of Computer Science*, John Wiley & Sons, New York, 1980.
73. Lin, S. and Costello, D.J., Jr., *Error control coding : Fundamentals and applications*, Englewood Cliffs, NJ : Prentice-Hall, 1983.
74. Lin, J., Proakis, J.G., Ling, F. and Lev-Ari, H., "Optimal tracking of time-varying channels : A frequency domain approach for known and new algorithms", *IEEE Trans. Select. Areas Commun.*, Vol. 13, pp. 141-153, Jan. 1995.
75. Long, G., Ling, F. and Proakis, J.G., "The LMS algorithm with delayed coefficient adaptation", *IEEE Trans. Acoust., Speech, Signal processing*, Vol. 37, pp 1397-1405, Sept. 1989.
76. Lucky, R.W., "Techniques for adaptive equalization of digital communication systems", *B.S.T.J.*, Vol. 45, pp 255-286, Feb. 1966.
77. Lucky, R.W., "A Survey of communication theory literature : 1968-1973", *IEEE Trans. Inform. Theory*, Vol. IT-19, pp 725-739, Nov. 1973.
78. Magee, F.R. and Proakis, J.G., "Adaptive maximum likelihood sequence estimation for digital signaling in the presence of intersymbol interference", *IEEE Trans. Inform Theory*, Vol. IT-19, pp. 120-124, Jan. 1973.
79. Magee, F.R. and Proakis, J.G., "An estimate of the upper bound on error probability for maximum-likelihood sequence estimation on channels having a finite-duration pulse response", *IEEE Trans. Inform. Theory*, Vol. IT-19, pp. 699-702, Sept. 1973.
80. Massey, J.L., "Coding and modulation in digital communications", in Proc. 1974 Int. Zurich Seminar Digital Commun., Zurich, Switzerland, pp. E2(1)-E2(4), 1974.
81. Mckay, R.G. and McLane, P.J., "Error bounds for trellis-coded MPSK on a fading mobile satellite channel", *IEEE Trans. Commun.*, Vol. 39, pp. 1750-1761, Dec. 1991.

82. McLane, P.J., Wittke, P.H., Ho, P.K.M. and Loo, C., "PSK and DPSK trellis codes for fast fading, shadowed mobile satellite communication channels", *IEEE Trans. Commun.*, Vol. 36, pp. 1242-1246, Nov. 1988.
83. Mehra, D.K., "Identification and equalization of fading dispersive channels", Ph.D. Thesis, Dept. Elec. Engg., Indian Institute of Technology, Kanpur, India, March 1978.
84. Mohanraj, P., Falconer, D.D. and Kwasniewski, T.A., "Baseband trellis-coded modulation with combined equalization/decoding for high bit rate digital subscriber loops", *IEEE J. Select. Areas Commun.*, Vol. 9, pp. 871-875, Aug. 1991.
85. Moher, M.L. and Lodge, J.H., "TCMP-A modulation and coding strategy for Rician fading channels", *IEEE J. Select Areas Commun.*, Vol. 7, pp. 1347-1355, Dec. 1989.
86. Mosen, P., "Feedback Equalization for Fading Dispersive Channels", *IEEE Trans. Inform. Theory*, Vol. IT-17, pp. 46-55, Jan. 1971.
87. Mosen, P., "Fading channel communications", *IEEE Commun. Mag.*, Vol. 18, no. 1, pp. 16-25, Jan. 1980.
88. Mui, S. and Modestino, J.W., "Performance of DPSK with convolutional encoding on time varying fading channels", *IEEE Trans. Commun.*, Vol. COM-25, pp. 1075-1083, Oct. 1977.
89. Omura, J.K., "On the Viterbi decoding algorithm", *IEEE Trans. Inform. Theory*, Vol. IT-15, pp. 177-178, Jan. 1969.
90. Pahlavan, K., and Holsinger, J.L., "Voice-band data communication modems - A historical review : 1919-1988", *IEEE Commun. Mag.*, Vol. 26, no. 1, pp. 16-26, Jan. 1988.
91. Panayirci, E., Aygolu, U. and Ucan, O.N., "Error performance analysis of quadrature partial response trellis coded modulation (QPR-TCM) in fading mobile satellite channels", *IEEE Trans. Commun.*, Vol. 43, no. 2/3/4, Feb./March/April, pp. 1653-1662, April 1995.
92. Pietrobon, S.S., Deng, R.H., Lafanechere, A., Ungerboeck, G. and Costello, D.J., Jr., "Trellis-coded multidimensional phase modulation", *IEEE Trans. Inform. Theory*, Vol. 36, pp. 63-89, January 1990.
93. Pietrobon, S.S. and Costello, D.J., Jr., "Trellis coding with multidimensional QAM signal sets", *IEEE Trans. Inform. Theory*, Vol. 39, pp. 325-336, March 1993.
94. Pottie, G.J. and Eyuboglu, M.V., "Combined coding and precoding for PAM and QAM HDSL systems", *IEEE J. Select. Areas Commun.*, Vol. 9, pp. 861-870, Aug. 1991.

95. Pottie, G.J. and Taylor, D.P., "An approach to Ungerboeck coding for rectangular signal sets", *IEEE Trans. Inform. Theory*, Vol. IT-33, pp. 285-290, March 1987.
96. Pottie, G.J. and Taylor, D.P., "Multilevel codes based on partitioning", *IEEE Trans. Inform. Theory*, Vol. 35, pp. 87-98, Jan. 1989.
97. Price, R. and Green, P.E., "A Communication technique for multi-path channels", *Proc. IRE.*, Vol. 46, pp. 555-570, March 1978.
98. Proakis, J.G., "Channel identification for high speed digital communication", *IEEE Trans. Auto. Control*, Vol. AC-19, pp. 916-922, Dec. 1974.
99. Proakis, J.G., "Performance capabilities of the Viterbi algorithm for combatting intersymbol interference on fading multipath channel", *Communication systems and random proces theory*, Ed. by Skwirzynski, J.K., Sijthoff and Noordhoff, 1978, pp. 403-424.
100. Proakis, J.G., *Digital Communications*, New York : McGraw-Hill, 1989, 2nd ed.
101. Proakis, J.G., "Adaptive equilization for TDMA digital mobile radio", *IEEE Trans. Veh. Tech.*, Vol. 40, pp. 333-341, May 1991.
102. Proakis, J.G. and Miller, J.H., "An adaptive receiver for digital signalling through channels with intersymbol interference", *IEEE Trans. Inform. Theory*, Vol. IT-15, pp. 484-497, July 1969.
103. Qureshi, S.U.H. and Newhall, E.E., "An Adaptive Receiver for Data Transmission over Time-Dispersive Channels", *IEEE Trans. Inform. Theory*, Vol. IT-19, pp. 448-457, July 1973.
104. Qureshi, S.U.H., "Adaptive equalization", *Proc. IEEE*, Vol. 73, pp. 1349-1387, Sept. 1985.
105. Raheli, R., Polydors, A. and Tzou, C.K., "Per-survivor processing : A general approach to MLSE in uncertain environments", *IEEE Trans. Commun.*, Vol. 43, no. 2/3/4, pp. 354-364, Feb./March/April, 1995.
106. Rissanen, J., "Recursive Identification of Linear Systems", *SIAM Journal of Control*, Vol. 9, pp. 420-430, 1971.
107. Rissanen, J. and Kailath, T., "Partial Realization of Random Systems", *Automatica*, Vol. 8, pp. 389-396, 1972.
108. Rouanne, M. and Costello, D.J., Jr., "An algorithm for computing the distance spectrum of trellis codes", *IEEE J. Select. Areas Commun.*, Vol. SAC-7, pp. 929-940, Aug. 1989.
109. Sayegh, S.I., "A class of optimum block codes in signal space", *IEEE Trans. Commun.*, Vol. COM-34, pp. 1043-1045, Oct. 1986.

110. Schlegel, C. and Costello, D.J., Jr., "Bandwidth efficient coding for fading channels : Code construction and performance analysis", *IEEE J. Select. Areas Commun.*, Vol. 7, pp. 1356-1368, Dec. 1989.
111. Schlegel, C., "Evaluating distance spectra and performance bounds of trellis codes on channels with intersymbol interference", *IEEE Trans. Inform. Theory*, Vol. 37, pp. 627-634, May 1991.
112. Seshadri, N., "Joint data and channel estimation using blind trellis search techniques", *IEEE Trans. Commun.*, Vol. 42, no. 2/3/4, pp. 1000-1011, Feb./March/April, 1994.
113. Seshadri, N. and Sundberg, C.E.W., "Multilevel trellis coded modulations for the Rayleigh fading channel", *IEEE Trans. Commun.*, Vol. 41, pp. 1300-1310, Sept. 1993.
114. Seshadri, N. and Sundberg, C.E.W., "List Viterbi decoding algorithms with applications", *IEEE Trans. Commun.*, Vol. 42, no. 2/3/4, pp. 313-323, Feb./March/April 1994.
115. Shannon, C.E., "A mathematical theory of communication", *B.S.T.J.*, Vol. 27, pp. 379-343, July 1948, and pp. 623-656, Oct. 1948.
116. Shannon, C.E., "Communication in the presence of noise", *Proc. IRE*, Vol. 37, pp. 10-21, Jan. 1949.
117. Sheen W.H. and Stuber, G.L., "MLSE equalization and decoding for multipath-fading channels", *IEEE Trans. Commun.*, Vol. 39, pp. 1455-1464, Oct. 1991.
118. Sheen W.H. and Stuber G.L., "Error probability of reduced-state sequence estimation for trellis-coded modulation on intersymbol interference channels", *IEEE Trans. Commun.*, Vol. 41, pp. 1265-1269, Sept. 1993.
119. Sheen, W.H. and Stuber G.L., "Error probability for maximum likelihood sequence estimation of trellis-coded modulation on ISI channels", *IEEE Trans. Commun.*, Vol. 42, no. 2/3/4, pp. 1427-1430, Feb./March/April 1994.
120. Simmons, S.J., "Alternative trellis decoding for coded QAM in the presence of ISI", *IEEE Trans. Commun.*, Vol. 42, No. 2/3/4, pp. 1455-1459, Feb/March/April, 1994.
121. Soleymani, M.R., and Kang, L., "TCM schemes with partially overlapped signal constellations", *IEEE Trans. Commun.*, Vol. 41, pp. 435-438, March 1993.
122. Stein, S., "Fading channel issues in system engineering", *IEEE J. Select Areas Commun.*, Vol. SAC-5, pp. 68-89, Feb. 1987.
123. Thapar, H.K., "Real-time application of trellis coding to high-speed voiceband data transmission", *IEEE J. Select Commun.*, Vol. SAC-2, pp. 648-658, Sept 1984.

124. Turgeon, J.M. and Mclane, P.J., "Minimal transmitter complexity design of analytical described trellis codes", *IEEE Trans. Commun.*, Vol. 38, pp. 1352-1358, Sept. 1990.
125. Ungerboeck, G., "Adaptive maximum-likelihood receiver for carrier-modulated data-transmission systems", *IEEE Trans. Commun.*, Vol. COM-22, pp. 624-636, May 1974.
126. Ungerboeck, G., "Channel coding with multilevel/phase signals", *IEEE Trans. Inform. Theory*, Vol. IT-28, pp. 55-67, Jan. 1982.
127. Ungerboeck, G., "Trellis-coded modulation with redundant signal sets - Part I: Introduction and Part-II:State of the art", *IEEE Commun. Mag.*, Vol. 25, no. 2, pp. 5-21, Feb. 1987.
128. Viterbi, A.J., "Error bounds for convolutional codes and an asymptotically optimum decoding algorithm", *IEEE Trans. Inform. Theory*, Vol. IT-13, pp. 260-269, April 1967.
129. Viterbi, A.J., "Convolutional codes and their performance on communication systems", *IEEE Trans. Commun. Tech.*, Vol. COM-19, pp. 751-772, Oct. 1971.
130. Viterbi, A.J. and Omura, J. K., *Principles of Digital Communications and Coding*, New York : McGraw-Hill, 1979.
131. Viterbi, A.J., Wolf, J.K., Zehavi, E. and Padovani, R., "A pragmatic approach to trellis-coded modulation", *IEEE Commun. Mag.*, Vol. 27, no. 7, pp. 11-19, July 1989.
132. Webb, W.T., Hanzo, L. and Steele, R., "Bandwidth efficient QAM schemes for Rayleigh fading channels", *IEE Proc.*, Vol. 138, no. 3, pp. 169-175, June 1991.
133. Wei, L.F., "Rotationally invariant convolutional channel codes with expanded signal space, Part I :  $180^\circ$  and Part II : Nonlinear codes", *IEEE J. Select. Areas Commun.*, Vol. SAC-2, pp. 659-686, Sept. 1984.
134. Wei, L.F., "Trellis-coded modulation with multidimensional constellations", *IEEE Trans. Inform. Theory*, Vol. IT-33, pp. 483-501, July 1987.
135. Wei, L.F., "Rotationally invariant trellis-coded modulations with multidimensional M-PSK", *IEEE J. Select. Areas Commun.*, Vol. 7, pp. 1281-1295, Dec. 1989.
136. Wei, L.F., "Two-level coding based on trellis-coded modulation and Reed-Solomon codes", *IEEE Trans. Commun.*, Vol. 42, pp. 3098-3108, Dec. 1994.
137. Wesolowski, K., "An efficient DFE and ML suboptimum receiver for data transmission over dispersive channels using two-dimensional signal constellations", *IEEE Trans. Commun.*, Vol. COM-35, pp. 336-339, March 1987.

138. Wesolowski, K., "Efficient digital receiver structure for trellis-coded signals transmitted through channels with intersymbol interference", *Electron. Lett.*, Vol. 23, no. 24, pp. 1265-1267, Nov. 1987.
139. Widrow, B., "Adaptive filters", in *Aspects of Network and System Theory*, part IV, R.E., Kalmau and N. Declaris, Eds. New York : Hold, Rinehart and Winston, 1971, pp. 563-587.
140. Widrow, B., McCool, J. and Ball M., "The complex LMS algorithm", *IEEE Proc.*, Vol. 63, pp. 719-720, April 1975.
141. Wilkinson, J.H. and Reinsch, C., *Handbook for Automatic Computation*, Vol. II: Linear Algebra, Springer-Verlag, New York, 1977.
142. Wong, L.N. and Mclane, P.J., "Performance of trellis codes for a class of equalized ISI channels", *IEEE Trans. Commun.*, Vol. 36, pp. 1330-1336, Dec. 1988.
143. Wu, J. and Lin, S., "Multilevel trellis MPSK modulation codes for the Rayleigh fading channel", *IEEE Trans. Commun.*, Vol. 41, pp. 1311-1318, Sept. 1993.
144. Wu, J.M. and Su, S.L., "Combination of block-coded modulation and trellis-coded modulation", *IEE Proc.*, Vol. 138, pp. 381-386, Oct. 1991.
145. Yamaguchi, K. and Imai, H., "Highly reliable multilevel channel coding system using binary convolutional codes", *Electron Lett.*, Vol. 23, no. 18, pp. 939-941, Aug. 1987.
146. Zehavi, E. and Wolf, J.K., "On the performance evaluation of trellis codes", *IEEE Trans. Inform. Theory*, Vol. IT-33, pp. 196-202, Mar. 1987.
147. Ziemer, R.E. and Kasahara, M., "Coded modulation : Development, theory and applications", *IEEE Commun. Mag.*, Vol. 29, pp. 8-11, Dec. 1991.
148. Zhou, K, and Proakis, J.G., "Decision-feedback equalization on time-dispersive channels with coded modulation", *IEEE Trans. Commun.*, Vol. 38, pp. 18-24, Jan. 1990.